Copy 2

THE PHYSICAL REVIEW

VOLUME 43 *Second Series* NUMBER 6

MARCH 15, 1933

Published for the

AMERICAN PHYSICAL SOCIETY

by the

AMERICAN INSTITUTE OF PHYSICS
Incorporated

LANCASTER, PA., AND NEW YORK, N. Y.

The American Physical Society

OFFICERS OF THE SOCIETY

Paul D. Foote, *President*
The Gulf Companies
Pittsburgh, Pennsylvania

Arthur H. Compton, *Vice-President*
University of Chicago
Chicago, Illinois

W. L. Severinghaus, *Secretary*
Columbia University
New York, New York

G. B. Pegram, *Treasurer*
Columbia University
New York, New York

John T. Tate, *Editor*
University of Minnesota
Minneapolis, Minnesota

L. B. Loeb, *Local Secretary for the Pacific Coast*
University of California
Berkeley, California

The Physical Review

BOARD OF EDITORS

John T. Tate, *Editor*

J. W. Buchta, *Assistant Editor*

Associate Editors

A. J. Dempster
David M. Dennison
J. C. Slater
R. C. Gibbs
E. O. Lawrence
J. H. Van Vleck
K. K. Darrow
J. C. Hubbard
A. E. Ruark

The Physical Review, which was established in 1893, is a journal of experimental and theoretical physics. It is published for the American Physical Society by the American Institute of Physics Incorporated. There are two volumes annually with twelve issues in each volume.

Manuscripts for publication should be submitted to John T. Tate, University of Minnesota, Minneapolis, Minnesota.

Proof and all correspondence concerning papers in the process of publication, should be addressed to the Editorial Secretary, American Institute of Physics, 11 East 38th Street, New York, New York.

Subscription price $15.00 per year. Single copies $1.50 each for issues prior to July 1, 1929 (Vols. 1-33); $.75 each for issues subsequent thereto. Subscriptions and orders for back numbers should be addressed to Prince and Lemon Streets, Lancaster, Pennsylvania, or to the American Institute of Physics, 11 East 38th Street, New York, New York.

Advertising is not accepted for the *Physical Review* but attention is called to the *Review of Scientific Instruments with Physics News and Views*, a companion publication of the Institute, and a medium through which the field of physics can be reached most effectively. Rates and other information will be furnished on request to the Editorial Secretary.

Changes of address and complaints of failure to receive the *Physical Review*, in the case of members of the American Physical Society, should be addressed to the Treasurer; in the case of other subscribers, to the Editorial Secretary. New copies can be sent free in response to complaints of non-delivery only if notice of non-delivery is received within three months of date of issue.

The Physical Review is published semi-monthly at Prince and Lemon Streets, Lancaster, Pennsylvania.

Entered at the Post Office at Lancaster, Pennsylvania, as second class matter.

Acceptance for mailing at special rate of postage provided for in section 1103, Act of October 3, 1917, authorized September 6, 1924.

THE
PHYSICAL REVIEW
A Journal of Experimental and Theoretical Physics
VOL. 43, No. 6 MARCH 15, 1933 SECOND SERIES

A Geographic Study of Cosmic Rays

ARTHUR H. COMPTON, *University of Chicago*
(Received January 30, 1933)

Data are given from measurements of the intensity of cosmic rays by 8 different expeditions at 69 stations distributed at representative points over the earth's surface. Each set of apparatus consisted of a 10 cm spherical steel ionization chamber filled with argon at 30 atmospheres, connected to a Lindemann electrometer, and shielded with 2.5 cm of bronze plus 5.0 cm of lead. Measurements were made by comparing the ionization current due to the cosmic rays with that due to a capsule of radium at a measured distance, the radium standards used with the several sets of apparatus having been intercompared. The method of detecting and correcting for the following disturbing effect is discussed: insulation leak and absorption, local gamma-radiation, radioactive contamination of the ionization chamber, and shielding from cosmic rays by roof and horizon. Intensity *vs.* barometer (altitude) curves are given for various latitudes. These show not only the rapid increase with altitude noted by previous observers, but also the fact that at each altitude the intensity is greater for high latitudes than near the equator. At sea level the intensity at high latitudes is 14 ± 0.6 percent greater than at the equator; at 2000 m elevation, 22 percent greater; and at 4360 m, 33 percent greater. This variation follows the geomagnetic latitude more closely than the geographic or the local magnetic latitude, and is most rapid between geomagnetic latitudes 25 and 40 degrees. Consideration of the conditions necessary for deflection of high-speed electrified particles by the earth's magnetic field indicates that if the cosmic rays are electrons, they must originate not less than several hundred kilometers above the earth. The data can be quantitatively explained on the basis of Lemaitre and Vallarta's theory of electrons approaching the earth from remote space. Acknowledgment is made of the cooperation of more than 60 physicists in this program, 25 of whom are named.

IN the summer of 1930, Professor R. D. Bennett, then of the University of Chicago, Professor J. C. Stearns of the University of Denver, and the writer initiated a coordinated study of the geographical distribution of cosmic rays. While it will be some years before this study is completed, the results already obtained give information whose publication should not be delayed. The present paper is thus a progress report[1] on the findings of our associated expeditions, and gives data which we hope to amplify in subsequent communications.

Previous studies of the relative intensity of the cosmic rays in different parts of the world have been made by J. Clay,[2] who made several trips between Java and Holland, and who found consistently a lower intensity near the equator; Millikan and Cameron,[3] who found but small

[1] Earlier reports of the work of these expeditions have appeared as follows: A. H. Compton, R. D. Bennett and J. C. Stearns, Phys. Rev. **38**, 1565, 1566 (1931); ibid. **39**, 873; **41**, 119 (1932). R. D. Bennett, Technology Review, July, 1932; A. H. Compton, Phys. Rev. **39**, 190; **41**, 111 and 681; **42**, 904 (1932); Scientific Mon., Jan., 1933. A. H. Compton and J. J. Hopfield, Phys. Rev. **41**, 539 (1932). J. C. Stearns, W. P. Overbeck and R. D. Bennett, Phys. Rev. **42**, 317 (1932). R. D. Bennett, J. L. Dunham, E. H. Bramhall and P. K. Allen, Phys. Rev. **42**, 446 (1932).

[2] J. Clay, Proc. Amsterdam Acad. **30**, 1115 (1927); **31**, 1091 (1928).

[3] R. A. Millikan and G. H. Cameron, Phys. Rev. **31**, 163 (1928).

differences between Bolivia and California in their measurements in mountain lakes, and no difference[4] between Pasadena and Churchill, close to the north magnetic pole; Bothe and Kolhörster,[5] who carried a counting tube from Hamburg (53°N) to Spitzbergen (81°N) and back, and who detected no variations in the cosmic rays larger than their rather large experimental error; Kennedy, who under Grant's direction[6] carried similar apparatus from Adelaide, Australia to Antarctica, and likewise found no measurable change; and Corlin,[7] who on going from 50°N to 70°N in Scandinavia found some evidence of a maximum at about 55°N. The prevailing opinion regarding the significance of these measurements has thus been expressed by Hoffmann[8] in a recent summary; "The results so far have on the whole been negative. Most of the observers conclude that within the errors of experiment the intensity is constant and equal, and those authors who do find differences give their results with certain reservations."

In view of the strong indication from the Bothe-Kolhörster double counter experiment[9] that the cosmic rays are high-speed electrical particles, this failure to find a variation of cosmic-ray intensity with latitude was of unusual interest. If the negative results of the experiments could be established with higher precision, it would mean that the cosmic rays could not be electrical particles coming from outside the earth's atmosphere, unless these particles had an unsuspectedly high energy. If, on the other hand, further experiments should confirm the tentative findings of Clay and Corlin, it might be found that a consistent theory of cosmic rays could be built on the assumption of high-speed electrical particles entering the earth's atmosphere.

[4] R. A. Millikan, Phys. Rev. **36**, 1595 (1930).
[5] W. Bothe and W. Kolhörster, Berl. Ber. p. 450 (1930).
[6] Kerr Grant, Nature **127**, 924 (1931).
[7] A. Corlin, Lund Medd. No. 121 (1930).
[8] G. Hoffmann, Phys. Zeits. **32**, 633 (1932). Hoffmann mentions also (without reference) that in their airship flight over the north pole, Malmgrön and Behounek observed the normal cosmic-ray intensity throughout the flight.
[9] W. Bothe and W. Kolhörster, Zeits. f. Physik **56**, 751 (1929).

Organization and Location of the Observing Stations

In order to get as extensive data as possible in the minimum possible time, several expeditions were organized to go into different parts of the world. Seven similar sets of apparatus were constructed, and measurements by the different observers were made with essentially the same procedure. The work has been done not only at sea level, but also at as great a variety of altitudes as possible, in order to learn whether the intensity-altitude relation was independent of the location.

Eight of these associated expeditions have so far reported data. They have been under the direction of:

1. J. C. Stearns and A. H. Compton, working in Colorado and Switzerland.
2. A. H. Compton, in Hawaii, New Zealand, Australia, Panama, Peru, Mexico, northern Canada, Michigan and Illinois.
3. R. D. Bennett, Massachusetts Institute of Technology, in Alaska, California, Colorado and Cambridge.
4. E. O. Wollan, University of Chicago, in Chicago, Spitzbergen and Switzerland.
5. Allen Carpe, of New York City, in Alaska.
6. S. M. Naude, University of Capetown, in South Africa.
7. J. M. Benade, Forman Christian College, Lahore, in India, Ceylon, Malaya, Java, Ladakh.
8. P. G. Ledig, Division of Terrestrial Magnetism, Carnegie Institution of Washington, in South America.

The locations of the major stations where measurements have been made and reported are shown in Fig. 1.

Apparatus

In designing the measuring apparatus, the two main characteristics kept in mind were freedom from sources of systematic error and portability. An ionization chamber was used rather than a counting tube, because of the better reproducibility and the lower statistical error of its readings. The chamber was made small, 10 cm diameter, in order that the weight of the pro-

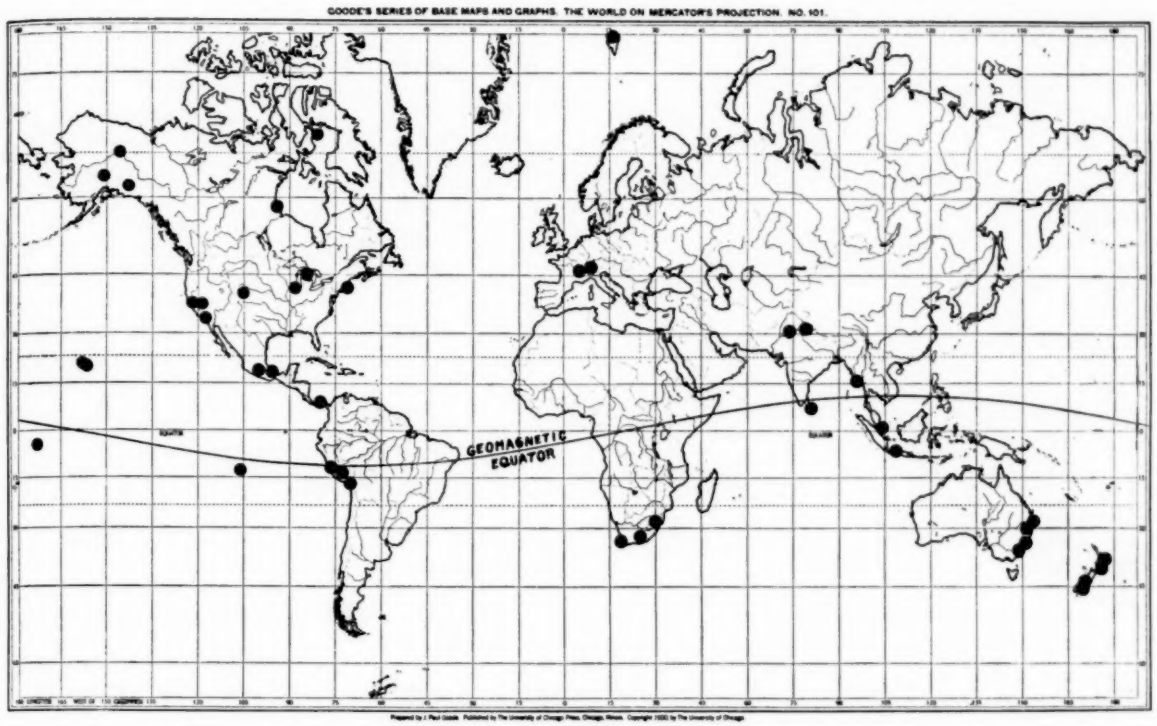

FIG. 1. Map showing location of our major stations for observing cosmic rays.

tecting shields should not be too great for transport by pack trains or porters. By filling the chamber with argon[10] at 30 atmospheres the ionization current was made large enough to be conveniently measurable with a Lindemann electrometer. At each station the ionization due to the cosmic rays was compared with that due to a standard radium capsule. Our measurements were thus independent of the pressure of the gas in the chamber, or of the sensitiveness of our electrical instruments, the reliability of our comparison between different stations depending rather upon the constancy of the radium capsule.

A partly diagrammatic plan of the apparatus is shown in Fig. 2. The ions produced in the argon-filled chamber are collected by a steel rod electrode, which conducts the ionization current to the needle of the electrometer. This electrode is insulated by an amber cone from the brass tube through which it passes. The brass tube serves as a support for the ionization chamber, and remains at ground potential. The chamber containing the key and the connection to the electrometer, though at atmospheric pressure, is kept nearly air-tight with a sponge rubber gasket *G*, and is dried with a phosphorus pentoxide tube. The electrometer is similarly dried by using a modified form of drying tube. The pressure chambers have shown little if any leak while in service in the field. The various battery potentials indicated in the diagram are supplied by commercial dry batteries. Spherical shells of bronze and of antimony lead encased in thin steel are fitted around the ionization chamber. These shells, each 2.5 cm thick, are sufficient to reduce the intensity of the local gamma-rays to about 5 percent of the cosmic-ray intensity.

For standardizing the instrument, a capsule containing about 1.3 mg of radium enclosed in about 1 cm of lead is placed with its center 1 meter from the center of the ionization chamber. The absolute magnitude of the ionization current due to the radium in this position was measured by the help of a standard cylindrical condenser, which is screwed in place of the grounding key *K*. This condenser has two pairs of concentric cylinders which may be used alternately. The difference in capacity between the larger and the

[10] Cf. A. H. Compton and J. J. Hopfield, Phys. Rev. **41**, 539 (1932).

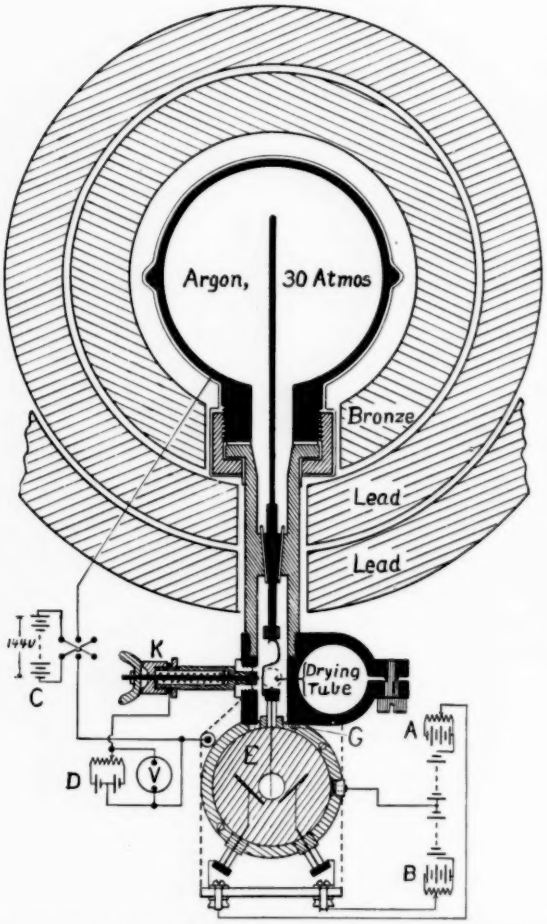

FIG. 2. Cosmic-ray ionization chamber, electrometer, and electrical connections.

smaller pair can be calculated from the dimensions as 14.95 cm. By comparing the rate of drift of the electrometer needle with and without the condensers, the capacity of apparatus No. 7, for a needle sensitivity of 0.01 volt per division, was found to be 12.72 cm. The ionization current due to the laboratory radium standard at 1 meter produced a potential change of 4.14×10^{-5} volts per second, when the chamber was filled with dry air at 741 mm pressure and 24.5°C, corresponding to 4.626×10^{-5} volts per second filled with air under standard conditions. The volume of the chamber was 430.8 cc. Thus the ionization in standard air due to the laboratory radium standard at 1 meter, through the lead and bronze shields, is,

$$I_s=\frac{1}{300}\times\frac{12.72\times4.626\times10^{-5}}{4.77\times10^{-10}\times430.8}$$
$$=9.53 \text{ ions cm}^{-3}\text{ sec.}^{-1}. \quad (1)$$

Each of the 7 sets of apparatus has with it its own secondary radium standard, which was compared with the laboratory standard before the equipment was sent out for use. These secondary standards were found to produce respectively in standard air at 1 meter, per cm³ per sec., the values given in Table I.

THE MEASUREMENTS

Each complete set of measurements at a given station consisted of two parts: (1) the determination of the ratio i_2/i_r of the ionization with the radium at a great distance to the ionization with the radium at 1 meter from the center of the ionization chamber, by using both lead shields; and (2) measurement of the ratio i_1/i_2 of the ionization with no radium present when only 1 lead shield surrounds the chamber to that with two lead shields in place. From these two data and the value of I_γ given in Table I can be calculated the ionization due to the cosmic rays (through both lead shields), and the intensity of the local gamma-rays which enter the chamber.

TABLE I. *Ionization by radium capsules.*

Capsule No.	Expedition No.	Ionization (I_γ)
1	3	11.05 ions
2	7	11.8
3	6	12.2
4	5	11.95
5	2 and 8	11.6
6	9	11.55
7	4 and 3	11.85

Let i_r be the observed ionization current in arbitrary units, through 2 lead shields, radium at 1 meter; i_1 the ionization through 1 lead shield, radium absent; i_2 the ionization through 2 lead shields, radium absent. The ratio of the ionization due to cosmic and local rays to that due to the gamma-rays alone is then,

$$R_2=i_2/(i_r-i_2)=(i_2/i_r)/(1-i_2/i_r). \quad (2)$$

Also, the ratio of the cosmic rays with 1 shield to the gamma-rays with 2 shields is,

$$R_1=(i_1/i_2)R_2. \quad (3)$$

To correct for the effect of the local radiation we

use the formulas,

$$C=[a/(a-b)](R_2-bR_1)I_\gamma \quad (4)$$

$$L=R_2I_\gamma-C. \quad (5)$$

Here C is the ionization through both lead shields, due to the cosmic rays alone, and I_γ is the ionization by the gamma-rays, so that if I_γ is expressed in ions per cc per second in standard air, C is expressed in the same units.[11] a is the ratio of the ionization due to the cosmic rays when 2 lead shields are used to that when 1 shield is used, and has a value of about 0.9. b is the same ratio for the local gamma-rays, and has a value of 0.286. L represents the ionization due solely to the local rays.

The derivation[12] of Eq. (4) involves the assumption that the ionization due to radioactivity in the chamber itself is negligible. This has been tested with three of our sets of apparatus by placing them in deep tunnels (one in Colorado, one in Thibet and one in Peru). If the assumption is justified, the calculated intensity of the cosmic rays inside the tunnel should be zero. In the Colorado and Thibet measurements it was found to be respectively about 0.2 and 0.1 percent of the intensity outside the tunnel, whereas in the Peruvian measurements there appeared an ionization of about 2 percent, which may have been due to temporary radioactive contamination.

The value of b was determined by using the radium capsule as the source of gamma-rays. In regions where thorium is abundant the resulting value may not be wholly reliable, but approximate tests on the local radiation inside a tunnel in Peru have confirmed the value obtained with radium within experimental error. It was found that the value of a varies so rapidly with altitude that it was necessary to adjust this constant according to the barometric pressure. The values of a used in calculating our results are given in Fig. 3. These values are somewhat arbitrary.

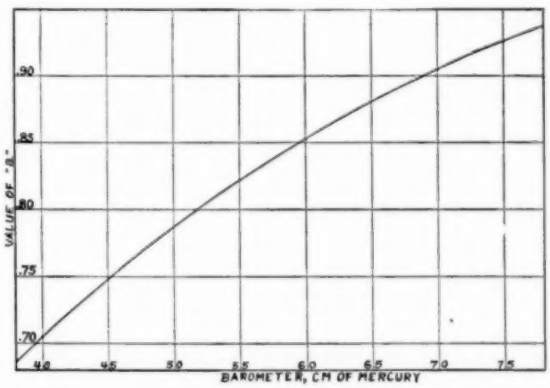

FIG. 3. a as a function of barometric pressure.

Approximate values of a have been determined by measurements of the relative ionization with 1, 2, and 3 shields. Such determinations are however unreliable because the cosmic rays are not exponentially absorbed by the shields. The values given in Fig. 2 are so chosen that the correction for local radiation is on the average about the same for different altitudes. Errors in the value of a will introduce errors in the absolute ionization by the cosmic rays, and in the

[11] This statement assumes that the value of R_2 will be independent of the nature and pressure of the gas in the ionization chamber. Its independence of pressure when air or CO_2 is used has been tested and confirmed by Stearns (Phys. Rev. **39**, 881 (1932)), Millikan (Phys. Rev. **39**, 397 (1932)) and Steinke and Schindler (Naturwiss. **20**, 15 (1932)), though Broxon working with nitrogen (Phys. Rev. **40**, 327 (1932)) and Hopfield using argon (Phys. Rev. **42**, 904A (1932)) find slight differences. If such differences exist, they will require a revision of our *absolute* cosmic-ray intensities, though not of our relative intensities at different altitudes and latitudes.

[12] Let C_1 and L_1 be the intensities of the cosmic rays and the local rays respectively through 1 shell of lead, C_2 and L_2 be the intensities through 2 shells of lead. Then

$$I_1=C_1+L_1 \quad (6)$$

and

$$I_2=C_2+L_2 \quad (7)$$

are the total observed intensities in the two cases, when no radium is present. Also, $a=C_2/C_1$ and $b=L_2/L_1$ are the fractions of the cosmic and the local rays respectively transmitted by the second shell of lead. Thus $C_2=aC_1$ and $L_2=bL_1$. Writing Eq. (7) as

$$I_2=aC_1+bL_1, \quad (8)$$

and combining with (6) we find,

$$C_1=[1/(a-b)](I_2-bI_1).$$

or, since $C_2=aC_1$

$$C_2=[a/(a-b)](I_2-bI_1). \quad (9)$$

However, I_2 is the same as the R_2I_γ, and $I_1=R_1I_\gamma$. Also, C_2 is identical with the C of Eq. (4). Hence,

$$C=[a/(a-b)](R_2-bR_1)I_\gamma, \quad (10)$$

which is Eq. (4) of the text

relative ionization at different altitudes. They will not affect however the relative ionization as calculated at different latitudes.

In any case, since the corrections introduced by Eqs. (3) and (4) for the local radiation are of the order of only 5 percent of the observed intensity, small errors in this correction are not serious.

A typical series of readings consists of: (A) Measurements with the bronze and both lead shields, with and without radium, and with the ionization chamber alternately at +144 and −144 volts. This serves to determine i_2/i_r. (B) Measurements with the bronze and one lead shield, without radium, and with the ionization chamber alternately at +144 and −144 volts. Comparison with A gives i_1/i_2.

Measurements of type A and B are made alternately over a period of from 8 hours to 240 hours, and then averaged. Most of the data reported for a given station represent about 30 hours of readings.

Corrections

In addition to the correction for local radiation, small corrections were necessary also for the absorption by the roof—if any—protecting the apparatus, and for the shielding due to neighboring mountains or buildings. The roof correction was made by adding to the observed barometric pressure an equivalent to the average weight per cm² of the roof. The maximum correction thus applied amounted to 5.3 mm of mercury. Wherever possible an unprotected site was of course chosen. In no case was the shielding by neighboring buildings significant. In many cases, however, neighboring mountains shielded the apparatus appreciably. A panorama of the altitude of the horizon was then made, and the loss from the shielded zones estimated from Table II. The maximum correction as thus estimated for any station was 10 percent. Since the angular altitude distribution of cosmic rays is known to depend on the elevation, this correction is of course only approximate.

Table II.

Degrees from zenith	Normal contribution
0–45°	0.6578
45–60°	0.2105
60–75°	0.1100
75–85°	0.0210
85–90°	0.0007

Several kinds of electrical troubles were encountered. Among these should be mentioned, leakage across the insulation supporting the electrode and the electrometer needle, dielectric absorption by this insulation, ionization in the air filling the electrometer and the tube connecting the electrometer to the ionization chamber, and insulation failures in the auxiliary battery box. Trouble with the batteries could introduce no systematic errors into our measurements, but occasionally reduced their precision. By drying the battery box and connections either with heat or with calcium chloride, the insulation could be kept in satisfactory condition in the dampest weather. Small leaks along the electrometer insulation and ionization in the connecting tube produced effects which average out when a complete series of readings as outlined above is taken. It can be shown that if the resistance of this insulation leak obeys Ohm's law, the average rate from −10 to +10 differs from the rate at 0 by less than 1 percent if the time from 0 to +10 does not exceed that from −10 to 0 by more than 20 percent. Under normal operating conditions the difference was much less than this, and any insulation leak was thus of negligible importance. Tests for such leaks were however a part of our regular routine.

Dielectric absorption showed itself by a faster rate of deflection just after reversing the potential of the sphere than after some minutes had elapsed. The effect could be reduced by careful drying of the air near the electrometer insulation. By using a "null method" of reading, for which each apparatus was wired, the effect of dielectric absorption could be completely eliminated. This method consisted in changing the voltage of the battery C continuously through 6 volts by means of a potentiometer, and thus inducing on the electrode a current which would just balance the ionization current, thus keeping the electrometer needle at zero. In this case the time was noted for which a change of 6 volts was required. This method was however used very little, since the direct deflection method was simpler, and no difference could be detected in the results of the two methods when suitable care was taken.

We have occasionally noted also that the readings taken immediately after changing the lead and copper shields have shown a slightly higher ionization than occurs after standing for 30 minutes or more. This may be due to a temporary active deposit falling on the outside of the electrically charged chamber when the shields are removed. This may have influenced some of the data taken at Summit Lake in Colorado. The effect is at most a few percent, and seems to be of short duration.

It will be especially noted that the value of the cosmic-ray intensity observed in the field does not depend at all upon the sensitivity of the electrometer nor the precision of our voltmeter, nor, within wide limits, upon the perfection of the insulation. We have relied rather upon the constancy of the radium sample as our only standard.

For measuring the barometric pressure, Paulin barometers and aneroids were chiefly used. Wherever possible, these instruments were compared with mercury barometers, and some boiling point tests were made. On the high mountain measurements, however, it is probable that our barometric errors are more serious than our errors in the cosmic-ray data.

Data

In Table III are recorded the data which have been reported before the end of 1932. All the measurements that have been made are included, except one in Australia, and several near Ceylon and Singapore, for which insulation troubles due to high humidity made the results highly erratic. The tabulated values of i_2/i_r and of i_1/i_2 are merely the averages of the observations, taken as described above, without any corrections. The horizon correction is calculated from Table II, and the values of I_γ are taken from Table I. For expedition 1, the laboratory standard capsule was used at a much shorter distance, thus accounting for the high value of I_γ. The values of C and L are then calculated from these data by using Eqs. (3) and (4). No corrections for radiation from the chamber walls have been applied in the tabulated values of C.

In Fig. 4 are plotted the values of the cosmic-ray intensity C as a function of the barometric pressure, including all the data given in Table III. The circles represent data obtained in the northern hemisphere, and the squares those from the southern hemisphere. The solid dots are values from geomagnetic latitudes[13] higher than 40 degrees, the open dots are between 25°S and 25°N, and the half shaded dots for intermediate latitudes.

In plotting these data, the values of C found by expeditions 1 and 4 have been adjusted so that they can be compared with those from the other expeditions. Expedition 1 used a somewhat larger ionization chamber, filled with air at 30 atmospheres instead of argon, and cylindrical instead of spherical shields. A reliable comparison of the data with the two sets of apparatus is however made possible by comparing the value of $C=6.10$ ions obtained from 240 hours readings at Summit Lake with apparatus number 1 in 1931 with the value of $C=5.70$ ions obtained from a series of readings of equal length at the same location with apparatus number 3. Thus all of the data obtained by expedition 1 have been multiplied by the factor $5.70/6.10=0.935$ to reduce them to the same basis as those obtained by the other expeditions. Expedition 4 used an ionization chamber with which a variety of auxiliary tests had been made over a period of four months. Just before its final filling with argon, it was noted that the residual ionization (radium re-

[13] By geomagnetic latitude we mean the latitude relative to the pole of the earth's uniform magnetization. The north geomagnetic pole, according to Bauer (Terrestrial Magnetism **28**, 1 (1923)), is at 78°32′N, 69°08′W. This is not identical with the north "magnetic pole" (90° dip), which Amundsen places at 71°N, 96°W (1903–6). The geomagnetic latitudes here used are calculated by the formula,

$$\sin\lambda=\sin\psi\cos\theta\cos\varphi+\cos\psi\sin\theta, \qquad (11)$$

where λ is the geomagnetic latitude, ψ is the colatitude of the north pole of uniform magnetization, θ is the geographic latitude of the point, and $\varphi+69°08'$ is the west longitude of the point.

The "magnetic latitude," as commonly used in papers on terrestrial magnetism, is commonly defined by the formula,

$$\tan\mu=\tfrac{1}{2}\tan\delta, \qquad (12)$$

where μ is the magnetic latitude and δ is the inclination or dip of the magnetic needle.

Thus the magnetic latitude is a function of the local magnetic field at the point, whereas the "geomagnetic latitude" depends upon the earth's resultant magnetic moment.

TABLE III. *Cosmic-ray intensities at various locations.*

Expt.	Expd.	Place	Lat.	Long.	Bar. (cm)	i_2/i_r	i_1/i_2	Hor. corr.	I_γ	C	L	C_{76}	C_{60}	C_{45}	Geo-mag. Lat.	Date
1	1	Mt. Evans	40N	106W	44.7	——	——	1.00	——	7.32	0.13†			6.69	49N	9/31
2	1	Summit Lake	40N	106W	47.4	0.0430	——	.995	137	6.10	.13†			6.71	49N	9/31
3	1	Denver	40N	105W	62.3	——	——	——	——	2.93	——		3.02		49N	9/31
4	1	Jungfraujoch	47N	6E	50.0	.0371	1.344	.944	137	5.45	.16			6.99	49N	10/31
5	2	Haleakala	21N	156W	54.7	.2264	1.504	.99	11.6	3.00	.42		2.42		21N	4/32
6	2	Idlewild	21N	156W	66.0	.1725	1.449	.99	11.6	2.12	.32		2.61		21N	4/32
7	2	Honolulu	21N	158W	76.4	.1304	1.230	1.00	11.6	1.63	.11	1.65			20N	4/32
8	2	SS Aorangi	4S	173W	75.3	.1391	1.500	1.00	11.6	1.65	.20†	1.64			7S	4/32
9	2	Ball Pass	44S	170E	60.2	.2120	1.249	.99	11.6	3.05	.10		3.08		50S	4/32
10	2	Ball Hut	44S	170E	66.3	.1757	1.281	.970	11.6	2.38	.16		3.01		50S	4/32
11	2	Dunedin	46S	170E	76.4	.1460	1.211	1.00	11.6	1.87	.11	1.88			51S	4/32
12	2	Wellington	41S	175E	75.8	.1464	1.235	.99	11.6	1.86	.14	1.86			44S	5/32
13	2	Sydney	34S	151E	76.6	.1614	1.480	1.00	11.6	1.86	.37	1.88			43S	5/32
14	2	Kosciusko	36S	148E	60.6	.2312	1.511	1.00	11.6	2.98	.50		3.06		45S	5/32
15	2	Brisbane*	28S	153E	76.8	.1444	1.510	1.00	11.6	1.61	.35	1.63			37S	5/32
16	2	Guyra*	30S	152E	64.8	.1893	1.232	1.00	11.6	2.60	.11	1.87			39S	5/32
17	2	Auckland	37S	175E	77.5	.1372	1.186	1.00	11.6	1.76	.08	1.81			42S	5/32
18	2	SS Mataroa	13S	106W	76.2	.1300	1.259	1.00	11.6	1.61	.13	1.61			5S	6/32
19	2	Panama	9N	80W	75.5	.1362	1.324	.995	11.6	1.66	.18	1.64			20N	6/32
20	2	Lima	12S	77W	75.0	.1356	1.313	1.00	11.6	1.65	.17	1.62			1S	6/32
21	2	Chosica	12S	77W	68.8	.1541	1.287	.978	11.6	1.99	.16	1.66			1S	7/32
22	2	Matucana	12S	77W	57.3	.1927	1.243	.924	11.6	2.93	.06		2.64		1S	7/32
23	2	Chicla	12S	77W	48.6	.2596	1.312	.932	11.6	4.32	.03			5.22	1S	7/32
24	2	Galera	12S	77W	42.8	.337	1.368	.976	11.6	6.03	0			5.24	1S	7/32
25	2	Huantapallacu	13S	74W	43.8	.3221	1.402	.995	11.6	5.41	.12			5.07	2S	7/32
26	2	El Misti	17S	71W	37.7	.4245	1.490	1.00	11.6	8.41	.125			5.10	6S	7/32
27	2	Monte Blanco	17S	71W	42.8	.3500	1.441	.980	11.6	6.15	.21			5.39	6S	7/32
28	2	Arequipa	17S	71W	57.6	.2061	1.300	.995	11.6	2.89	.14		2.63		6S	7/32
29	2	Mollendo	17S	72W	76.8	.1266	1.179	1.00	11.6	1.61	.07	1.63			6S	7/32
30	2	Vera Cruz	19N	96W	76.0	.1306	.998	1.00	11.6	1.68	.06†	1.68			29N	8/32
31	2	Orizaba	19N	97W	66.1	.1619	1.066	.995	11.6	2.19	.06†		2.77		29N	8/32
32	2	Mexico City	19N	99W	58.5	.2039	1.264	1.00	11.6	2.87	.10		2.69		29N	8/32
33	2	Nevado Toluco	19N	100W	46.5	.3204	1.386	.981	11.6	5.44	.13			5.95	29N	8/32
34	2	SS Ocean Eagle	67N	80W	75.3	.1400	1.150	.982	11.6	1.86	.06	1.84			78N	8/32
35	2	Churchill*	59N	94W	76.0	.1386	1.186	.99	11.6	1.80	.09	1.80			69N	9/32
36	2	Otsego Lake	45N	85W	73.2	.1469	1.184	1.00	11.6	1.91	.08	1.80			56N	9/32
37	2	Chicago	42N	88W	74.5	.1514	1.205	1.00	11.6	1.96	.10	1.88			53N	10/32
38	3	Fort Yukon	67N	145W	75.1	.1500	1.190	(1.00)	11.05	1.88	.09	1.84			71N	6/32
39	3	Kennecott	62N	143W	61.0	.2092	1.214	(1.00)	11.05	2.88	.06		3.01		66N	7/32
40	3	Berkeley	38N	122W	75.1	.1465	1.220	(1.00)	11.05	1.81	.11	1.78			46N	7/32
41	3	Tioga Pass	38N	119W	53.0	.2788	1.307	(1.00)	11.05	4.18	.13		3.04		46N	8/32
42	3	Pasadena	34N	118W	73.6	.1537	1.250	(1.00)	11.05	1.88	.14	1.79			42N	8/32
43	3	Denver	40N	105W	62.3	.2026	1.271	(1.00)	11.05	2.69	.14		2.96		49N	8/32
44	3	Summit Lake	40N	106W	48.1	.3466	1.372	(1.00)	11.05	5.70	.20			6.96	49N	9/32
45	4	Chicago	42N	88W	74.5	.1838	1.168	1.00	11.85	2.57	.09	1.80			53N	7/32
46	4	Advent Bay	78N	16E	75.5	.1844	1.152	.98	11.85	2.59	.09	1.86			75N	8/32
47	4	Zurich	47N	9E	71.7	.1930	1.184	.995	11.85	2.74	.10	1.82			49N	10/32
48	4	Eiger Gletcher*	47N	8E	57.4	.2460	1.236	.90	11.85	4.21	.07		3.14		49N	10/32
49	4	Wengen	47N	8E	65.5	.2208	1.195	.99	11.85	3.36	.07		3.20		49N	10/32
50	4	Jungfraujoch	47N	8E	50.1	.3246	1.260	.99	11.85	5.68	.06†			6.84	49N	10/32
51	5	Mt. McKinley*	63N	151W	50.0	.333	1.312	.98	11.95	6.00	.10			8.50	67N	5/32
52	6	Capetown	34S	18E	76.0	.1294	1.234	(1.00)	12.2	1.70	.12	1.70			32S	6/32
53	6	Lootsberg	32S	25E	62.2	.1875	1.292	(1.00)	12.2	2.65	.16		2.91		32S	7/32
54	6	Johannesburg	26S	28E	62.6	.1799	1.224	(1.00)	12.2	2.59	.09		2.88		27S	7/32
55	6	Vlakfontein	27S	30E	63.9	.1749	1.328	(1.00)	12.2	2.38	.20		2.75		28S	7/32
56	6	Pretoria	27S	28E	65.6	.1644	1.252	(1.00)	12.2	2.31	.12		2.81		28S	7/32
57	6	Lodewykslust	27S	31E	67.7	.1560	1.290	(1.00)	12.2	2.09	.16	1.69			28S	7/32
58	6	Nat. Park, Natal	29S	29E	64.9	.1674	1.270	(1.00)	12.2	2.31	.14		2.77		30S	7/32
59	6	Mt-aux-Sources	29S	29E	54.5	.2264	1.300	(1.00)	12.2	3.51	.05		2.80		30S	7/32
60	7	Lahore	31N	74E	74.3	.127	1.20	1.00	11.8	1.63	.08	1.59			21N	8/32
61	7	Lal Tibba	30N	78E	58.2	.184	1.27	.98	11.8	2.62	.09		2.44		20N	8/32
62	7	Rohtang La	32N	77E	47.7	.281	1.375	.98	11.8	4.51	.15			5.24	22N	8/32
63	7	Sarchu	33N	78E	46.1	.297	1.37	(1.00)	11.8	4.87	.12			5.21	23N	8/32
64	7	Lachalung La	33N	78E	42.8	.315	1.41	.96	11.8	5.32	.10			4.65	23N	8/32
65	7	Bara Lacha La	33N	77E	42.5	.343	1.42	.99	11.8	6.09	.13			5.21	23N	8/32
66	7	Telekonka*	33N	78E	41.2	.384	1.43	(1.00)	11.8	7.24	.10			5.60	23N	8/32
67	7	Lanyar La	30N	78E	37.7	.421	1.48	.99	11.8	8.58	.07			5.25	20N	8/32
68	8	Lima	12S	77W	74.6	.1306	1.255	1.00	11.6	1.61	.13	1.58			1S	12/32
69	3	Cambridge	42N	71W	76.8	.184	1.140	1.00	11.85	2.55	.12	1.87			53N	12/32

* Values at these stations have low statistical weight, because of either low reproducibility of the data or a small number of readings.

† These values of L are estimated, because of insufficient data for their reliable calculation.

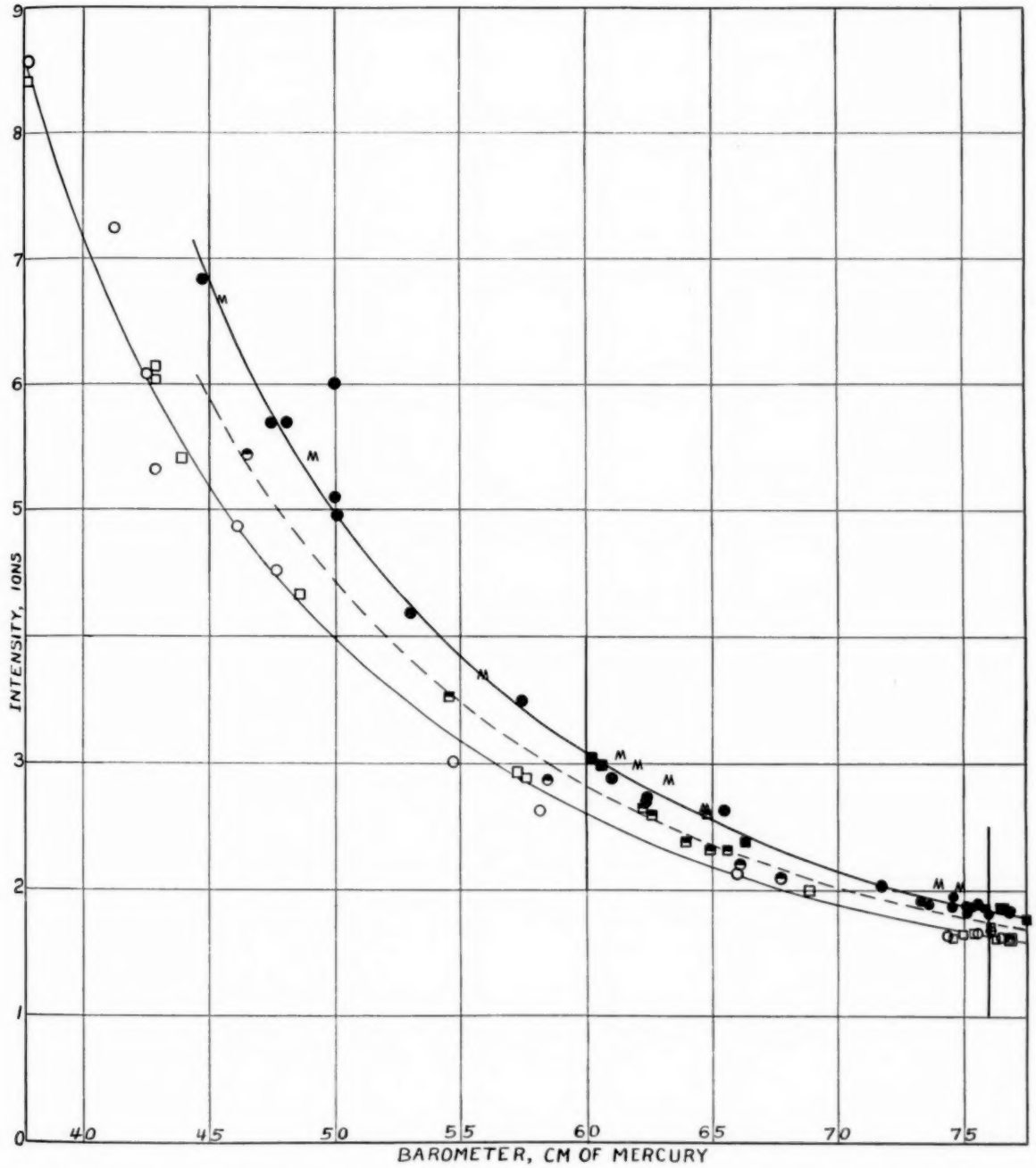

FIG. 4. Cosmic-ray intensity at different elevations. Squares, southern hemisphere. Circles, northern hemisphere. Solid dots, 90° to 40°. Shaded dots, 40° to 25°. Open dots, 0° to 25°.

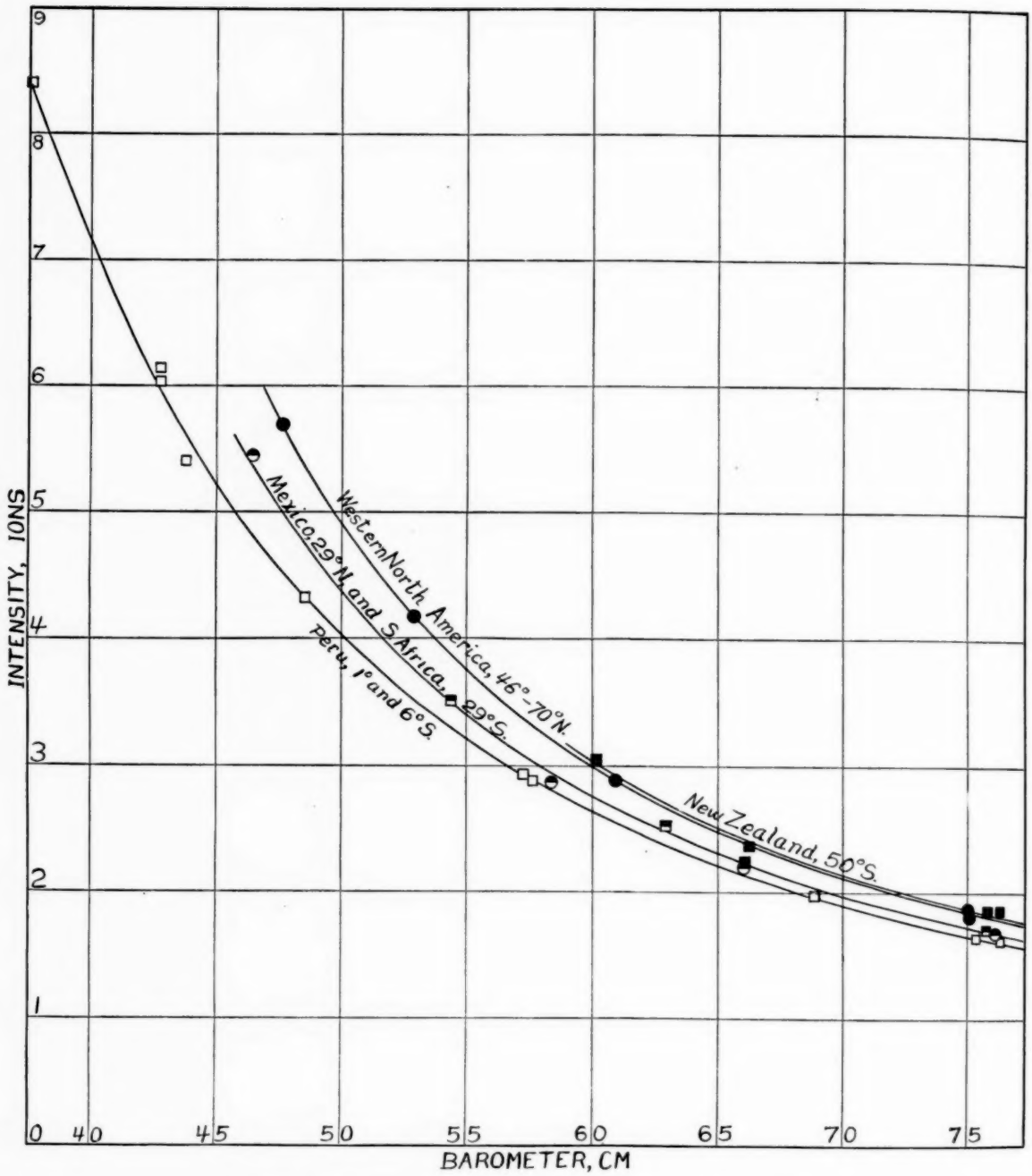

FIG. 5. Typical intensity *vs.* altitude curves for various latitudes.

moved and shields in place) was greater with air at 1 atmosphere than with air at 100 atmospheres. This could only mean an alpha-ray contamination, whose ionization is reduced by pressure. The magnitude of this ionization from the walls has been estimated by comparing the mean value of $C_{76}=2.55$ ions from experiments 45, 46 and 69 (Chicago, Spitzbergen and Cambridge) with the mean value of $C_{76}=1.84$ ions obtained for similar latitudes by expeditions 2 and 3. Thus, by subtracting 0.71 ion from the data obtained with apparatus 4, its results become comparable with those from the other sets of equipment.[14]

On the same figure are plotted the data of Millikan and Cameron,[15] indicated by the symbol *M*. The agreement between their values and ours is satisfactory, in view of the differences in the type of apparatus employed.

In Fig. 4 all of the data are included, without choice on the basis of statistical weight. The fact that all of the solid dots lie higher than the open ones over the whole range of barometric pressures is definite evidence that the cosmic rays are more intense at high latitudes than near the equator. This difference is shown more clearly in Fig. 5, which shows the results of six series of intensity *vs.* altitude measurements, made under favorable conditions, at six different latitudes. Those in New Zealand, Mexico and Peru were taken with apparatus number 2, Western North America with number 3, and South Africa with number 6. The excellent agreement between the New Zealand and the North American data, and between the South African and Mexican data indicates the reliability of our method of measurement. This figure shows also how the difference in intensity between the tropic and polar zones becomes much more prominent at the higher elevations.

Variation of Cosmic-Ray Intensity with Latitude

In order to make a precise comparison of the data for different latitudes, the data plotted in Fig. 4 have been reduced to three standard barometric pressures, by using the smooth curves drawn in this figure as guides in effecting the reduction. All data for pressures over 67.5 cm have been reduced to 76 cm; those between 52.5 cm and 67.5 cm to 60 cm; and those between 37.5 cm and 52.5 cm to 45 cm. The values as thus standardized are given in Table III in columns C_{76}, C_{60} and C_{45}, and are plotted in Fig. 6 as functions of the geomagnetic latitude. In making this graph, the values in brackets in columns C_{76}, C_{60} and C_{45} have been averaged and plotted as a single point, in order to avoid unnecessary complexity. The numbers within the datum points indicate the apparatus with which the different values were obtained.

All the data agree in showing a marked difference between the intensities found within 20 degrees of the magnetic equator as compared with those at a higher latitude than 50° north or south. The increase in going to the higher latitudes averages 14 percent at sea level, 22 percent at 2000 meters (barometer 60 cm), and 33 percent at 4360 meters (barometer 45 cm).

In order to show the sea level values more clearly, they have been plotted in Fig. 7 on a larger scale. There have been added to this figure the data of Millikan,[16] taken at Pasadena and Churchill; and the recent ones of Clay and Berlage,[17] obtained with a set of Steinke recording equipment, compared with a standard at Amsterdam and carried on a ship from Genoa to Singapore. The values in Table IV, read from Clay and Berlage's curve, have been used in

[14] It is probable that there may be wall corrections of a similar type that should be applied to the other sets of apparatus. If so, however, the corrections are certainly much smaller than those for chamber number 4. Lacking exact information regarding the magnitude of these corrections, we have preferred to make none at all for the other sets of equipment. This procedure is partially justified by the small magnitude of the correction as found for the three sets of equipment that have been tested, and by the consistency of the data as here shown. It is probable that an even better agreement will, however, appear when it becomes possible to determine this zero correction by direct experiment. It will be about a year before such tests can be completed. Of course any possible zero correction cannot affect the differences observed at different latitudes and altitudes when using the same set of apparatus.

[15] R. A. Millikan and G. H. Cameron, Phys. Rev. **37**, 235 (1931). The ionization values given in their Table III are divided by the factor 13.80 given by Millikan (Phys. Rev. **39**, 397 (1932)) to reduce their measurements at 30 atmospheres air pressure to 1 atmosphere.

[16] R. A. Millikan, Phys. Rev. **36**, 1595 (1930).

[17] J. Clay and H. P. Berlage, Naturwiss. **37**, 687 (1932).

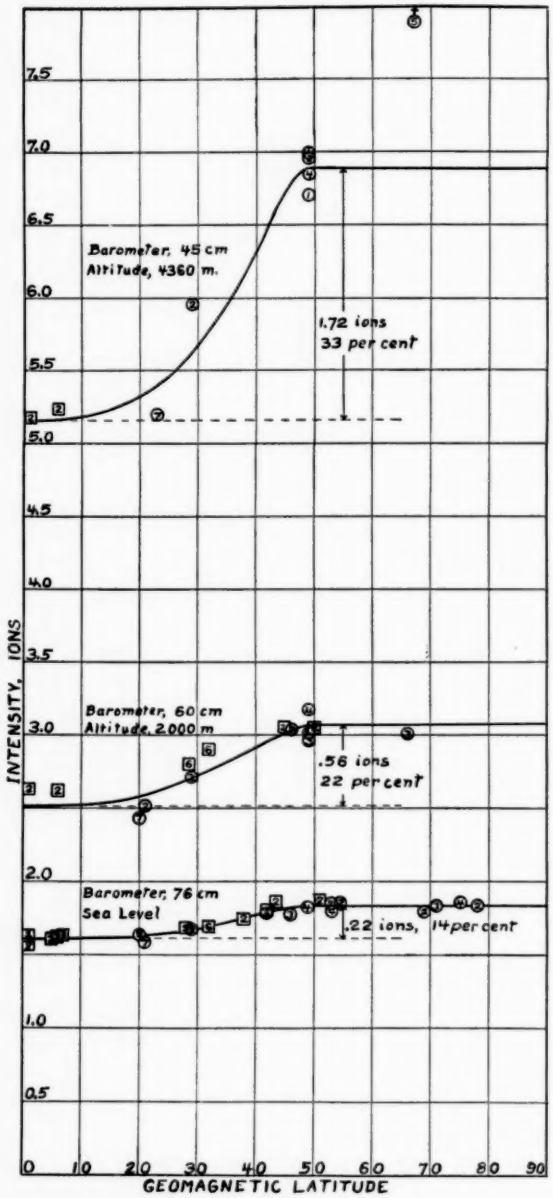

FIG. 6. Intensity *vs.* geomagnetic latitude for different elevations.

Fig. 5. These values have been plotted as crosses without any adjustment of the constants. Millikan's values are given for an ionization chamber pressure of 30 atmospheres; which, as he notes in a later paper,[18] multiplies the ionization by 13.80. With this reduction factor, his value at Pasadena is 2.050 ions for barometer 74.0 cm, and at Churchill is 2.020 ions for barometer 74.8 cm. Reduced to sea level according to the curves of Fig. 4, these intensities become 1.970 and 1.974 respectively. These values have been compared with ours by multiplying by the factor 1.79/1.97, which makes his value at Pasadena and ours at the same place identical. This gives for Millikan's value at Churchill (on our scale) 1.793 ions, plotted as a plus sign, which is to be compared with our value at Churchill of 1.80 ions. Our data are thus in good accord with those of the other observers who have made measurements in the same regions.

It is significant that most of the datum points recorded in Fig. 7 were taken with the same set of apparatus (expedition 2). It was carried from geomagnetic latitude $\lambda = 53$ N to 51 S. After crossing the equator four times at different longitudes it was brought back to 78 N, and then sent once more across the equator with expedition 8.

The 15 experimental points plotted in Fig. 7 for this instrument were all taken under essentially the same conditions, so that we cannot find any source of systematic error that might affect the results. The readings with instruments 3 and 4 confirm the absence of appreciable variation north of $\lambda = 42°$, and comparison with the data from instruments 6 and 7 confirms both the magnitude of the variation observed by instrument 2 and the latitude at which it occurs.

TABLE IV. *Cosmic-ray intensities from Clay and Berlage's curve.*

Place	Lat.	Long.	C	Geomag. Lat.
Amsterdam	52 N	5 E	1.87	54 N
Genoa	44 N	9 E	1.79	44 N
At sea	37 N	19 E	1.72	35 N
Suez	30 N	32 E	1.66	27 N
Guardafui	12 N	51 E	1.61	6 N
Colombo	7 N	80 E	1.59	4 S
Singapore	1 N	104 E	1.58	11 S

The average of our 8 datum points taken for geomagnetic latitudes less than 22 degrees is 1.620 ± 0.006 ions. For our 9 datum points at latitudes higher than 48°, the average is 1.839 ± 0.006 ions. The difference between the two latitude ranges is thus 0.219 ± 0.0085 ion; that is, more than 25 times the probable error. This probable error is also approximately that estimated also on the basis of statistical fluctuations in the readings taken under uniform conditions.

[18] R. A. Millikan, Phys. Rev. **39**, 397 (1932).

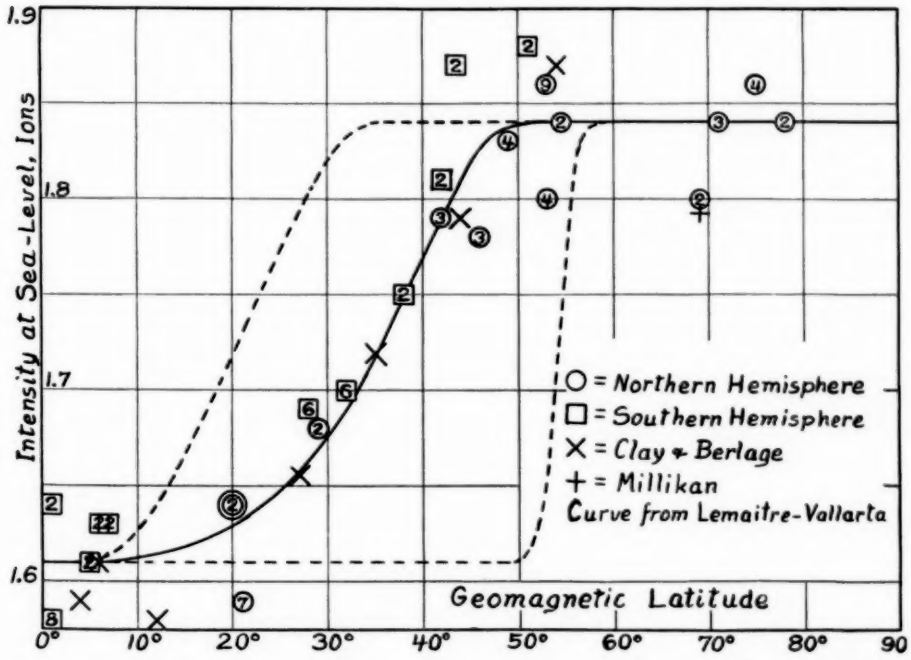

FIG. 7. Intensity *vs.* geomagnetic latitude at sea level, including data of Clay and Millikan.

There is thus no indication of any serious systematic error. From a statistical standpoint, therefore, the probability of the existence of this latitude effect amounts practically to a certainty.

COMPARISON WITH LEMAITRE-VALLARTA THEORY

The sharpness of the increase in intensity between geomagnetic latitudes 25° and 45° is a major feature of these data. This shape of curve is just what may be expected from the new theory of Lemaitre and Vallarta,[19] which considers the effect of the earth's magnetic field on the motion of electrons approaching the earth from remote space. To show that this is true, the smooth curves drawn in Figs. 6 and 7 have been calculated from the Lemaitre-Vallarta theory (by graphical interpolation in their family of $F(x)$ *vs.* latitude curves). The arbitrary constants used for Fig. 7 are: 1.605 ions due to rays unaffected by the earth's magnetic field (neutral rays, or electrons of energy over 4×10^{10} electron-volts), and a band of electrons approaching the earth with energies between 0.5×10^{10} and 1.3×10^{10} electron-volts, which reach the earth at latitudes higher than 50°, producing 0.235 ion, but which fail to reach the earth at the geomagnetic equator.[20] The excellent agreement between this curve and the experimental data means that the variation of cosmic-ray intensity with latitude is that to be expected if a considerable portion of the ionization at high latitudes is due to electrons coming from remote space with energies of about 7×10^9 electron-volts.

At the higher altitudes, as shown in Fig. 6, the latitude effect is so large as to be unquestionable, even without statistical analysis. Within experimental error, the zone over which the cosmic-ray intensity varies with latitude is the same as that found at sea level. There is one datum, of 8.5 ions at geomagnetic latitude 67 degrees, which perhaps indicates a continued increase in intensity at the higher latitudes at high elevations. This datum, however, is starred in Table III, because it represents a single unchecked result obtained by the ill-fated Carpe expedition[21] on Mt. McKinley. Bennett and his

[19] G. Lemaitre and M. S. Vallarta, Phys. Rev. **42**, 914 (1932).

[20] In calculating the ionization due to this band of rays, 4 equally ionizing groups were assumed, having respectively the following values of Lemaitre and Vallarta's x: 0.30, 0.35, 0.40 and 0.45.

[21] Both observers, Allen Carpe and Theodore Koven, were killed by falling into a crevasse in the Muldrow

coworkers (data here recorded under expedition 3) have concluded from their Alaskan measurements at 1840 meters that the shape of the intensity-altitude curve is the same for geomagnetic latitude 66°N as at 48°N.[22] This is further supported, to much higher altitudes, by Millikan's recently reported[23] airplane measurements at 64°N, which showed the same increase with altitude as did experiments at 55°N. We thus seem justified in neglecting Carpe's datum, and in assuming that, as at lower altitudes, the intensity-latitude curve is flat north of 50°. This means, according to the Lemaitre-Vallarta theory, that there is no marked difference in the energy distribution of the particles responsible for the latitude effect as observed at different altitudes up to 4360 meters.

On the other hand, it will be seen from Fig. 6, that the extra component of cosmic rays which appears at the higher latitudes is more rapidly absorbed than is the main body of the rays. This would be anticipated if the portion of the rays that is unaffected by the earth's magnetic field consists of electrons of greater energy. Other interpretations are however possible. Thus, the uniform background may be due to some electrically neutral ray, such as photons, neutrons, or high speed neutral atoms.

Electrified Particles Bombarding the Earth from Remote Space

We have shown that the variation in intensity with latitude, which our experiments have brought to light, can be accounted for satisfactorily on Lemaitre and Vallarta's theory, which assumes that the rays consist of electrons of high energy coming from remote space, but are deflected by the earth's magnetic field. May there not, however, be alternative explanations?

A guide to possible interpretations is given by plotting the cosmic-ray intensity against the different variables of which it may be supposed to be a function. In Fig. 8 the same data as those used in Fig. 5 are plotted against the geographic latitude. Though there is clearly some correlation, in the intermediate latitudes, such as 30°, the scattering is definitely greater than is to be expected from the probable error of the experiments. Thus, the intensity is probably not a direct function of the geographic latitude.

In Fig. 9 the data are plotted against the local "magnetic latitude."[13] Though the correlation in this case is somewhat better than with the geographic latitude, the scattering in the neighborhood of 40°, where the change is most rapid, is again larger than would be expected from the probable error. This result indicates that the latitude variation is not due to the local magnetic field, which presumably would be effective for several hundred kilometers above the ground. It is thus difficult to attribute the latitude variation to any magnetic effect on the rays which occurs primarily within the earth's atmosphere.

The absence of any systematic variation of the atmospheric electric gradient with the latitude makes it hopeless to attempt to correlate the present effect with the electric field of the earth's atmosphere. Also, there is no systematic difference detectable between the data obtained at sea, such as experiments 5, 6, 7, 8, 18, 34, 46; and those taken at corresponding geomagnetic latitudes in mid-continental stations, such as 25, 28, 32 and 60 at the lower latitudes and 14, 37, 39 and 47 at the higher latitudes. This uniformity of the rays with respect to oceanic and continental areas makes it difficult to ascribe the latitude variation to any kind of atmospheric phenomenon.

It can be shown further that this latitude effect cannot be due to any bending of the cosmic-ray particles within the earth's atmosphere. For an electron moving with a speed nearly equal to that of light, the radius of curvature of the path when crossing a magnetic field of strength H is approximately,

$$R = mc^2/eH. \tag{13}$$

With 0.3 gauss as the value of H at the equator, where the magnetic effect is a maximum, this

---

Glacier, on which the observation tent was pitched. Some parts of the apparatus, and their notebook, were later recovered, but their Paulin barometer remains on the mountain. Though the cosmic-ray data appear reliable, the unchecked barometer might be in error by enough to bring this point in line with the others.

[22] R. D. Bennett, J. L. Dunham, E. H. Bramhall, P. K. Allen, Phys. Rev. **42**, 447 (1932).

[23] R. A. Millikan as quoted in New York Times, Dec. 31, 1932.

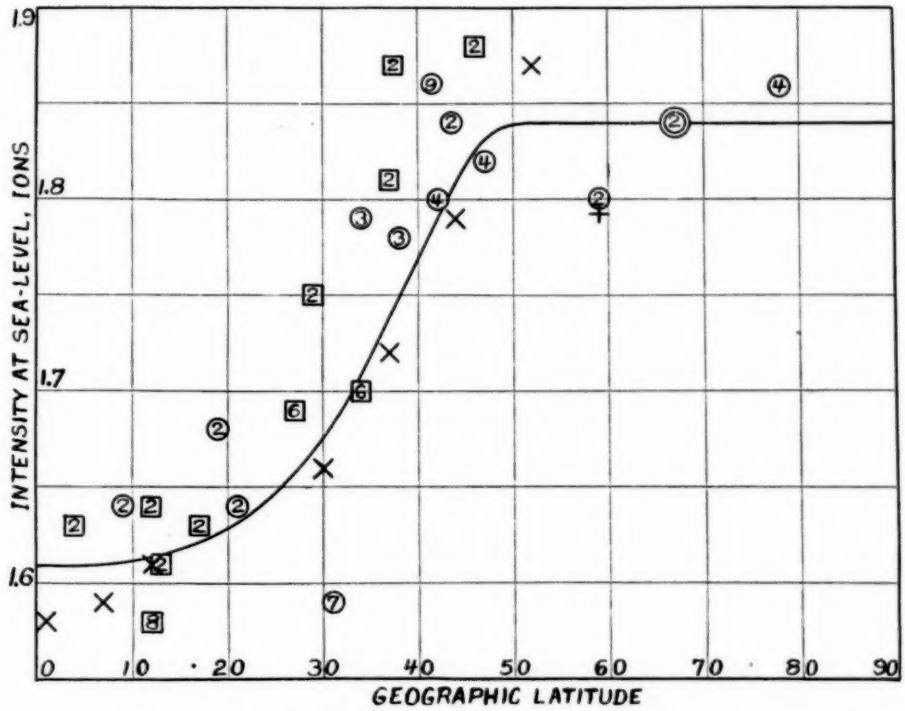

FIG. 8. Intensity *vs.* geographic latitude.

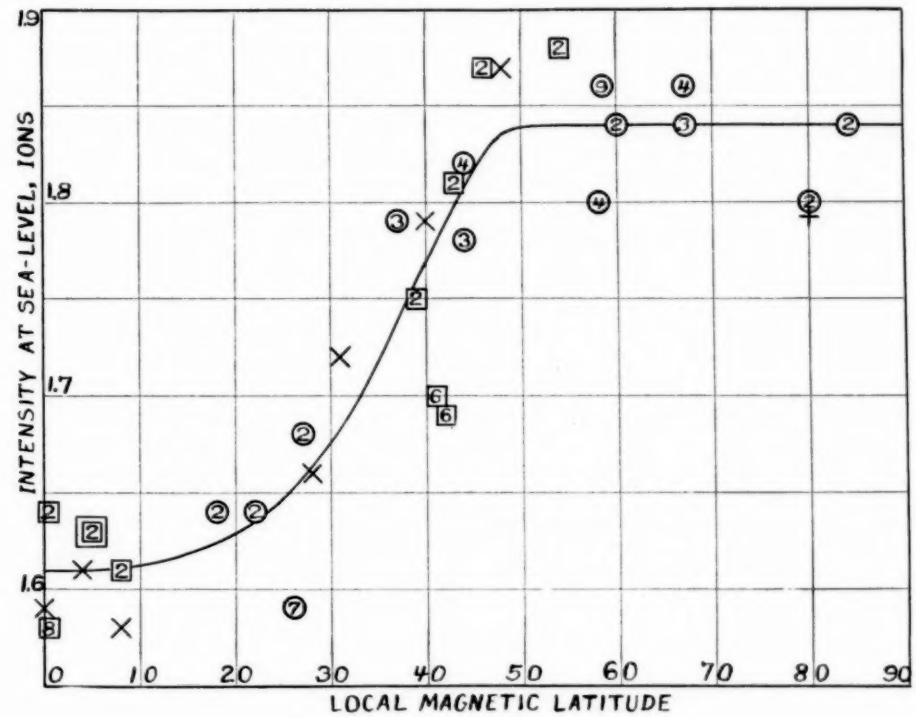

FIG. 9. Intensity *vs.* local magnetic latitude.

becomes,

$$R=6\times10^{30}m \text{ cm}, \qquad (14)$$

where m is the mass of the moving particle expressed in grams. The range of beta-particles has been discussed at length by Rutherford, Chadwick and Ellis,[24] chiefly on the basis of Bohr's theory of beta-ray absorption. From their formulas (10), p. 438; and (7), p. 442, the range of a beta-particle in air at atmospheric pressure can be written approximately as:

$$r=0.2\times10^{30}m \text{ cm}, \qquad (15)$$

if the mass m of the electron in motion is much larger than the rest mass. That is, the radius of curvature in the earth's magnetic field is at atmospheric pressure, $6/0.2=30$ times the particle's range. Thus, at atmospheric pressure the curvature produced in the path of an electron by the earth's magnetic field is negligible. At an altitude of 25 kilometers, where the density of the earth's atmosphere is about 1/30 of that at sea-level, the range of an electron should be about equal to its radius of curvature, and above this altitude the earth's magnetic field should have an appreciable effect on the particle's range. This means that, if the cosmic rays which are affected by the earth's magnetic field are electrons, they must originate at an altitude of more than 25 km. For other electrified particles, protons, alpha-particles, etc., the limiting altitude as thus calculated is still higher.

Supposing that it is such electrons, originating high in the earth's atmosphere, which are detected by our ionization chambers at the earth's surface; how much energy is necessary to penetrate the atmosphere? If in Eq. (15) we place the range $r=8.0\times10^5$ cm, which is the equivalent of 1 atmosphere if the air were of uniform density equal to that under standard conditions, we obtain $m=4\times10^{-24}$g. Multiplying by the conversion factor, $300c^2/e$, this means an energy of 2.3×10^9 electron-volts.[25] This would be the minimum possible energy for an electron passing vertically through the atmosphere without deflection. For such an electron, however, according to Eq. (14), the radius of curvature is 240 kilometers. This means that, if a beta-particle capable of penetrating the earth's atmosphere is appreciably affected by the earth's magnetic field, it must originate not less than some hundreds of kilometers above the earth's surface. This conclusion supports the comparison of Figs. 7 and 9, which indicated that it is the average rather than the local magnetic field of the earth which is responsible for the latitude variation.

It would seem that an effect due to a magnetic field necessarily implies that the rays thus affected are moving charged particles. If so, our data mean that a portion at least of the cosmic rays consists of high speed particles. But we have seen also that these particles must originate high above the earth. It is accordingly not permissible to assume that these cosmic electrons are secondary beta-rays produced within the earth's atmosphere by some form of electrically neutral rays such as photons. Our experiments seem to require rather that the portion of the cosmic rays which varies with the geomagnetic latitude shall consist of electrified particles approaching the earth from distances of not less than some hundreds of kilometers.

The quantitative agreement of the curve taken from Lemaitre and Vallarta's theory, with the data plotted in Fig. 7, strongly supports this conclusion. Though in fitting this curve to the data several arbitrary constants were available, it is by no means true that any arbitrary set of data could thus be fitted. If the cosmic-ray intensities at the equator and the poles are to be respectively 1.61 and 1.84 ions, the Lemaitre-Vallarta theory requires that the intensities at intermediate latitudes shall lie between the two broken curves of this figure. Of these, that for the higher latitude represents the minimum energy (2.3×10^9 electron-volts) that an electron can have which will penetrate the earth's atmosphere,

[24] E. Rutherford, J. Chadwick, C. D. Ellis, *Radiations from Radioactive Substances* pp. 434-444, 1930.

[25] Neglecting a small correction due to the different ratio of (atomic weight)/(atomic number), this corresponds to an energy loss of 2.5×10^7 electron-volts per cm of lead traversed by a β-particle. This is in substantial accord with the loss of 3.5×10^7 electron-volts per cm of lead as reported recently by C. D. Anderson (Bulletin Am. Phys. Soc. **7**, No. 7, p. 15, Dec. 7, 1932). With Anderson's value, the energy lost by an electron traversing the atmosphere would be slightly greater than that here estimated.

superposed on a background of radiation that is unaffected by the earth's field. The curve for the lower latitude represents the maximum energy the electrons can have (3.2×10^{10} electron-volts) if the difference in intensity between the equator and the poles is to be of the specified amount. It would be a surprising coincidence that the experimental curve should fall within the rather narrow limits defined by this theory if the latitude variation has some other origin.

The experimental data thus give very strong support to Lemaitre and Vallarta's theory of the variation of cosmic-ray intensity with latitude. This means that this variation seems to be due to the presence in the cosmic rays of charged particles coming into the earth's atmosphere from remote space with an energy, if they are electrons, of about 7×10^{9} electron-volts.

ACKNOWLEDGMENTS

In addition to the leaders of the various expeditions mentioned above, the help of the following persons should be specially mentioned: Dr. Marcel Schein, of the University of Zurich, who helped in organizing the two Alpine expeditions; Dr. J. J. Hopfield, Dr. E. O. Wollan and Dr. V. J. Andrew, who have helped with the design, construction and testing of the apparatus at Chicago; Professor Harry Kirkpatrick of the University of Hawaii, who organized the Hawaiian expedition; Professor P. W. Burbidge of Anckland University College, who made the plans for New Zealand and gave valuable help with the measurements; Professor O. U. Vonwiller of the University of Sydney, who planned the Australian program; Dr. Robert Enders, who arranged for the experiments in Panama; Mr. P. G. Ledig and Dr. J. E. I. Cairns of the Huancayo Magnetic Observatory of the Carnegie Institution, without whose help the Peruvian measurements could hardly have been completed; Professor M. S. Vallarta of Massachusetts Institute of Technology, who looked after all arrangements in Mexico; Mr. George Kydd, engineer in charge of construction at Churchill, who made possible the trip to Foxe Channel; Dr. J. L. Dunham, Dr. E. H. Bramhall and Dr. P. K. Allen, who worked with expedition 3 for several months; Mr. Theodore Koven, who with Mr. Allen Carpe gave his life in the effort to secure data on Mt. McKinley; Professor B. F. J. Schonland, of the University of Capetown, who has helped with the experiments in South Africa; Professors Ross Wilson of Lahore and Sharma of Allahabad, who have helped with the Himalayan measurements, and Dr. J. A. Fleming of the Carnegie Institution of Washington, who has supplied valuable information. There have been in addition more than thirty other physicists who have given generously of their time in performing these experiments.

A grant from the Carnegie Foundation made possible a survey on a world-wide scale. Among the other institutions which have contributed support in money or equipment are: the University of Chicago, Massachusetts Institute of Technology, the Rumford Fund, the University of Denver, the University of Hawaii, Auckland University College, the government of New South Wales and the Radium Service Corporation of America. Most of the members of the various expeditions have also borne a large share, or all, of their own expenses while engaged in these experiments. Without such remarkable cooperation, the progress of this survey would have been greatly delayed.

A Determination of e/m for an Electron by a New Deflection Method

FRANK G. DUNNINGTON,* *University of California*

(Received December 27, 1932)

To fill the need of a new deflection determination and to provide a more accurate value, a new measurement of e/m is being made. The method used was conceived by Professor E. O. Lawrence. The essential points of the method are: acceleration of electrons to a continuous range of velocities by a radiofrequency electrostatic field, choice of a particular velocity by magnetic field resolution, measurement of this velocity through radiofrequency fields applied to a pair of accelerating slits and a pair of decelerating slits. A most important advantage of this method is that no acceleration voltage need be measured. This, combined with other properties of the method, practically eliminates errors due to contact potentials. Another advantage is the very high observational precision the method makes possible. The present results, although not considered final, are of an accuracy comparable with published values. The value obtained from two groups of observations made at different electron velocities (the corresponding electron voltages being about 1420 and 844 volts) is

$$e/m_0 = (1.7571 \pm 0.0015) \times 10^7 \text{ e.m.u.}$$

The uncertainty stated is a conservatively calculated probable error. A comparison of six recent and probably most reliable e/m determinations is made. The spectroscopic and free electron averages are now in good agreement. The weighted average of these six determinations is

$$e/m_0 = (1.7598 \pm 0.0005) \times 10^7 \text{ e.m.u.}$$

INTRODUCTION

INTEREST in the correct value of the specific charge of an electron has been considerably increased in the past year through the work of Bond[1] and Birge.[2] Bond in the articles referred to presents a new method for the evaluation of e and h which uses all of the existing data from experiments designed to measure h. The method is of considerable importance because it offers a more reliable method of evaluating e than has been attained by direct determination and of even greater importance it provides a means of obtaining an accurate set of values of the basic physical constants which are *self-consistent*. Birge has corrected and improved the work of Bond, giving solutions based on the more recent and reliable data. In the conclusion of his article Birge states (p. 260) that "The most probable values of e, h, and $1/\alpha$ depend primarily on the value adopted for e/m." Thus it is doubly important to obtain an accurate value of e/m, not only in order that the uncertainty as regards the discrepancy[3] of the deflection and spectroscopic values may be definitely settled, but also for the increased accuracy that will be possible in the values of e, h and α.

As is well known, the various determinations of e/m do not agree, the differences amounting in some instances to many times the stated probable error. The situation at the present time as regards the value of e/m may be briefly put as follows. The most probable value based on all of the work previous to 1929 was given by Birge[3] as

Deflection, $e/m_0 = (1.769 \pm 0.002) \times 10^7$ e.m.u.,

Spectroscopic, $e/m_0 = (1.761 \pm 0.001) \times 10^7$ e.m.u.,

two values being given because the two types of experiments gave results differing much more than their probable errors. Since 1929 no deflection measurements have been published. Two free electron measurements, however, have been made, one by Perry and Chaffee[4] in 1930 and one by Kirchner[5] in 1931–32. Essentially the same method was used by both: electrons were

* National Research Fellow.

[1] W. N. Bond, Phil. Mag. **10**, 994 (1930) and **12**, 632 (1931).

[2] R. T. Birge, Phys. Rev. **40**, 228 (1932).

[3] R. T. Birge, Phys. Rev. Sup. **1**, 1 (1929).

[4] C. T. Perry and E. L. Chaffee, Phys. Rev. **36**, 904 (1930).

[5] F. Kirchner, Ann. d. Physik [5] **8**, 975 (1931) and [5] **12**, 503 (1932).

allowed to fall through a known potential difference and their velocity then determined by the time required to travel between two points having a known separation. The third determination of e/m made since 1929 was that by Campbell and Houston[6] in 1931. This was a spectroscopic measurement based on the Zeeman patterns of certain cadmium and zinc lines. The values obtained in these three measurements are of interest:

Free electrons:	Perry and Chaffee:	$e/m_0=(1.761\pm0.001)\times10^7$ e.m.u.,
	Kirchner:	$e/m_0=(1.7585\pm0.0012)\times10^7$ e.m.u.,
		$(1.7590\pm0.0015)\times10^7$ e.m.u.,
Bound electrons: (Spectroscopic)	Campbell and Houston:	$e/m_0=(1.7579\pm0.0025)\times10^7$ e.m.u.

Thus for the first time measurements on free electrons have given "low" values in agreement with the 1929 spectroscopic value, Kirchner's value even falling so low as to be more than twice the probable error lower. Campbell and Houston's spectroscopic value is even lower but in this measurement the uncertainty is twice as large. Recent evidence thus strongly indicates a low value. On the other hand, there still remains the fact that no deflection method has given a low value. The most recent deflection determination carefully performed by Wolf[7] in 1927 gave $e/m_0=(1.7689\pm0.0018)\times10^7$ e.m.u. Thus it is still most desirable to obtain a very accurate deflection value of e/m.

The present determination is being made in view of the above need. A new deflection method conceived by Professor E. O. Lawrence and most kindly offered to the author has been used because it seemed capable of giving a higher precision. The method has been found successful, and the results have reached a degree of precision comparable with the other recent determinations, hence they are being published at this stage. This report, however, is not to be considered final, as it is hoped to carry the measurements to a still higher precision.

Method and Apparatus

(A) Method and e/m measuring tube

The new method used for the determination of the value of e/m is a deflection method in which the electrons after being given an initial velocity are deflected in a circular path by a magnetic field. The most important difference between this method and others is that the energy of the electrons need not be known, that is, *the electron accelerating voltage is not measured.* This feature is of major importance because it very largely eliminates the errors and uncertainties due to contact potentials. A second feature of the method is that the determination of the electron velocity is accomplished through the measurement of the frequency of a radiofrequency oscillator. This is done by adjusting the electron velocity (more properly, the speed) so that the time to travel a given length of arc is exactly equal to one period of the oscillator. In this respect the method may suggest that used by Perry and Chaffee[4] and Kirchner[5] but the manner of use of the radiofrequency fields is quite different as will be seen presently. For the determination of e/m by this method three quantities must be measured: the frequency of the oscillator ν, the angle θ subtended by the circumferential path used in timing the electrons and the deflecting magnetic field H_0.

e/m measuring tube. The general scheme of the measuring tube is shown schematically to approximate scale in Fig. 1 and the more important parts in greater detail in a cross-sectional view in Fig. 2. A heavy brass box B about 31 cm square and 12 cm deep is evacuated through a vacuum line at V. The box contains a series of adjustable slits A_1, A_2, S_1, S_2, D_1, D_2, which are arranged on the circumference of a circle of radius r. The filament cylinder FC (see

[6] J. S. Campbell and W. V. Houston, Phys. Rev. **39**, 601 (1932).

[7] F. Wolf, Ann. d Physik **83**, 849 (1927).

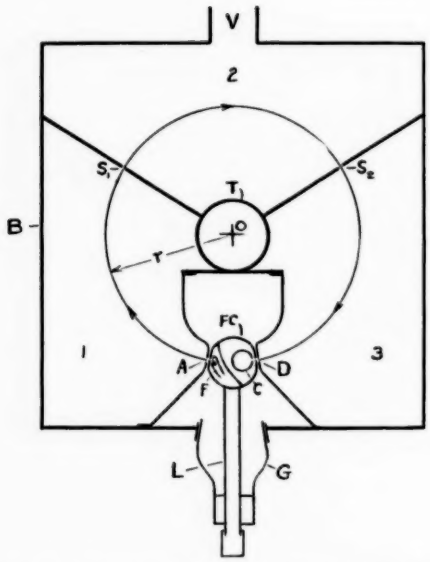

FIG. 1. Schematic diagram of measuring tube.

especially Fig. 2), made of a 3 cm length of 4.1 cm diameter brass tubing, is divided into two parts by the partition P (all parts are of brass unless otherwise stated). The ends of the left half of this tube are closed, thus making an enclosed semi-cylinderical box in which is placed the filament F, the source of the electrons. Two faces are machined on the outside of the cylinder to hold the adjustable slits A_1 and D_2. The cylinder is mounted at right angles on the long lead-in tubing L, which is supported from the box by the glass insulator G. Inside the tubing and in line with D_2 is another slit D_3 which is

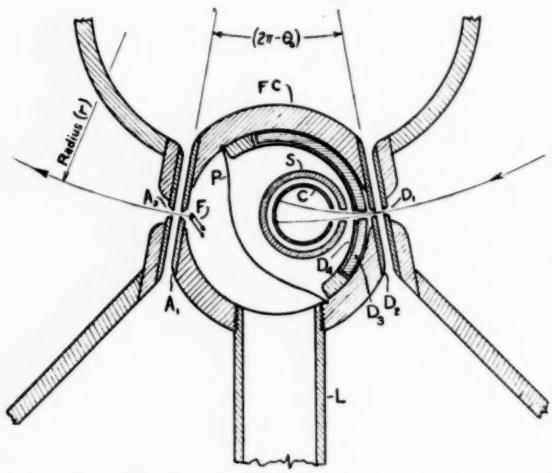

FIG. 2. Cross section of tube in vicinity of filament and collector.

completely enclosed by a shield extending from the tubing and having a slit D_4 in it. D_3 is insulated with mica. The purpose of enclosing the slit D_3 and the filament F is simply to shield them from radiofrequency fields. Coming up from the bottom of the box B and extending into the right half of the filament cylinder but not touching it is a shield S which encloses the collector C, the latter being connected to an electrometer.

The output of a radiofrequency oscillator is connected to the lead L and to the box B, the latter being grounded. Thus radiofrequency fields exist between the pairs of slits A_1-A_2, D_1-D_2, and D_4-S. The regions of the box made up of compartments (1), (2) and (3) are field free. Suitable baffles between compartments allow free circulation for evacuation. In order that the controls of the circuits associated with the filament and with the slit D_3 shall be at ground potential, their leads are brought out *through* the lead-in L and the coil I (made of tubing). Since the end of the coil connected to the box is at ground potential, the filament and D_3 leads can be brought out at this point. However, all circuits associated with the measuring tube were completely shielded with copper to protect against radiofrequency fields.

The magnetic field is produced by two large coils forming a Helmholtz system. The coils are symmetrically placed above and below the box on an axis through O. The magnetic field is thus perpendicular to the section of the tube as shown in Fig. 1 and is uniform around the circumference of any circle about O.

Simplified description of action in tube. A somewhat simplified description of the action will be given first. Electrons from the filament are accelerated across the slits A_1, A_2, during the half of each cycle of the impressed voltage in which the box is positive. There are therefore electrons passing through A_2 with velocities corresponding to all voltages from zero to the peak voltage of the oscillator. These electrons will be bent in circles of various radii by the magnetic field. For any magnetic field H (within a limit determined by the peak voltage of the oscillator) there will be electrons having a related voltage V that will be bent in a circle of radius r and that therefore will pass through the defining

slits S_1 S_2 and arrive at D_1. In passing from D_1 to D_2 these electrons will experience an acceleration or deceleration depending on their time of arrival relative to the voltage cycle. With the frequency remaining constant the experimental procedure is to find the value of the field H_0 so that the time required for the electrons to travel from the slits A_1 A_2 to D_1 D_2 is equal to one period of the radiofrequency oscillator. When this is the case the electrons in passing from D_1 to D_2 experience a deceleration equal to the acceleration gained in passing from A_1 to A_2 and hence do not reach the collector C. Reference to Fig. 3 shows that the electrons accelerated at the times t_1 and t_2 and which therefore have a voltage V_0 (corresponding to the magnetic field H_0) are completely decelerated at the times t_1' and t_2', respectively. For any value of the field other than H_0, the deceleration is less than the acceleration for half of the electrons. These electrons passing on through D_2 are again accelerated in the gap between D_2 and S (disregard D_3 and D_4 for the present) and thus reach the collector C. For example if the field is smaller, corresponding to the voltage V_1, elec-

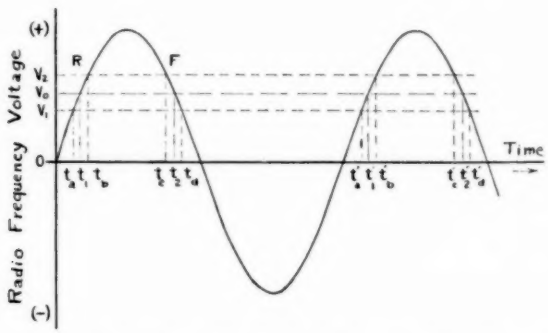

FIG. 3. Voltage-time relations for electron acceleration and deceleration.

trons accelerated at the time t_a will arrive at the decelerating slits later than t_a' and be completely stopped, while those leaving at t_d will likewise arrive later than t_d' and, experiencing only a partial deceleration, will pass on to the collector. For fields in the neighborhood of H_0, the current to the collector i_c should vary with the field in the manner shown by the solid curve (1) of Fig. 4. The resonance value of the field H_0 is indicated by zero (or minimum) current. The

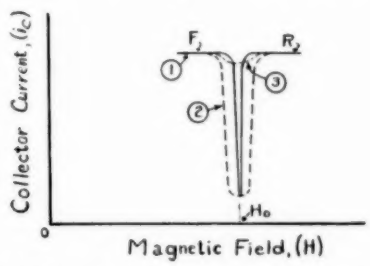

FIG. 4. Variation of collector current near resonance.

branch F is made up of electrons starting on the falling part of the cycle (as at t_d, Fig. 3) and branch R of those starting on the rising part (as at t_b, Fig. 3).

Derivation of equation for e/m. The equation giving e/m in terms of the experimentally observed quantities and the geometry of the apparatus is very simply obtained. For any magnetic field H, electrons having a velocity v given by the radial force equation

$$mv^2/r = Hev \text{ (e.m.u.)} \tag{1}$$

will be bent around through the defining slits at a radius r. The electron velocity necessary to travel from A_1 to D_2 (see Fig. 2) in one cycle is

$$v_0 = r\theta/T, \tag{2}$$

where θ is the angle in radians subtended by the path and T is the period of the oscillator. Since the oscillator frequency $\nu = 1/T$, the velocity can be written also as

$$v_0 = r\theta\nu. \tag{2'}$$

Elimination of the velocity by combining Eqs. (1) and (2') gives the desired result:

$$e/m = \theta\nu/H_0 \text{ (e.m.u.)}, \tag{3}$$

where θ is the angle in radians subtended by the electron path, the path being that which the electron would travel with constant velocity v_0 in one period, ν is the oscillator frequency in cycles per second and H_0 is the magnetic field in gauss.

Description of action in tube. The above description of the method must be slightly modified to correspond to the actual method of operation. In order to draw electrons from the filament through the slit A_1, it is necessary to apply an accelerating potential V_A between the

filament and the filament cylinder *FC*. In order to balance this an equal or slightly greater retarding potential V_D is applied between D_2 (i.e., the filament cylinder) and D_3. The effect of this initial velocity is simply to shift the time (relative to the radiofrequency voltage cycle) at which those electrons which pass on through the defining slits cross the gap A_1-A_2. For example if we let $V_0=V_A+V_1$, then with a magnetic field H_0, electrons crossing the gap A_1-A_2 at a time t_a (see Fig. 3) will experience a voltage acceleration V_1 and hence will leave A_2 with a velocity corresponding to the resonant voltage V_0. These electrons will then be decelerated in the gap D_1-D_2 by a voltage V_1 and further decelerated to zero velocity in the gap D_2-D_3 by a voltage V_D and hence will not reach the collector. With values of the magnetic field other than the resonance value half the electrons, as explained before, will be able to pass through D_3. They will be accelerated in the gaps D_3-D_4 and D_4-S and will reach the collector.

Contact potentials and retarding voltage V_D. From the foregoing discussion it is seen that with a magnetic field H_0 the existence of an initial electron velocity or of a continuous distribution of initial electron velocities does not in any way affect the equality of the acceleration in the A_1-A_2 slits with the deceleration in the D_1-D_2 slits. It is for the same reason that *the existence of contact potentials at any point other than* in the regions 1, 2 and 3, Fig. 1, *is immaterial.* Such contact potentials are taken care of in the adjustment of the retarding voltage V_D. This retarding voltage is adjusted experimentally to the value that gives the sharpest current minimum (see curve 1, Fig. 4). Too large a value gives a minimum with a rather flat bottom (curve 2) due to the appreciable interval of the magnetic field over which the electrons are stopped. Too small a value, instead of giving no minimum at all as might at first be expected, gives a shallow minimum, as curve 3. This is due to the fact that for conditions near resonance the electrons passing D_3 must travel a path of about 2 mm length with average velocities corresponding to a few volts before they can reach the strong accelerating field between D_4 and S and be shot into the collector. In travelling at these slow velocities the paths of the electrons are bent inward from the original circle and some are intercepted by the edges of D_3 and D_4. Thus no matter what the value of V_D (within reasonable limits of course) there is always at least a shallow minimum to be found. No variation of the observed values of e/m has been found with small variations of V_D. This is most important.

Bending of the electron path. Two things have been done to allow for the bending of the electron path mentioned above. First, the slits D_3, D_4, S and C have been widened relative to the other slits and in increasing amounts in the order given (see Fig. 2). These slits are aligned with their outer edges on the same circle as all the preceding slits. This allows electrons to reach the collector that have had their paths changed quite appreciably as well as those having paths practically unchanged. The result of this change is a narrower current minimum. Second, in order to determine if small changes in the radial location of the collector and shield relative to D_4 influence the results, the collector and its shield have been mounted eccentrically on a tapered plug in such a manner that they can be moved past the slit D_4 while measurements are being made. No changes in the observed e/m have been found with such displacement.

Effective angle subtended by the electron path. The angle θ appearing in Eq. (3) is a function of the accelerating voltage V_A. The variation, however, is quite small being of the order of one part in a thousand for the values of V_A used in the present work. As before stated the angle θ is determined by the distance (call it D) which the electrons would travel in one period *if* they maintained constant throughout this period the velocity v_0 that they have between the slits A_2 and D_1 (see Fig. 2). The electron acceleration between the slits A_1-A_2 and the deceleration between D_1-D_2 both require a finite though small time interval, the interval being of the order of 1/300 of the period T. This time interval is, of course, a function of the initial accelerating voltage V_A, being less the larger V_A. Less time taken in getting up to maximum velocity means a larger fraction of the period left to travel at that maximum velocity. Thus, increasing the accelerating voltage V_A decreases slightly the

maximum velocity v_0, and hence decreases slightly the distance D that could be travelled in a whole period.

The quantitative relation between the accelerating voltage and the angle can easily be obtained if the following approximations are made. Since the time interval for acceleration, or deceleration, is about 1/300 of a period, the voltage can, to a high approximation, be assumed to vary linearly with time over such an interval. Further, since the change in accelerating voltage over such a time interval is only of the order of 1.5 percent and the change in θ that is being calculated is only of the order of 0.1 percent, the acceleration can also be assumed constant for present precision. The result is:

$$\theta=\theta_0-(2d_1/r)[1/((V_0/V_A)^{\frac{1}{2}}+1)], \qquad (4)$$

where θ_0 is the angle in radians subtended by the electron path from A_1 around to D_2 (see Fig. 2), d_1 is the spacing between the slits A_1 and A_2 and between D_1 and D_2, r is the electron radius, V_A is the initial accelerating potential and V_0 is the potential corresponding to the electron velocity between A_2 and D_1. The magnitude of the variation in θ can be visualized by noting that the limits of the path corresponding to θ are for $V_A=0$ at the slits A_1 and D_2 and for $V_A=V_m$ at the midpoints between A_1-A_2 and between D_1-D_2. To evaluate Eq. (4) it is necessary to know *approximately* the voltages V_A and V_0. V_A (of the order of 100 to 200 volts) is measured by a voltmeter, allowance being made for the filament drop in potential. V_0 (of the order of 1000 volts) is easily computed from the electron radius r, the magnetic field H_0 and any reasonable assumption for the value of e/m, being given by

$$V_0=0.08795H_0^2r^2. \qquad (5)$$

It should be emphasized that V_A and V_0 need not be known accurately. For example, an error in V_A and one volt (due, say, to a contact potential) would cause an error in the computed value of e/m of only about six parts in a million.

Method of measurement of factors determining e/m. The three factors entering directly into the determination of e/m (see Eq. (3)) were determined as follows: The angle θ was obtained through the angle $(2\pi-\theta_0)$ indicated on Fig. 2. This smaller angle was found by measuring the chord from the slit A_1 to A_2. The chord was measured for both the inner and outer slits, the mean of which in combination with the radius gave the angle. The method of measuring the radius is given in the next section. The frequency ν was obtained by harmonics from the carrier waves of various broadcast stations. The magnetic field H_0 is made up of two parts: that produced by the current i_H in the Helmholtz coils and that by the earth's field. The current i_H was measured in the usual manner by using a standard resistance immersed in oil with a potentiometer and a standard cell. Since the Helmholtz coils of No. 20 enamel wire were carefully layer-wound on accurately turned aluminum wheels, it was considered sufficiently accurate for the present precision to compute the Helmholtz constant k_r from the micrometered dimensions. This was done by formulae which take into account the finite cross section of the coils. The determination of the earth's field is explained in the next section.

(B) Auxiliary apparatus

Amplifier for magnetic field measurement and adjustment. Since the magnetic fields used in this work were of the order of 10 to 12 gauss, the earth's magnetic field of the order of 0.4 gauss could not be neglected. An audio amplifier terminated with a vacuum tube voltmeter aided in the two phases of this problem. The amplifier was of the usual resistance coupled type but was designed to respond to frequencies as low as 5 cycles per second. The over-all amplification was 300,000 and imput levels as low as 3 microvolts could be used. The imput to the amplifier came from one or the other of two 5000 turn coils placed in the brass tube T passing through the box B, Fig. 1. The coils could be rotated at any desired speed by a small motor located some distance away. The axis of one coil was coincident with the axis through O, that of the other was perpendicular. The center of the latter coil was located accurately in the plane of the electron orbit and on the axis through O. In order that there be no radial component of the earth's field in the measuring tube, the axis through O, Fig. 1, was made parallel to the earth's field. This was accomplished through the

use of the parallel axis coil, a null reading on the output voltmeter indicating the desired condition. The adjustment was made by three levelling screws supporting the measuring tube. Secondly, the magnitude of the earth's field was measured through the use of the perpendicular axis coil. The field from the Helmholtz coils was adjusted to equality with the earth's field at the point O by opposing the two and again obtaining a null reading on the voltmeter. The Helmholtz current i_e so obtained, when multiplied by the Helmholtz constant at the point O, gives the earth's field. In either case the field could be adjusted to within 4×10^{-4} gauss. Since fields of the order of 10 gauss were used, this represents an accuracy of about 4 parts in 10^5.

Apparatus for aligning slits and measuring radius. The alignment of all the slits on the same radius and with the same slit width must be done very accurately. This was accomplished by having end caps on the tubing T, Fig. 1, with accurately located centers. Two dead centers supported on a U-shaped framework fit into these centers, so that the whole measuring tube (with the cover and Helmholtz coils removed) can be swung freely on the axis through O. A microscope with two cross-hairs is mounted with axis parallel but at a distance equal to the desired radius r. The slits have all been built so that they project about 0.4 mm from the face of the material mounted in, hence they can be seen from the side as viewed in the microscope. The two cross-hairs are adjusted to give the desired slit width. The pairs of slits are then adjusted consecutively to coincide with the cross-hairs.

The radius r (needed for calculation of the magnetic field and the angle) can be measured by the above arrangement with the addition of a large micrometer and an accurately turned and centered rod which is placed between the dead centers after the slits have been aligned and the measuring tube removed. The inner and outer slit radii can then be accurately measured by adjusting one edge of the bar to coincidence with the proper cross-hair, the bar being held by a framework with the other edge against the rod. The mean of the two is taken as r.

Radiofrequency source and control. The source of radiofrequency applied between the lead-in L, in Fig. 1, and the box was a short wave power-oscillator of the usual tuned-grid tuned-plate type. The circuit is given in Fig. 5. The capacity C_2 shown across the plate inductance L_2 is simply the capacity between the slits in the e/m tube and between the lead-in L and the return lead L_R which is large concentric cylinder

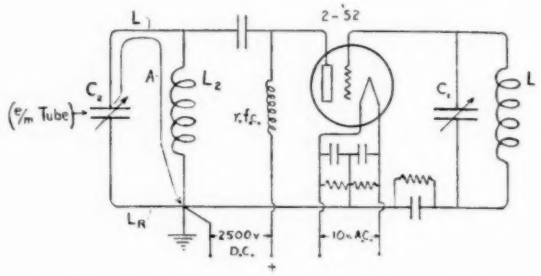

FIG. 5. Oscillator for supplying the radiofrequency voltage.

surrounding L. There is no possibility in the present method of any appreciable phase displacement of the radiofrequency voltage between the accelerating and decelerating slits. This follows from the very short path between these slits and the complete symmetry of the construction even to the symmetrically placed return lead L_R so that the capacity currents to both sets of slits have the same path lengths. The part of the tank circuit through which the filament and slit D_3 leads are led before being brought out at ground potential is indicated by the arrow A. Although only one tube is shown, actually two 75 watt tubes were connected in parallel. A well-filtered source of d.c. for the plate is necessary to avoid modulation which would alter the time between equal voltage ordinates of successive cycles.[8] The wave-length range used was from 7.5 to 10.5 meters. The peak voltage delivered to the e/m tube could be varied from zero to 3000 volts.[9]

The frequency was controlled and measured in the present preliminary work by a heterodyne method schematically shown in Fig. 6. As mentioned before, the carrier waves of various broadcast stations were used as frequency standards. Oscillator 1 is tuned to the carrier

[8] The average time would, of course, remain constant.

[9] The e/m measuring tube can be used as a high-frequency peak voltmeter by finding the maximum value of the magnetic field at which electrons can be sent around.

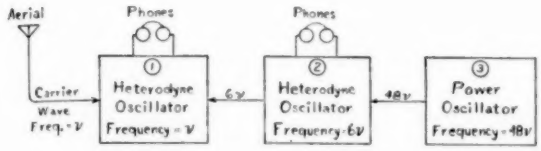

FIG. 6. Scheme for frequency control.

frequency by adjusting for zero beat note. Oscillator 2 is then turned on and its frequency adjusted so that its fundamental gives zero beat with the sixth harmonic of oscillator 1. Finally the power oscillator is adjusted to zero beat with the eighth harmonic of 2. The adjustments were monitored continuously during the taking of measurements. These zero beat adjustments were made with small vernier condensers of such size that a beat note of about 30 cycles occurred at least 7 to 10 dial divisions either side of resonance. Hence an adjustment to ± 4 cycles was easily possible.

RESULTS

General collector current variation

The hope that this new method would have a very sharp current minimum at the resonant adjustment has been realized. A typical collector current curve obtained by varying the magnetic field, the frequency being held constant, is shown by curve 1, Fig. 7. The resonant minimum at B is much narrower than the width of the printed line. At H there is a trace of a shallow second order resonance, that is, the adjustment in which the electrons take two periods instead of one to travel the required path. The value of the magnetic current at H is not exactly half of that at B due to the earth's field, but the net fields are exactly in the ratio of 1 : 2.

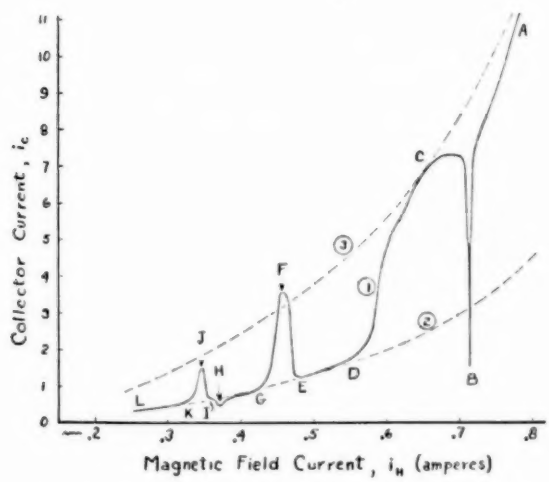

FIG. 7. Variation of collector current with magnetic field at a frequency of 3.7920×10^7 cycles and a peak voltage of 2400 volts.

The two peaks at F and J respectively are due to special electron velocity *versus* voltage phase relations, existing only in those localized regions, and of such a nature that both R and F groups of electrons (see discussion with Fig. 4) get through the collector. The collector current is made up of these two groups in the following manner: A to B, and G to I of the R group alone, B to E and K to L of the F group alone, E to G and I to K of both groups.

Slope of collector current curve

In Fig. 4 the collector current was indicated as being constant on either side of the resonant point. That this simplified picture is not to be expected can be seen from the following. A finite slit width Δr means a finite range of electron voltage Δv which can satisfy the resonance condition. For a given slit width this voltage range is a constant and is given by

$$\Delta V/V = 2(\Delta r/r). \tag{6}$$

The magnitude of ΔV therefore is proportional to the electron voltage V. Considering a sine wave (see Fig. 3), the time interval over which a given voltage range exists depends not only on the voltage range but also on the ratio of the electron voltage to the peak voltage V_P. It is given by

$$\Delta t/T = [1/\pi[(V_P/V)^2 - 1]^{\frac{1}{2}}](\Delta r/r), \tag{7}$$

where T is the oscillator period. The quantity of current travelling to the collector in a pulse is, of course, proportional to Δt, hence the collector current i_c is proportional to Δt. By Eq. (5), the electron voltage is proportional to the square of the total magnetic field and therefore it is proportional to the square of the Helmholtz current i equivalent to that field. Eq. (7) may then be written in the working form

$$i_c = K/[(V_P/2593i^2)^2 - 1]^{\frac{1}{2}}, \tag{8}$$

where K is the proportionality factor and the

numerical constant comes from the electron radius and the Helmholtz constant of the present apparatus.

Curve 2 of Fig. 7 has been computed from Eq. (8), correcting i for the current equivalent to the earth's field and adjusting the constant K to give current equality at $i_H = 0.5$ ampere. V_P was 2400 volts. It is seen that the general rise of the collector current is in perfect agreement up to about $i_H = 0.55$ ampere. If instead of making the fit at $i_H = 0.5$ ampere it is made at 0.65 ampere, curve 3 is obtained which fits fairly well above $i_H = 0.65$ ampere. There is thus a threefold current increase between $i_H = 0.55$ and 0.65 ampere, before and after which the collector current varies in the manner to be expected. The cause of the threefold increase is unknown. The effect of the general positive slope in the neighborhood of the minimum is to shift the minimum to a smaller value of magnetic current which in turn gives a value of e/m too high. Fortunately, however, with good experimental conditions the minimum is so sharp that the shift is very small, being of the order of 2 parts in 100,000.

The current minimum

To show the sharpness of the current minimum the region in the vicinity of the resonant point B (Fig. 7) has been plotted in Fig. 8 with an abscissa scale 40 times that of Fig. 7. The sharpness of the minimum easily allows single readings to one part in 10,000. The two side minimum at B and C are due to geometry of the slit system since in one particular adjustment of the apparatus they disappeared (see dotted lines) only to reappear on subsequent adjustments. The heights of B and C are influenced by the magnitude of the accelerating potential V_A and the decelerating potential V_D, *but any reasonable adjustment does not affect the location of the minimum A.*

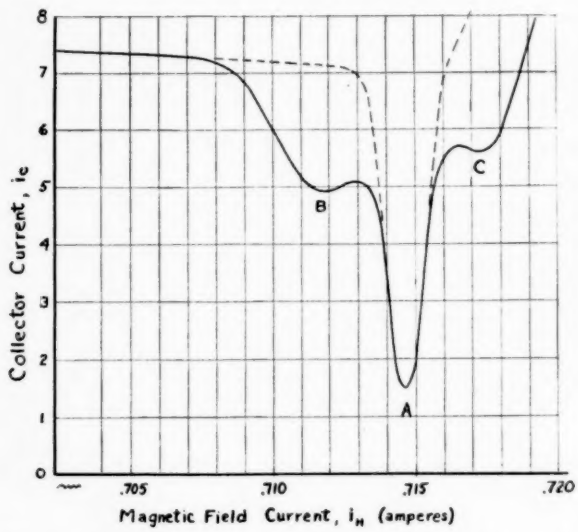

FIG. 8. The current minimum of Fig. 7 with abscissa scale magnified 40 times.

Summary of results

A summary of the results is given in Table I. The data were taken at two frequencies (see column 1) and for various accelerating potentials V_A (column 2), each run consisting of the number of observations of the current minimum given in column 4. The corresponding electron voltages were respectively about 1420 and 844 volts. The average Helmholtz current for each run appears in column 5. This has been corrected for the change with temperature of the standard resistance. These average currents have in turn been averaged by least squares in groups depending on the accelerating potential (column 6). The very high consistency of the readings of any group is evident from the observational probable errors given below each average, this error being less than 2 parts in 100,000 for the best experimental conditions. The values of e/m corresponding to these group averages are given in column 6.[10] These have been computed on the basis of θ_0 (i.e., without allowing for the change in angle with V_A as given in Eq. (4)) in order that a comparison between the computed and experimentally observed change with V_A could be made. This comparison appears in Table II. The observed changes are simply differences of values in column 7 of Table I, and the calculated changes are differences in the values of column 8, the latter computed by Eq. (4). The observed changes are greater than the calculated, that for the higher frequency

[10] The numerical values used in Eqs. (3) and (4) were as follows: angle $\theta = 5.9348$ radians, electron radius $r = 9.907$ cm, Helmholtz constant at this radius $k = 17.3616$, mean value of the earth's magnetic field $= 0.43291$ gauss, and slit spacing $d_1 = 0.128$ cm. The electron voltages V_0 are given above. The slit width was 0.066 cm.

TABLE I. *Summary of e/m data and results.*

1 Frequency and station	2 Run No.	3 V_A (volts)	4 No. observations	5 Average i_H (amp.)	6 Group average i_H (amp.)	7 Corresponding e/m uncorrected	8 $(\Delta e/m)_\theta$ Angle correction	9 e/m_0	10 Frequency average e/m_0
3.7920×10^7 (KGO_{48})	1	71	13	0.71424	0.71426 ± 1	1.75354 ± 3	−0.00140	1.75701 ± 3	1.75699 ± 2 (R_e/R_i =0.80)
	2	71	10	0.71424					
	3	71	12	0.71424					
	4	71	20	0.71430					
	5	121	10	0.71415	0.71415 ± 2	1.75381 ± 4	−0.00173	1.75695 ± 4	
	6	121	10	0.71414					
	7	121	10	0.71416					
	8	171	10	0.71403	0.71397 ± 5	1.75423 ± 12	−0.00197	1.75713 ± 12	
	9	171	10	0.71391					
2.9280×10^7 ($KFRC_{48}$)	10	81	30	0.54518	0.54518 ± 3	1.75555 ± 9	−0.00183	1.75661 ± 9	1.75679 ± 12 (R_e/R_i =1.86)
	11	121	20	0.54497	0.54498 ± 3	1.75617 ± 9	−0.00210	1.75696 ± 9	
	12	121	20	0.54499					
	13	121	12	0.54496					

being within the experimental error but that for the lower frequency being considerably outside. The reason for this discrepancy is apparent when the effect is considered of the width of the current minimum on its location. The minimum becomes broader as the accelerating voltage is increased. This should make the values of e/m obtained at higher accelerating voltages too large and such is the case (see column 7 and "observed" values Table II). The reason that

TABLE II. *Calculated and observed angle corrections.*

Frequency $\times10^{-7}$	Change in V_A (volts)	Change in Uncorrected e/m ($\times10^6$) Computed	Observed
3.7920	71 to 171	57	69±15
2.9280	81 to 121	27	62±18

at the lower frequency the observed change is so much larger than the computed is because the current minimum even for the best conditions is much broader. Hence the effect is increased at the lower frequency.

The values of e/m_0 containing the angle as well as the relativity correction are given in column 9 for each accelerating voltage. The relativity corrections in e/m for the higher and lower frequency data are respectively +0.00487 and +0.00289.

The least squares average for each frequency with the probable error is tabulated in column 10. In all cases in this paper the probable error given is the larger of the two errors computed by external and internal consistency. The consistency of the various e/m_0 values for a given frequency is shown by the ratio of the external to the internal probable errors[11] as given below each average. For the higher frequency the ratio is less than unity. This indicates that the error due to broadening and consequent shifting of the minimum as V_A is raised to 171 volts has no appreciable effect on the result, that is, runs 8 and 9 have little weight. This is due to their relatively large probable error. For the lower frequency the ratio of two errors is 1.86. The chance of the error varying by this fraction due purely to statistical fluctuation is only 1 to 3.8. In this case the error due to the shifting of the minimum with increasing V_A is noticeable. This results from two things: the magnitude of the shift is greater due to a broader minimum and second, the number of observations taken at the two accelerating potentials happened to be such that the two resulting probable errors are equal. The agreement, however, between the two frequency values is good since they differ by only 1 part in 10,000. Changing the frequency changes the energy of the electrons being measured. The

[11] R. T. Birge, Phys. Rev. 40, 207 (1932).

TABLE III. *A comparison of the constancy of e/m_0 with change in electron energy.*

Experimenter	Percent electron energy change	$\Delta e/m$ $\times 10^4$	Relative change in e/m for same percent energy change
Dunnington	40.9	2	1.00
Kirchner	5.87	5	17.4
Perry and Chaffee	41.6	11	5.4

constancy of the present results with change in energy is compared with that obtained in other e/m determinations in Table III. The data for Perry and Chaffee were taken from the two frequency groups whose percentage difference in electron energy is nearest to that of the author.

The final value of e/m_0 as computed by least squares from the two frequency averages is $e/m_0=(1.75699\pm0.00002)\times10^7$ e.m.u. The correction of the magnetic field from international to absolute units[5] requires an increase of 0.5 parts in 10^4. The result then becomes:

$$e/m_0=(1.75708\pm0.00002)\times10^7 \text{ e.m.u.}$$

The uncertainty given is the observational probable error determined simply by observations on the minimum. The ratio of the external to internal probable errors for this average is 1.12 and the chance of the error varying by this fraction solely because of statistical fluctuations is 1 to 1.25. This shows that the frequency variation does not appreciably affect the magnitude of the result or its probable error. This is because of the much larger probable error at the lower frequency. In other words, the result largely depends on runs 1 through 7. This mathematically attained result is in agreement with the author's estimate of the relative reliability of the data. The previously mentioned effect of the shifting of the minimum with its increased breadth would lead one to expect a slightly higher value at the lower frequency. Since the results obtained were lower for the lower frequency, there is apparently some other effect that is a function of the frequency and that varies in a sense opposing the first.[12]

[12] The effect may at least partially be due to one or both of the broadcast stations consistently maintaining an average frequency above or below their assigned frequency. In this case the uncertainty can be eliminated by using various harmonics of the same carrier wave.

ERRORS

A summary of the various probable errors and their sources is given in Table IV. The formula for e/m (Eq. (3)) has three factors, θ, ν and H_0 but actually the determination of the field H_0 involves two things: the Helmholtz constant k and the current i equivalent to the total field. These four factors are listed at the left of the table. The quantities that enter into the determination of these factors are listed in the next column with their estimated (or calculated) uncertainties in the third column. The probable errors calculated by least squares appear in the last column. The probable error in e/m_0, also calculated by least squares is given below the table.

It should be noted that in the case of the angle θ_0, the probable error computed from the uncertainties of the radius and chord is that for the small angle $(2\pi-\theta_0)$, shown in Fig. 2. Since θ_0 is about 17 times greater, its proportional uncertainty is only 1/17th as large.

Since the constant of the Helmholtz coils was calculated and not checked by any experimental method, an allowance has been made of 4×10^{-4} for unknown errors (i.e., other than from uncertainties in the dimensions). This should allow for such things as an appreciable permeability of the brass and aluminum used in and about the tube, etc. A generous allowance has also been made in the field current i for the possible existence of any factors disturbing the location of the minimum. It should be noted that the final probable error in e/m_0 (given below the table) depends almost entirely on these two allowances, all other errors being small in comparison.

In computing the frequency error, the computed error in the setting of the heterodyne oscillators was based on an assumed uncertainty of each individual setting of 10 cycles. This latter is twice the precision of a single setting.

The estimated uncertainties given in the third column are not probable errors, that is, they are not the errors which are as likely to be exceeded as fallen short of. Rather they are the errors for which the chance is small that the true error will exceed them, probably about one chance in five. This means that they are twice

TABLE IV. *Summary of probable errors.*
Probable error in e/m_0: 6.77 parts in 10,000 or $\Delta e/m_0 = \pm 0.00119$.

Factors	Quantities entering into factors	Estimated uncertainty Parts in 10^4	Probable error Parts in 10^4
Angle θ_0	Radius Chord (of $2\pi-\theta$)	5 14	0.90
Field constant k	Effect of uncertainty in radius of electron orbit Effect of uncertainty in radius of Helmholtz coils Allowance for unknown errors	0.75 1 4	4.19
Field current i	Observational uncertainty (including frequency correlation) as given by twice the obs. p. e. Voltage of standard cell (by Bur. Standards) Resistance of standard resistance (by Bur. Standards) Precision of Wolf potentiometer Allowance for factors disturbing location of minimum	0.25 1.0 0.5 0.2 4	5.23
Frequency ν	Standards, limit of error { KGO -0.63×10^{-4} / KFRC -0.82×10^{-4} } Errors in setting heterodyne oscillators	0.30 0.13	0.33

the probable errors. However, to be conservative, these estimated uncertainties will be taken as the probable errors.

On the foregoing assumption, the probable error in e/m_0 is ± 0.00119. Retaining only four decimals and allowing still more for additional uncertainties because of the preliminary nature of the work, the value that will be adopted for the present work is

adopted probable error in

$$e/m_0 = (\pm 0.0015)\times 10^7 \text{ e.m.u.}$$

In view of the above manner of determination, this is considered a conservative estimate.

CONCLUSION

Author's value of e/m_0

The value of e/m_0 and its probable error found in the present investigation is[12a]

$$e/m_0 = (1.7571 \pm 0.0015)\times 10^7 \text{ e.m.u.}$$

The present probable value of e/m_0

For the purpose of comparing this result with that of preceding experimenters and of obtaining the present most probable value of e/m, the data of Table V is offered. The table contains the results of all important determinations of e/m made in the last ten years.[13] The only exception is that of Wolf[7] whose result now appears to be in conflict with those of all other methods.

The table may be divided into two parts, the first consisting of three spectroscopic determinations and the second consisting of three free electron determinations. The value of e/m_0 given for Houston is the result as corrected by Birge[3] and the value given for Kirchner is the weighted mean of his two frequency determinations with the probable error based on internal consistency. The probable error quoted for Babcock is that based on his statement that he believed his result good to one part in a thousand. His observational probable error was 0.0012. The weights as computed by least squares have been listed in column 6. These were used in computing the averages of columns 7 and 8 and the probable errors given under each average. A separate average for the spectroscopic and free electron data has been computed to emphasize the present agreement between the two classes of data.

A final average of e/m_0 based on all the data is given in column 8. This value is

[12a] This result differs from that published in a letter, Phys. Rev. **42**, 734 (L) (1932), because of a change in the value used for the standard resistance (the certificate arriving from the Bureau of Standards after the letter was published) and because of a new and more accurate calculation of the magnetic field constant k of the Helmholtz coils.

[13] A comparison has recently been made by Birge using three previous determinations and the author's uncorrected value,[12a] Phys. Rev. **42**, 736 (1932).

TABLE V. *Probable value of e/m based on six recent determinations.*

Experimenter	Date	Method	e/m_0 $\times 10^{-7}$	Probable Error (r) $\times 10^4$	Weight $=10^{-6}/r^2$	e/m_0 $\times 10^{-7}$	e/m_0 $\times 10^{-7}$
Houston[14]	1927	Fine structure	1.7608	8	1.563	1.7605±7 ($R_e/R_i=0.526$)	1.7598±5 ($R_e/R_i=0.88$)
Babcock[15]	1929	Zeeman effect	1.7606	18	0.309		
Campbell and Houston[6]	1932	" "	1.7579	25	0.160		
Perry and Chaffee[4]	1930	Linear acceleration	1.761	10	1.000	1.7593±7 ($R_e/R_i=1.12$)	
Kirchner[5]	1932	" "	1.7587	9	1.235		
Dunnington	1932	Magnetic deflection	1.7571	15	0.444		

probable value based on six determinations

$$e/m_0=(1.7598\pm0.0005)\times10^7 \text{ e.m.u.}$$

It is important to note that in all three averages the ratio of the error based on external consistency to that based on internal consistency (R_e/R_i) is near to or less than unity. This shows that the errors assumed by each investigator have been quite conservative. The agreement of the six determinations made with such widely varying methods indicates the reliability of their average.

Discussion

The author's value of e/m_0 is seen to be lower than that of the other recent determinations. The improvement, however, of the present method over preceding ones is indicated by the constancy of the value of e/m_0 with change in frequency, that is, with change in electron energy, the energy correlation being 5 to 17 times better than in the two most recent free electron determinations. The improvement is also indicated by the high observational precision and by the greatly reduced effect of contact potentials.

However, it is to be emphasized that the measurements have all been made with one alignment of the slit system and are not considered by the author to be of a final nature. The apparatus has now been moved to the California Institute of Technology and the measurements will be continued at that institution with the aim of confirming or disproving the present results and of increasing the accuracy as much further as is reasonably possible and desirable.

It is also desirable to emphasize the importance of the human equation in accurate measurements such as these. It is easier than is generally realized to unconsciously work toward a certain value. One cannot, of course, alter or change natural phenomena (for example, the location of the current minimum in the present experiment), but one can, for instance, seek for those corrections and refinements which shift the results in the desired direction. Every effort has been made to avoid such tendencies in the present work.

The author desires to thank Professor E. O. Lawrence for the use of the method which made possible the present results and for suggestions during the course of the work. He also wishes to thank Professor R. T. Birge for his interest and for his criticism of the paper and David H. Sloan for suggestions on the radiofrequency apparatus.

[14] W. V. Houston, Phys. Rev. **30**, 608 (1927).
[15] H. D. Babcock, Astrophys. J. **69**, 43 (1929).

A Determination of e/m by Means of Photoelectrons Excited by X-Rays

G. G. KRETSCHMAR, *Ryerson Physical Laboratory, University of Chicago*

(Received December 29, 1932)

A value of e/m has been obtained by a magnetic deflection method by making use of x-ray photoelectrons and the magnetic spectrograph. Electrons were ejected from thin evaporated or sputtered films of gold, silver, copper and platinum by the x-radiation from a molybdenum target metal tube placed close to the film and working at an input of 1.5 kilowatts. The velocity of ejection of the photoelectrons was computed from the difference between the energies associated with Mo K radiation and the various absorption limits of the metal films. Relativity corrections were made since these velocities correspond to from 8000 to 15,000 equivalent volts. The α_1 and α_2 components of the molybdenum $K\alpha$ line were clearly resolved since the magnetic field was kept very constant by the use of a potentiometer and continuous hand control. The weighted mean value of e/m_0 obtained from five plates is $1.7570\pm0.0026\times10^7$ e.m.u. per gram. This result is based upon a value of $h/e=1.3737\pm0.0005\times10^{-17}$ as taken from x-ray crystal measurements. By taking h/e from x-ray data the resulting value of e/m is independent of the uncertainty involved in the crystal grating constant.

DURING the past forty years there have been many determinations of the specific charge of the electron. In the *Handbuch der Radiologie*[1] for instance, there is a compilation of not less than forty-five separate experiments up to the year 1913, for the evaluation of this important constant. Gerlach[2] gives a compilation of the researches from 1901 to 1911, in which he gives the value 1.766×10^7 e.m.u. as the most probable value at that time. More recently, the value of 1.7609 ± 0.0012 obtained by Babcock[3] by the Zeeman effect, and Houston's value[4] of 1.7608 ± 0.0008 by an interferometric measurement of the Rydberg constant of H and He has emphasized a lower result, while the cathode-ray measurement of 1.7689 ± 0.002 made by Wolf[5] has agreed with the prevailing higher estimates. Birge[6] suggested that there might be a difference in the value of e/m depending on whether the electron is free or bound in the atom. This suggestion probably has had the effect of stimulating experimentation in this interesting field, for we have since had a surprisingly large number of researches on the evaluation of e/m.

The work of Campbell and Houston,[7] making use of the Zeeman effect, has given us the value of 1.7579 ± 0.0025 in substantial agreement with the previous spectroscopic determinations. Then, recently, we have had the experiments of Perry and Chaffee[8] and Kirchner[9] giving values corresponding to those obtained by the spectroscopic methods. This work is of especial interest, because the lower values are obtained by a nonspectroscopic method.[10] However, the method is not a deflection method, and it is still extremely important, as Birge[11] suggests in a recent paper, to obtain a really reliable value of e/m from magnetic deflection. The present experiment[12] represents an attempt in this direction.

[1] A. Bestelmeyer, Handb. d. Radiologie **5**, 1–79 (1919).

[2] W. Gerlach, Handb. d. Physik **22**, 41–82 (1926).

[3] H. D. Babcock, Astrophys. J. **58**, 149 (1923); **69**, 43 (1929).

[4] W. V. Houston, Phys. Rev. **30**, 608 (1927).

[5] F. Wolf, Ann. d. Physik **83**, 849 (1927).

[6] R. T. Birge, Phys. Rev. Sup. **1**, 48 (1929).

[7] J. S. Campbell and W. V. Houston, Phys. Rev. **39**, 601 (1932).

[8] Charlotte Perry and E. L. Chaffee, Phys. Rev. **36**, 904 (1930).

[9] F. Kirchner, Ann. d. Physik, **8**, 975 (1931); **12**, 503 (1932).

[10] Although the recent determinations of e/m have tended to confirm the lower value, W. N. Bond (Proc. Phys. Soc. **44**, 374 (1932)) from the theoretical work of Eddington, gives reasons for believing that the higher value is correct.

[11] R. T. Birge, Phys. Rev. **40**, 228 (1932).

[12] As early as 1906 A. Bestelmeyer (Ann. d. Physik **22**, 429 (1907)) experimented with x-ray photoelectrons for obtaining a value of e/m. He was able to show experimentally that the value of e/m depends on the velocity, and he made the relativity corrections.

Method

The present experiment makes use of the magnetic spectrograph method, originally developed by Robinson and Rawlinson[13] and used by de Broglie[14] and Robinson[15] for determining atomic energy levels, and more recently by Watson[16] for obtaining data on spatial distribution of x-ray photoelectrons. Watson has shown that the optimum direction of ejection of the electrons is a little forward of 90° from the direction of the x-ray beam. Also, he has shown that by the use of very thin films, the lines obtained are very much sharper, and approximate more closely to a true image of the slit than when thicker films are used. These facts have been of great help in the present work. It has been possible by the use of very thin films, and by holding the magnetic field very constant, to produce sufficient resolution to show clearly the doubling in the lines due to the α_1 and α_2 components of the Mo $K\alpha$ line in the radiation which was used.

It is now apparently well established that photoelectrons are ejected by x-rays, with a definite energy, given by the Einstein relation:

$$\tfrac{1}{2}mv^2 = hc(1/\lambda_K - 1/\lambda_L), \qquad (1)$$

where λ_K is the wave-length of the incident radiation and λ_L is the wave-length of the absorption limit of the electron shell from which the particles have their origin. Also, since the electrons are bent into a circular path, by a magnetic field of H gauss, we have:

$$mv^2/r = Hev. \qquad (2)$$

Solving these two equations for e/m we obtain:

$$e/m = 2c^2(h/e)(1/\lambda_K - 1/\lambda_L)/(Hr)^2. \qquad (3)$$

The result, it is seen, involves the constant h/e. Fortunately, this constant, as Birge[17] has pointed out, is much more accurately known than e. One of the most precise methods for obtaining h/e is by means of the limit of the x-ray spectrum, as has been done by Duane, Palmer and Yeh[18] and by Feder.[19] It can be shown that if the x-ray value of h/e is used[20] the resulting value of e/m is independent of the grating space assumed since the effect of the grating space on the value of h/e is just balanced by its effect on the value of the wave-lengths. Thus the value of e/m obtained by this magnetic spectrograph method is more reliable than might appear, in view of the discussion of the correctness of crystal wave-lengths.

Since the electron velocities in this experiment were of the order of 8000 to 15,000 equivalent volts ($\beta = 0.16$ to 0.24) it is necessary to replace Eqs. (1) and (2) with the equations which involve the relativity corrections. They are:

$$m_0c^2(1/(1-\beta^2)^{\frac{1}{2}} - 1) = hc(1/\lambda_K - 1/\lambda_L) \qquad (4)$$

$$\beta c/(1-\beta^2)^{\frac{1}{2}} = Hr(e/m_0), \qquad (5)$$

where $m = m_0/(1-\beta^2)^{\frac{1}{2}}$, $\beta = v/c$ and m_0 is the rest mass and m is the mass at the velocity v and c is the velocity of light. Eq. (4) may be put into the form:

$$\frac{\beta c}{(1-\beta^2)^{\frac{1}{2}}} = \beta \frac{e}{m_0}\frac{h}{e}\left(\frac{1}{\lambda_K} - \frac{1}{\lambda_L}\right) + \beta c$$

and equating to (5) and solving for e/m_0 we get:

$$\frac{e}{m_0} = \frac{2c^2(h/e)(1/\lambda_K - 1/\lambda_L)}{(Hr)^2 - c^2(h/e)^2(1/\lambda_K - 1/\lambda_L)^2}. \qquad (6)$$

It is seen that this form is identical with the form obtained with the simple equations with the addition of a second order term in the denominator.

Experimental Arrangement

The experimental arrangement consists of, first, a metal x-ray tube rigidly mounted with a three-stage mercury diffusion pump on a heavy wooden support. Second, a large solenoid

[13] H. Robinson and W. F. Rawlinson, Phil. Mag. **28**, 277 (1914).

[14] M. de Broglie, C. R. **172**, 274, 527, 746, 806 (1921).

[15] H. Robinson, Proc. Roy. Soc. **A104**, 455 (1923).

[16] E. C. Watson, Phys. Rev. **30**, 479 (1927).

[17] R. T. Birge, Rev. Mod. Phys. **1**, 72 (1929).

[18] W. Duane, H. H. Palmer and Chi-Sun Yeh, Proc. Nat. Acad. Sci. **7**, 237 (1921).

[19] Ann. d. Physik **5** (1), 494 (1929).

[20] The value used in the computations of this paper is $1.3737 \pm 0.0005 \times 10^{-17}$. This value is obtained from the arithmetical average of the results of the experiments of Duane, Palmer and Yeh, and of Feder as given by R. T. Birge, Phys. Rev. **40**, 247 (1932).

mounted on a rigid framework, so that the axis of the solenoid is parallel to the earth's field. Third, a heavy brass camera with supports so arranged that it may be placed in the middle of the solenoid and carefully aligned with respect to the direction of the x-ray beam and the axis of the solenoid.

The solenoid was 100 cm long and 22 cm in diameter wound with a single layer of No. 18 enameled wire, held in place by layers of shellac, baked on, above and below the wire. The solenoid was very carefully made as it was originally planned to obtain the solenoid constants from the dimensions, but this was found to be impractical, and the field was finally calibrated by a standard solenoid and flip coil method, which will be described later. Two heavy brass rings were securely fastened to the ends of the solenoid and two pins projecting into the lower one and a special clamp on the upper one permitted the exact alignment of the solenoid and insured its return to the same position whenever it was necessary to remove it. A hole in the middle of the solenoid, 6 mm in diameter was made into the wall during its construction, and the wire was distorted slightly on the two sides of this hole during the winding, thus producing a small opening through which the x-ray beam was sent.

The source of x-rays was a metal tube designed by Dr. Elmer Dershem of this laboratory. It contained a water-cooled molybdenum target such as is used in commercial tubes. The vacuum system to which the tube was permanently attached, was made as short and direct as possible, of large diameter tubing. The excitation was from a large capacity transformer (20 kw) and it was found possible to run the tube consistently for long periods with an input of 75 to 85 milliamperes with a voltage of approximately 30,000 volts.

The camera was in the form of a circular disk 21.5 cm outside diameter and 6.5 cm high. The bottom and top were made of heavy brass plate 1.22 cm thick and the side wall was a short length of large diameter seamless brass tubing. A groove cut into the bottom plate contained a rubber gasket. Twelve screws clamped the upper part onto this gasket making a convenient and vacuum-tight joint.

The distribution of parts inside the camera is best described from the diagram Fig. 1, which represents a section through the middle of the camera and perpendicular to the axis of the solenoid. The surfaces in the planes AB and CD were carefully scraped flat to within 0.003 mm and these surfaces were parallel to each other to the same accuracy.

Eastman x-ray plates were used. They were held in contact with the plane AB by the spring T. A fine slit at S' served to make a fiducial mark on the plate by means of optical light. The slit S, through which the electrons passed, was very carefully made by working the two parts down to a knife edge and finishing by means of the finely ground surface of a glass flat. This slit was 0.12 mm wide. The lead shield L served to keep any scattered x-rays from affecting the plate, and the heavy lead well W was for absorbing the main x-ray beam after it had passed through the metal film at M. The x-rays were admitted to the camera in the direction shown through a 6 by 10 mm opening in the camera wall which was covered with a thin window of cellophane on the outside, cemented on so that it was vacuum tight, and a thin sheet of black paper on the inside to keep out any optical light.

The metal films used were gold, silver, copper and platinum. The first three were evaporated onto cellophane by the method suggested by Cartwright and Strong.[21] The platinum was a sputtered film on cellophane. The films were very thin and transparent, of about the thickness known as "half-silvered" or less. In use a strip was cut out of the metalized cellophane about 3 mm wide, and cemented across the two prongs so that the center line of the strip was exactly under the slit. Of course, it was necessary to get the metal side above, as the x-rays passed through the cellophane before driving electrons out of the film.

The fixed dimensions of the camera focussing device were measured on a small Gaertner comparator the least count of which was 0.001 mm. This instrument was carefully checked against a standard decimeter, which has been checked by the United States Bureau of Stand-

[21] C. H. Cartwright and J. Strong, Rev. Sci. Inst. **2**, 189 (1931).

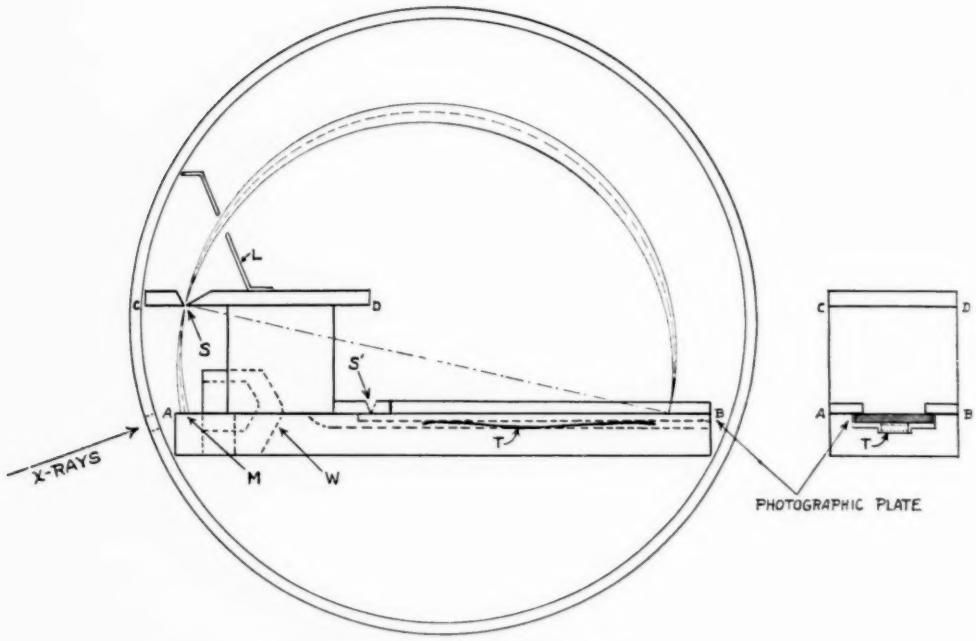

FIG. 1. Diagram of camera box.

ards. The vertical distance was 31.868±0.002 mm and the horizontal distance from the center of S to the center of S' was 52.890±0.002 mm at 23°C. Temperature corrections were always made in the computations.

The support for the camera was built up from four brass rods securely anchored to the supporting framework. It was independent from the solenoid, thus producing no distortion in the latter. The top of this support, consisted of heavy brass rings which contained two pins which projected into the base of the camera. These pins served to orient the camera so that the small hole through which the x-rays entered could be put into exact alignment with the hole in the solenoid. The camera support also served as a rigid support for the standard solenoid by extending one of the rods.

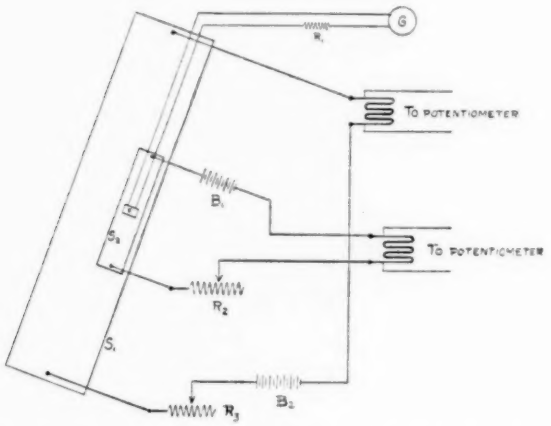

FIG. 2. Circuit diagram showing method of calibration of solenoid.

CALIBRATION OF THE MAGNETIC FIELD

The standard solenoid was wound on a bronze cylinder which was cast from S. A. E. 62 bronze made up from virgin metals to avoid any trace of magnetic impurity. This bronze cylinder was 6.4 cm in diameter and turned perfectly true. It had a 90° thread cut into the surface as accurately as possible, and the wire was wound into these thread grooves. Before winding on the wire the cylinder was supported on the bed of a large Geneva Society comparator and measured at short intervals by sighting the cross hair in the exact centers of the thread cuts. A series of six sets of measurements made in this way were found to agree within one part in 28,000. A check measurement made a number of weeks later after the wire was wound on the cylinder, agreed with the original measurement to one part in 10,000.

The cylinder was insulated with three coats of lacquer and wound with 243 turns of No. 18 enamelled wire, and the ends were taken off at right angles and along the same element of the cylinder. The diameter of the solenoid was obtained from micrometer measurements on the outside of the winding in different azimuths. The thickness of the enamel was estimated from tables and from measurements.

The magnetic field strength of the solenoid was computed from the formula: $H=KI$ gauss, where I is the current in amperes and $K=0.4\pi N \cos\alpha$. N is the number of turns per cm and α is the angle subtended at the center by the radius at one end. This simple formula is applicable in this case since the flip coil is small and located at the center of the solenoid. The flip coil mechanism contained a coil of nearly 12,000 turns of No. 40 enameled wire 32 mm outside diameter and 16 mm wide. This coil was mounted in the center of the solenoid on carefully aligned pivots, and arranged with a trip mechanism so that it could be controlled from a distance, and caused to turn quickly through exactly 180°, under the tension of small rubber bands.

The mounting of the standard solenoid was so placed that the flip coil rotated in a position which corresponded to the centers of the electron trajectories during the exposures.

The actual calibration was by a null method. The diagram Fig. 2 gives the connections during a calibration. By using two separate potentiometer circuits, the current was held constant in the large solenoid at one value and simultaneously, in the standard solenoid, at a series of values above and below the neutral point, and the deflections of a ballistic galvanometer observed at these points. It was found possible to plot a straight line through the resulting points, the intersection of which on the axis, gave very accurately the current required in the standard solenoid to neutralize the field of the large solenoid. The galvanometer used for the field calibration was a type HS Leeds and Northrup instrument of 25,000 ohms external critical damping resistance. It was used critically damped by placing an extra 20,000 ohm unit in series, in the galvanometer circuit.

The calibrations were made under the same conditions as obtained during the exposures, for the current was maintained in the large solenoid during calibrations, at the value which was used while most of the plates were being made. The earth's field, including any stray field effects, was determined by running the calibration currents both in the normal and the reversed directions.

A series of measurements taken over a period of ten days showed very excellent agreement. The weighted mean of nine calibrations was taken. It is 11.434 ± 0.005 gauss per ampere and this value was used in all the computations of this paper. The weights were taken with respect to the accuracy with which the ballistic galvanometer deflections corresponded to a straight line, and the closeness with which the conditions of the calibration simulated the conditions during the exposures.

A small magnetometer, designed by Mr. A. E. Shaw of this laboratory, was mounted on the apparatus. This served to show the effect of the placement of magnetic objects, such as tools, steel chairs, and the opening of the steel windows. No ferromagnetic materials were used in the construction of any of the apparatus or supports, and a slight magnetic effect of running the x-ray tube was neutralized by placing a steel chair in a position about two meters distant from the apparatus. This was afterward verified by making calibrations both with and without the tube running. These calibrations failed to show a detectable difference.

Making the Exposures

The high input into the x-ray tube and the short distance which was about 8 cm from the target to the metal film in the camera, made possible the obtaining of plates in a shorter time than would be possible with a glass x-ray tube. It was found possible to get good lines with about 18 hours exposure and some of the later exposures were made in 8 and 10 hours, but a little more time would have been an advantage.

During the exposures the magnetic field was kept constant to about one part in 5000 by fine rheostatic controls. The current was measured by means of a standard 0.1 ohm shunt and a Wolff potentiometer. The shunt was calibrated

recently by the Bureau of Standards, and was certified to an accuracy of one part in 4000 for the current used. Two Weston normal cells were used, which were frequently intercompared and checked against a Weston cell with a recent Bureau of Standards certificate. These cells were contained in insulating boxes and corrected for temperature variations.

It was found that the careful control of the solenoid current permitted sufficient resolution to show all the lines as close doublets. The separation is accounted for as due to the α_1 and α_2 components of the Mo $K\alpha$ line. Fig. 3 is a

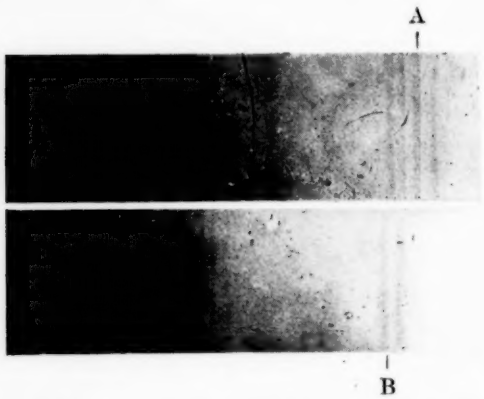

FIG. 3. Reproduction of two plates, C-3 with gold and C-7 with a silver film; A indicates position of line due to Mo $K\alpha$ − Au M_{111}; B the position of line due to Mo $K\alpha$ − Ag L_{111}.

reproduction of two of the plates. C-3 was taken with a gold and C-7 with a silver film. The arrow at A indicates the position of the line due to Mo $K\alpha$ − Au M_{111}. The arrow at B shows the position of the line due to Mo $K\alpha$ − Ag L_{111}. These lines show very plainly as close doublets on the original plates.

The plates were measured on a large comparator built by the Société Gènévoise. The instrument was checked by comparison with the decimeter standard and found to be accurate within the errors of reading. The lines were best seen by reflected light and it was found possible to place a mark in the center of the line with a fine needle point and then measure to this mark. This process gave very consistent measurements as may be seen from column 5 of Table I in which the probable error computed from 6 or more measurements on each line is given.

RESULTS

The results of all measurements on five plates are given in Table I. The values given in the last two columns have been calculated from Eq. (6). The wave-length of Mo $K\alpha_1$ (λ_K) has been taken as 0.707830A as recently determined by Compton.[22] While it is recognized that this wave-length is not known absolutely, the recent work of Tu[23] shows that it is probably a very excellent value. There is considerable variation in the data on the absorption wave-length limits (λ_L). The values chosen are taken from the more recent work and are believed to represent the most accurate data available at present.

The value of h/e was taken as 1.3737×10^{-17}. As already mentioned[20] this value is taken from an average of two h determinations by the method of the limit of the x-ray spectrum.[24] The last column of the table gives one value selected from each plate which gives what the author believes to be the best values of e/m_0 obtained from the present work. The basis of the selection was that the lines selected were the most intense and the easiest to see on the plates. The last three plates were made each in a single day, giving less opportunity for any changes due to temperature variations, and plate C-13 was washed in ice water giving less possibility for the gelatin to soften. The values from C-11 and from C-12 have, therefore, been given double weight and the value from C-13 has been given three times the weight of the first two.

Taking, then, the weighted average of the last column of Table I we obtain the value: $e/m_0=1.7570\pm0.0026\times10^7$ e.m.u. per gram in which the precision has been estimated by assuming that the data on the wave-lengths of the absorption limits is accurate to approximately 0.1 percent.

[22] A. H. Compton, Rev. Sci. Inst. **2**, 365 (1931).

[23] Y. Tu, Phys. Rev. **40**, 662 (1932).

[24] By taking the value of $h/e=1.3751\times10^{-17}$ as obtained from the work of Duane, Palmer and Yeh,[18] I obtain for the weighted mean value of e/m_0, 1.7588×10^7 e.m.u. This is in excellent agreement with the very recent value of 1.7592×10^7 given by Dunnington (Phys. Rev. **42**, 734 (1932)). (See also the preceding paper in this issue. Editor.) It also agrees closely with the value of $1.759\pm0.001\times10^7$ given by Birge in a new summary of values of e/m. Phys. Rev. **42**, 736 (1932).

TABLE I. *Data and computed values of* e/m_0.
Weighted mean of the selected values of e/m_0 is $1.7570 \pm 0.0026 \times 10^7$ e.m.u. per gram.

Plate	Line Mo K	Absorption L	Authority	Plate measurement	Hr	$e/m_0 \times 10^7$ (e.m.u.)	$e/m_0 \times 10^7$ (e.m.u.)
C-3	Au M_{I}	3603	Johnson[25]	8.0493±0.0009	402.201	1.7565	
	M_{II}			8.1918± .0017	406.240		
	M_{III}	4508	Lindberg[26]	8.3952± .0005	412.043	1.7569	1.7569
	M_{IV}	5330	Lindberg[26]	8.6183± .0008	418.439	1.7532	
	M_{V}	5529	Lindberg[26]	8.6647± .0009	419.741	1.7521	
C-7	Ag L_{I}	3247.4	V. and L.[27]	7.8663± .0003	396.960	1.7543	
	L_{III}	3690.8	V. and L.[27]	8.0972± .0002	403.537	1.7554	1.7554
C-11	Cu K	1377.7	Average[28]	8.3832± .0023	311.891	1.7581	1.7581
C-12	Pt M_{I}	3742	Johnson[25]	8.1314± .0008	404.317	1.7539	
	M_{II}	4085	Johnson[25]	8.2658± .0012	408.125	1.7556	
	M_{III}	4676	Lindberg[26]	8.4563± .0009	413.588	1.7554	1.7554
	M_{IV}	5544	Lindberg[26]	8.6658± .0004	419.565	1.7542	
	M_{V}	5746	Lindberg[26]	8.7221± .0008	421.176	1.7496	
C-13	Pt M_{I}	3742	Johnson[25]	8.1259± .0021	404.165	1.7555	
	M_{II}	4085	Johnson[25]	8.2559± .0009	407.868	1.7580	
	M_{III}	4676	Lindberg[26]	8.4470± .0010	413.318	1.7580	1.7580

It is, of course, recognized that this method cannot claim to produce an absolute value of e/m in view of the fact that the wave-lengths are taken from crystal measurements, and since it involves also a knowledge of h/e. Nevertheless, since the factor involving the crystal grating constant balances out of the equation, as suggested earlier in this paper, the value of e/m_0 obtained is believed to be quite reliable and it is of more than ordinary interest since it has been obtained by the magnetic deflection of free electrons.

In conclusion, the author wishes to express his appreciation to Professor A. H. Compton who suggested the problem and gave valuable advice, and to Dr. Elmer Dershem for much helpful counsel and assistance. It is a pleasure, also, to acknowledge the friendly interest and helpful suggestions of Professor A. J. Dempster and Professor S. K. Allison. The work of Mr. Ivar Kalberg, who constructed the standard solenoid and flip coil, is also, very much appreciated.

[25] Arthur J. M. Johnson, Phys. Rev. **34**, 7 (1929).
[26] E. Lindberg, Zeits. f. Physik **54**, 632 (1929).
[27] G. D. Van Dyke and G. A. Lindsay, Phys. Rev. **30**, 562 (1927).
[28] M. Siegbahn, *Spektroskopie der Rontgenstrahlen*, 2nd edition, page 265 (1931). The average of the last five values, which have been obtained since 1925, was taken.

The Masses of Ne^{20} and B^{11}. The Mass of Ne^{22} and the Disintegration of F^{19}.[1]

K. T. BAINBRIDGE, *Bartol Research Foundation of the Franklin Institute*

(Received January 17, 1933)

The mass of Ne^{20} measured from ten spectra is 19.9967 $\pm$0.0009. This value is outside the limit of error of Aston's measurement and an explanation for his high mass value is suggested. The mass of B^{11} was measured from two spectra as a test of the method used to determine the mass of Ne^{22}. The mass of B^{11} from these measurements is 11.0107$\pm$0.001. The mass of Ne^{22} from five spectra is 21.9947$\pm$0.0009. The maximum value for the mass of Ne^{22} is 21.9925$\pm$0.0015 calculated from Aston's value for F^{19} and from the F^{19} disintegration experiments of Chadwick and Constable. The discrepancy between the two values for the mass of Ne^{22} is discussed.

THE determination of the masses of the isotopes of certain light elements has been valuable, in conjunction with disintegration experiments, as a check on the relationship $\Delta E = c^2 \Delta m$.[2] Possible errors in the measurement of the energies of the products of disintegration, stated in terms of the equivalent mass, are in general small compared to the errors involved in the direct measurements of the masses of atoms. Accepting the equivalence of mass and energy it has been possible to obtain a value for the mass of a neutron.[3] In several cases the evidence for a particular mode of disintegration and synthesis has been clarified and reinforced.[4] The evidence from investigation of the disintegration of F^{19} by α-particle bombardment[5, 6] points to the formation of Ne^{22} by the process $F^{19}+\alpha \rightarrow Ne^{22}$ +proton. If the provisional value for the mass of Ne^{22} reported by Aston[7] is correct, the disintegration of F^{19} and the synthesis of Ne^{22} would be impossible as a result of α-particle bombardment, unless there can exist for Ne^{22} in the simplest case two distinct nuclear conformations whose mass defects differ by 0.0123 mass units, equivalent to 11.4×10^6 electron-volts.

The present work was undertaken to obtain a reliable figure for the mass of Ne^{22} to aid in the interpretation of the mode of disintegration of F^{19}. At the same time the masses of Ne^{20} and B^{11} were determined, and as the measurement of the mass of Ne^{22} to some extent is dependent upon them, these measurements will be reported first.

The Mass of Ne^{20}

The mass of Ne^{20} was measured by comparison of the position of its line on a spectrum in relation to the lines of the hydrides of carbon, oxygen and the carbon molecule C_2. Spectrum *A*, Fig. 1, shows in the upper spectrum the lines due to the ions CH_3, O^{16}, CH_4, OH_1, Cl^{35++}, OH_2, Cl^{37++}, OH_3, Ne^{20}, $Ne^{20}H$ and Ne^{21} (?), Ne^{22}, Na (?), C_2, C_2H, etc.

To a first approximation the mass scale is linear[8] so that $D+E=KM$, where D is the distance from the fiducial line to any line of mass M, and E is the distance from the fiducial line to the source. Accordingly two lines of known masses, CH_3 and C_2, or CH_3 and OH_3 are selected to solve for E and K. With E and K known the

[1] This paper was presented before the American Physical Society at the Atlantic City meeting, December 28, 1932.

[2] R. T. Birge, Phys. Rev. **37**, 841 (1931). $B^{10}+\alpha \rightarrow C^{13}$ +proton.

[3] J. Chadwick, Proc. Roy. Soc. **A136**, 701 (1932). $B^{11}+\alpha \rightarrow N^{14}$+neutron.

[4] For example Li^7+proton$\rightarrow 2\alpha$, F^{19}+proton$\rightarrow O^{16}+He^4$. J. D. Cockcroft and E. T. S. Walton, Proc. Roy. Soc. **A137**, 229 (1932).

[5] Radiations from Radioactive Substances. Rutherford, Chadwick and Ellis, p. 307. E. Rutherford and J. Chadwick, Proc. Camb. Phil. Soc. **25**, 186 (1929); J. Chadwick, J. E. R. Constable and E. C. Pollard, Proc. Roy. Soc. **A130**, 463 (1931).

[6] J. Chadwick and J. E. R. Constable, Proc. Roy. Soc. **A135**, 48 (1932).

[7] F. W. Aston, Proc. Roy. Soc. **A115**, 487 (1927).

[8] K. T. Bainbridge, Phys. Rev. **40**, 130 (1932), and a paper shortly to appear in the Journal of the Franklin Institute.

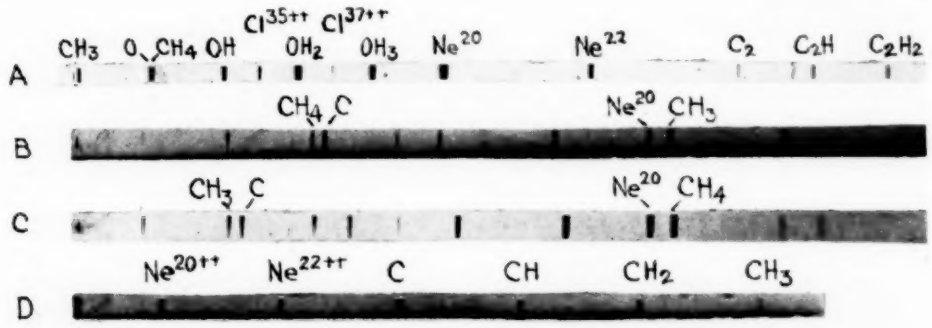

FIG. 1. Mass-spectra of Ne^{20} and Ne^{22}. Natural size.

masses corresponding to all the other lines are evaluated. The deviation of the mass scale from absolute linearity is easily found by comparison of the positions of the known masses CH, CH_2, CH_3, CH_4, OH, OH_2, OH_3, C_2H, C_2H_2 with their positions as calculated under the assumption of strict linearity. The mass of any intermediate line, such as Ne^{20}, may be derived from the position of the line *E*, *K*, and the correction curve. The deviations from linearity range from one part in 10,000 over the first 8 cm of the plate to 10 parts in 10,000 near the other extremity of the plate.

TABLE I. *Mass determinations of* Ne^{20}.

19.99792	19.99672
19.99292	19.99619
20.00154	19.99370
20.00081	19.99444
19.99600	19.99686

Table I lists the measurements of the mass of Ne^{20} from ten different spectra taken on five different plates. The mass[9] of Ne^{20} is 19.9967 $\pm$0.0009 referred to O^{16}, a value much lower than the 20.0004$\pm$0.0007 reported by Aston[7] and outside of the confines of his limit of error, $\pm$0.002 mass units. The probable error in the present determination is $\pm$0.0006. When the effective proportional uncertainty in the mass of C^{12} is included, the probable error of the mass of Ne^{20} referred to O^{16} becomes $\pm$0.0009.

It is suggested that the high value of the mass of Ne^{20} obtained by Aston may be traced to the experimental conditions. The ratio Ne^{20} : O was evaluated in terms of the ratio CH_3 : C. Under the conditions of the experiment CH_4 may have been present in an abundance very nearly equal to that of O.[10] If the O$-$$CH_4$ doublet was in the region of lowest dispersion, or if the resolving power of the apparatus was below par at the time, the Kostinsky and related effects[11] might tend to increase the separation of the O$-$$CH_4$ traces and in consequence depress the position of the O trace and so raise the Ne : O ratio. This hypothesis should be easy to test if the ratios Ne : CH_4 :: CH_3 : C or Ne : CH_3 :: CH_4 : C are used with the oxygen line weak or absent.[12] Spectra *B* and *C*, Fig. 1, are of this type. To account for the difference between the present value of the mass of Ne^{20} and that reported by Aston would only require a shift in the position of O, because of the Kostinsky or other effects of about 0.005 cm.[13]

Aston[7] measured the mass of A^{40} by means of the ratios A^{++} : O^+ :: CH_3^+ : C^+, a method identical with that used for Ne^{20}; accordingly the

[9] All mass values refer to the masses of neutral atoms.

[10] In general CH_4 is admitted to a discharge tube, and the lines C, CH, CH_2, CH_3, CH_4 appear in approximately equal abundance.

[11] F. E. Ross, Atrophys. J. **53**, 349 (1921).

[12] If the suggested ratios are used a loss in accuracy results because the mass of Ne^{20} no longer is compared with O^{16}. The mass of CH_4 however has been accurately determined (reference 7) and it constitutes a valuable secondary standard of mass.

[13] Two serious objections exist which militate against the Kostinsky effect *per se* as the correct explanation. First, the density of the O$-$$CH_4$ traces, in the absence of any direct statement, may be assumed to be low, and the Kostinsky effect only attains an appreciable magnitude for high photographic densities. Secondly, it is possible that ethane was used to provide the CH_2 and C lines which would reduce the amount of CH_4 present in the discharge below that which would be present if methane had been used to give the lines C and CH_3.

argon determination might also be in error. The writer made a rough check of the ratio of the masses of A^{40} and Ne^{20} by direct comparison on two adjacent spectra. For the first exposure the discharge tube contained only argon and nitrogen and the lines due to A^{++} and the nitrogen molecule were recorded. Immediately following this exposure the argon was pumped out and the tube was washed out with neon, before admitting a mixture of neon and nitrogen. On an adjacent strip of the recording photographic plate the lines due to Ne^{20}, $Ne^{20}H$, Ne^{22} and $Ne^{22}H$ and the nitrogen molecule were then recorded.[14] The mass of A^{40} was determined provisionally as 39.9724 evaluated in terms of $Ne^{20}=19.9967$. On the basis of this measurement we may say that whatever error appeared in the measurement of the mass of Ne^{20} when the ratios $Ne^{20}:O::CH_3:C$ were used by Aston did not occur in the evaluation of the mass of A^{40} from the similar ratios $A^{40++}:O^{+}::CH_3^{+}:C^{+}$. The close agreement of the value 39.9724 with Aston's value 39.971 may be fortuitous to some extent as the error in a single determination of this type may be as great as one part in 10,000. Even if an error of this magnitude were present, however, it could not invalidate the argument that the present value of the mass of Ne^{20} and Aston's value of the mass of A^{40} are more consistent than are Aston's values for the masses of Ne^{20} and A^{40}.

Mass of B^{11}

A rough determination of the mass of B^{11} was made as a test of the method which was planned for use with Ne^{22++}. Out of 18 spectra taken, with BCl_3 and CH_4 in the discharge tube, two spectra in which the B^{11+} line was photographed together with the lines of the ions C, CH_1, CH_2, CH_3, were suitable for measurement. The latter lines gave the values of E and K in the relationship $D+E=KM$. Then the mass of B^{11+} was evaluated from this equation by substitution of D, the distance from the B^{11+} line to the fiducial line. The two measurements gave for the mass of the neutral B^{11} atom, 11.0098 and 11.0117 or a mean value 11.010_{75}. Aston[7] has reported the value 11.0110 ± 0.0005 from a more extended and exact series of measurements.

Mass of Ne^{22}

Doubly ionized Ne^{22} was compared with Ne^{20++} and C^{+} and its hydrides on five spectra on five different plates of which spectrum D, Fig. 1 is an example. The values obtained were, 21.99468, 21.99583, 21.99309, 21.99488 and 21.99518. The average value is 21.99473 with a probable error[15] in the determination of ±0.00033. On the O^{16} scale $Ne^{22}=21.9947\pm0.0009$ when the effective proportional probable errors of the reference masses are included. Aston[7] has reported the provisional value 22.0048 for Ne^{22} measured in relation to Ne^{20} using the approximate ratios $Ne^{22}:Ne^{20}::CH:C$.

The Mass of Ne^{22} and the Disintegration of F^{19}

The mass of Ne^{22} is 21.9925 ± 0.0015 calculated from the F^{19} disintegration experiments of Chadwick and Constable.[6, 16] $F^{19}+\alpha+E_\alpha+e\rightarrow Ne^{22}+\rho+E_\rho+E_n$ where α, e, and ρ are the masses of an α-particle, electron, and proton respectively, E_α, E_ρ, and E_n are the kinetic energies of the α-particle, proton and the residual nucleus. This

[14] This method of measurement is one which appears to be peculiarly suited for the spectrographs of the type described by W. R. Smythe, Phys. Rev. **28**, 1275 (1926) and by J. Mattauch, Phys. Zeits. **33**, 899 (1932).

[15] The probable error was calculated on the basis of a theory of errors for small samples. H. Jeffreys, Proc. Roy. Soc. **A138**, 48 (1932).

[16] The calculation of the mass of Ne^{22} from the F^{19} disintegration experiments has been given using earlier and less exact data for the proton and α-particle energies and omitting the kinetic energy of the Ne^{22} nucleus. (Reference 5.) The present calculation has been made on the basis $F^{19}=19.0000\pm0.00127$, $He=4.00216\pm0.00013$ (Aston, reference 7), $H^1=1.007775\pm0.000035$ (Bainbridge, Phys. Rev. **43**, 103 (1933), mass of electron 0.000548 (Birge, Phys. Rev. Supplement **1**, 1 (1929)), energy of incident α-particle 5.25×10^6 $e-$volts $=0.00564$ mass units, energy of proton of 56 cm range and velocity 3.58×10^9 cm/sec. $=6.82\times10^6$ e-volts $=0.00732$ mass units, all masses referred to the O^{16} scale. The velocity-range data for protons has been given by P. M. S. Blackett, Proc. Roy. Soc. **A135**, 132 (1932).

The kinetic energy of the nucleus was calculated under the assumption that the protons, which had been measured in the forward direction, were, on the average, emitted at 10° from the direction of the projected track of the incident α-particle. Under this assumption the kinetic energy of the nucleus is 0.192×10^6 e-volts $=0.00021$ mass units.

equation does not include the possible loss in mass by γ-ray emission from the residual nucleus and assumes that both the proton before and the α-particle after disintegration occupy the ground states in their respective nuclei.

If the 2×10^6 *e*-volt quanta observed by Webster[17] are attributed to Ne^{22} the mass 21.9925 must be decreased to 21.9903. Consequently on the basis of the disintegration experiments and the mass of F^{19} the mass of Ne^{22} cannot exceed 21.9925 ± 0.0015 and the agreement with the mass-spectrograph value 21.9947 ± 0.0009 is unsatisfactory. Other possible modes of disintegration of F^{19} are eliminated for various reasons.[18]

An explanation which has the benefit of being consistent with the chemical data is that the mass-spectrograph value[7, 19] for the mass of F^{19} is too low by approximately 0.0022 mass units. Moles and Batuecas[20, 21] determined the molecular weight of methyl fluoride as 34.025. If the accepted values 12.0025 and 1.00777 are used for the atomic weights of carbon and hydrogen, the atomic weight of fluorine on the chemical scale is 18.999_2. The mass of F^{19} on the O^{16} scale, assuming no other isotopes, is $19.0034\pm.005$. This is to be compared with the minimum value for the mass of F^{19}, 19.0022, if the disintegration experiments on F^{19} and the present mass-spectrograph determination of the mass of Ne^{22} are taken to be correct.

In conclusion the writer wishes to thank Dr. A. Bramley for his interest and helpful discussions and to thank Professor John A. Miller and the members of the Swarthmore College Observatory for their generous permission to use their measuring instruments.

Note added in proof: The faint lines of mass 17 in spectra *B* and *C*, Fig. 1, are definitely CH_5^+ lines as determined by accurate mass measurements. CH_5^+ only appears rarely and the conditions essential to its formation are not known.

---

[17] H. C. Webster, Proc. Roy. Soc. **A136**, 428 (1932).

[18] Other possible modes of disintegration of F^{19} are:

1. $F^{19}+\alpha\rightarrow\alpha+p+O^{18}$
2. $F^{19}+\alpha\rightarrow\alpha+n+p+O^{17}$
3. $F^{19}+\alpha\rightarrow\alpha+H^2+O^{17}$
4. $F^{19}+\alpha\rightarrow n+p+Ne^{21}$
5. $F^{19}+\alpha\rightarrow H^2+Ne^{21}$
6. $F^{19}+\alpha\rightarrow n+Na^{22}$
7. $F^{19}+\alpha\rightarrow Na^{23}$

From considerations of the masses and energies involved numbers 1, 2, 3, 4 and 5 may be ruled out. 6 is possible but bears no relation to the observations of Chadwick and Constable (reference 6). The possibility of neutron emission is not definitely ruled out (J. Chadwick, Proc. Roy. Soc. **136**, 705 (1932)) but the observed scarcity of Na^{22} indicates that Na^{22} may be unstable and may not exist (K. Bainbridge, J. Frank. Inst. **212**, 336, 1931). 7 is incompatible with the γ-emission experiments of H. C. Webster (reference 15).

[19] Aston compared the mass of fluorine with that of carbon by means of the progression $C : CH_3 : F : C_2$. The limit of error for carbon was given as ±0.0012 mass units or one part in 10,000. The limit of error of the fluorine determination was also given as one part in 10,000 which, as the mass of fluorine was determined in terms of carbon and hydrogen, does not allow for any error in the fluorine determination itself. Assuming equal accuracy in the fluorine determination the limit of error becomes ±0.0038 instead of ±0.0019 mass units as given by Aston and the probable error is ±0.00127, under the usual convention. If probable errors alone are dealt with, the p.e. in the mass of F^{19} is $(2)^{\frac{1}{2}}(19/30{,}000)=\pm0.0009$. In view of the uncertainty in the mass of F^{19} the value ±0.00127 is indicated.

[20] E. Moles and T. Batuecas, J. Chim. Phys. **18**, 353 (1920). The data used by R. T. Birge, Phys. Rev. **37**, 1669 (1931). was taken from the first paper of Moles and Batuecas, J. Chim. Phys. **17**, 539 (1919).

[21] H. S. Patterson, R. Whytlaw-Gray and W. Cawood, give several reasons for not accepting the results of Moles and Batuecas. It appears however that Patterson, Whytlaw-Gray and Cawood were troubled by systematic errors as their value for the mass of carbon 12.010, derived from the density of ethylene, is high compared to the accepted value 12.0025 and their value for methyl fluoride may also be high in the ratio 28.05108 : 28.03608 or $(\mathbf{C}\,H_2)_2 : (C\,H_2)_2$ where **C** is 12.010 and C is the accepted value 12.0025. Assuming that systematic errors were present of the magnitude indicated above and no other isotopes are present the mass of F^{19}, is 19.0022 on the chemical scale or 19.0064 on the O^{16} scale when the measured molecular weight of FCH_3 is reduced from 34.046 to 34.028 by multiplication by the conversion factor $(CH_2)_2 : (\mathbf{C}\,H_2)_2$.

Thermionic and Adsorption Characteristics of Thorium on Tungsten

WALTER H. BRATTAIN AND JOSEPH A. BECKER, *Bell Telephone Laboratories*

(Received January 19, 1933)

Variation of thermionic emission of tungsten with surface density of adsorbed thorium.—Thorium was deposited on a tungsten ribbon by evaporation from a thorium wire. A study was made of the dependence of the thermionic emission on the two parameters: T, the temperature, and f, a quantity which is proportional to the amount of thorium on the tungsten surface. At a fixed temperature 1274°K it was found that as the amount of thorium on the tungsten surface was increased, the thermionic emission increased to a maximum, then decreased, and asymptotically approached a constant value. For the maximum, f is defined to be 1.0. The maximum value and the final constant value of the emission current were respectively 5.7×10^5 and 5.7×10^4 times the value of emission current characteristic of clean tungsten. Moreover the final constant value of the emission agreed to within a factor of 2 with the value characteristic of clean thorium. From $f=0.0$ to $f=0.8$ the relation between the emission current and f satisfied the following empirical equation

$$\log_{10} i = -3.14 - 6.54\, \epsilon^{-2.38f},$$

where i is the emission current in amperes per cm². For $0.8<f<2.0$, the values of emission currents are tabulated. For any fixed f, the emission obeys Richardson's equation. All the Richardson lines for $0<f<1$ intersect in a common point at an extrapolated temperature of 12,500°K, and for $f\geq1$ the lines intersect in a common point for which the temperature is 3250°K. These results obtained by depositing thorium on a tungsten ribbon have been compared with results obtained from thoriated tungsten wire. Thoriated tungsten wire can be activated by diffusion of thorium from the interior to the surface. For a while every atom that diffuses to the surface sticks to it so that f increases linearly with the time; later when evaporation is no longer negligible the rate of accumulation, df/dt, gets less and less; a steady state is reached when the diffusion rate equals the evaporation rate. It is unnecessary to assume "induced evaporation" to explain these results.

Variation of emission from thoriated tungsten with applied field.—It was found that for both the ribbon and the thoriated tungsten wire the dependence of emission on applied field changed as f was varied. For the thoriated tungsten wire the dependence of the thermionic constants A and b on applied field was most pronounced for $0.3<f<0.6$.

Evaporation and migration of thorium on tungsten surface.—Evaporation and migration of thorium on the tungsten surface were studied. The evaporation rate depends on the temperature and the fraction of the surface covered (f). For $0.2<f<1.0$ the rate of evaporation is approximately an exponential function of f. At 2200°K and $f=0.2$ the rate of evaporation was 10^{-4} layers/sec. and at $f=0.8$ was 31×10^{-4} layers/sec. It was found that thorium could be deposited on one side of the tungsten ribbon and then made to migrate to the other side of the ribbon. This migration occurred at an appreciable rate above 1500°K and was not complicated by evaporation up to 1655°K. It was found that the migration coefficient depended on f as well as on T. For a given set of conditions an approximate value of the heat of migration was calculated to be 110,000 calories per mol.

INTRODUCTION

THE saturated electron emission per unit area from a clean tungsten surface is a function of two variables, the absolute temperature and the applied field tending to pull the electrons away from the tungsten. When the tungsten surface is covered with one or two layers of foreign material the electron emission depends also on the amount and nature of foreign material. Thorium on tungsten is an example of such a case.

Langmuir[1] investigated the electron emission from thoriated tungsten filaments. He determined the activity[2] as a function of the time of flashing the filament at some activating temperature between 1800°K and 2200°K. His results are expressed in terms of a parameter θ which he defined as the fraction of the surface covered with thorium. Actually, however, all of his numerical values of θ are based on a theoretical formula which states that the logarithm of the electron emission from the surface varies linearly with θ. Dushman and Ewald[3] made a determi-

[1] Langmuir, Phys. Rev. 4, 544 (1914) and 22, 357 (1923).

[2] Saturated electron emission current per sq. cm at a particular temperature.

[3] Dushman and Ewald, Phys. Rev. 29, 857 (1927).

nation of log i as a function of the absolute temperature for various activities of the thoriated tungsten wire. In both cases the thorium was brought to the tungsten surface by diffusion from the interior.

A more direct method of studying this problem is to deposit thorium on a tungsten ribbon by evaporation from a filament of pure thorium. This method has two distinct advantages. The first is that the amount of thorium deposited on the side of the ribbon towards the thorium wire is proportional to the time of evaporation at a fixed temperature. The second is that the amount of thorium that can be deposited on the tungsten is not limited to about one layer. This method of deposition of thorium on tungsten has been used in this investigation.

Experimental Procedure

The procedure followed can be outlined in the following manner. The dependence of the activity on the amount of thorium on the tungsten surface was determined. This was done for a particular temperature of the surface and for a given applied field. Then the activity was determined as a function of the temperature for various amounts of thorium on the surface and for the same value of the applied field. This much was sufficient to determine the activity as a function of the two parameters, temperature and amount on the surface. The relation between the activity and the amount on the surface was then used to study changes in the amount of thorium on the tungsten ribbon caused by flashing the tungsten ribbon at given temperatures. This treatment can cause migration from one side of the tungsten ribbon to the other, diffusion into the tungsten or evaporation from the tungsten surface.

Three similar tubes were used in this work. The essential features of one of the tubes are shown in Fig. 1. A tungsten ribbon filament B was mounted in the axis of the tube. In the plane of the ribbon were two shields S. On both sides of this plane, sectored cylindrical collectors were placed. The side view indicates that each collector was divided into three sections, two end collectors and a central one. A thorium wire,[4] A, was mounted on one side of and parallel to the tungsten ribbon. On the other side a 4-mil thoriated tungsten wire, C, was mounted. Four auxiliary 4-mil thoriated tungsten filaments were mounted on the outside for outgassing and clean-up purposes. Except for the filaments, the platinum leads in the press and molybdenum

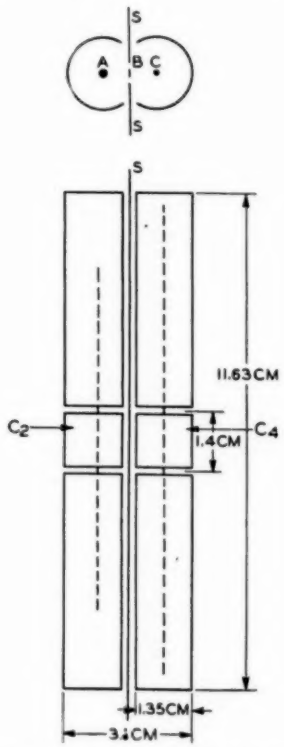

Fig. 1. Simplified diagram of filaments and plates. A, 0.038 cm, thorium wire, 7.9 cm long; B, 0.035 x 0.0036 x 11.1 cm, tungsten ribbon; C, 0.01 cm, thoriated tungsten wire; S, nickel shields; distance $AB=0.635$ cm.

springs to keep the filaments taut, the parts were constructed of preglowed nickel. An ionization manometer was sealed onto the side of the tube.

The design was based on the following considerations. A tungsten ribbon was used in order that the thorium could be deposited *uniformly* on a definite portion of the tungsten surface. It was essential to design the tube so that the electron emission from the two sides of the tungsten ribbon could be separated. This was the purpose of the shields. The central collectors C_2 and C_4 made it possible to measure the emission from a small central portion of the tungsten ribbon. This served two purposes. It reduced the effect of temperature variation along the ribbon

[4] We are indebted to the Westinghouse Lamp Company for this wire

due to end cooling and also reduced the effects due to non-uniform deposition of thorium along the length of the tungsten ribbon.

The emission from the tungsten ribbon was measured by maintaining the potential of all the plates positive with respect to the ribbon. Different applied potentials on the shields were tried. All of the readings used were taken with the shields at the same potential as the plates.

The temperature of the tungsten ribbon was determined as a function of the heating current by sighting on the ribbon with a Siemens and Halske optical pyrometer. Correction was made for the absorption of the glass wall of the tube. The true temperature was determined from the brightness temperature by using the known values[5] of spectral emissivity for tungsten. A temperature scale for the ribbon can also be determined from the tables given by Langmuir and Jones.[6] These two temperature scales agreed to within 10°, for the range 1200°K to 2000°K. Below 1200°K, Langmuir and Jones' table, because of end cooling, was not applicable.

Preliminary Treatment of Tubes

Each tube was thoroughly treated on the pumps for three days and sealed off at a pressure of 10^{-6} mm of mercury. During seal-off all the plates in the tube were kept hot (barely visible), by electron bombardment from the auxiliary filaments.

After a tube was sealed off, it was cleaned up by glowing the auxiliary filaments at 2500°K until the pressure was less than 10^{-8} mm of mercury. During this process a small current was drawn from these filaments to ionize the atoms of the residual gas. The other filaments were flashed from time to time to clean their surfaces and to condition them. The approximate value of the final pressure obtained was 5×10^{-9} mm of mercury. The final working condition of the tubes was such that any and all of the filaments could be moderately heated without affecting the pressure reading on the manometer. Severe heating of a filament, such as glowing the tungsten ribbon at 2800°K however, always caused a small temporary increase in pressure.

At first the surface of the thorium wire was not clean and consequently the material evaporating from it was not pure thorium. Hence it was necessary to clean the surface of the thorium filament during the clean-up process. This could not be accomplished on the pumps because, at pressures from 10^{-7} to 10^{-6} mm of mercury, glowing the thorium filament caused it to take up gas. It was only at pressures of 10^{-7} or better that this effect ceased to be appreciable. The thorium wire could not be cleaned quickly because parts of it became clean before the rest. The clean parts had a lower emissivity than the others and consequently a higher temperature and a faster rate of evaporation. If therefore, the filament was run at too high an average temperature the increased evaporation from the clean parts reduced the size of the filament in spots. This effect would have rendered the filament useless. It was found that the filament could be got to a uniformly clean state by heating it at a low enough temperature for a long enough time (1000 hr. or more).

The effect of the material which evaporated from the thorium wire on the activity of the side of the tungsten ribbon towards the wire was studied. This was accomplished in the following manner. The tungsten was first flashed at 2800°K to clean it. Then the thorium wire was glowed for definite successive intervals. After each interval the activity of the tungsten ribbon was measured at some low testing temperature.

It was found that the results of successive tests of this kind changed continuously as the thorium wire was being cleaned off. At first, the deposited material decreased the activity of the tungsten; later it increased the activity up to some limiting value. Still later, a stage was reached where the deposited material first increased the activity to some peak value, and then decreased it.

At this stage another type of test was made. After a certain amount of material had been deposited on the tungsten, it was then removed slowly by glowing the tungsten ribbon at moderately high temperatures. The changes in activity during this removal process were followed. It was found that if the deposition had been carried to a stage where the activity passed through a peak, the activity on removal went back through a peak. Furthermore, the heights

[5] Worthing and Forsythe, Astrophys. J. **61**, 146 (1925).
[6] Langmuir and Jones, Gen. Elec. Rev. **30**, 310 (1927).

of the peaks on successive removal tests were always approximately the same. At first the height of the peak on deposition was somewhat less than the height on removal. For each successive test the peak on deposition increased until finally it was somewhat higher than the peak on removal. As the treatment of the thorium wire progressed still further the peak on deposition decreased and approached a height approximately equal to the height on removal. It was also found that at first the rate of removal of the deposited material, as determined by the rate of change of activity, decreased with successive tests. Finally a stage was reached where the rate of removal was much smaller than at first but did not change for successive tests.

These results were interpreted in the following manner. At first the material coming from the thorium wire was not pure thorium. The percentage of foreign material decreased with time. The heights of peaks on deposition and the rates of removal were affected by the percentage of foreign material deposited. On removal, most of the foreign material evaporated at low temperatures and the height of the peak was approximately characteristic of pure thorium on tungsten. As the percentage of foreign material becomes negligible, the height of the deposition peak and the rate of removal approach values characteristic of pure thorium.

It was essential that the rate of deposition of thorium on different parts of the front surface of the ribbon be approximately the same. The effects of non-uniform deposition on the tungsten ribbon could be studied by noting the differences in activity of the ribbon as measured by the current to the different collectors. When only one or two spots on the thorium wire were clean, this effect was of course quite large. However, as the thorium wire was cleaned off, this effect decreased.

In each of the three tubes used, the object was to carry these preliminary treatments to the stage where the results for successive runs were consistent and did not change with continued aging of the tube. Actually this ideal stage was not reached in all cases. Filaments will break or burn out, especially thorium filaments. However, the ideal conditions were approximately reached in two of the tubes and the experimental data upon which the following analysis is based were all taken under conditions in which the various spurious effects described above were at least minimized and the ideal stage approximately reached.

Experimental Results on Tungsten Ribbon

The first problem was to determine from the experimental data how i, the electron emission in amperes per cm^2, measured at a fixed temperature (1274°K) and fixed applied field varies with the amount of thorium on the tungsten surface. Since i varies by such large factors, it is convenient to use log i rather than i. It was found that log i passed through a maximum as t, the time of glowing the thorium wire, progressed. Let t_m be the time required for log i to reach this maximum. As was to be expected, t_m decreased rapidly as the glowing temperature for the thorium wire increased. Furthermore it was found that if t/t_m was plotted in place of t, the results of various tests in which the thorium wire was glowed at different temperatures, could all be represented by a single curve. It is obvious that the maximum activity occurs at some critical, definite and reproducible amount of thorium on the surface of the tungsten, and that any amount on the surface can be expressed in terms of the amount corresponding to the maximum activity. We will therefore define a quantity f by the equation $f=t/t_m$. f is a measure of the amount of thorium on the tungsten surface. All of our results will be expressed in terms of f.

If the peak activity occurs at the time when just one layer of thorium atoms has been deposited on the tungsten ribbon, then f, as defined, is equal to the fraction of the surface covered or the number of layers on the surface of the tungsten ribbon. There is some evidence[7] that this is the case for caesium on tungsten. If subsequent work should definitely establish that the peak activity does not quite correspond to one layer, it will nevertheless be desirable to express amounts on the surface in terms of f because this quantity can be determined easily and precisely. Furthermore whenever the amount on the surface corresponding to the peak activity

[7] Becker, Phys. Rev. **28**, 341 (1926).

is determined, f can very readily be converted to number of layers or number of atoms.

In order to determine the relation between log i and f, experimental values of log (i/i_m) were plotted against t/t_m. The plot was made for log (i/i_m), rather than log i, in order to compensate for small differences in the value of log i at the peak for different runs. Log i was determined by measuring the current to the central collector (C_2) on the side of the tungsten ribbon towards the thorium wire. This current was usually measured when the tungsten ribbon was maintained at a temperature of 1274°K. Measurements of i were made after each successive interval of glowing the thorium wire at a fixed temperature.

Fig. 2 is a plot of log (i/i_m) *vs.* t/t_m or f for several runs, taken after the thorium wire had reached a condition where the evaporation from the central part of the thorium wire was fairly uniform and the indications were that the peak on deposition was the same as the peak on removal.

The value of log (i/i_m) at $f=0$ was obtained by extrapolating a log $i-2$ log T *vs.* $1/T$ plot for the clean tungsten ribbon to $1/T=1/1274$. The values for log (i/i_m) for small f were not very accurate as the currents were small and almost at the limit of sensitivity of the galvanometer used. Beyond the peak the different runs diverge somewhat probably because of the different effects of non-uniformities on different runs.

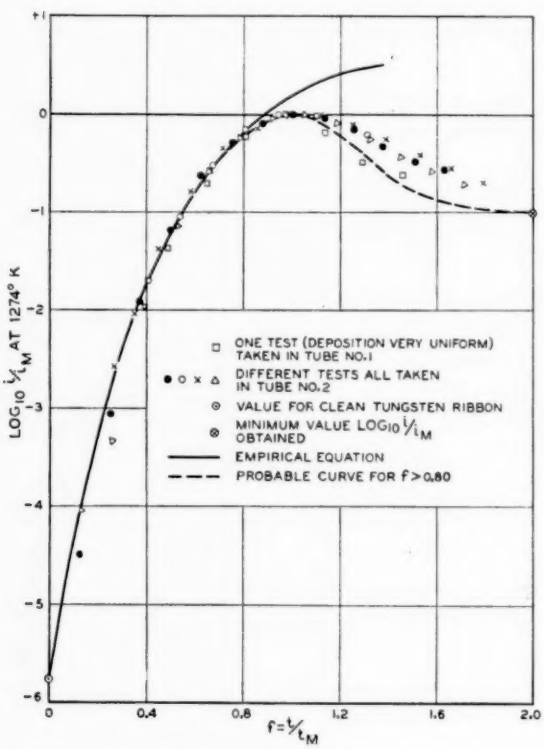

FIG. 2. The thermionic activity of the tungsten ribbon *vs.* the time of deposition from the thorium wire.

In order that the amount of thorium deposited on the ribbon be proportional to the time t, it is necessary that the evaporation rate from the thorium wire remain constant, and that no appreciable migration, evaporation or diffusion occur on the tungsten ribbon at the testing temperature. The first requirement was repeatedly tested and found to be satisfied. It was also found that the ribbon could be maintained at 1274°K for indefinite periods of time without changing the activity of the ribbon. Some tests were made by depositing the thorium on the ribbon while the ribbon was at room temperature. The ribbon was raised to 1274°K only for the short times necessary to test the activity. Other tests were made by maintaining the tungsten ribbon at 1274°K all the time. If appreciable migration, diffusion, or evaporation took place at 1274°K the resulting log i *vs.* time curves should have had different shapes. This, however, was not the case. Hence, the amount accumulated is proportional to t and likewise proportional to f.

It is to be noted here that log (i/i_m) is evidently not a linear function of f between $f=0$ and 1, and therefore log i is not a linear function of the amount of thorium on the tungsten surface.

For the case of barium on tungsten, Becker[8] found a log i *vs.* f curve very similar to that in Fig. 2. The relation between log i and f, for f from 0 to 0.8 or 0.9, was found to obey an empirical equation of the form

$$\log i = \log i_w + a(1-\epsilon^{-cf}), \qquad (1)$$

where a and c are constants, and i_w is the current from clean tungsten.

If this form of equation holds for Fig. 2, then we should have the following relation

$$\log (i/i_m) = \log (i_w/i_m) + a(1-\epsilon^{-cf}). \qquad (2)$$

The values of a and c which gave the best fit

[8] Becker, Phys. Rev. **33**, 1082 (1929).

were: $a=6.54$ and $c=2.38$. While an equation of the form of (2) probably holds if the current i is measured at some other testing temperature, the values of the constants a and c may be different. This question will be considered later.

The solid curve in Fig. 2 is a plot of log (i/i_m) *vs.* f as determined by Eq. (2) and these values of the constants. With the exception of a few points for small values of f, the empirical curve fits the experimental data quite well up to $f=0.8$. Since the experimental points for $f<0.3$ are quite inaccurate, as mentioned before, it can be said that the agreement between Eq. (2) and experiment is as good as the experimental accuracy. Except for differences in the values of the constants the same empirical relation between log i and f holds for both barium and thorium on tungsten for $f<0.8$.

The values of log (i/i_m) for f greater than 1 spread considerably because of non-uniformities in the deposition of thorium on the tungsten ribbon. The differences in amount of thorium deposited on different parts of the ribbon become greater as the time of deposition increases. Hence in this part of the curve even small non-uniformities in rate of deposition have quite an effect. It was found that log (i/i_m) approached a constant value for $f>2$. This constant value is indicated on Fig. 2 at $f=2.0$. A study of the influence of non-uniform deposition shows that beyond the peak the experimental points should lie above the true curve. Therefore, knowledge of this constant value of log (i/i_m) for $f>2$ and the general trend of the deposition curve, enables one to interpolate approximately for values of log (i/i_m) between f equal to 1 and f equal to 2. One has then as shown by the curve in Fig. 2 a relation between log (i/i_m) and f for thorium on a tungsten ribbon when the ribbon is at a temperature of 1274°K.

The average value of log i_m at 1274°K was determined from the experimental data. This value was log $i_m=6.08-10$. With this value, log i at 1274°K was plotted as a function of f as shown in Fig. 3.

The next step was to determine the relation between log i and T, the temperature, for various values of f and constant applied field. A Richardson plot can be made, even though the value of f for a particular surface condition may not be known. The procedure was to determine i for various values of T and constant f and then to plot log $i-2$ log T *vs.* $1/T$. Since these Richardson plots give straight lines they can be represented by an equation of the form

$$\log i-2\log T=\log A-b/2.3\,T, \qquad (3)$$

where log A and b are the intercept and slope respectively of a Richardson plot. The values of A and b are different for each straight line and therefore depend on f. The value of f for a particular straight line can be obtained by determining log i at 1274°K and consulting the data presented in Fig. 3. If A and b as functions of f were known, then log i as a function of f and T for constant applied field would be determined. Since the relation between log i at 1274°K and f is already known it is sufficient to determine b as a function of f or of log i at 1274°K. It is then possible to draw Richardson plots for any given value of f.

The procedure adopted was to determine log i at 1274°K, as well as b, from the various experimental Richardson plots; and then to plot b *vs.*

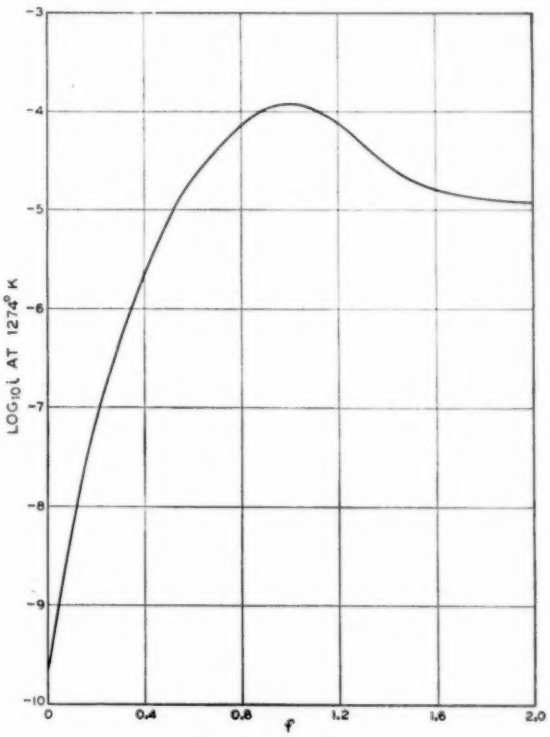

FIG. 3. Log$_{10}$ i at 1274°K *vs.* f; i expressed in amperes per sq. cm.

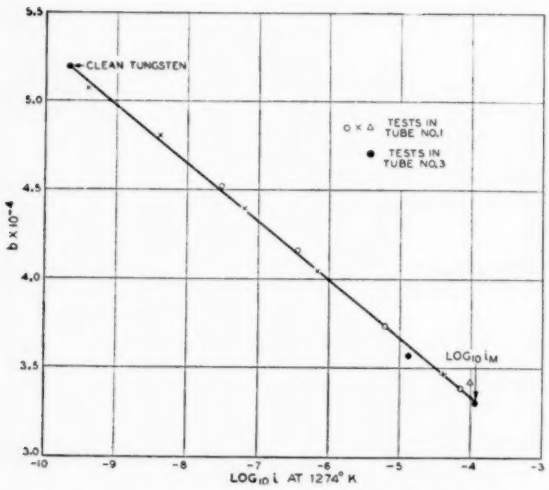

FIG. 4. b *vs.* $\log_{10} i$ at 1274°K. b is the slope of a Richardson plot in °K. i is the current in amp./cm².

$\log i$. Such a plot is shown in Fig. 4 for $f<1$. We have found such a plot advantageous because b is quite accurately a linear function of $\log i$ at 1274°K. For $f<1$, it follows that

$$b=b_w+\beta_1 \log (i/i_w)_{1274°K}, \tag{4}$$

where b_w is the value of b for the clean tungsten ribbon, and i_w is the electron emission for the clean tungsten ribbon. The symbol β_1 stands for the slope of the plot in Fig. 4 and is equal to -3.26×10^3.

It has been found that a relation can be developed between $\log (i/i_w)$ at any temperature and $\log (i/i_w)_{1274°K}$; and since $\log (i/i_w)_{1274°K}$ as a function of f is known, such a relation is the solution of this part of our problem. This relation can be developed as follows: For clean tungsten

$$\log i_w-2\log T=\log A_w-b_w/2.3T. \tag{5}$$

Subtracting Eq. (5) from (3) for a particular value of T gives

$$\log \frac{i}{i_w}=\log \frac{A}{A_w}-\frac{b-b_w}{2.3T}. \tag{6}$$

This equation is general and holds true for all values of T in the experimental temperature range. For T equal to 1274°K, substitution of $b-b_w$ from (4) into (6) gives

$$\log \frac{A}{A_w}=\left(1+\frac{\beta_1}{2.3\times1274}\right)\log\left(\frac{i}{i_w}\right)_{1274°K}. \tag{7}$$

Now by using (6) for any temperature, let us substitute values of $b-b_w$ and $\log (A/A_w)$ from (4) and (7) in (6). We have as a result

$$\log\left(\frac{i}{i_w}\right)_T=\left[1+\frac{\beta_1}{2.3}\left(\frac{1}{1274}-\frac{1}{T}\right)\right]\log\left(\frac{i}{i_w}\right)_{1274}. \tag{8}$$

This Eq. (8) gives $\log (i/i_w)$ at any temperature in terms of $\log (i/i_w)$ at 1274°K. Since (4) only holds for $f<1$ Eq. (8) is only valid for that range.

It was found that an equation of the form

$$b=b_m+\beta_2 \log (i/i_m)_{1274} \tag{9}$$

also held for $f>1$ where b_m and i_m are the values of b and i for $f=1$, and $\beta_2=-4.82\times10^3$. We can then by a similar analysis arrive at the equation

$$\log\left(\frac{i}{i_w}\right)_T=\left[1+\frac{\beta_2}{2.3}\left(\frac{1}{1274}-\frac{1}{T}\right)\right]\log\left(\frac{i}{i_w}\right)_{1274}+\frac{\beta_1-\beta_2}{2.3}\left(\frac{1}{1274}-\frac{1}{T}\right)\log\left(\frac{i_m}{i_w}\right)_{1274} \tag{10}$$

which is valid for $f>1$.

In order to use Eqs. (8) and (10) it is necessary to know the values of $\log i_w$ and $\log i_m$ at 1274°K. The value of $\log i_m$ has already been given; it is 6.08–10. The electron emission per sq. cm from the clean tungsten ribbon was determined several times. Analysis gave $b_w=5.20\times10^4$°K and $\log A_w=1.84$ or $A_w=69$ amp. per cm² per deg.². From these values, $\log i_w$ at 1274°K was computed and found to be 10.32–20. The value for b_w obtained compares quite well with the accepted value 5.24×10^4°K for clean tungsten.

An interesting consequence of Eq. (4) or Eq. (8) is that the family of Richardson lines for thorium on tungsten ($0<f<1$) all have a common intersection point. This intersection point occurs

at the value of T for which $\log (i/i_w)_T$ is equal to zero. On solving Eq. (8) for the value of T that satisfies this condition we obtain $T=12{,}500°K$. If this intersection point had occurred at a value of $1/T$ equal to zero then the values of A for all the Richardson lines would have been the same. For this to be true it would be necessary that β_1 have the value -2.93×10^3 instead of -3.26×10^3.

In a similar way it follows from Eq. (9) that for $f\geq1.0$ all Richardson lines have a common intersection point at an extrapolated temperature of 3250°K. Hence for $f\leq1.0$ all Richardson lines cross the clean tungsten line at a common point for which $1/T=8.00\times10^{-5}$ or $T=12{,}500°K$ while for $f\geq1.0$ all Richardson lines cross the line for $f=1.0$ at a common point for which $1/T=3.08\times10^{-4}$ or $T=3250°K$.

Equations (8) and (10) enable one to calculate $\log (i/i_w)$ for any value of T and f provided the relation between $\log (i/i_w)_{1274}$ and f is known. This analysis therefore has determined the activity as a function of the two independent variables, temperature and amount of thorium on the tungsten surface for constant applied field.

The validity of Eqs. (8) and (10) may be tested by using them to determine Richardson lines and comparing these with experimentally determined ones. Such a comparison for $f<1$ is shown in Fig. 5 where the points represent actual experimental determinations and the lines are determined from Eq. (8). The comparison for $f>1$ is shown in Fig. 6. It is apparent that the empirical formulae give results in good agreement with actual experimental determinations for all values of f which have been investigated. In Fig. 7 a graded series

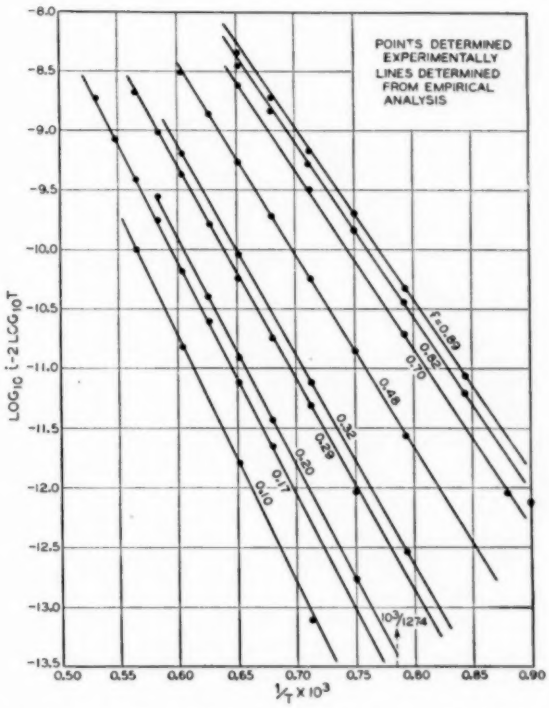

FIG. 5. Richardson plots for various amounts of thorium on tungsten; $f<1.0$.

of Richardson lines is given for f in the range 0 to 1.

For the range of f from 0 to 0.8 for which Eq. (2) holds we can substitute for $\log (i/i_w)_{1274}$ in terms of f in Eq. (8).

From Eq. (2) we have

$$\log (i/i_w)_{1274}=6.54(1-\epsilon^{-2.38f}). \tag{11}$$

Substitution of this value of $\log (i/i_w)_{1274}$ in Eq. (8) gives

$$\log\left(\frac{i}{i_w}\right)_T=6.54\left[1-1.42\times10^3\left(\frac{1}{1274}-\frac{1}{T}\right)\right](1-\epsilon^{-2.38f}). \tag{12}$$

This equation gives $\log (i/i_w)$ at any temperature in terms of f. We see therefore that $\log (i/i_w)$ at any temperature is given by an equation of the form

$$\log (i/i_w)_T=a'(1-\epsilon^{-c'f})$$

where c' is a constant equal to 2.38 while a' depends on temperature and is given by

$$a'=6.54[1-1.42\times10^3(1/1274-1/T)].$$

We will have occasion to use the expression

$$[(\log i-\log i_w)/(\log i_m-\log i_w)]_T$$

in terms of $\log (i/i_w)_{1274}$. This relation can be developed from the preceding equations and the result is

$$\left(\frac{\log i-\log i_w}{\log i_m-\log i_w}\right)_T=\frac{1}{\alpha}\log\left(\frac{i}{i_w}\right)_{1274}$$

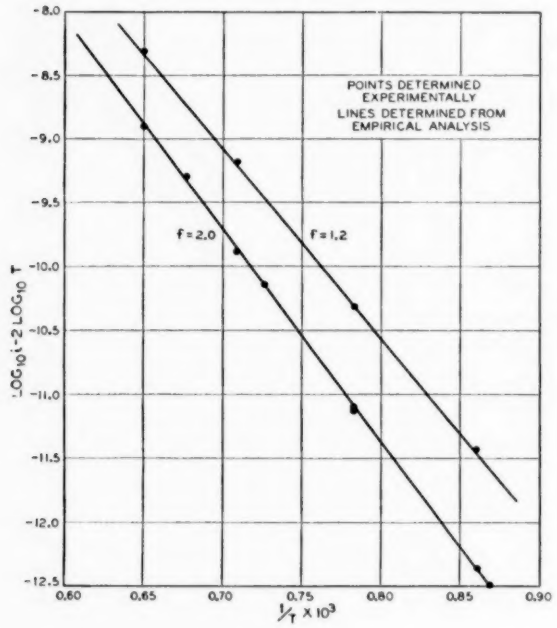

FIG. 6. Richardson plots for thorium on tungsten; $f>1.0$.

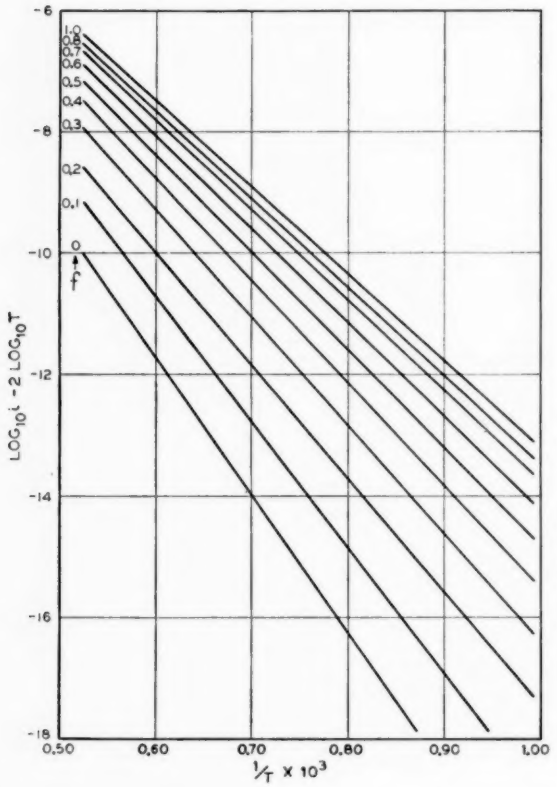

FIG. 7. A graded series of Richardson plots for $0<f<1.0$; applied potential 100 volts.

where α is $(\log i_m/i_w)_{1274}$, and is equal to 6.08–10–(10.32–20) or 5.76.

For the range of f from zero to 0.8 we have then that

$$\left(\frac{\log i-\log i_w}{\log i_m-\log i_w}\right)_T=\frac{a}{\alpha}(1-\epsilon^{-cf}), \qquad (13)$$

where $a=6.54$, $c=2.38$ and $a/\alpha=6.54/5.76=1.13$. Since a/α and c are constants independent of temperature, the function on the left side of Eq. (13) is also independent of T and the subscript T can be omitted. Let θ represent this function.

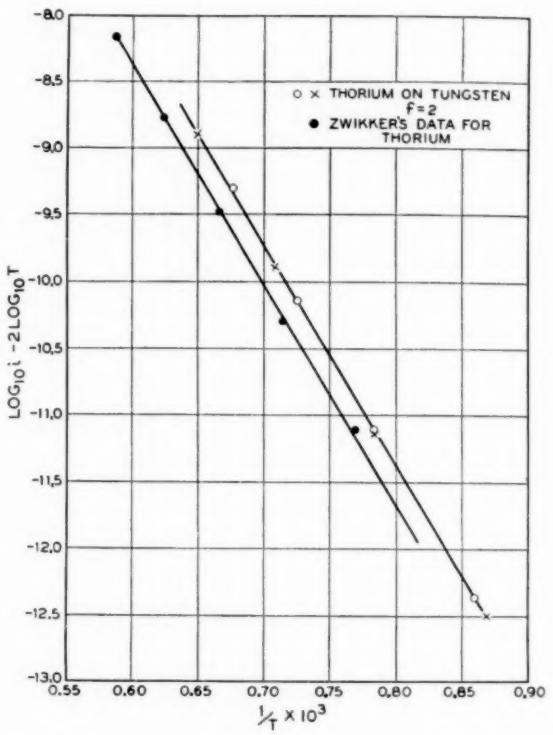

FIG. 8. Comparison of Richardson plots for thorium and for thorium on tungsten, $f=2.0$.

It is of interest to compare the values of emission from the tungsten ribbon when f is greater than 2 with the emission from clean thorium as determined by Zwikker.[9] Fig. 8 shows a plot of $\log i-2\log T$ *vs.* $1/T$ as determined for $f=2$ and as determined for clean thorium by Zwikker. While the values for $\log i-2\log T$ for f approximately 2 on the ribbon are

[9] Zwikker, Proc. Amst. Acad. Sci. **29**, 792 (1926).

a factor of 2 larger than Zwikker's values for clean thorium it is somewhat surprising that such a small amount of thorium on tungsten will give a surface whose thermionic characteristics are approximately the same as those of a clean thorium surface.

The results thus far are summed up in Table I

TABLE I. *Summary of numerical results.*

f	θ	$b\times10^{-4}$	A	log i_{1274}	log$(i/i_w)_{1274}$
0	0	5.20	69	0.32–10	0
0.1	0.24	4.75	48	1.71–10	1.39
0.2	0.43	4.39	36	2.80–10	2.48
0.3	0.58	4.11	29	3.66–10	3.34
0.4	0.70	3.89	24	4.34–10	4.02
0.5	0.79	3.71	21	4.88–10	4.56
0.6	0.86	3.58	19	5.30–10	4.98
0.7	0.92	3.46	17	5.65–10	5.33
0.8	0.97	3.39	16	5.86–10	5.54
0.9	0.99	3.34	15.6	6.02–10	5.70
1.0	1.00	3.32	15.5	6.08–10	5.76
1.2	*	3.43	20	5.87–10	5.55
1.4		3.61	37	5.46–10	5.14
1.6		3.74	53	5.20–10	4.88
1.8		3.79	61	5.11–10	4.79
2.0		3.80	65	5.07–10	4.75

* θ not defined for $f>1$.

which gives corresponding values of f, θ, b, A, $(\log i)_{1274}$ and $\log (i/i_w)_{1274}$.

Comparison with Thoriated Tungsten

It is interesting to compare these results with those obtained for thoriated tungsten wire. As Langmuir[1] has shown, thorium can be brought to the surface of a thoriated tungsten wire by diffusion from the interior. The steps in such an activation process are: The wire is first glowed at approximately 2800°K in order to reduce thorium oxide to metallic thorium and to clean the surface of the wire. The wire is quickly cooled. It is then kept at an activating temperature, 1800 to 2200°K, for various intervals of time in order to allow thorium to diffuse to the surface. After each such interval, the activity is tested by measuring the electron emission at some fixed testing temperature at which the activity does not change with time. Most of the adsorbed thorium can subsequently be removed by flashing the filament at a high temperature, such as 2600°K for a short time.

Fig. 9 gives the results of two such tests on the 4 mil thoriated tungsten wire marked C in Fig. 1. The testing temperature was 1549°K in both tests. Log (i/i_m) at 1549°K was plotted against t, the time of activation. For run 1, the activation temperature was 1940°K, and for run 2 it was 1845°K. Except for the difference in rate of activation, the curves are quite similar: Both curves go through a maximum and then approach an equilibrium activity. The equilibrium activity for the run at 1845°K was definitely lower than that at 1940°K.

From our previous results it is possible to determine for these tests how f varies with the time of activation. The curve for f *vs.* log (i/i_m) at 1549°K can be obtained from Figs. 5 and 6. Values of f for each value of log (i/i_m) corresponding to various values of t in Fig. 9, can be determined. In Fig. 10, f has been plotted against time of activation for the two runs in Fig. 9. It is seen that for some time f increases linearly with the time; then it increases more and more slowly until it approaches a constant value. The rate of increase of f with time is greater for the run at 1940°K while the final constant value approached by f is greater for the run at 1845°K. It is to be noted that f is not zero when t is zero. This is to be expected since the thoriated tungsten wire may not be completely clean at 2800°K and should activate somewhat on cooling from 2800°K.

From these results we draw the following conclusions: Thorium diffuses to the surface at a rate which is constant for a particular run; this rate depends on the activation temperature and on the amount and distribution of thorium in the tungsten. At first, the rate of evaporation of thorium from the surface is negligible, so that the amount of thorium accumulated increases linearly with time. As the surface concentration of thorium increases, the rate of evaporation increases rapidly.[10] When the evaporation becomes comparable with the diffusion rate, the rate of accumulation of thorium on the surface is no longer equal to the rate of diffusion, but gets less and less until equilibrium is reached between evaporation and diffusion. The rate of evaporation increases more rapidly with temperature

[10] It will be shown later that the rate of evaporation of thorium from a tungsten surface is an exponential function of the amount on the surface.

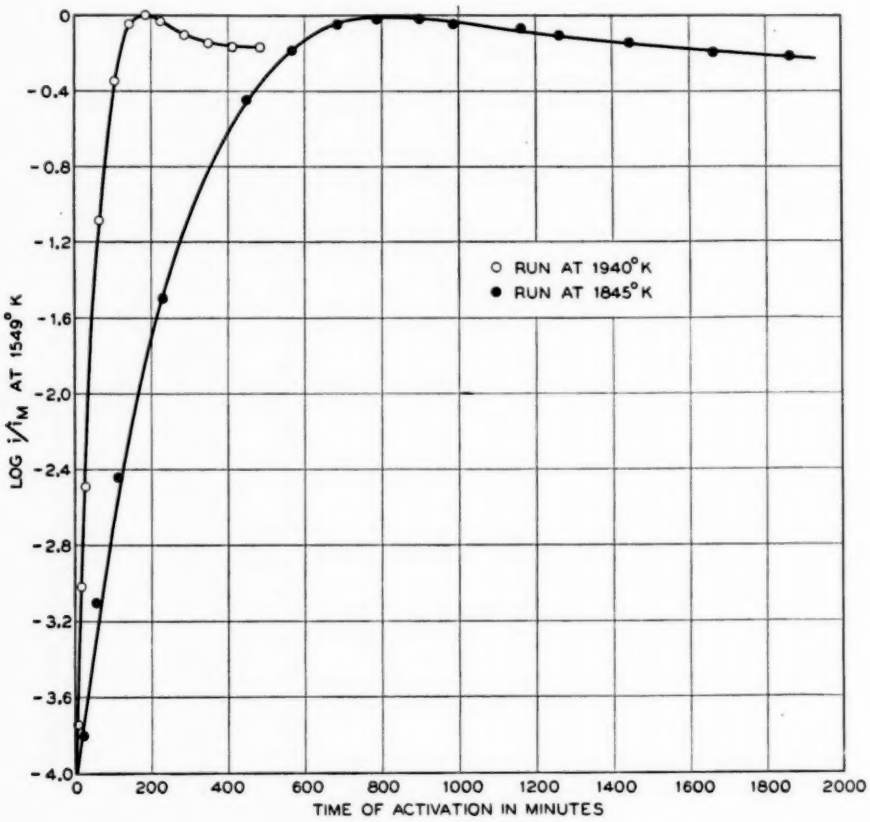

FIG. 9. Activation curves for thoriated tungsten wire.

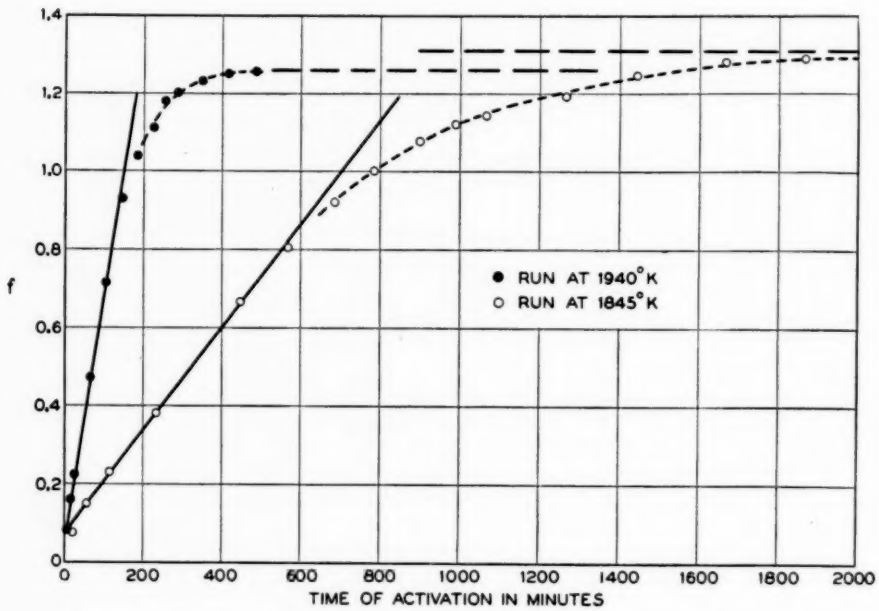

FIG. 10. f *vs.* time of activation for data shown in Fig. 9.

than the rate of diffusion, and therefore as the activation temperature increases, the equilibrium value of f decreases. Numerous subsidiary experiments showed that if the activation temperature is high enough, the equilibrium value of f is less than 1.0.

One would expect that the dependence of log i on temperature should be the same for a thoriated tungsten wire as it is for the tungsten ribbon when the value of f for the two surfaces is the same. If, therefore, we make a plot of b *vs.* log i at 1274°K from experimentally determined values for thoriated tungsten wire and compare it with the similar plot for the tungsten ribbon (Fig. 4), the two should agree. In Fig. 11, such a comparison is shown. The dashed line represents the results for the ribbon and is taken from Fig. 4. For the case of thoriated tungsten we have the plotted points determined from Dushman's[3] data and some points obtained by analyzing the data that we have taken on thoriated tungsten. While all the points obtained for thoriated tungsten lie approximately on a straight line this straight line does not quite agree with the one determined for the ribbon. In analyzing the results shown in Fig. 11 it is to be noticed that the value that Dushman determined for log i_m does not quite agree with the value we obtained for thoriated tungsten. Note the largest values of log i for which points are given from our data and Dushman's data. It was found that this difference might be explained by a difference in temperature scale as a shift in temperature scale will change the values of both log i at 1274°K and b in such a way that points still lie approximately on the same line.

This comparison shows that our results for thoriated tungsten agree with Dushman's results except for a possible difference in temperature scale and that the combined results for thoriated tungsten do not agree exactly with our results for thorium on the tungsten ribbon. Since the tungsten ribbon is different from the thoriated tungsten wire in that the wire contains thorium oxide and that as a result of this thorium oxide the wire has a much smaller crystal size it may be reasonable to suppose that the differences shown in Fig. 11 are due either to the difference in crystal size of the two filaments or to the direct effects of the presence of thorium oxide in the wire.

Comparison with Langmuir's Results

Since our work leads to an interpretation which in some respects is radically different from that of Langmuir and others who have followed his method, it seems desirable to discuss this work. In comparing Langmuir's results with our own, it is necessary to compare his θ with our f. While Langmuir[1] defines θ as "the fraction of the surface covered by thorium atoms," all of his numerical values of θ are based on a theory from which it follows that "the logarithm of the emission is a linear function of θ so that θ may be calculated from the equation[11]

$$\theta = (\log i - \log i_w)/(\log i_m - \log i_w)." \qquad (14)$$

So far as we know, no derivation of this equation has been published. Langmuir and others have, nevertheless, used this equation in the calculation of evaporation rates, diffusion rates, heats of evaporation and heats of diffusion. We have shown that this formula is not in agreement with experiment. Hence numerical quantities based on it are generally erroneous. Furthermore, it has led to certain false concepts with regard to the mechanism of adsorption.

At first sight, it might appear that Langmuir's experimental data differ from ours; but this is not the case, as can be shown in the following two ways:

Fig. 12 is a plot of f *vs.* time of activation for an activation run taken from Langmuir's data at 2000°K. For comparison, we have plotted the results of our run at 1940°K, previously shown in Fig. 10. It is seen that Langmuir's results are quite similar to our own. They differ somewhat in that the diffusion rate at 2000°K in Langmuir's case was less than the diffusion rate we obtained at a lower temperature, 1940°K; also, the equilibrium value of f in his case was 1.0 or slightly less, while in our case it was greater than 1.2. It is to be expected that the diffusion rate should depend upon the concentration of thorium in the wire and should consequently vary from one wire to the next. Since, in Langmuir's case, the rate of diffusion is less than in ours, and since the rate of evaporation is higher, because of the higher

[11] This function is the same as the left side of Eq. (13) which we have designated by θ.

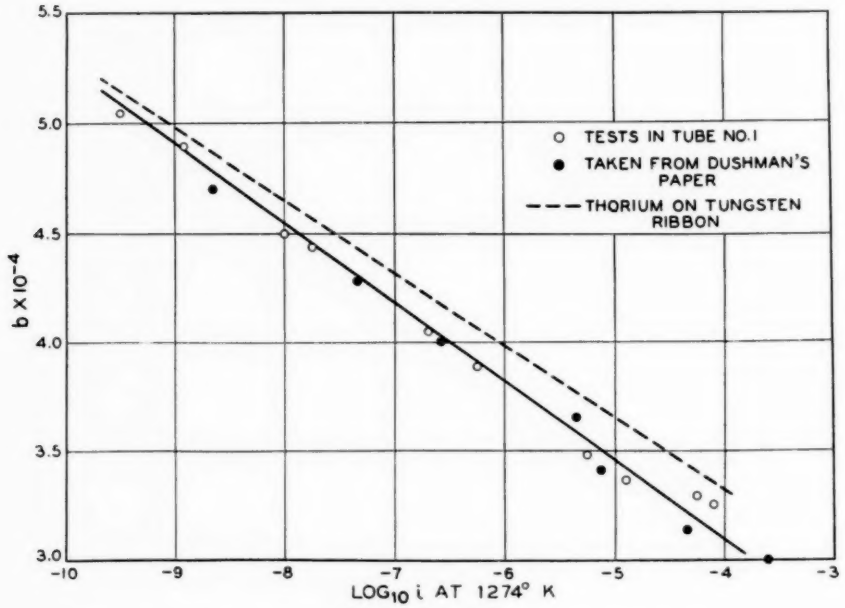

FIG. 11. b *vs.* $\log_{10} i$ at 1274; b in °K and i in amp./cm².

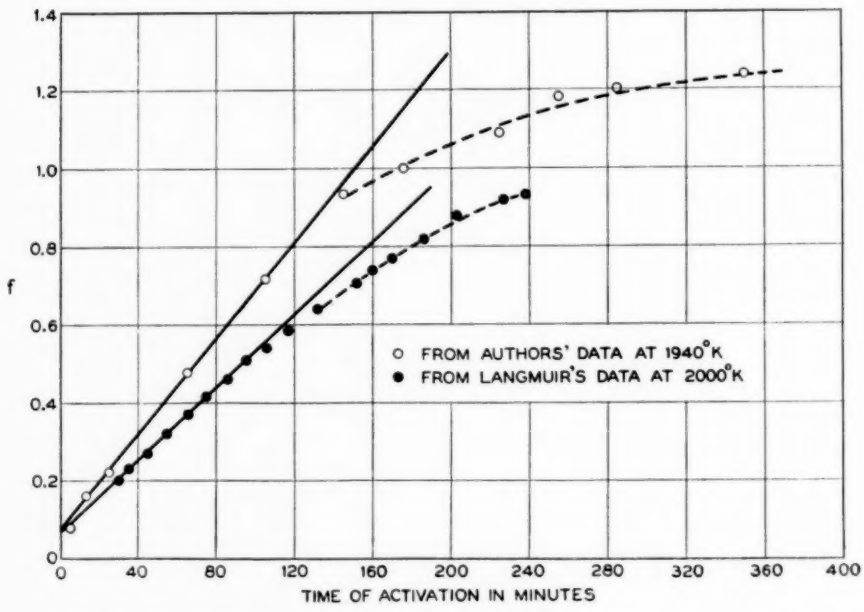

FIG. 12. f *vs.* time of activation—comparison of Langmuir's and author's data.

temperature, his equilibrium value of f should be lower; and it is.

The second proof that Langmuir's experimental results yield a log i *vs.* t curve agreeing with our own, is based on Langmuir's empirical equation[1]

$$d\theta/dt = k(1-\theta). \tag{15}$$

The solution of this differential equation is

$$\theta = 1-\epsilon^{-kt} \tag{16}$$

since $\theta = (\log i - \log i_w)/\alpha$, where $\alpha = \log i_m - \log i_w$, it follows that Langmuir's experimental results are given by the equation

$$\log i = \log i_w + \alpha(1-\epsilon^{-kt}), \qquad (17)$$

which is of the same form as our empirical Eq. (1).

It is clear then, from Langmuir's experiments as well as our own, that $\log i$ is not a linear function of t. Langmuir explains this departure from linearity by his principle of "induced evaporation," which states that whenever a thorium atom diffuses to the surface from the interior of the tungsten at a spot which is already occupied by a thorium atom, it "induces" this atom to evaporate. Consequently, the rate of accumulation of thorium should not be constant, but should be proportional to the fraction of the surface which has not yet been covered, i.e., to $(1-\theta)$. In this way, Langmuir accounted for his empirical relation given in Eq. (15) and for the nonlinearity of the $\log i$ *vs.* t curve.

In contrast with this, we believe that the principle of induced evaporation is not applicable in any case similar to thoriated tungsten, for the following two reasons. As will be shown later, thorium atoms migrate on the surface of tungsten at temperatures which are even lower than activating temperatures, and migration can be brought about without any appreciable evaporation. Consequently, if a thorium atom ever does diffuse to the surface just underneath another thorium atom, it will push this atom aside rather than "induce" it to evaporate. In other words the tendency would be for the thorium atoms to distribute themselves over the surface rather than to leave it. In the second place, Clausing[12] has shown that thorium diffusion does not occur through the tungsten lattice, but between the boundaries of the tungsten crystals. Consequently the only way in which the surface can be covered with thorium is by migration from the grain boundaries, and the rate of accumulation of thorium on the surface should not be proportional to the amount of bare surface, $(1-\theta)$. Now the only evidence presented by Langmuir for induced evaporation of thorium from tungsten is that on his view the rate of accumulation is proportional to $(1-\theta)$. Hence Clausing's work also shows that the induced evaporation hypothesis is not in accord with the experimental facts.

[12] Clausing, Physica **7**, 193 (1927).

What then is to be inferred from the nonlinearity of the $\log i$ *vs.* t, or *vs.* f, curve? We have always maintained that this nonlinearity means that the effectiveness of an individual electropositive atom in reducing the work function of the surface is not constant, but decreases as f increases.[13] This in turn must mean that the fraction of the adsorbed thorium which is ionized or, if one prefers, the average electric moment of a thorium adatom, decreases with the surface concentration. In this connection, it is interesting to note that in his most recent work,[14] Langmuir apparently accepts this interpretation for caesium and barium on tungsten.

Langmuir's activation curves for thoriated tungsten never pass through a maximum. The reason, undoubtedly, is that his activation temperatures were too high for the maximum to appear. If the activation temperatures are low enough, or if thorium is deposited from an external source, the maximum always appears.

The following equations will be found useful in comparing Langmuir's numerical values with our own. It was shown above that the relationship between $\log i$ and f is given by Eq. (2) for $f<0.8$. This range is approximately the same as that for which Langmuir claims his equation (Eq. (15)) holds. It follows from Eq. (13) that

$$\theta = (a/\alpha)(1-\epsilon^{-cf}) \qquad (18)$$

where $\alpha = \log i_m - \log i_w$, and that

$$\frac{d\theta}{dt} = \frac{ac}{\alpha}\epsilon^{-cf}\frac{df}{dt} = \frac{ac}{\alpha}\left(1-\frac{\alpha}{a}\theta\right)\frac{df}{dt}. \qquad (19)$$

By means of the last equation, it is possible to convert Langmuir's evaporation rates in terms of $d\theta/dt$ to the true evaporation rates in terms of df/dt. The comparison of evaporation data will be discussed later.

This discussion may be summarized as follows: Everyone agrees that when a thoriated tungsten filament is activated, $\log i$ does not increase linearly with the time of activation. Langmuir interprets this nonlinearity as evidence for

[13] J. A. Becker, see Phys. Rev. **28**, 341 (1926), Trans. Am. Electro-Chem. Soc. **55**, 153 (1929) and Faraday Society Symposium on Adsorption, January, 1932.

[14] Langmuir, J. Am. Chem. Soc. **54**, 2798 (1932). See particularly p. 2820.

induced evaporation and for the correctness of his formula which states that log i increases linearly with the amount of surface covered. On the other hand, we present new evidence which shows that the rate of accumulation of thorium on the surface is directly proportional to the time and conclude that log i does not vary linearly with the amount of adsorbed thorium. From this nonlinearity we conclude that the electrical moment per atom decreases as the number of adatoms increases. Hence it is no longer necessary to assume induced evaporation. Furthermore, the evidence of surface migration and Clausing's[12] work which shows that thorium diffuses along grain boundaries rather than through the body of the tungsten crystals, lead to the conclusion that induced evaporation does not exist.

Dependence of Emission on Applied Field

All measurements of the current from the tungsten ribbon were made with an applied potential of 100 volts between it and the surrounding electrodes. As pointed out in the introduction the activity of the ribbon depends on the applied field. For example when the tungsten surface was clean, ($f=0$), reducing the applied potential from 100 volts to 10 volts reduced the thermionic current by approximately 15 percent. For $f=0.7$ and $f=2.0$ the corresponding reductions in currents were respectively 25 and 15 percent. It was not feasible to make a detailed study of these effects for the tungsten ribbon since the field is not uniform over the surface of the ribbon. It is quite probable that the exact dependence of the activity on applied field will be characteristic of the particular filament used rather than being characteristic for thorium on tungsten. Moreover, the significant point here is that the dependence of activity on applied field is so small in comparison to the dependence on f and T that the exact field used will not greatly affect the conclusions.

The study of the dependence of activity on applied field is a problem in itself and is really beyond the scope of this paper. However, in this connection some data were taken on the 4-mil thoriated tungsten filament. For this filament the field is uniform and is directly proportional to the applied potential; and the dependence of emission current on plate potential was found to be much more pronounced than in the case of the tungsten ribbon. The results can be summarized most conveniently by determining how the parameters A and b vary with the applied potential. For an amount of thorium on the tungsten surface such that $f=0.6$ it was found that both A and b decreased as the potential was increased. For $f=1$ it was found that A was approximately constant and independent of the potential and that the change in b with potential was much less than it was at $f=0.6$. The dependence of A and b on applied potential was most pronounced in the region for f from 0.3 to 0.6. These results are shown in Figs. 13 and 14. There were only comparatively few data available with which to make the calculations. The results therefore are only approximate and it would be necessary to make a more thorough investigation before final conclusions could be reached. The absolute values of b are not accurate and therefore the values for log A are approximate since a small error in b can make a large error in the value of log A. However, relative values of b and of log A should be quite reliable.

Evaporation of Thorium from Tungsten

We can now proceed to study the rate of evaporation of thorium from tungsten for various values of f at one or more temperatures. Results have been obtained for a range of f from 0.05 to 0.9 at a temperature of 2200°K. These results were obtained in the following manner. First several layers of thorium were deposited on one side of the tungsten ribbon. In order to determine the rate of removal of thorium from the tungsten it was essential to eliminate the effect of removal from the front due to migration of the thorium to the back of the tungsten ribbon. The discussion of migration will be taken up later. It is sufficient here to state that the thorium on the front was uniformly distributed over the surface of the ribbon by migration. The thorium was then removed from both sides by flashing the ribbon for successive intervals at 2200°K. Between each interval the activity of the tungsten ribbon was measured at some low testing temperature. This sufficed to determine the amount on the surface (f) as a function of the time of flashing at 2200°K. Then $\Delta f/\Delta t$ in layers per sec. was calculated for various values of f. In Fig. 15 is

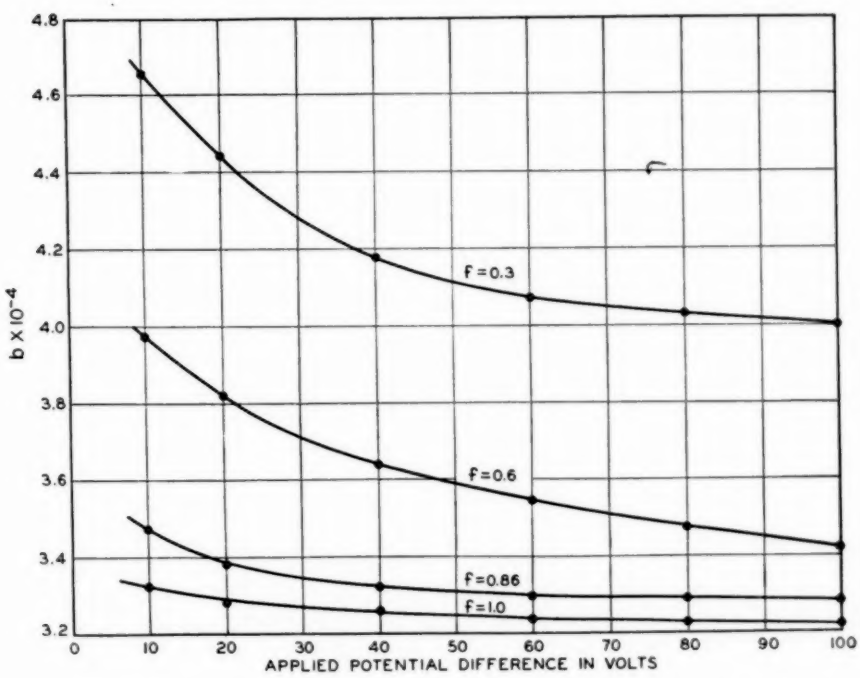

FIG. 13. Dependence of b on applied potential for thoriated tungsten wire.

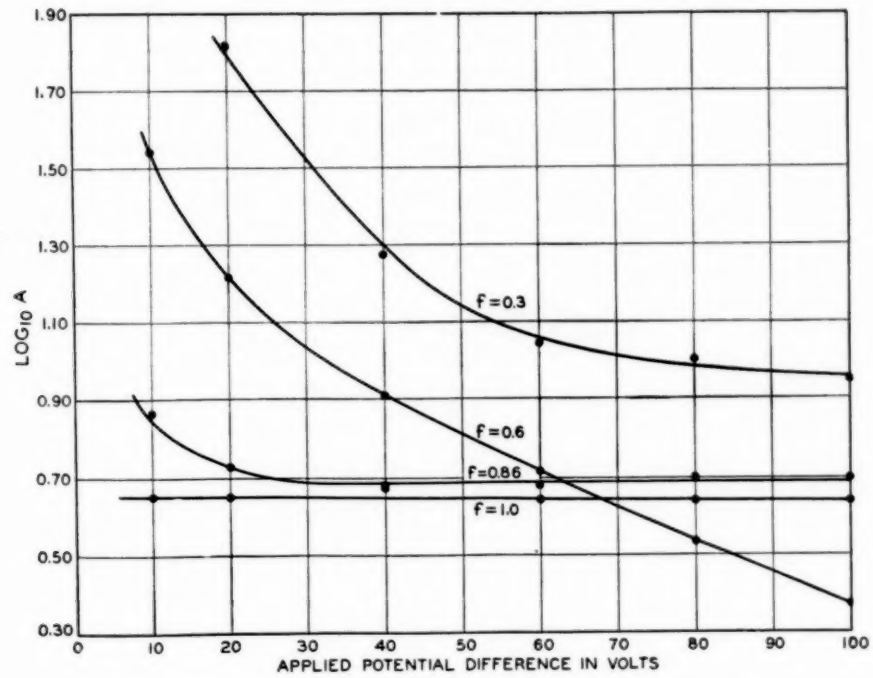

FIG. 14. Dependence of A on applied potential for thoriated tungsten wire.

shown a plot of log $(\Delta f/\Delta t)$ *vs.* f. Between $f=0.2$ and $f=0.9$, log $(\Delta f/\Delta t)$ is approximately a linear function of f. Therefore $\Delta f/\Delta t$ is an exponential function of f. For f less than 0.2, log $(\Delta f/\Delta t)$ falls off more rapidly.

When one attempts to see the significance of the main features of Fig. 15, one is led to the consideration of the factors that should determine the rate of evaporation of adatoms (E_a). It has been proposed[13] that E_a is given by an equation of the form

$$E_a=\Delta f/\Delta t=KT^n f\epsilon^{-w/T},$$

in which K is a constant, n is a small number, and w represents the work function for evaporation of adatoms. The work function w very likely depends on f and may also depend on the temperature T. The factor f is introduced since it is to be expected that the number of atoms which evaporate should be proportional to the number on the surface as well as to the probability that an individual atom evaporates. If E_a, for thorium on tungsten, is given by an equation of this form, a plot of log $[(1/f)(\Delta f/\Delta t)]$ *vs.* f might be expected to yield a curve which would no longer show the steep rise shown in Fig. 15 for small values of f. Fig. 16 shows such a plot. For a complete analysis of the dependence of the evaporation rate on f and T it would be necessary to have evaporation data at other temperatures. However from the fact that $(1/f)(\Delta f/\Delta t)$ increases with f it follows that the work to remove a thorium atom from the tungsten surface decreases as the number of thorium atoms on the surface increases.

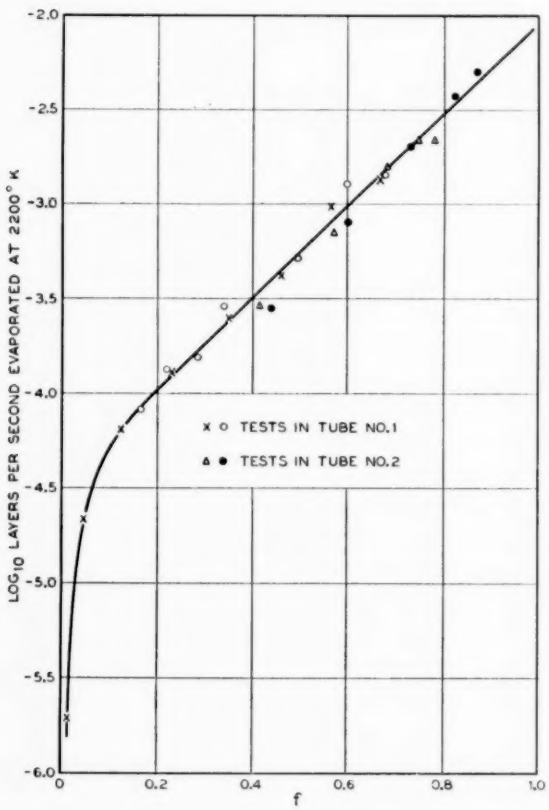

FIG. 15. Rate of evaporation of thorium from tungsten ribbon at 2200°K *vs.* f.

Since it is possible for some of the thorium to diffuse into the tungsten ribbon, $\Delta f/\Delta t$ represents the sum of the rates of diffusion and evaporation. If the rate of diffusion is not negligible, then $\Delta f/\Delta t$ should depend on the concentration of thorium in the tungsten. The concentration in the tungsten should in turn depend on the treatment given the tungsten ribbon between successive tests. As mentioned before in the preliminary treatment of the tube, the rate of removal at first decreased with each successive test. However, this behavior was most likely due to foreign material coming from the thorium wire, rather than to diffusion of thorium into the tungsten ribbon. After the preliminary treatment was more or less complete the rate of removal became independent of the previous treatment of the ribbon. There was then no evidence leading to the conclusion that the rate of removal depended on the time of flashing the tungsten ribbon between successive tests. Furthermore, if the concentration of thorium in the tungsten is appreciable, then after the tungsten ribbon is cleaned off by glowing at 2200°K, it should activate on glowing at some lower temperature. This was tried but no evidence of activation was obtained. The conclusion then is that the rate of diffusion into the tungsten was small compared to the rate of evaporation at 2200°K. Examination of the ribbons after removal from the tube has shown that the ribbons are made up of several large single crystals. If appreciable diffusion can take place only along grain boundaries,[12] then diffusion of thorium into the ribbon should be small.

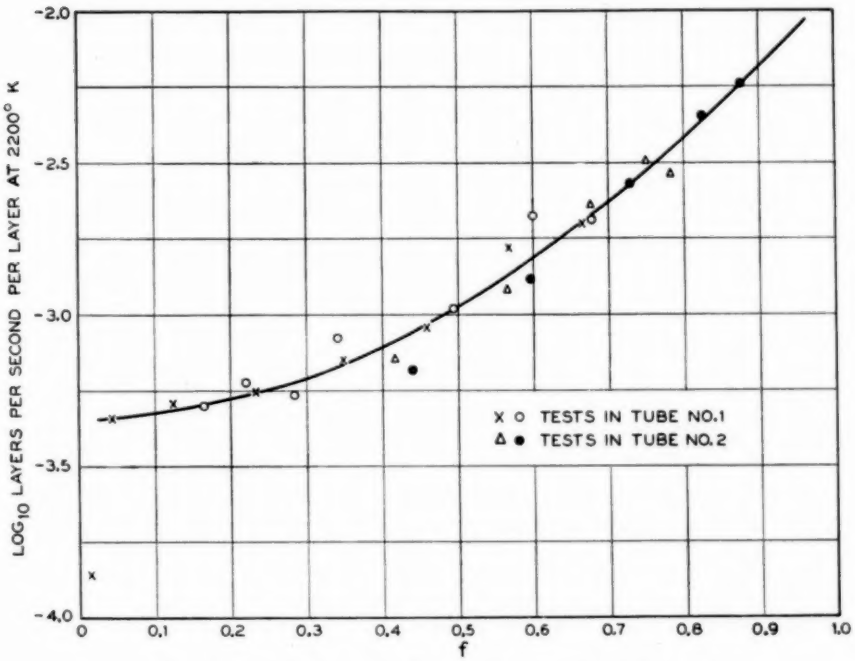

FIG. 16. Rate of evaporation per layer at 2200°K *vs.* f.

Langmuir's[1] and Andrew's[15] results on evaporation of thorium from tungsten are not directly comparable with our results because their results are given in terms of the parameter θ. It is, however, possible to convert their results to the same basis as ours.

From Eq. (19) we have

$$\frac{df}{dt}=\frac{1}{c(a/\alpha-\theta)}\frac{d\theta}{dt}=\frac{0.368}{(1-0.88\theta)}\frac{d\theta}{dt}. \quad (20)$$

If we substitute for $d\theta/dt$ in (20) values of E/N_0 from Langmuir's data or values of $2.3\theta d(\log_{10}\theta)/dt$ from Andrew's data we obtain corresponding values of df/dt in layers per sec. for particular values of θ or for particular values of f.

In Fig. 17 we have plotted the results of such a conversion. The curves give values of $\log_{10}(df/dt)$ as a function of f where df/dt represents the evaporation rate in layers per sec. at 2200°K. The data for curve 1 was obtained from Andrew's results. Curve 2 was obtained from Langmuir's results. Curve 3 represents our own results. Curve 4 is taken from some unpublished data obtained by J. M. Eglin at these laboratories. Eglin studied the rate of evaporation from a 4-mil thoriated tungsten wire by measuring the rate of deposition of the evaporated thorium on a tungsten ribbon. All the curves agree approximately as to shape and trend. The values of df/dt vary by more than a factor of ten. If this discrepancy is due to differences in temperature scales used, a spread of 50° from the mean would be sufficient to explain the differences. Considering that 50° is less than 3 percent of 2200°K, this explanation is not improbable. The ranges of f which the various data cover are indicated approximately by the extent of the curves.

MIGRATION OF THORIUM ON TUNGSTEN

For caesium[7] and for barium[16] on tungsten it has been shown that the adatoms move about or migrate over the surface. In this section we will show that thorium adatoms migrate over the surface; that the rate of migration increases rapidly with temperature, and that the rate of migration is appreciable at temperatures so low that evaporation is negligibly small. From a detailed study of this process we can obtain additional evidence that the parameter f is indeed a correct measure of the surface concen-

[15] Andrews, Phys. Rev. **33**, 454 (1929).

[16] Becker, Trans. Am. Electro-Chem. Soc. **55**, 153 (1929).

tration. It is also possible to draw some conclusions in regard to the nature of the mechanism involved in the migration process. This mechanism it appears is different from that involved in the ordinary case of diffusion in which the diffusion coefficient is independent of the concentration. On the other hand, it can be deduced that some of the migration, and perhaps most of it, is caused by atoms which rise above the surface at one point and return to it at another point. A preliminary value for the heat of migration is found to be 110,000 calories per mol.

The study of migration of thorium on the surface of the tungsten ribbon offers another means of testing whether or not the parameter f is proportional to the amount on the surface. Suppose for example we cover just one side of the tungsten ribbon until the current per sq. cm from this side has a given value at a given testing temperature. This value determines a value of f for this side of the ribbon, and f for the reverse side is zero. If now the thorium initially on one side of the ribbon can be uniformly distributed over both sides by migration then the emission per sq. cm from both sides should be the same. If this can be done at a temperature so low that appreciable thorium is not lost by evaporation, then the original amount of thorium should be distributed over twice the area. Therefore, if f is proportional to the fraction of the surface covered, the value of f as determined by the new value of emission per sq. cm should be just half of the original value of f.

In order to study migration, a given amount of thorium was first deposited on the side of the tungsten ribbon towards the thorium wire; then the tungsten ribbon was flashed for successive intervals at low temperatures such that no appreciable evaporation took place. The activity of each side of the tungsten was measured after each interval of flashing. The plot in Fig. 18 is based on a typical test. In the previous deposition of thorium on tungsten, the total time of deposition was 11.25 hours and the time at which the maximum activity occurred was 6.35 hours. The value of f on this side of the ribbon at the start of the migration test was 11.25/6.35 or 1.77. The tungsten ribbon was then flashed for definite intervals of time at 1535°K. Fig. 18 shows the plot of log (i/i_m) as measured at 1261°K after

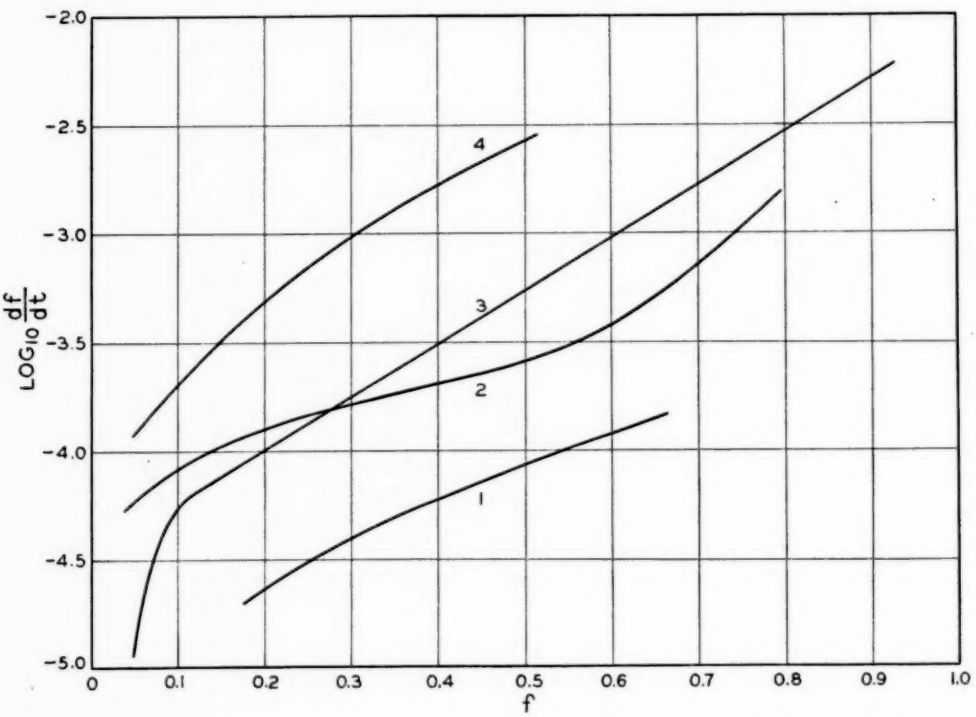

FIG. 17. Comparison of evaporation rates as determined by Andrews (1), Langmuir (2), authors (3) and Eglin (4).

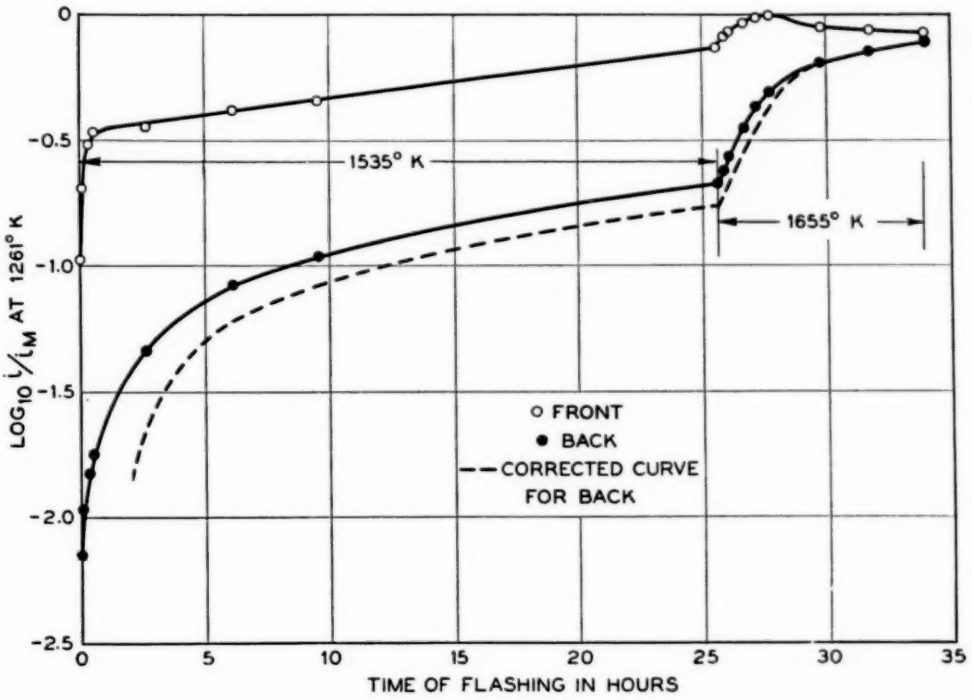

FIG. 18. Changes in activity of front and back of the tungsten ribbon caused by migration of thorium.

each interval of flashing at 1535°K. After 25.5 hours of this treatment the flashing temperature was raised to 1655°K and the procedure continued.

It is to be noticed that log (i/i_m) for the front passes through a maximum and that f for the front goes from $f>1$ to $f<1$. Since about 1 electron in 16 from the front side of the ribbon is eventually collected by the back electrodes, the first few values of log (i/i_m) for the back are too large. This effect of course cancels out when the emission currents from the two sides are nearly equal. Approximate correction can be made for this and the dashed curve in Fig. 18 gives these corrected values.

It is now easy to compare the initial and final values of f. At the end of the run log (i/i_m) for the front was 9.930–10 and for the back 9.894–10. The corresponding values of f are 0.89 and 0.87 and the average value is 0.88, whereas one-half of the initial value of f for the front side is 1.77/2 or 0.885. In other words, the average value of f at the end of the run agrees with the half value of the initial f to within 1 percent. This is probably better agreement than might be expected on consideration of the probable experimental error.

We can learn more about the nature of the migration process by comparing the experimental results for migration with calculated results based on a treatment which is similar to that used in the study of diffusion. Such a treatment leads to the following differential equation

$$\partial f/\partial t = \alpha(\partial^2 f/\partial x^2 + \partial^2 f/\partial y^2),$$

in which f is equal to the surface concentration at any point, t is the time, x and y are the distances in two mutually perpendicular directions on the surface, and α is a quantity, analogous to the diffusion coefficient, which we will call the migration coefficient. α is defined as the net number of atoms crossing a line of unit length in unit time per unit concentration gradient across the line. In most problems on diffusion, the diffusion coefficient does not depend on the concentration. Whether α depends on the surface concentration f, is a question that can at present be decided only by experiment. If experiment should show that α is independent of f then it could be concluded that the nature of the forces causing migration are similar to those causing

diffusion. On the other hand if α depends on f, then the forces causing migration must differ from those causing diffusion. We shall, (1) assume that α is independent of f; (2) deduce from this how the emission current from the front side of the ribbon should vary with time of migration; and (3) compare this with the experimental result.

In order to apply the above migration equation to our case[17] we set up a system of coordinate axes and take into account the initial conditions and the boundary conditions. Consider a line parallel to the axis of the ribbon and in the middle of the front side. Call this the front axis. Let x be any distance on the surface of the ribbon measured normal to this line. A point in the middle of the back of the ribbon will have a value of $x=w$ where w is the width of the ribbon. Then if y is measured parallel to the axis of the ribbon, $\partial f/\partial y$ and $\partial^2 f/\partial y^2$ will be zero and we can omit $\partial^2 f/\partial y^2$ in the migration equation. When a migration experiment is performed, the initial conditions are: $f=f_0$ for all values of x between $-w/2$ and $w/2$; $f=0$ for all values of x between $w/2$ and w and between $-w/2$ and $-w$. f_0 is the value of f on the front side of the ribbon when $t=0$. The boundary conditions are that for all values of t, $\partial f/\partial x=0$ at $x=0$ and at $x=w$; this follows from the symmetry of the conditions to the right and left of the front axis. Subject to these conditions the solution of the migration equation is

$$f=\frac{f_0}{2}+\frac{2f_0}{\pi}\sum_{m=1}^{m=\infty}\left(\frac{1}{m}\epsilon^{-m^2\alpha\pi^2 t/w^2}\cos\frac{m\pi x}{w}\sin\frac{m\pi}{2}\right).$$

The indicated series converges rapidly and it is not difficult to compute f for any value of x and t. From such a computation a plot was made of f as a function of x between $x=0$ and $x=w/2$ for a series of values of t, expressed in units of $w^2/\alpha\pi^2$. From the log i *vs.* f curve and the computed f *vs.* x curve, i was determined as a function of x. Then by graphical integration i or log i for the front of the ribbon was determined for various values of t. In order to compare t with the time in the experiment we can assign various values to α. The effect of this is to expand or contract the time scale for the computed curve. α is the only disposable constant in the calculation.

Fig. 19 is a plot of the experimental and calculated results. The constant α was chosen so as to make the calculated and experimental values of log (i/i_m) agree at $t=25.5$ hours. This gave a value of α equal to 1.84×10^{-9} cm^2 per sec. at 1535°K. Beyond $t=25.5$ hrs. the time scale for the calculated values of log (i/i_m) was adjusted by a factor equal to the ratio of the slopes of the experimental curves at $t=25.5$ hrs. The corresponding value of α for this new time scale was 2.44×10^{-8} cm^2 per sec. at 1655°K.

From Fig. 19 it is evident that the experimental values of log (i/i_m) increased faster at first and then slower than the calculated values of log (i/i_m). This holds for the entire test including the latter part at 1655°K. From this it follows that the experimental results cannot be explained by choosing a migration coefficient α dependent on temperature only but that α must also depend on the concentration f. As f decreases, α must decrease. This means that the rate of migration at a given temperature and for a given concentration gradient decreases as the concentration decreases. In the experiment the decrease in α with concentration amounted to at least a factor of 2 or 3.

These results are to be expected if our picture of the migration process is similar to that for evaporation. When evaporation takes place, the number of atoms that have sufficient energy to escape from the surface is very small compared with the number that have energy enough to temporarily rise above the surface. It is very probable that these atoms will not return to the surface at the point they started from especially if there is a component of force acting on the atoms in the direction of decreasing concentration. If this is the mechanism of migration then the ease with which atoms can rise above the surface will greatly affect the rate of migration. We know from the evaporation data that the number of atoms that escape from the surface increases as f increases. Hence the number of atoms which rise above the surface should also increase as f increases, and according to our picture the rate of migration should increase with increase in concentration other things being the same.

[17] We are greatly indebted to Mr. R. W. Sears of these laboratories for the mathematical solution of this problem.

This hypothesis for the mechanism of migration may be unnecessarily detailed or too pictorial. A more general hypothesis can be stated as follows: Ordinarily the adatoms are held in equilibrium positions on the underlying surface. These equilibrium positions are determined by the structure of the underlying surface and by the nature of the adatoms. Between any two neighboring positions a potential hill exists. Let us call the lowest value of this potential hill the work function for migration. If an atom is to go from one equilibrium position to a neighboring one it must first be given sufficient kinetic energy to cross this

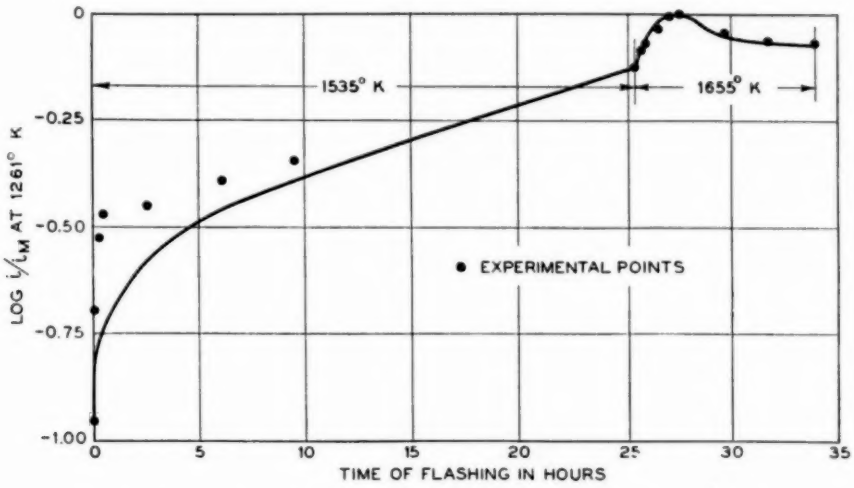

FIG. 19. Comparison of experimental and calculated migration curves for front side of ribbon.

potential hill. This kinetic energy is supplied by thermal agitation and hence the migration rate should increase as the temperature increases.

If the migration work is determined by the nature of the underlying atoms and is not influenced by the concentration of the adatoms, then the rate of migration should be directly proportional to the concentration gradient and should not depend on the concentration. Our experiments show that the migration rate increases with the concentration. Hence it follows that the migration work function must decrease as the concentration increases.

A rough value of the heat of migration can be determined by assuming that an equation of the form

$$\Delta H = 2.3kT^2 (\log \alpha_2/\alpha_1)/(T_2 - T_1) \qquad (21)$$

holds. Where ΔH is the heat of migration and k is Boltzmann's constant. (1.37×10^{-16}.) In the migration experiment, T is roughly 1600°K, $T_2 - T_1$ is 120° and $\log \alpha_2/\alpha_1 = 1.12$. The resulting value of ΔH is 7.5×10^{-12} ergs per particle or 110,000 calories per mol or 4.7 equivalent volts per particle. These values are only approximate and as we have pointed out, they must depend on concentration.

CONCLUSION

In conclusion we wish to emphasize the following points. We have shown that for thorium on tungsten log i is not a linear function of the surface covered as has been assumed in all previous work on thorium on tungsten. The concept of induced evaporation which has been extensively used in the explanation of adsorption phenomena is inapplicable in cases similar to thoriated tungsten. Not only can the activation curves be explained without the use of induced evaporation, but the fact that thorium migrates over the surface at temperatures at which evaporation is negligible shows that an atom which diffuses to the surface at a place occupied by another atom, causes this atom to move along the surface rather than "inducing" it to evapo-

rate. The migration phenomena cannot be explained as a simple process in which the migration rate is directly proportional to the concentration gradient. Finally the data on thermionic and adsorption characteristics of thorium on tungsten presented in this paper are qualitatively the same as in the case of caesium or barium on tungsten. In each of these cases the electron activity passes through an optimum, the evaporation rate at a given temperature varies exponentially with f, and migration takes place more readily than evaporation.

Transformations in the Theory of Complex Spectra

GEORGE H. SHORTLEY, *Palmer Physical Laboratory, Princeton University*

(Received January 27, 1933)

Four transformations are considered in detail: that from the zero-order nlm_lm_s scheme to the *LS*-coupling scheme, that from the zero-order $nljm_j$ scheme to the *jj*-coupling scheme, that connecting these two zero-order schemes, and that connecting the *LS*- and the *jj*-coupling schemes. A correlation between the states of the configuration with ϵ electrons in shell S plus η other electrons and those of the configuration with ϵ electrons missing from shell S plus the same η other electrons is found such that all of these transformations are the same for the two configurations. The transformation between zero-order states in two different schemes is considered in general and a general expression (3.10) is found giving this transformation for an almost closed shell in terms of the transformation for the corresponding simple configuration. Finally, a direct method is found for obtaining the transformation from *LS*-coupling to *jj*-coupling for any two-electron configuration, and this transformation is given explicitly for all such configurations up to *dd*. This then furnishes the *LS-jj*-coupling transformation also for p^4, p^5s, p^5p, p^5d, d^8, d^9s, d^9p, and d^9d, the configurations for which the *jj*-coupling scheme is most useful.

IN the course of the calculations on the spectra of configurations containing almost-closed shells which the writer is making, it became desirable to use the *jj*-coupling scheme for certain configurations, such as p^5p and p^5d of the rare gases. The problem of transforming the electrostatic energy matrix to this scheme led to the following considerations of the transformations involved in the theory of complex spectra.

There are four representations which are of importance in the theory, the two zero-order schemes which we shall designate as the m_lm_s scheme and the jm_j scheme, and the two schemes characterized by quantized resultant J and M_J, which we shall call the *LS*-coupling scheme and the *jj*-coupling scheme. The four most interesting transformations between these schemes may be represented diagrammatically as follows:

$$\begin{array}{ccc} nljm_j & \rightleftharpoons & nlm_lm_s \\ \updownarrow & & \updownarrow \\ jjJM_J & \rightleftharpoons & LSJM_J. \end{array}$$

Our principal objective will be the determination of the relation between the *LS*- to *jj*-coupling transformation for a simple configuration and for the corresponding configuration involving an almost closed shell. To this end, we shall first consider this relation for each of the other transformations. We shall then obtain explicitly the *LS-jj* transformation by a direct method for all two-electron configurations up to *dd* (and hence for their almost-closed shell correspondents).

§1. The transformation $nlm_lm_s \rightleftharpoons LSJM_J$

In the m_lm_s scheme one specifies a set nlm_lm_s of quantum numbers for each electron in the configuration. In forming an antisymmetric zero-order wave function (cf. 3.2) these sets are arranged in a specified order. We shall take as standard an order in which sets of a given n and l, i.e., sets belonging to the same shell, are arranged in order of decreasing m_l, with $m_s=+\frac{1}{2}$ before $m_s=-\frac{1}{2}$ in case both occur for a given m_l. The transformation from this scheme to a scheme in which $\mathbf{L}^2$, $\mathbf{S}^2$ and $\mathbf{J}^2$ are diagonal may be obtained by several methods.[1] The relation between this transformation for a configuration (L) containing ϵ electrons in shell S plus η electrons in other shells to that for the configuration (R) having ϵ electrons missing from shell S plus the same η other electrons has been determined by the writer.[2] To a given zero-order state of L we correlate that state of R whose ϵ missing electrons have the negatives of the m_l and m_s values of the ϵ electrons of L and whose η additional electrons have the same quantum numbers as those of L,

[1] See Ufford and Shortley, Phys. Rev. **42**, 167 (1932), §2.

[2] Shortley, Phys. Rev. **40**, 185 (1932). The letters L and R refer to left and right in the periodic table.

taken when in standard order with a phase (-1) to the sum of the m_l values of the electrons in shell S. With this correlation it was shown that the matrices of $\mathbf{L}^2$, $\mathbf{S}^2$ and $\mathbf{L}\cdot\mathbf{S}$ are the same in the two cases and hence that the transformation to LS-coupling is the same.

§2. The transformation $nljm_j \rightleftharpoons jjJM_j$

In the jm_j scheme a set $nljm_j$ of quantum numbers is specified for each electron in the configuration. Within a given shell we shall take for the standard order of arrangement of these sets, first those with $j=l+\frac{1}{2}$ in descending order of m_j, then those with $j=l-\frac{1}{2}$ in descending order of m_j. In the jj-coupling scheme, $\mathbf{J}^2$ has been diagonalized so that one obtains states characterized by a set of j values for the electrons and resultant J and M_J. The transformation between these two schemes may be obtained by methods analogous to those of reference 1.

Let us consider the matrix of $\mathbf{J}^2$ in the jm_j scheme. Its elements may be written down in exact analogy to those of $\mathbf{L}^2$ in the m_lm_s scheme.[3] It has nondiagonal elements only between states which differ in regard to two individual sets of quantum numbers; say that state A contains sets a and b where A' contains a' and b'. This element has the value

$$(A\,|\,\mathbf{J}^2\,|\,A') = \pm 4\{(a\,|\,J_x\,|\,a')(b\,|\,J_x\,|\,b') - (a\,|\,J_x\,|\,b')(b\,|\,J_x\,|\,a')\},$$

where

$$(a\,|\,J_x\,|\,b) = (n^a l^a j^a m_j{}^a\,|\,J_x\,|\,n^b l^b j^b m_j{}^b) = \delta(n^a l^a j^a; n^b l^b j^b)\,\delta(m_j{}^a \pm 1, m_j{}^b)\,\tfrac{1}{2}\bar{h}[(j^b \pm m_j{}^b)(j^b \mp m_j{}^b + 1)]^{\frac{1}{2}}.$$

The diagonal element of $\mathbf{J}^2$ is

$$(A\,|\,\mathbf{J}^2\,|\,A) = \bar{h}^2 M_J{}^2 + \bar{h}\sum_a\{j^a(j^a+1) - (m_j{}^a)^2\} - 4\sum_{a<b}(a\,|\,J_x\,|\,b)^2.$$

Now to a given state of L (in the jm_j scheme) let us correlate that state of R whose ϵ missing electrons have the same j values but the negatives of the m_j values of the ϵ electrons of L, and whose η additional electrons have the same quantum numbers. With this correlation it is easily seen, by an argument which is the direct analogue of that previously given for $\mathbf{L}^2$ in the m_lm_s scheme,[3] that the matrix of $\mathbf{J}^2$ is the same for the two configurations and hence that the same matrix will transform them to jj-coupling. Since the matrix of $\mathbf{J}^2$ is diagonal with respect to the number of electrons in shell S with $j=l-\frac{1}{2}$, this result still holds if our correlation involves a phase which depends in an arbitrary way on this number; this property will be of use later. In jj-coupling, to a given state of L is correlated that state of R of the same JM_J whose ϵ missing j values are those present in shell S of L, and whose η additional j values are the same as those of L.

§3. The transformation $nlm_lm_s \rightleftharpoons nljm_j$

Let us consider a k-electron configuration for which there are n possible sets of one-electron quantum numbers.[4] In the m_lm_s scheme let us denote these sets, in standard order, by the numbers $1, 2, \cdots n$, and the corresponding states by $\psi(1), \psi(2), \cdots \psi(n)$. In the jm_j scheme let us use the notation $1', 2', \cdots n'$ for the quantum numbers, and $\phi(1'), \phi(2'), \cdots \phi(n')$ for the states.[4] The transformation between these two one-electron systems[5] is given by

$$\psi(\alpha) = \sum_{\beta=1}^{n} \phi(\beta')(\beta'\,|\,\alpha). \tag{3.1}$$

The zero-order antisymmetric function belonging to the complete set $\alpha_1, \alpha_2, \cdots \alpha_k$ of quantum numbers is defined by

[3] Cf. §5 of reference 2 for details and notation.

[4] For example, for the configuration $2s3p^2$, $k=3$ and $n=8$, the possible sets of quantum numbers being given, for the m_lm_s scheme by $1=2s\,0^+$, $2=2s\,0^-$, $3=3p\,1^+$, $4=3p\,1^-$, $5=3p\,0^+$, $6=3p\,0^-$, $7=3p\,-1^+$, $8=3p\,-1^-$; and for the jm_j scheme by $1'=2s\,\frac{1}{2}\,\frac{1}{2}$, $2'=2s\,\frac{1}{2}\,-\frac{1}{2}$, $3'=3p\,\frac{3}{2}\,\frac{3}{2}$, $4'=3p\,\frac{3}{2}\,\frac{1}{2}$, $5'=3p\,\frac{3}{2}\,-\frac{1}{2}$, $6'=3p\,\frac{3}{2}\,-\frac{3}{2}$, $7'=3p\,\frac{1}{2}\,\frac{1}{2}$, $8'=3p\,\frac{1}{2}\,-\frac{1}{2}$.

[5] Most of the considerations of this section will be more general than is implied by the jm_j and m_lm_s designations; we shall prefer for a while the designations primed and unprimed schemes.

$$\Psi(\alpha_1, \alpha_2, \cdots \alpha_k) = \frac{1}{(k!)^{\frac{1}{2}}} \sum_P (-1)^p P\psi_1(\alpha_1)\psi_2(\alpha_2)\cdots\psi_k(\alpha_k), \tag{3.2}$$

where P is a permutation of the electron indices 1, 2, $\cdots$ k which are written as subscripts to the ψ's. $\alpha_1, \alpha_2, \cdots \alpha_k$ are k numbers of the set 1, 2, $\cdots$ n, arranged in the order $\alpha_1 < \alpha_2 < \cdots < \alpha_k$.

The transformation of this state to the primed scheme is given by the following calculation. From (3.2) and (3.1)

$$\Psi(\alpha_1, \alpha_2, \cdots \alpha_k) = \frac{1}{(k!)^{\frac{1}{2}}} \sum_P (-1)^p P \sum_{\beta_1=1}^{n} \phi_1(\beta_1')(\beta_1'|\alpha_1)\cdots \sum_{\beta_k=1}^{n} \phi_k(\beta_k')(\beta_k'|\alpha_k)$$

$$= \sum_{\beta_1, \cdots \beta_k} (\beta_1'|\alpha_1)\cdots(\beta_k'|\alpha_k) \frac{1}{(k!)^{\frac{1}{2}}} \sum_P (-1)^p P\phi_1(\beta_1')\cdots\phi_k(\beta_k').$$

If two of the β's are equal the antisymmetric factor $\sum_P \cdots$ vanishes, while for a given set of β's this term is the same, irrespective of the order of the β's, to within a sign which is just correct to give us a determinant of the transformation coefficients; i.e.,

$$\Psi(\alpha_1, \alpha_2, \cdots \alpha_k) = \sum_{\beta_1 < \beta_2 < \cdots < \beta_k} \boldsymbol{D}\begin{pmatrix} \beta_1' \cdots \beta_k' \\ \alpha_1 \cdots \alpha_k \end{pmatrix} \Phi(\beta_1', \beta_2', \cdots \beta_k'), \tag{3.3}$$

where we use the notation

$$\boldsymbol{D}\begin{pmatrix} \beta_1' \cdots \beta_k' \\ \alpha_1 \cdots \alpha_k \end{pmatrix} = \begin{vmatrix} (\beta_1'|\alpha_1) & \cdots & (\beta_1'|\alpha_k) \\ \cdots & \cdots & \cdots \\ \cdots & \cdots & \cdots \\ (\beta_k'|\alpha_1) & \cdots & (\beta_k'|\alpha_k) \end{vmatrix}. \tag{3.4}$$

The transformation coefficient connecting the state $\beta_1', \beta_2', \cdots \beta_k'$ with the state $\alpha_1, \alpha_2, \cdots \alpha_k$ (quantum numbers in standard order) is given, then, by just this determinant:

$$(\beta_1', \beta_2', \cdots \beta_k'|\alpha_1, \alpha_2, \cdots \alpha_k) = \int \overline{\Phi}(\beta_1', \beta_2', \cdots \beta_k')\Psi(\alpha_1, \alpha_2, \cdots \alpha_k) = \boldsymbol{D}\begin{pmatrix} \beta_1' \cdots \beta_k' \\ \alpha_1 \cdots \alpha_k \end{pmatrix}. \tag{3.5}$$

Suppose now that the configuration consists of g electrons in shell $\boldsymbol{S}$ and $k-g$ in other shells. Since the transformation (3.1) has no components connecting sets belonging to different shells, the coefficient (3.5) becomes just the product of two determinants:

$$(\beta_1', \cdots \beta_g', \beta_{g+1}', \cdots \beta_k'|\alpha_1, \cdots \alpha_g, \alpha_{g+1}, \cdots \alpha_k) = \boldsymbol{D}\begin{pmatrix} \beta_1' \cdots \beta_g' \\ \alpha_1 \cdots \alpha_g \end{pmatrix} \boldsymbol{D}\begin{pmatrix} \beta_{g+1}' \cdots \beta_k' \\ \alpha_{g+1} \cdots \alpha_k \end{pmatrix}. \tag{3.6}$$

Because of this property, in considering the relation between these coefficients for $\boldsymbol{L}$ and $\boldsymbol{R}$ we may restrict ourselves purely to the shell $\boldsymbol{S}$ so long as the other quantum numbers are the same for the correlated states of $\boldsymbol{L}$ and $\boldsymbol{R}$. We shall suppose that there are altogether m states in the shell $\boldsymbol{S}$, and consider the relation of these components for the configuration consisting of ϵ electrons to that consisting of $m-\epsilon$ electrons in this shell.

Let us seek an invariant correlation between an ϵ-electron state and the $(m-\epsilon)$-electron state whose ϵ missing electrons have the same quantum numbers. This correlation is to be independent

of the system of zero-order states used in the description. We shall denote a given ϵ-electron state by $\Psi(\alpha_1, \alpha_2, \cdots \alpha_\epsilon)$ and the corresponding $(m-\epsilon)$-electron state by $\Psi(a_1, a_2, \cdots a_{m-\epsilon})$, where the α's and a's together make up the set 1, 2, $\cdots m$.

Let us define a linear operator Z by the relations

$$Z\Psi(\alpha_1, \alpha_2, \cdots \alpha_\epsilon) = (-1)^{\alpha_1+\alpha_2+\cdots+\alpha_\epsilon}\bar{\Psi}(a_1, a_2, \cdots a_{m-\epsilon}). \quad (3.7)$$

This operator is seen to be unitary, since the states on the right form a normalized orthogonal system. In the primed scheme we shall define a corresponding operator Z' by

$$Z'\Phi(\beta_1', \beta_2', \cdots \beta_\epsilon') = (-1)^{\beta_1+\beta_2+\cdots+\beta_\epsilon}\bar{\Phi}(b_1', b_2', \cdots b_{m-\epsilon}'). \quad (3.8)$$

The relation between Z' and Z is given by the following calculation.

$$\begin{aligned} Z'\Psi(\alpha_1, \alpha_2, \cdots \alpha_\epsilon) &= Z' \sum_{\beta_1<\cdots<\beta_\epsilon} D\begin{pmatrix}\beta_1' \cdots \beta_\epsilon' \\ \alpha_1 \cdots \alpha_\epsilon\end{pmatrix}\Phi(\beta_1', \beta_2', \cdots \beta_\epsilon') \\ &= \sum_{\beta_1<\cdots<\beta_\epsilon} D\begin{pmatrix}\beta_1' \cdots \beta_\epsilon' \\ \alpha_1 \cdots \alpha_\epsilon\end{pmatrix}(-1)^{\Sigma\beta_\nu}\bar{\Phi}(b_1', b_2', \cdots b_{m-\epsilon}') \\ &= \sum_{\beta_1<\cdots<\beta_\epsilon} (-1)^{\Sigma\beta_\nu} D\begin{pmatrix}\beta_1' \cdots \beta_\epsilon' \\ \alpha_1 \cdots \alpha_\epsilon\end{pmatrix} \sum_{c_1<\cdots<c_{m-\epsilon}} D\begin{pmatrix}b_1' \cdots b_{m-\epsilon}' \\ c_1 \cdots c_{m-\epsilon}\end{pmatrix}\bar{\Psi}(c_1, c_2, \cdots c_{m-\epsilon}) \\ &= (-1)^{\Sigma\alpha_\nu} D\begin{pmatrix}1' \cdots m' \\ 1 \cdots m\end{pmatrix}\bar{\Psi}(a_1, a_2, \cdots a_{m-\epsilon}), \end{aligned}$$

since the terms for $c_1 = a_1, \cdots c_{m-\epsilon} = a_{m-\epsilon}$ furnish just the Laplace expansion of $D\begin{pmatrix}1' \cdots m' \\ 1 \cdots m\end{pmatrix}$ while the other terms vanish. Since any state may be expressed in terms of the $\Psi(\alpha_1, \alpha_2, \cdots \alpha_\epsilon)$, we see by comparison with (3.7) that

$$Z' = D\begin{pmatrix}1' \cdots m' \\ 1 \cdots m\end{pmatrix} Z. \quad (3.9)$$

This shows the operator Z to be invariant to within a constant factor. If we apply this operator to an ϵ-electron state and then take the complex conjugate we obtain an invariantively correlated $(m-\epsilon)$-electron state.[6,7] We take the complex conjugate because by (3.7) Z acting on a state gives a state in the dual space, whereas we want a state in the same space.

We may now calculate the relation between the transformation coefficients:

$$\begin{aligned} (b_1', b_2', \cdots b_{m-\epsilon}'|a_1, a_2, \cdots a_{m-\epsilon}) &= \int \bar{\Phi}(b_1', b_2', \cdots b_{m-\epsilon}')\Psi(a_1, a_2, \cdots a_{m-\epsilon}) \\ &= (-1)^{\Sigma\alpha_\nu+\Sigma\beta_\nu}\int Z'\Phi(\beta_1', \beta_2', \cdots \beta_\epsilon')\overline{Z\Psi(\alpha_1, \alpha_2, \cdots \alpha_\epsilon)} \\ &= (-1)^{\Sigma\alpha_\nu+\Sigma\beta_\nu} D\begin{pmatrix}1' \cdots m' \\ 1 \cdots m\end{pmatrix}\int \overline{Z\Psi(\alpha_1, \alpha_2, \cdots \alpha_\epsilon)}Z\Phi(\beta_1', \beta_2', \cdots \beta_\epsilon') \\ &= (-1)^{\Sigma\alpha_\nu+\Sigma\beta_\nu} D\begin{pmatrix}1' \cdots m' \\ 1 \cdots m\end{pmatrix}(\alpha_1, \alpha_2, \cdots \alpha_\epsilon|\beta_1', \beta_2', \cdots \beta_\epsilon'), \end{aligned} \quad (3.10)$$

since a transformation coefficient is invariant under a unitary transformation.

[6] This correlation was suggested by Professor E. P. Wigner, whom I wish to thank for his kind assistance with this section.

[7] This correlation is not linear, since taking the complex conjugate is an invariant, but not linear, operation. A linear correlation such as is obtained directly by omitting the bar on the right side of (3.7) is invariant only under real orthogonal transformations of the zero-order states.

These considerations have been rather more general than we need for the schemes $m_l m_s$ (unprimed) and jm_j (primed) in which we are particularly interested. In this case the transformation (3.1) is completely real, and its inverse is given by

$$\phi(nl, l\pm\tfrac{1}{2}, m_j) = \pm\left(\frac{l\pm m_j+\frac{1}{2}}{2l+1}\right)^{\frac{1}{2}}\psi(nl, m_j-\tfrac{1}{2}, \tfrac{1}{2}) + \left(\frac{l\mp m_j+\frac{1}{2}}{2l+1}\right)^{\frac{1}{2}}\psi(nl, m_j+\tfrac{1}{2}, -\tfrac{1}{2}), \qquad (3.11)$$

where the $\psi(nlm_l m_s)$ are chosen with such phase that the matrix of L_x is entirely positive (cf. reference 1). The determinant of this transformation for an l shell is easily shown to be $(-1)^l$. This value is to be inserted in (3.10). Moreover from the standard order of listing quantum numbers (§§1 and 2) it is seen that $(-1)^{\Sigma\alpha_\nu}=(-1)^{M_S+\epsilon/2}$, and $(-1)^{\Sigma\beta_\nu}=(-1)^{-M_J+q+\epsilon(l-\frac{1}{2})}$, where ϵ is the number of electrons in the configuration and q is the number in $\Phi(\beta_1', \beta_2', \cdots\beta_\epsilon')$ with $j=l-\frac{1}{2}$. Since $M_J=M_L+M_S$, (3.10) becomes

$$(b_1', b_2', \cdots b_{m-\epsilon}'|a_1, a_2, \cdots a_{m-\epsilon}) = (-1)^{-M_L+q+l(\epsilon+1)}(\beta_1', \beta_2', \cdots \beta_\epsilon'|\alpha_1, \alpha_2, \cdots \alpha_\epsilon). \qquad (3.12)$$

The states on the right side of this equation have just the quantum numbers which are missing on the left; we should prefer (because later we shall add η electrons in other shells and should then like to compare states of the same M_L, M_S, M_J) them to have the negatives of the m_l, m_s, and m_j values missing on the left. But this is easily accomplished. Let the coefficient on the right of (3.12) be

$$(l+\tfrac{1}{2} : m_j^1, m_j^2, \cdots m_j^p; l-\tfrac{1}{2} : m_j^1, m_j^2, \cdots m_j^q|m_l^1 m_s^1, m_l^2 m_s^2, \cdots m_l^\epsilon m_s^\epsilon), \qquad (3.13)$$

where $p+q=\epsilon$. The coefficient we would like to compare with this is

$$(l+\tfrac{1}{2} : -m_j^p, \cdots, -m_j^1; l-\tfrac{1}{2} : -m_j^q, \cdots, -m_j^1|-m_l^\epsilon - m_s^\epsilon, \cdots, -m_l^1 - m_s^1). \qquad (3.14)$$

If (3.13) is in standard order, (3.14) is seen to be also. Now from a comparison of the two determinants of type (3.5) which give the values of these two coefficients, and by using the relations (cf. 3.11)

$$(l+\tfrac{1}{2}, m_j|m_l, m_s) = (l+\tfrac{1}{2}, -m_j|-m_l, -m_s),$$

$$(l-\tfrac{1}{2}, m_j|m_l, m_s) = -(l-\tfrac{1}{2}, -m_j|-m_l, -m_s),$$

it is seen that

$$(3.14) = (-1)^q\cdot(3.13).$$

Hence, returning to (3.12), it is seen that the ratio of the transformation coefficient for the almost closed shell to that of the ϵ-electron configuration whose electrons have the negatives of the m_l, m_s, m_j values of those missing from the closed shell is

$$(-1)^{M_L+(\epsilon+1)(q+l)}. \qquad (3.15)$$

If we make the correlation of §1 which includes a phase factor $(-1)^{M_L}$ for the $m_l m_s$ scheme, and if in the jm_j correlation we insert a phase $(-1)^{(\epsilon+1)(q+l)}$—a function of the number of electrons with $j=l-\frac{1}{2}$ for which provision was made at the end of §2—we may say that the $m_l m_s$-jm_j transformation is the same for the two configurations.

These same results hold, as shown by (3.6), when we add η electrons in other shells with the same quantum numbers to both configurations.

§4. The transformation $jjJM_J \rightleftharpoons LSJM_J$

We have found a correlation between the zero-order states of $\boldsymbol{L}$ and $\boldsymbol{R}$ such that the transformations $jjJM_J \rightleftharpoons nljm_j$, $nljm_j \rightleftharpoons nlm_l m_s$, and $nlm_l m_s \rightleftharpoons LSJM_J$ are the same for the two configurations. This is seen to imply that the transformation $jjJM_J \rightleftharpoons LSJM_J$ is the same. More explicitly, the situation is as follows: A given state of the configuration $\boldsymbol{L}$ characterized by the quantum numbers $LSJM_J$ (this state is not uniquely determined for two reasons—first, there is an arbitrary phase; second, the set $LSJM_J$ of quantum numbers is not in general complete for more than two electrons so there may be two independent states characterized by the same $LSJM_J$) is a certain linear combination of the $m_l m_s$ states; the same linear combination of the correlated $m_l m_s$ states of $\boldsymbol{R}$ is a state of $\boldsymbol{R}$ characterized by this same $LSJM_J$. A similar

statement holds for a $jjJM_J$ state except that the *missing* j's of $\boldsymbol{R}$ are those of $\boldsymbol{L}$. The transformation between the LS- and jj-coupling states of $\boldsymbol{R}$ obtained in this way is the same as the corresponding transformation for $\boldsymbol{L}$.

Now to obtain this LS-jj transformation by the combination of the other three is in general a very tedious process involving the multiplication of three matrices of high order, for no two of the three transformations are diagonal in common with respect to more than M_J. On the other hand the resulting transformation is diagonal with respect to both J and M_J and splits in general into steps of a relatively low order. For example, no two-electron configuration or its equivalent can have more than four states of the same J and M_J, while pp or p^5p has altogether 10 states of $M_J=0$, dd or d^9d has 19.

It seems, then, to be desirable to find a direct method which will enable this transformation to be calculated with greater ease. The following accomplishes this result for two-electron configurations, this being in general the only case in which the quantum numbers $LSJM_J$ or $jjJM_J$ define a unique state (to within a phase).

The procedure we shall follow is that of calculating the matrices of $\mathbf{L}^2$ and $\mathbf{S}^2$ in the jj-coupling scheme and then diagonalizing them to obtain the transformation to LS coupling. Since these matrices will split into steps of at most fourth order, and since their eigenvalues are known, this diagonalization is a very simple procedure.

The matrices of $\mathbf{L}^2$ and $\mathbf{S}^2$ in a non-antisymmetric scheme in which the first electron has quantum numbers n_1, l_1, j_1, and the second electron has quantum numbers n_2, l_2, j_2, with resultant J, M_J, may be obtained by the method of Güttinger-Pauli and Johnson.[8] $\mathbf{L}^2=\mathbf{L}_1^2+\mathbf{L}_2^2+2\mathbf{L}_1\cdot\mathbf{L}_2$. The first two terms have known diagonal matrices. The matrix of the third term is diagonal with respect to n_1l_1, n_2l_2, JM_J. If we omit these quantum numbers, using simply the notation $(j_1, j_2|2\mathbf{L}_1\cdot\mathbf{L}_2|j_1', j_2')$, the elements of this matrix are given, with the abbreviation

$$w_i=l_i+\tfrac{1}{2},$$

by

[8] Güttinger and Pauli, Zeits. f Physik **67**, 743 (1931). The formulas given are exactly analogous to those obtained by M. H. Johnson, Phys. Rev. **38**, 1628 (1931) for the matrix of $\mathbf{L}_1\cdot\mathbf{S}_1$ in the LS-coupling scheme.

$$\left.\begin{aligned}
&(l_1\pm\tfrac{1}{2}, l_2\dot{\pm}\tfrac{1}{2}|2\mathbf{L}_1\cdot\mathbf{L}_2|l_1\pm\tfrac{1}{2}, l_2\dot{\pm}\tfrac{1}{2})\\
&\qquad=\frac{(2w_1\mp1)(2w_2\dot{\mp}1)}{4w_1w_2}\{J(J+1)-w_1(w_1\pm1)-w_2(w_2\dot{\pm}1)\}\\
&(l_1\pm\tfrac{1}{2}, l_2+\tfrac{1}{2}|2\mathbf{L}_1\cdot\mathbf{L}_2|l_1\pm\tfrac{1}{2}, l_2-\tfrac{1}{2})\\
&\qquad=\frac{2w_1\mp1}{4w_1w_2}\{(J\mp w_1+w_2)(J\pm w_1-w_2+1)(J\pm w_1+w_2+1)(w_2\pm w_1-J)\}^{\frac{1}{2}}\\
&(l_1+\tfrac{1}{2}, l_2\pm\tfrac{1}{2}|2\mathbf{L}_1\cdot\mathbf{L}_2|l_1-\tfrac{1}{2}, l_2\pm\tfrac{1}{2})\\
&\qquad=-\frac{2w_2\mp1}{4w_1w_2}\{(J+w_1\mp w_2)(J-w_1\pm w_2+1)(J+w_1\pm w_2+1)(w_1\pm w_2-J)\}^{\frac{1}{2}}\\
&(l_1+\tfrac{1}{2}, l_2+\tfrac{1}{2}|2\mathbf{L}_1\cdot\mathbf{L}_2|l_1-\tfrac{1}{2}, l_2-\tfrac{1}{2})\\
&\qquad=-\frac{1}{4w_1w_2}\{(J+w_1+w_2+1)(J+w_1+w_2)(w_1+w_2-J)(w_1+w_2-J-1)\}^{\frac{1}{2}}\\
&(l_1-\tfrac{1}{2}, l_2+\tfrac{1}{2}|2\mathbf{L}_1\cdot\mathbf{L}_2|l_1+\tfrac{1}{2}, l_2-\tfrac{1}{2})\\
&\qquad=\frac{1}{4w_1w_2}\{(J-w_1+w_2)(J-w_1+w_2+1)(J+w_1-w_2)(J+w_1-w_2+1)\}^{\frac{1}{2}}
\end{aligned}\right\}. \qquad (4.1)$$

(In the first formula either the upper or lower undotted sign is to be taken with either the upper or lower dotted sign.) The elements of the matrix of $2\mathbf{S}_1\cdot\mathbf{S}_2$ are exactly the same except that in the first two expressions the factor $(2w_1\mp1)$ is to be replaced by ∓1, in the first and third expressions the factor $(2w_2\mp1)$ is to be replaced by ∓1.

In terms of these non-antisymmetric matrix components, the components between antisymmetric states may be obtained by considerations such as previously used by the writer.[9] Let $\alpha=nl$, $\beta=n'l'$ and let all differences in quantum numbers be indicated by primes, subscripts merely denoting the electrons. Then unless $\alpha=\beta$ and $j=j'$, the antisymmetric

$$\Psi(\alpha j\beta j' JM_J)=2^{-\frac{1}{2}}[\Psi(\alpha_1 j_1\beta_2 j_2' JM_J)-\psi(\alpha_2 j_2\beta_1 j_1' JM_J)]. \quad (4.2)$$

Now if v is a symmetric observable diagonal with respect to n_1l_1 and n_2l_2 it is easily seen that for *non-equivalent electrons*

$$(\alpha j\beta j'|v|\alpha j''\beta j''')=(\alpha_1 j_1\beta_2 j_2'|v|\alpha_1 j_1''\beta_2 j_2'''), \quad \alpha\neq\beta \quad (4.3)$$

where we have for brevity omitted J and M_J throughout.

Consideration of the matrix element

$$(\alpha j\alpha j' JM_J|v|\alpha j''\alpha j''' JM_J)=(jj'|v|j''j''')$$

for *equivalent electrons* must be divided into three cases. First, if $j\neq j'$, $j''\neq j'''$, (4.2) applies to both states, and

$$(jj'|v|j''j''')=\tfrac{1}{2}[(j_1j_2'|v|j_1''j_2''')+(j_2j_1'|v|j_2''j_1''')-(j_1j_2'|v|j_2''j_1''')-(j_2j_1'|v|j_1''j_2''')]$$
$$=(j_1j_2'|v|j_1''j_2''')-(j_1j_2'|v|j_2''j_1''').$$

Now the order of the quantum numbers here is significant, and the second term must be evaluated by the relation

$$\psi(j_2''j_1'''JM_J)=(-1)^{j''+j'''-J}\psi(j_1'''j_2''JM_J) \quad (4.4)$$

which has been given by Wigner,[10] with whose scheme of vector addition (4.1) are consistent. This gives us

$$(jj'|v|j''j''')=(j_1j_2'|v|j_1''j_2''')-(-1)^{j''+j'''-J}(j_1j_2'|v|j_1'''j_2'').\quad j\neq j',\ j''\neq j''' \quad (4.5a)$$

Second, if $j\neq j'$, $j''=j'''$, from (4.4) we see that $\psi(j_1''j_2'')$ is already either antisymmetric or symmetric, corresponding to allowed and excluded states.[11] For an allowed state we have

$$(jj'|v|j''j'')=2^{-\frac{1}{2}}[(j_1j_2'|v|j_1''j_2'')-(j_2j_1'|v|j_1''j_2'')]=2^{-\frac{1}{2}}[(j_1j_2'|v|j_1''j_2'')+(j_2j_1'|v|j_2''j_1'')]$$

or

$$(jj'|v|j''j'')=2^{\frac{1}{2}}(j_1j_2'|v|j_1''j_2''). \qquad j\neq j' \quad (4.5b)$$

Third, if $j=j'$, $j''=j'''$, and both states are allowed, we have simply

$$(jj|v|j''j'')=(j_1j_2|v|j_1''j_2''). \quad (4.5c)$$

These formulas, then, enable us to calculate the matrices of $\mathbf{L}^2$ and $\mathbf{S}^2$ for antisymmetric states in jj-coupling using the non-antisymmetric values (4.1). These have been obtained and diagonalized for all two-electron configurations up to dd. The results are presented in the accompanying set of transformation matrices (see Fig. 1). On the left of the matrices are given the two j values of the state in jj-coupling, the J value being shown at the top in the Russell-Saunders notation. The transformations are independent of M_J. These matrices also give the transformations for the configurations p^4, p^5s, p^5p, p^5d, d^8, d^9s, d^9p, and d^9d, if the given j values are taken as the missing j values of the almost closed shells. It should be noted that while the phases in LS coupling are chosen here in no special way, the phases in jj coupling are those given by using Wigner's formula[10] for the vector addition of j_1 and j_2' (Wigner's l and $\tilde{l}$) in the first term on the right of (4.2).

It might be mentioned incidentally that these transformations furnish a very simple means of

[9] See Part II of reference 2.

[10] Wigner, *Gruppentheorie*, p. 206.

[11] This gives us the general rule for the allowed states in jj-coupling for two equivalent electrons, *viz.*, all J values for $j\neq j'$, even J values for $j=j'$.

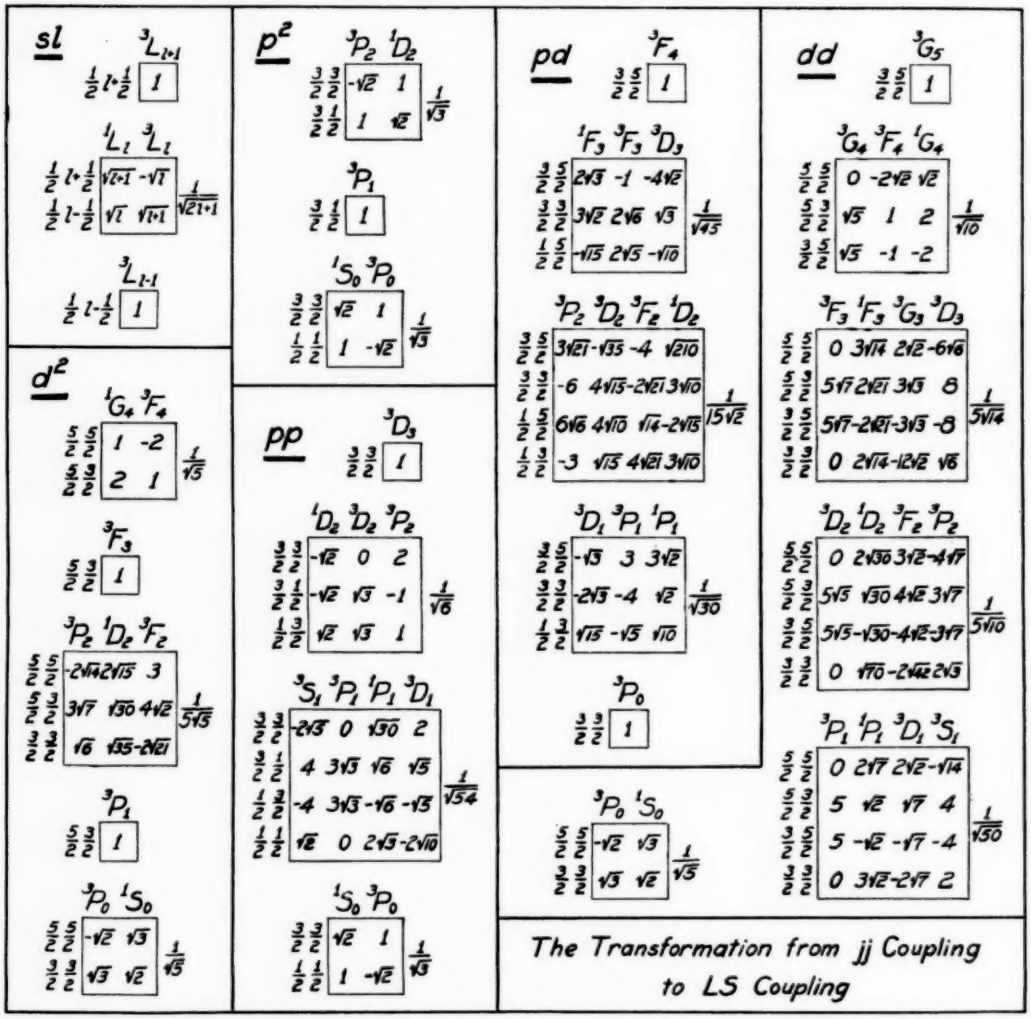

FIG. 1.

obtaining the matrix of spin-orbit interaction in *LS*-coupling, since this matrix has a simple diagonal form in *jj*-coupling. As a check of the transformations, this matrix has been obtained in this way and compared with that given by Johnson.[12] The transformation to *jj* coupling can alternatively be obtained by diagonalizing the matrix of spin-orbit interaction in *LS* coupling. This method applies not only to two-electron configurations but to any configuration in which the matrix of spin-orbit interaction is nondegenerate.

[12] Johnson, reference 8. We find no error in Johnson's matrices other than that pointed out by Inglis and Ginsburg, Phys. Rev. **43**, 194 (1933); that for *pp* the ${}^3P_0$-${}^1S_0$ element should read a_1+a_2 in place of a_1-a_2.

The Zeeman Effect of Lead II, III and IV

J. B. GREEN AND R. A. LORING, *Mendenhall Laboratory of Physics, Ohio State University*

(Received September 1, 1932)

Zeeman Effect of Pb II, III and IV, have been studied at fields of about 40,000 gauss with the newly completed outfit at the Mendenhall Laboratory. Gieseler's results on Pb II are in general correct, although a few minor discrepancies have been found. The $6d\,^2D_3$ level shows an anomalous g-value which may be attributed to the fact that the $6d\,^2D$ levels are inverted, or to perturbations caused by neighboring configurations. In Pb III a similar perturbation is found in the $6s\,7p$ configuration. Here the g-sum of $^3P_1$ and $^1P_1$ is slightly higher than the theoretical value, while the $^3P_2$ level, which should be unaffected by ordinary changes in coupling, yields a value 1.35 instead of 1.50.

CLASSIFICATIONS of the spark spectra of lead have been suggested by Gieseler[1] for Pb II and by Smith[2] for Pb III and Pb IV. Pb II shows a system of doublets and quartets and Pb III a system of singlets and triplets, while Pb IV shows doublets. The Zeeman effect for these spark spectra has not been measured except for a very few of the Pb II lines. Back[3] has measured λ6660, λ5608 and λ2203 and shown that they are $^2S-{}^2P$ transitions. Earlier work by Van der Harst[4] indicated unresolved Zeeman patterns for λ5608, λ4386, λ4245 and λ2698. Kimura and Nakamura[5] have classified the spectra into different degrees of ionization by means of the lengths of the lines in a condensed spark discharge. The present problem was undertaken to check the above classifications with the Zeeman effect patterns.

The apparatus consisted of a large Weiss type water-cooled electromagnet constructed in this laboratory, which gave a field strength of about 40,000 gauss when operated with a current of 90 amperes. Pole faces of 10 mm and about 3 mm pole gap were used. The magnet was operated well up on the saturated part of the magnetization curve, so that variations of 2–3 amperes in the current gave practically no variation in the field strength. The spectroscopic apparatus consisted of a 21 foot concave grating ruled with 30,000 lines per inch by R. W. Wood, mounted in a Paschen-Runge mounting in the basement of this laboratory. Spectra from 2000A in the first order to 4000A in the third order could be observed simultaneously. The grating room, being well insulated, gave good temperature stability. To insure more constant temperature operating conditions, a wooden box, open on one side, was placed over the grating, and the temperature of the room itself was controlled by a thermostat. The extremely good definition of the Zeeman patterns, even with exposure times of 30 hours, showed that conditions were unusually good.

The light source was a rotating-disk vacuum arc similar to that used by the authors[6] on the spectra of tin. It consisted of a thick walled brass vacuum chamber, placed so that the magnet pole pieces formed a part of the two sides, as shown in Fig. 1. Here HH' is the magnetic field axis. $BBBB$ shows the vacuum chamber; D is a brass disk 8 inches in diameter, which rotates counterclockwise in this figure about the axis A. This disk forms one electrode. The other electrode is a 1.5 mm brass or tungsten wire W, which slides vertically in a hollow brass rod C and touches D at the field axis. R is a hard rubber insulator, threaded to take the hollow brass tube G. Contact is made between W and G by a flexible wire F, which is fastened to the light brass weight E.

[1] Gieseler, Zeits. f. Physik **42**, 265 (1927).
[2] Smith, Phys. Rev. **34**, 393 (1929).
Smith, Phys. Rev. **36**, 1 (1930).
[3] Back, Zeits. f. Physik **73**, 193 (1926).
[4] Van der Harst, Proc. Amster. Acad. Sci. **22**, 300 (1920).
[5] Kimura and Nakamura, Japanese J. Phys. **3**, No. 7–10, 197 (1924).
[6] Green and Loring, Phys. Rev. **30**, 574 (1927).

A vacuum seal is maintained between R and B by soft wax and between G and R by a soft rubber gasket and stopcock grease. One electrical connection is made to the outside of G. Some slight adjustment of the centering of W may be obtained by sliding R on the top of the box. K is a long steel tapered shaft carrying a sprocket L

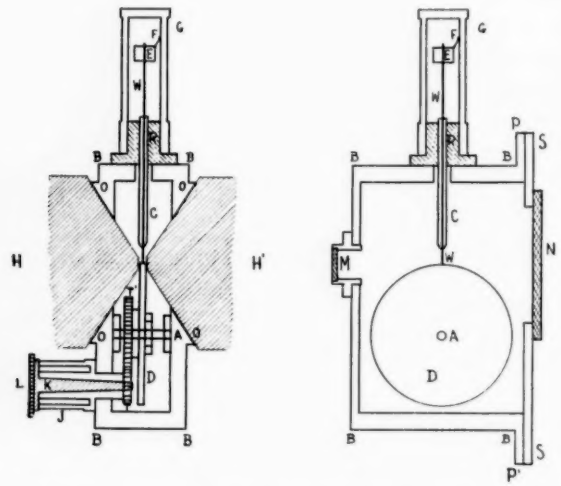

FIG. 1. Vacuum discharge source in magnetic field.

at one end and a small brass gear T at the other end, which in turn engages the gear, T'. This sprocket is connected by a chain drive to another sprocket and reducing gear. A motor drives the whole mechanism and causes the disk to rotate. Windows are placed in the front and back of the box at M and N. M is a fused quartz window cemented onto a brass collar which is fastened by soft wax to the vacuum box. N is a large plate glass window attached with soft wax to the back plate S. This plate covers the whole back of the vacuum box and can be removed for the purpose of changing the disk and cleaning the interior of the box. Soft wax seals are used here also as at M and N. Suitable manometer and pump connections make it possible to measure and maintain the vacuum.

The material used for the disk D depends upon the element being investigated. For the spectrum of zinc a $\frac{1}{8}$ inch brass disk and a 1.5 mm brass wire make a good combination. The principal SP multiplet lines are sufficiently strong to give a good exposure in about five minutes with an a.c. current of 3 amp., an air pressure of about 8 mm of mercury, a 4× normal slit-width in the spectroscope and an Eastman 40 plate. For silver a 2 mm silver wire was silver soldered to the circumference of a copper disk and knurled flat. A tungsten wire made the other connection. For lead and tin a lead wire, a 40–60 solder wire or a tin wire was soldered on the rim of the wheel, knurled flat and used with a brass wire or a tungsten wire. For antimony and bismuth and other nonmalleable metals a brass disk may have its circumference turned down until it is about 1 mm thick and the metal cast on the outer surface and trued up in a lathe or in a grinding wheel.

The intensity of the discharge seems to depend somewhat upon the pressure between the wire and the disk and so it is necessary to experiment with the size of weight E and the stiffness of flexible wire F. The character of the arc is quite different when it takes place in the magnetic field. Without the presence of the field the arc strings out along the periphery of the disk. In the presence of the field and with the intersection of the disk and the wire exactly centered in the magnetic axis the spark appears to stretch out along the field and form a very narrow bright line. The character of the spectrum is decidedly different also. With no field the spectrum is arc-like in type, while, with a field, the first, second and third spark spectrum lines appear with good intensity and with no apparent diminishing of the arc lines. In the case of tin, some first, second and third spark lines that are very strong in the magnetic field are very weak lines or do not appear at all in a condensed spark. This is seen in the case of Sn λ5597, Sn λ5369 and Sn λ4215.

In order to get the optimum operating conditions, a series of low-dispersion plates was made with a Gaertner constant deviation spectrograph. Five-minute exposures were made on d.c. Ortho plates with the pressure varying in steps of 1 mm from 4–20 mm of Hg, and a current of about 2 amp. and 110 volts a.c. An air pressure of 8 mm of Hg gave the most intense spark spectrum and the least intense band spectrum. Higher pressures made the arc more stable but the lines were not so sharp and the band spectrum became objectionable. A second series was run with hydrogen as residual gas.

A hydrogen atmosphere causes the discharge to become slightly more unstable although it is still manageable. The arc current was kept below 4 amp. to minimize spattering of small pieces of molten lead against the window. Even under these conditions it was necessary to clean the window every three hours to prevent excessive absorption of the light.

Twenty 2×10 inch Eastman 40 plates were set up in the blue and ultraviolet regions and, at the same time, four 2×10 inch W and W Panchromatic plates were set up in the first-order green and red regions. More recently we have found that the Eastman 1G Special Spectroscopic[7] plates are much more satisfactory for the green region.

Altogether we made eleven exposures ranging from two hours to thirty hours net time. The first six sets were run without separating the polarizations. 40–60 solder was used on the rim of the disk. The last five exposures were run with lead strips cut from $\frac{1}{8}$ inch commercial lead sheeting soldered to the edge of the brass disk. Polarizations were separated by placing a large calcite crystal between the window M and the condensing lens of fused quartz of 12 inch focal length. Two 5X enlarged images were focussed at the slit about an inch apart horizontally, so that either polarization could be selected and introduced into the spectroscope with no chance of contamination by the other polarization. Even under the best operating conditions, it was necessary to change the wire *W* and clean the window *M* every three hours. The disk *D* had usually to be refaced after about fifteen hours.

The plates were developed in a modified Eastman D-76 fine-grain developer with 50 percent more than the recommended amount of sodium sulphite. They were fixed in an acid-hypo bath.

In the few years immediately following the proposal of Hund's theory of complex spectra, the Zeeman effect was used principally as a check on the classification of spectra but recent work on complex spectra has developed the necessity for accurate measurements of the magnetic splitting-factor *g*. With this idea in mind, the plates were dried slowly and carefully to prevent possible distortions of the emulsion. They were then measured on a Société Gènévoise measuring engine. Each line was measured in five different positions along the length of the line, with two settings in each position. In several cases, the same line was remeasured on the same plate, and the agreement between the measured patterns for sharp lines was usually better than 0.5 percent.

With unresolved patterns, the method suggested by Shenstone and Blair[8] were used for calculating *g*-values. One must, however, exercise considerable care and discretion in the application of these equations. It will be noted that the formulas apply only in case the blackening were proportional to the intensity of the light. Overexposure and plate inertia might serve to shift considerably the center of intensity of an unresolved group of lines. Thus, the relative intensities in a 5-line group vary theoretically from 1 to 15. With underexposure, the weaker lines may not appear at all because of plate inertia. The apparent center of intensity is thus shifted toward the stronger lines. With overexposure, the stronger lines are not blackened proportionately and the apparent center of intensity is shifted toward the weaker components. An example of this effect is shown by Table I.

TABLE I. *Effect of intensity on the apparent center of intensity of Pb* 3176.*

Plate	Pattern	Order	Plate	Pattern	Order
My-6-d	(0) 1.151	I	My-1-7	(0) 1.111	II
My-6-6	(0) 1.111	II	My-1-16	(0) 1.099	III
My-6-16	(0) 1.089	III	A-19-6	(0) 1.158	II
My-1d	(0) 1.135	I			

* The theoretical pattern of this line consists of three groups of seven lines each. The intensity of the zero group is shaded with decreasing intensities symmetrically outward on both sides of the zero position. Its position, therefore, would be unaffected by change of intensity. The perpendicularly polarized components are each shaded outward with decreasing intensities. Note that the measured apparent center of intensity progresses inward with increasing diffraction order in the same set of plates (the intensity of the line decreases with increasing order number), and also that corresponding orders of different sets give consistent patterns, except A-19-6 which was about as strong in the second order as the other two sets in the first order.

[7] Mees, J. Opt. Soc. Am. **21**, 753 (1931).

[8] Shenstone and Blair, Phil. Mag. **8**, 765 (1929).

TABLE II. *Zeeman effects in the first spark spectrum of Pb.*

λ	ν	Classification (Gieseler[1])	Pattern	Plates measured
2203	45367.7	$2^3P_2-2^3S_1$	(0.310) 0.99 1.68	3
2719	36756.8	$p^3D_2-5^3F_3$	(0) 1.07	1
2948	33903.1	$3^3D_3-5^3F_4$	(0) 0.95	2
3016	33140.1	$3^3D_2-5^3F_3$	(0) 0.84	3
3279	30480.4	$3^3P_2-5^3S_1$	(0) 0.91	4**
3452	28963.8	$p^3D_3-5^3F_4$	(0) 0.80	1
3718	26886.9	$3^3P_1-4^3S_1$	(.64) 1.30	3
3786	26404.0	$p^3D_2-4^3F_3$	(.40) (1.20) .44 1.08	5
3909	25574.4	$3^3D_2-4^3P_2$	(.30) 1.28	4
4153	24074.1	$3^3P_2-4^3S_1$	(.32) 1.01 1.60	2
4242	23566.2	$3^3D_3-4^3F_3$	(.18) (.65) (1.10) .20 .62 1.07 1.52 1.96	5
4245	23550.5	$3^3D_3-4^3F_4$	(0) 0.88	3
4386	22790.5	$3^3D_2-4^3F_3$	(0) 0.86	3
5042	19824.8	$p^4\bar{P}_1-3^3P_2$	(0) 0.84	2
5372	18609.5	$p^3D_3-4^3F_4$	(0) 0.47	2†
5608	17823.8	$2^3S_1-3^3P_2$	(.33) 1.00 1.67	2
5857	17067.6	$p^4\bar{P}_2-3^3P_2$	(0) 1.30	1*
5876	17012.4	$p^4\bar{P}_1-3^3P_1$	0.77	1

* Also assigned as Pb III $6^3D_3-7^3P_2$. (Smith[2].)

† Parallel components show six equally spaced lines with a separation of about 0.30.

** This classification is obviously incorrect. The pattern suggests an unresolved $^2P_1{}^2D_2$ which calculates ±(1/15) 11/15 13/15.

Table II shows the measured Zeeman effects for the spectrum of Lead II, and Table III gives the *g*-values calculated from the patterns in Table II.

In addition to the remarks made in connection with the tables, we note the following interesting facts. The *g*-values for 3^2D_3 and 4^2F_3 calculated from the precision measurement on λ4242 are 1.29 and 0.85 as compared with the theoretical values of 1.20 and 0.86. No theory has yet been proposed to account for perturbation of *g*-values of one-electron systems. We must therefore look for the explanation of the large perturbation in the *g*-value of 3^2D_3 in perturbations due to interactions of neighboring electronic configurations, or in the fact that the 3^2D terms are inverted. In the spectrum of Pb III we find similar difficulties which will be discussed later.

The quartet system also shows considerable perturbations, but here we have the case of a three-electron system (p^2s) and the *g*-values could be calculated by the method of Inglis and Johnston.[9]

The assignments given in Tables II and III are those of Gieseler,[1] and the authors' observations of the *g*-values indicate that the assignments are in general correct, although there is some room for doubt as to the validity of the classifications of the sp^2 configuration.

Table IV shows the measured Zeeman effects for Pb III, and Table V shows the *g*-values calculated from the measured patterns of Table IV.

The spectrum of Pb III offers an excellent opportunity for the comparison of theory and experiment. The theory of the Zeeman effect for two-electron systems of the simpler types has been developed by Houston[10] and by Goudsmit,[11] along with the theory of multiplet separations. Discrepancies in the mutiplet separations of 6^3D and 5^3F have already been noted by the authors.[12] The present work indicates serious discrepancies in the present status of the Zeeman effect according to this theory.

The $6s\ 7s^3S_1-6s\ 7p$ multiplet has been studied with especial care. This group of four lines appeared with very good intensity on all our plates, and were remarkably sharp for such high excita-

[9] Inglis and Johnston, Phys. Rev. **38**, 1642 (1931).

[10] Houston, Phys. Rev. **33**, 297 (1929).

[11] Goudsmit, Phys. Rev. **35**, 1325 (1930).

[12] Green and Loring, Phys. Rev. **38**, 1289 (1931).

TABLE III. *g-value table for Pb II.*

	2^2P_2	$p^4\overline{P}_1$	2^2S_1	$p^4\overline{P}_2$	p^2D_2	p^2D_3	3^2P_1	3^2P_2	3^2D_2	3^2D_3	4^2S_1	4^2P_2	4^2F_3	4^2F_4	5^2F_3	5^2F_4	
λ2203	1.33		2.02														
2719					0.55										0.85		§
2948										1.29						1.14	
3016									0.85						0.85		
3452						1.42										1.14	
3718							0.66				1.94						†
3786					1.65								0.85				‡
3909									1.16			1.40					*
4153								1.33			1.97						†
4242										1.29			0.85				†
4245										1.29				1.11			
4386									0.85				0.85				
5042		2.34						1.34									
5372						1.39								1.11			
5608			2.02					1.34									†
5857				1.27				1.33									
5876		2.20					0.66										
Mean	1.33	2.27	2.02	1.27	X	1.40	.66	1.33	.85	1.29	1.95	1.40	.85	1.11	.85	1.14	
Theor.	1.33	2.67	2.00	1.73	.80	1.20	.67	1.33	.80	1.20	2.00	1.33	.86	1.14	.86	1.14	

* This pattern is ±(0.30) 1.28. The *g*-values chosen give ±(0.12) (0.36) 1.04 1.08 1.52. If only the perpendicular components are matched we can take $g_1=0.85$ $g_2=1.71$. This line is assigned to the triplet system also. (Smith.[3] See Table IV.)

† Precision measurement.

‡ This is an unusual type. It calculates with these *g*-values to give. ±(0.40) (1.20) −0.35 0.45 1.25 2.05 which is good in comparison with the measured pattern of ±(0.40) (1.20) 0.44 1.08 Graphically the pattern is as shown in Fig. 2.

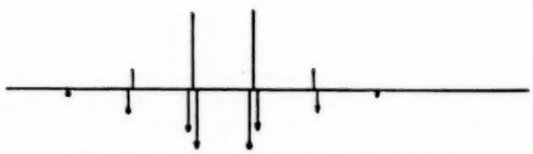

FIG. 2. Possible structure of Pb λ3786.

§ This line may possibly be confused with a copper line. This line calculates at about λ2718.8. The copper line is at λ2718.9. Kayser lists a Pb line at λ2717.2. A line appears on our plates at λ2717.5. Gieseler, on the other hand, lists a Pb line at λ2719.78. Our line at λ2717.5 appears to have a pattern similar to that of λ3786. It is not measurable due to its position on the plate.

tion spark lines. The intervals between the members of the 6s 7*p* levels are not in very good agreement with each other according to Houston's theory. However, if we calculate the parameters according to his suggestions, the *g*-values of $^3P_1$ and $^1P_1$ are in fairly good agreement with experiment. The *g*-sum which should be 2.50, is somewhat larger, 2.53, a value too high to be accounted for by experimental error. The *g*-value of the $^3P_2$ term which should be unaffected by changes in coupling turns out to be 1.34_5 instead of 1.50. There is no other level in the neighborhood whose combinations are sufficiently strong; so that the trouble cannot be attributed to incorrect classification. This suggests, then, a perturbation due to a level with $j=2$ from some other configuration of electrons. An inspection of Table VIII (unclassified lines) suggests the possibility of such a level. The line λ4183, from its Zeeman effect, appears to be a combination between a $^3S_1$ level and a level with $j=2$ and a *g*-value of 0.97. Strangely enough, the wave number of this line is exactly halfway between 7^3S_1 and 8^3S_1, so that it might be either $7^3S_1 - x_2$ or $x_2 - 8^3S_1$, with $x_2=84{,}795$, and only 2034 wave numbers from 7^3P_2, sufficiently close to produce a considerable perturbation.

In order for this level to produce a perturbation on the $^3P_2$ level, it is not sufficient that its *j*-value should be the same. Because of the nature of the integrals involved, Condon[13] has shown that to

[13] Condon, Phys. Rev. 36, 1121 (1930).

TABLE IV. *Zeeman effects in the second spark spectrum of lead.*

λ	ν	Classification (Smith[2])	Pattern	Plates measured
2562	39016.2	$6^1D_2-5^1F_3$	(0) 0.95	5
3031	32975.8	$6^3D_2-5^1F_3$	(0) 0.83	1
3044	32842.8	$6^3D_1-5^3F_2$	(0) 0.77	3
3089	32361.9	$6^3D_2-5^3F_2$	0.65 (1.02) 1.65	2
3138	31859.0	$6^3D_2-5^3F_3$	(0) 0.98	4
3176	31471.0	$6^3D_3-5^3F_4$	(0) 1.12	7
3242	30828.1	$6^3D_3-5^3F_3$	(0.64) 1.12	4
3276	30514.5	$7^3P_1-7^3D_2$	(0) 1.00	4
3280	30479.9	$7^3P_0-7^3D_1$	(0) 0.49	4
3297	30316.0	$7^3P_1-7^3D_1$	0.52 (0.86) 1.42	3
3689	27097.6	$6s\,7s^3S_1-6s\,7p^1P_1$	(0.849), 1.140, 1.972	7‡
3706	26974.7	$7^3P_0-8^3S_1$	(0) 2.00	3
3728	26810.5	$7^3P_1-8^3S_1$	(0.58) 1.32 2.00	4
3833	26083.0	$pp^1D_2-5^1F_3$	(0) 0.51	4†
3841	26023.3	$7^3P_2-7^3D_3$	(0) 1.30	4
3854	25939.5	$7^3P_2-7^3S_1$	(0) (0.65) 0.68 1.33 1.97	6‡
3909	25573.7	$7^3P_2-7^3D_2$	(0.30) 1.27	4
3952	25296.9	$6s\,6d^1D_2-6s\,7p^1P_1$	(0) 1.01	3
4004	24967.0	$pp^1D_2-5^3F_3$	(0) 0.78	1
4094	24415.1	$6s\,7p^1P_1-6s\,7d^3D_2$	(0) 1.15	1
4128	24316.8	$6s\,7p^1P_1-6s\,7d^3D_1$	0.54 1.06	1‖
4141	24139.5	$6^1D_2-7^3P_2$		1
4272	23398.2	$6s\,7s^1S_0-6s\,7p^1P_1$	(0) 1.14	4‡
4500	22218.4	$6s\,7p^1P_1-6s\,7d^1D_2$	(0) 1.13	2§
4571	21869.3	$7^3P_2-8^3S_1$	(0) (0.63) 0.65 1.29 1.91	3
4761	20998.0	$7^3P_1-7^3S_1$	(0.59) 1.38 1.98	6‡
4798	20834.0	$7^3P_0-7^3S_1$	(0) 1.98	5‡
5857	17067.5	$6^3D_3-7^3P_2$	(0) 1.30	1*

* Also assigned as Pb II $p^4\bar{P}_2-3^2P_2$ (Gieseler.[1] See Table II).

† Components broad—Shaded out.

‡ Precision measurement.

§ See text.

‖ Only perpendicular components measurable.

TABLE V. *g-values of Pb III.*

Line	7^1S_0	7^3S_1	8^3S_1	7^3P_0	7^3P_1	7^3P_2	7^1P_1	6^1D_2	p^1D_2	6^3D_1	6^3D_2	6^3D_3	7^3D_1	7^3D_2	7^3D_3	7^1D_2	5^1F_3	5^3F_2	5^3F_3	5^3F_4
2562								1.05									1.00			
3031											1.15						0.99			
3044										0.50								0.67		
3089											1.15							0.67		
3138											1.15								1.09	
3176												1.33								1.25
3242												1.33							1.09	
3276					1.38_3									1.13_2						
3280				√									0.49							
3297					1.38_2								0.52							
3689		1.97_5					1.14_9													
3706			2.00	√																
3728			2.01		1.37_8															
3833									?								?			
3841						1.34_7									1.33_4					
3854		1.98_7				1.34_3														
3909						1.35_7								1.20_4						
3952							1.14_9	1.06												
4004									1.40										1.09	
4094							1.14_7							1.15_3						
4128							(1.06)						(0.54)							
4141						?		?												
4272	√						1.14_5													
4500							1.14_5									1.13_8				
4571			2.00			1.36_5														
4761		1.98_2				1.38_4														
4798		1.99_0		√																
5857						1.34_5						1.32_5								
Aver.	√	1.98_3	2.00	√	1.38_3	1.34_5	1.14_7	1.06	1.40	0.50	1.15	1.33	0.50	1.16	1.33	1.14	1.00	0.67	1.09	1.25
Theoretical normal	√	2.00	2.00	0/0	1.50	1.50	1.00	1.00	1.00	0.50	1.16_7	1.33_3	0.50	1.16_7	1.33_3	1.00	1.00	0.66_7	1.08_3	1.25
Houston	√	2.00	2.00	√	1.37_1	1.50	1.12_9	1.00_1	?	0.50	1.16_6	1.33_3	0.50	1.16_6	1.33_3	1.00_1	?	0.66_7	?	1.25

perturb each other both levels must belong to the same kind of electronic configuration, i.e., both of the configurations must be odd or both even. It would seem, therefore, that the level x_2 must belong to a *pd* configuration. In addition, it should be mentioned that the two levels need not necessarily be very close together to perturb each other. The perturbation calculation usually involves a term containing the difference in energy values of the perturbing terms in the denominator, and thus would ordinarily decrease as the distance between the terms increases. But if all the elements of the perturbation integral have the same phase for some interval, the value of the integral may be appreciable.

The accuracy of the measurements also indicates a discrepancy, just barely detectable, in the g-value of 7^3S_1. The measured value is 1.98_3, a value just on the limit of the accuracy of separable from the theoretical value 2. This effect does not come about as the result of the averaging of several discordant observations. Every line involving this level gives a g-value less than the theoretical.

Fig. 3 is included to show the effect on the Zeeman pattern of a charge from *ls* to *jj* coupling. Fig. 3a is the Zn line λ4722, II order, and 3b is the Pb III line λ4761, I order. Both of these lines involve the same transition, $^3P_1-{}^3S_1$.

Fig. 4 shows the effect on the Zeeman pattern

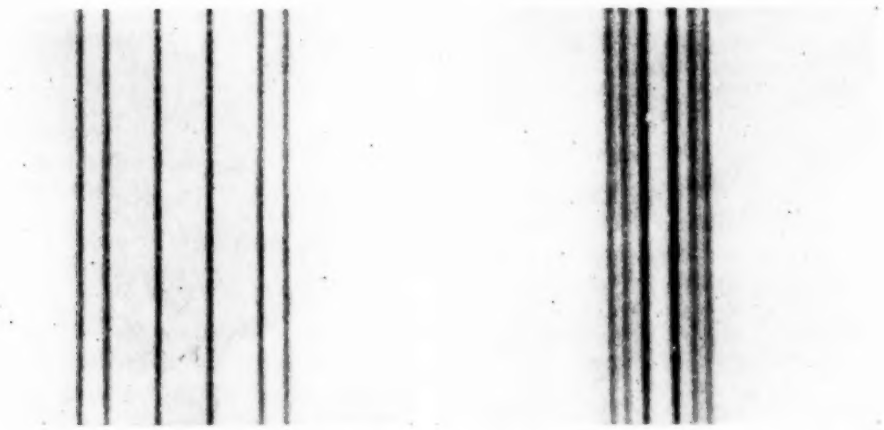

a b

FIG. 3. (a) Zn 4722, II order, $L-S$ coupling. (b) Pb III 4761, I order, $J-J$ coupling.

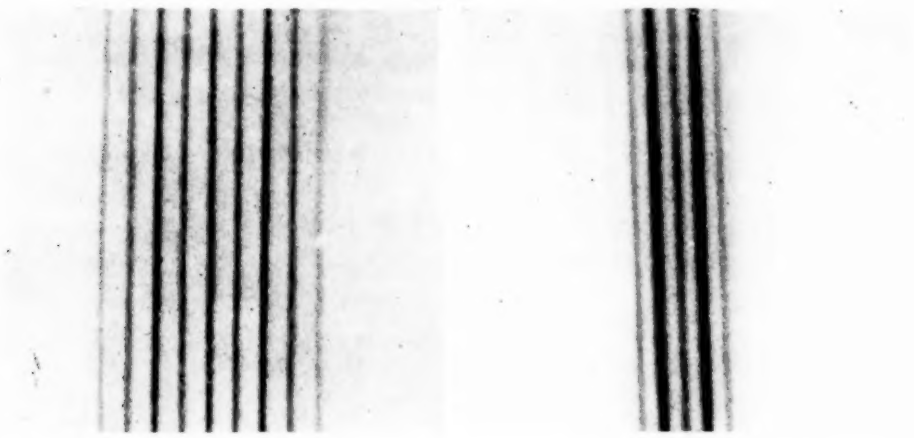

a b

FIG. 4. (a) ZnI 4810, II order, LS coupling. (b) PbIII 3854, I order, JJ coupling.

of the perturbation of the g-value of the $^3P_2$ term. Fig. 4a is the Zn line λ4810, II order, and 4*b* is the Pb III line, λ3854; both lines involve the same transition, $^3P_2-{}^3S_1$. The blackest lines on the photograph Fig. 4b are overlapped parallel and perpendicular components, an effect which causes the pattern to look like a seven-line pattern instead of the nine-line pattern which it really is.

We should like also to suggest an alternate classification for the line λ4500, classified by Smith[2] as $6s\,7p^1P_1-6s\,7d^1D_2$. The level $^1D_2$ occurs in only one other transition, with $6s\,6p^1P_1$, and might, therefore, as well be 8^1S_0, a classification much more consistent with the Zeeman pattern of 4500, and also consistent with the position of 8^3S_1.

Table VI gives the measured Zeeman effects for the third spark spectrum of lead and Table VII gives the g-values calculated from these patterns.

The lines of Pb IV are not sufficiently sharp to be able to draw any conclusions from the g-factors the values of which fit the theoretical values within experimental error.

Table VIII shows the magnetic resolution of unclassified lines in the lead spark that appeared on our plates.

TABLE VI. *Zeeman effects in the third spark spectrum of lead.*

λ	ν	Classification (Smith[2])	Pattern	Plates measured
2864	34899.4	$6d^2D_3-7p^2P_2$	0.21 (0.77) 1.76	5
3052	32748.8	$7s^2S_1-7p^2P_2$	(0.32) 0.97 1.62	4
3087	32383.5	$7p^2P_2-7d^2D_3$	(0) 1.11	1
3145	31781.3	$7p^2P_2-7d^2D_2$	———	1†
3221	31034.4	$6p^2D_3-7p^2P_2$	(0) 1.08	3
3962	25229.8	$6d^2D_2-7p^2P_1$	(0) 0.81	3*
4050	24685.7	$7s^2S_1-7p^2P_1$	(0.61) 1.28	3

* Smith[2] has suggested two alternative sets of classifications for Pb IV. This line is given the same classification in both sets.

† Not measurable, but qualitatively correct, i.e., the pattern shows that $\Delta j=0$.

TABLE VII. *g-value table for Pb IV.*

Line	$6d^2D_2$	$6d^2D_3$	$7s^2S_1$	$7p^2P_1$	$7p^2P_2$	$7d^2D_3$
2864						*
3052			1.939		1.295	
3087					1.295	
3221		1.174			1.295	1.19
3962	0.783			0.676		
4050			1.902			
Mean	0.783	1.174	1.92	0.676	1.295	1.19
Theor.	0.800	1.200	2.00	0.667	1.33	1.200

* The g-values for this pattern calculate to be $g_1=2.534$ and $g_2=0.986$ with $j_1=1/2$ and $j_2=3/2$. This was in an alternative classification which is obviously incorrect.

TABLE VIII. *Magnetic resolution of unclassified lines in the lead spark.*

λ	Pattern	Plates measured
2192	(0) 0.967	1
2242	(0) 1.17	1
2247	(0) 1.21 [−2.24]	1*
2568	(0) 0.917	1
2770	(0) 1.26	1
2977	(0) 1.63	1
2978	(0) 1.07	1
3455	(0) 1.17	3
3483	(0) 0.905	3
3586	(0) 1.02	3
3590	(0) 0.900	3
3593	(0) (0.89) 0 1.07	4
3655	(0) 0.92	3
3714	(0) 1.03	3
3736	(0) 1.13	3
3827	(0.58) 0.92	5
3993	(0) 0.94	1
4023	0.88	
4031	(0) 1.13	
4183	(0) (0.99) 0.95 1.91 [2.89]	†
4401	(0) 0.84 1.12	‡
4802	(0) 1.14	4
5545	(0) 1.07	2

* A fourth weak comp on short wave side at 2.24.

† Some doubt about 2.89 comp. Only appears on one side. See also text on Pb III.

‡ Parallel component doubled on one plate; possible $\Delta j=0$.

Infrared Absorption Bands of Methane

WILL V. NORRIS AND HILBERT J. UNGER, *University of Oregon*

(Received January 3, 1933)

The *fine structure of the infrared bands of methane* in the region 1–2μ has been observed, and four new bands located at 1.135, 1.187, 1.330 and 1.734μ. The 1.66μ band observed by Moorhead was re-observed with the result that some 14 new lines were added to it. The line spacing in all the bands in this region is of the order of 10.5 cm^{-1}, but varies from 9.44 to 10.8 cm^{-1}. All the bands have sharp zero branches with a tendency to shade off on the low-frequency side, except for the one at 1.33μ, which is quite symmetrical in all its branches. The positive branch of the 1.66μ band decidedly converges to the red (line spacing increases towards the high frequencies), which was also observed by Cooley in the 3.5μ band. The infrared data in the region observed favors the tetrahedral model assumed by Dennison for theoretical work. It is possible to use as a fundamental frequency $\nu_1 = 2913$ cm^{-1}, found in the Raman spectrum, in representing the harmonic and combination bands of methane instead of the usually assumed 4217 cm^{-1} ($=\nu_1+\nu_4$).

INTRODUCTION

THE infrared region from 1–2μ has been investigated with a spectrometer of sufficient resolving power to obtain the fine structure of six methane bands. All of these bands have been reported before, except for the ones at 1.135, 1.187, 1.33 and 1.738μ, but the fine structure has not been reported on any but the 1.66μ band.[1] The position of the bands as found by Ellis[2] agrees with our results within the experimental error of his wave-length determinations. The 1.37μ band was not investigated as it lies at the center of the 1.38μ water vapor band, which is very strong, and would require a vacuum spectrograph to eliminate it.

APPARATUS AND EXPERIMENTAL PROCEDURE

The experimental work was done with an automatic recording spectroscope of the Littrow type, consisting of two 60° and one 30° prisms with faces 10 x 15 cm, and a collimating mirror with a 60 cm focus. The prisms were so arranged that the light traversed the path twice, giving a dispersion equivalent to five 60° prisms. A more complete description of the apparatus may be found in a previous paper.[3]

The methane gas used was obtained in small cylinders from the Fisher Scientific Co., Pittsburgh, and contained a small amount of ethane. However, comparison with the ethane spectrum showed there was not enough present to be detected. The methane was released into the case of the spectroscope (equivalent to a three meter path), but the gas pressure was not determined.

DISCUSSION

D. M. Dennison and S. B. Ingram[4] have reported a series of methane bands in the photographic, infrared region, 8900A, which they consider to be the third overtone $n=0\rightarrow4$ of the fundamental, $\nu_3 = 3014$ cm^{-1}, at 3.3μ. They give the equation $\nu = 3085n - 66n^2$, which for $n=3$ gives $\nu = 8661$ cm^{-1}. The band at 1.16μ has its center at 8606 cm^{-1}, which agrees well with the above calculated value. According to Dennison's theory of degenerate energy states for the methane molecule there should be five groups of nearly coincident levels. The resulting pattern of lines would give a series of groups of lines which by the continuous recording method with an effective slit width of about 6A would be the apparent spacing of a single band. The grouping of the lines in the 8900A band gives a series of maxima about 10 cm^{-1} apart. This is the spacing of most of the bands of methane, and would help

[1] J. G. Moorhead, Phys. Rev. **39**, 83 (1932).
[2] J. W. Ellis, Proc. Nat. Acad. Amer. **42**, 202 (1927).
[3] H. J. Unger, Phys. Rev. **43**, 123 (1933).
[4] D. M. Dennison and S. B. Ingram, Phys. Rev. **36**, 1451 (1930).

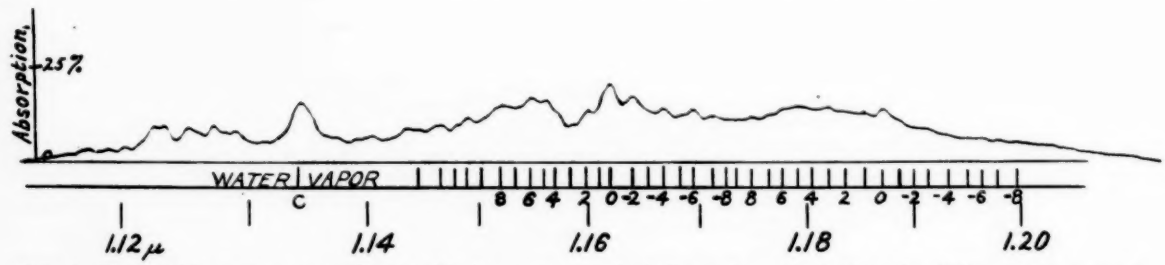

FIG. 1. The 1.134μ water vapor band with its center marked C overlaps the 1.13 and 1.162μ methane bands, but comparison allowed eight lines to be determined in each branch of the last band.

to explain the irregular intensity of the lines in some of the bands.

The 1.13μ band could not be investigated because it lies in the region of the 1.134μ water vapor band, but several lines were determined by comparison with the water band, and the separation was found to be approximately 10 cm^{-1}, which agrees with the other bands of methane. The lines in this water vapor band were first investigated by McAlister and Unger,[5] but the results have never been published. This band contains about forty lines with a fairly sharp zero branch, and the wave-lengths are in excellent agreement with Abbot's[6] work on the atmospheric absorption of the solar radiation.

Fig. 1 shows the 1.13μ water vapor band and the superimposed methane band as well as the

TABLE I. 1.162μ *methane band.*

$\nu = 8606.41 + 8.728M - 0.0456M^2 + 0.0121M^3$

M	λ	ν	$\Delta\nu$
8	1.1522	8679.04	
			8.27
7	1.1533	8670.77	
			12.10
6	1.1549	8658.67	
			8.16
5	1.1560	8650.51	
			8.98
4	1.1572	8641.53	
			8.19
3	1.1583	8633.34	
			10.43
2	1.1597	8622.91	
			8.17
1	1.1608	8614.74	
			8.98
0	1.1620	8605.76	
			15.44
−2	1.1641	8590.32	
			10.32
−3	1.1655	8580.00	
			10.29
−4	1.1669	8569.71	
			10.36
−5	1.1683	8559.35	
			9.51
−6	1.1696	8549.84	
			11.59
−7	1.1712	8538.25	
			10.20
−8	1.1726	8528.05	
			Av. = 9.44

TABLE II. 1.187μ *methane band.*

$\nu = 8425.57 + 11.514M - 0.0274M^2 - 0.0104M^3$

M	λ	ν	$\Delta\nu$
9	1.1735	8521.51	
			10.91
8	1.1750	8510.60	
			10.09
7	1.1764	8500.51	
			9.39
6	1.1777	8491.12	
			9.36
5	1.1790	8481.76	
			10.06
4	1.1804	8471.70	
			10.75
3	1.1819	8460.95	
			12.15
2	1.1836	8448.80	
			12.83
1	1.1854	8435.97	
			13.50
0	1.1873	8422.47	
			9.92
−1	1.1887	8412.55	
			9.19
−2	1.1900	8403.36	
			10.58
−3	1.1915	8392.78	
			11.96
−4	1.1932	8380.82	
			11.92
−5	1.1949	8368.90	
			11.89
−6	1.1966	8357.01	
			9.77
−7	1.1980	8347.24	
			10.44
−8	1.1995	8336.80	
			Av. = 10.86

[5] E. D. McAlister and H. J. Unger, Phys. Rev. **37**, 1012 (1931).

[6] C. G. Abbot and H. B. Freeman, Smithsonian Misc. Col., Vol. 82, No. 1.

1.162μ and 1.187μ methane bands. Wave-lengths of the lines in the latter bands will be found in Tables I and II. Eight lines in each branch of the last two bands were selected and equations calculated to represent their spacings. It is customary to use a second degree equation of the form $\nu = A + BM - CM^2$, where M is an integral number taking positive and negative values, but a cubic equation gives better agreement. An equation for each band will be found in its wave-length table; they were calculated by the least square method as modified by Birge and Shea.[7]

A very interesting band was found at 1.330μ, which has not been reported before (Table III). It has a narrow symmetrical zero branch, the base of which is about 20 cm^{-1} in width. The positive branch consists of eleven distinct lines with the seventh one enhanced. This enhancement is similar to that of the lines in the positive branch of the 1.66μ band, Fig. 2. Little is known of the relative intensity of the negative branch as it runs into the 1.38μ water vapor band, but the position of six lines was determined by comparison with the known water vapor lines. Because of the symmetry of the zero branch and

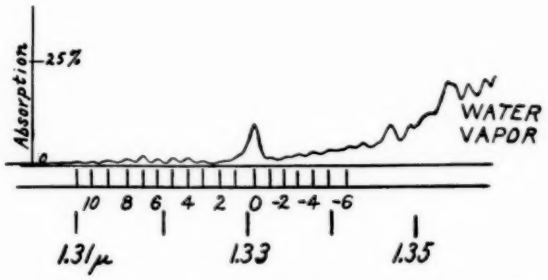

FIG. 2. The negative branch of this band overlaps the last few lines of the intense 1.37μ water vapor band. The zero and positive branches are very symmetrical.

[7] R. T. Birge and J. D. Shea, University of California Publications in Mathematics, **2**, 67–118 (1927).

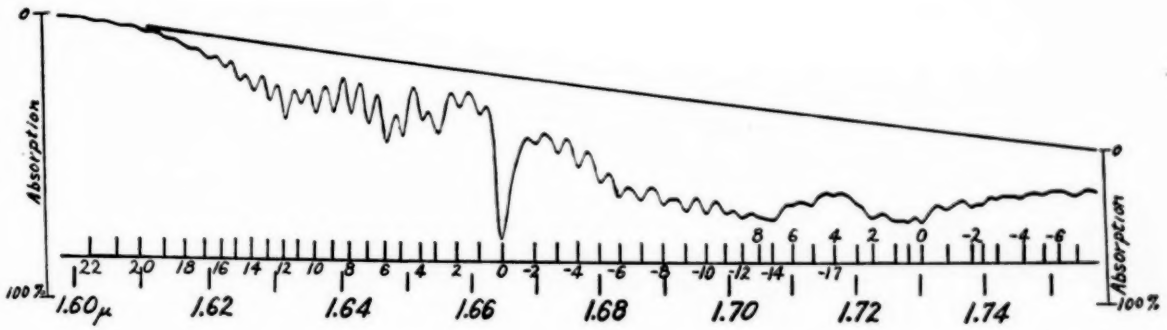

FIG. 3. The 1.66μ band, first investigated by Moorhead, shows an increase in line spacing towards the high-frequency end of the positive branch. The energy curve, which has been drawn in, slopes down rapidly in the direction of long wave-lengths because of strong absorption by the glass prisms.

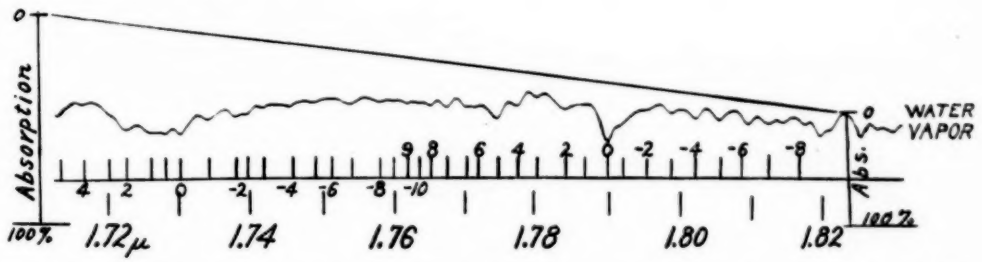

FIG. 4. This is a continuation of the curve in Fig. 3. The long wave-length end of the 1.79μ band runs into the 1.87μ water vapor band.

TABLE III. 1.33μ *methane band.*
$\nu = 7517.46 + 11.106M + 0.00859M^2 - 0.01515M^3$

M	λ	ν	$\Delta\nu$
11	1.3099	7634.2	
			9.3
10	1.3115	7624.9	
			11.0
9	1.3134	7613.8	
			11.6
8	1.3154	7602.2	
			12.1
7	1.3175	7590.1	
			10.2
6	1.3191	7580.9	
			9.8
5	1.3208	7571.1	
			10.3
4	1.3226	7560.8	
			9.7
3	1.3243	7551.1	
			10.8
2	1.3262	7540.3	
			10.8
1	1.3281	7529.5	
			13.6
0	1.3305	7515.9	
			11.3
−1	1.3325	7504.7	
			10.1
−2	1.3343	7494.6	
			9.0
−3	1.3359	7485.6	
			10.1
−4	1.3377	7475.5	
			10.6
−5	1.3396	7464.9	
			11.7
−6	1.3417	7453.2	
			Av. = 10.65

the uniform spacing of the positive and negative branch lines, this band indicates that it arises from a vibration that is only slightly, if at all, coupled with the rotation of the molecule.

The 1.66μ methane band investigated by Moorhead[1] was recorded as shown in Fig. 3; the zero branch is quite sharp and intense with a slight broadening on the low-frequency side, indicative of slight coupling between rotational and vibrational states. Wave-lengths are given in Table IV. The line spacing decreases towards the high frequencies for about 13 lines and then increases again. This increase in spacing is very decided, and is too large to be accounted for by experimental error. Because of the overlapping of this band with the 1.734μ band it was not possible to determine whether this divergence also occurs in the negative branch. Cooley[8] has found that the 3.5μ band of methane converges on the low-frequency side of the branches.

The spectral region from 1.60 to 1.81μ (Figs. 3 and 4) shows a continuous absorption with only the stronger lines resolved. There seem to be two other bands in this region besides the one at 1.66μ, and they have quite definite zero branches. Their positions are 1.734μ and 1.790μ, and the line spacings agree well with those of the other bands (Tables V and VI). Because of the intensity of the absorption under these bands it is very probable that there are other bands present.

Table VII gives the average line spacing of the entire group of methane bands and the corresponding moments of inertia of the molecule. The moment of inertia varies considerably for the different bands, and very probably represents a real difference in it for the various modes of vibration. It is interesting to note that the 3.5μ band lines have spacings of about 1.5 times the 10.5 cm^{-1} which is the spacing of the lines of all the other bands with the exception of the 7.67μ band where the spacing is about 0.5 times 10.5 cm^{-1}. It may be due to a combination band $\nu = \nu_2 + \nu_4$ of which ν_2 has not been investigated, and ν_4 exhibits the half spacing. The line spacing of overtones of ν_4 has not been determined. This still leaves the question unsettled as to whether the methane model is a tetrahedron or a pyramid with the four hydrogen atoms at the corners of the base.

Calculation of the moment of inertia of the methane molecule, I', from the most probable rotational frequency, ν_r, of the positive and negative branches, gives a rough check on that obtained from the line spacing. The I' calculated for the 7.67μ band agrees with the larger moment of inertia (see Table VII), which would favor the pyramid structure.

The data presented in this paper show that the overtone and combination bands of methane in the 1–2μ region can be explained as combinations of four fundamental frequencies required by the regular tetrahedron model for methane.

[8] J. P. Cooley, Astrophys. J. 62, 73 (1925).

TABLE IV. 1.665μ *methane band.*

The mean square average of $\Delta\nu$ for the + and − branches is 10.81 cm^{-1} and 10.72 cm^{-1}, respectively, while the average value is 10.62 in each.

$$\nu = 6009.70 + 11.131M - 0.0449M^2 - 0.00341M^3$$

Positive branch M	μ	ν	$\Delta\nu$
0	1.6645	6007.8	
			12.3
1	1.6611	6020.1	
			12.4
2	1.6577	6032.5	
			11.3
3	1.6546	6043.8	
			9.1
4	1.6521	6052.9	
			10.4
5	1.6492	6063.5	
			8.9
6	1.6468	6072.4	
			11.1
7	1.6438	6083.5	
			9.6
8	1.6412	6093.1	
			9.3
9	1.6387	6102.4	
			9.3
10	1.6362	6111.7	
			10.1
11	1.6333	6121.8	
			8.7
12	1.6312	6130.5	
			9.0
13	1.6288	6139.5	
			8.7
14	1.6265	6148.2	
			9.4
15	1.6240	6157.6	
			8.4
16	1.6218	6166.0	
			8.7
17	1.6195	6174.7	
			11.5
18	1.6165	6186.2	
			12.7
19	1.6132	6198.9	
			13.8
20	1.6096	6212.7	
			13.2
21	1.6062	6225.9	
			15.5
22	1.6022	6241.4	
		m.s. av. = 10.81	

Negative branch M	μ	ν	$\Delta\nu$
0	1.6645	6007.8	
			18.0
2	1.6695	5989.8	
			13.2
3	1.6732	5976.6	
			11.4
4	1.6764	5965.2	
			12.1
5	1.6798	5953.1	
			11.0
6	1.6829	5942.1	
			11.6
7	1.6862	5930.5	
			11.7
8	1.6897	5918.2	
			12.2
9	1.6932	5906.0	
			10.8
10	1.6963	5895.2	
			10.8
11	1.6994	5884.4	
			9.6
12	1.7022	5874.8	
			9.7
13	1.7050	5865.1	
			9.6
14	1.7075	5856.5	
			9.2
15	1.7102	5847.3	
			9.6
16	1.7130	5837.7	
			10.5
17	1.7161	5827.2	
		m.s. av. = 10.72	

TABLE V. *1.734μ methane band.*

$\nu = 5767.62 + 12.471M + 0.0280M^2 - 0.0256M^3$

M	λ	ν	$\Delta\nu$
8	1.7075	5856.5	
			9.2
7	1.7102	5847.3	
			9.6
6	1.7130	5837.7	
			10.5
5	1.7161	5827.2	
			12.2
4	1.7197	5815.0	
			9.5
3	1.7225	5805.5	
			11.8
2	1.7260	5793.7	
			13.4
1	1.7300	5780.3	
			11.6
0	1.7335	5768.7	
			14.0
−1	1.7377	5754.7	
			12.9
−2	1.7416	5741.8	
			12.1
−3	1.7453	5729.7	
			10.5
−4	1.7485	5719.2	
			8.8
−5	1.7512	5710.4	
			8.5
−6	1.7538	5701.9	
			13.3
−7	1.7579	5688.6	
			5.8
−8	1.7597	5682.8	
			11.3
−9	1.7632	5671.5	
			10.5
−10	*	5661.0	
			10.6
−11	1.7698	5650.4	
			Av. = 10.85

* Calculated.

TABLE VI. *1.790μ methane band.*

$\nu = 5588.88 + 9.607M - 0.0546M^2 + 0.00853M^3$

M	λ	ν	$\Delta\nu$
9	1.7615	5677.0	
			11.0
8	1.7649	5666.0	
			8.3
7	1.7675	5657.7	
			12.1
6	1.7713	5645.6	
			9.6
5	1.7743	5636.0	
			8.5
4	1.7770	5627.5	
			9.5
3	1.7800	5618.0	
			10.1
2	1.7832	5607.9	
			9.7
1	1.7863	5598.2	
			11.0
0	1.7898	5587.2	
			7.8
−1	1.7923	5579.4	
			9.3
−2	1.7953	5570.1	
			10.5
−3	1.7987	5559.6	
			10.8
−4	1.8022	5548.8	
			10.8
−5	1.8057	5538.0	
			10.1
−6	1.8090	5527.9	
			11.3
−7	1.8127	5516.6	
			13.0
−8	1.8170	5503.6	
			Av. = 10.2

TABLE VII. *Average line spacing of the entire group of methane bands.*

Band μ	Line separation $\Delta\nu$ cm^{-1}	Moment of inertia I (c.g.s.)	I' (c.g.s.)
1.162	9.44	5.86×10^{-40}	5.8×10^{-40}
1.187	10.86	5.10	4.6
1.330	10.65	5.20	4.5
1.665	10.62, 10.4*	5.21, 5.31*	4.2
1.738	10.85	5.10	
1.790	10.2	5.42	6.0
2.2	10.7	5.17*	
3.31	9.77	5.66†	4.3†
3.5	15.3	3.61	
7.67	5.41	(5.1 or 10.2)†	11.0†
$I = h/4\pi^2c^2(\Delta\nu)$		$I' = 3RT/8\pi^2N\nu_r^2$	

* Moorhead.
† Cooley.

TABLE VIII. *Fundamental frequencies of methane and the possible classification of the bands in the 1–2μ region.*

$\nu_1 = 2913$ cm^{-1} (Raman spectrum) $\nu_3 = 3014$ cm^{-1}
$\nu_2 = 1520$ $\nu_4 = 1304$
$n\nu_1 = 2913n - 15n^2$ represents the overtones of ν_1.

Band μ	ν (obs.) cm^{-1}	Classification*
1.135	8800	$\nu_1 + 2\nu_3 = 8819$ cm^{-1}
1.1620	8606	$3\nu_3 = 8661$
1.1873	8423	$2\nu_1 + 2\nu_4 = 8434$
1.3305	7516	$\nu_2 + 2\nu_3 = 7548$
1.6645	6008	$2\nu_3 = 6028$
1.7335	5769	$\nu_1 + \nu_2 + \nu_4 = 5737$
1.7898	5587	$\nu_1 + 2\nu_4 = 5521$

* $\nu = 3085n - 66n^2$ used for ν_3.

A New Band in the Spectrum of the OH Molecule

HERRICK L. JOHNSTON, DAVID H. DAWSON[1] AND MARGERY K. WALKER, *Department of Chemistry, Ohio State University*

(Received December 16, 1932)

Although the ultraviolet "water vapor" bands were among the earliest molecular spectra to undergo extensive investigation, heretofore only six bands have been reported. These involve transitions between the (0, 1, 2) vibrational levels of an excited $^2\Sigma$ state and the (0, 1) vibrational levels of the normal $^2\Pi$ state. With improved conditions for exciting the spectrum we have obtained 91 lines, heretofore unreported, in the neighborhood of the (0′, 1″) band at λ3428. 44 of these lines prove to be extensions of λ3428; 54 lines (including 11 in common with λ3428) form a new band with a head at λ3484; and 4 lines remain unidentified. Analysis of the new band identifies it as the (1′, 2″) band of the water vapor system. Rotational constants for the normal $^2\Pi$ electronic state of OH are: $B_e''=19.025$, $\alpha''=0.724$, $D_e''=-1.97\times10^{-3}$, $\beta''=5.0\times10^{-6}$, and $r_e''=0.964\times10^{-8}$ cm. Vibrational constants are: $\omega_e''=3734.9$ and $x_e''\omega_e''=82.6$. Rotational and vibrational constants for the excited $^2\Sigma$ state are also evaluated and are tabulated.

INTRODUCTION

THE well-known "water vapor" bands which are produced in the combustion of substances rich in hydrogen, and in an electrical discharge through water vapor, are among the earliest molecular spectra recorded in the literature,[2] and have been the subject of numerous subsequent investigations.[3] At one time assigned to H_2O, then to O_2,[4] the bands were eventually identified with the neutral OH molecule.[5] The bands, of which those heretofore reported are listed in Table I, belong to a ($^2\Sigma\rightarrow{}^2\Pi$) transition and occur in the ultraviolet region of the spectrum. The $^2\Pi$ term has been identified with the normal state of the molecule. Each band possesses six principal branches (double P, double Q, and double R branches). Intense exposures of the strong λ3064 band shows additional satellite branches, a portion of which also make their appearance on long exposures of the weaker bands.[6]

TABLE I. *Wave-lengths (international Angstroms) of the band heads of the OH system, with the vibrational assignments.*

	$v''=0$	1
$v'=0$	3064	3428
1	2811	3122
2	2608	2875

The difficulty of obtaining satisfactory photographs of the weaker bands, or of the weaker lines of the strong bands, is greatly enhanced by the presence of a very considerable continuous background, presumably due to hydrogen, which increases toward the red end of the spectrum. Probably for this reason, as well as the fact that the bands removed from the (0, 0) member at λ3064 are progressively more difficult to excite, only the bands at λ3064 and at λ2811 have been subject to any very thorough analysis, and even for these bands the analyses are incomplete with respect to the classification of numerous weak lines which appear throughout the bands.

[1] Dawson, Du Pont Fellow in Chemistry.

[2] Liveing and Dewar, Proc. Roy. Soc. **A30**, 498, 580 (1880); ibid. **A33**, 274 (1882); Phil. Trans. **129**, 271 (1880), cf. also Deslandres, Ann. Chim. Phys. **14**, 257 (1888); Comptes Rendus **100**, 854 (1888).

[3] Among the more notable of these are: Grebe and Holtz, Ann. d. Physik **39**, 1243 (1913); Heurlinger, *Dissertation*, Lund (1918); Fortrat, J. Phys. Radium **5**, 20 (1924); Watson, Astrophys. J. **60**, 145 (1924); Dieke, Proc. Acad. Sci. Amsterdam **28**, 174 (1925); Jack, Proc. Roy. Soc. **A115**, 373 (1927) and, ibid. **A118**, 647 (1928); Tanaka, Proc. Roy. Soc. **A108**, 594 (1925); Kemble, Phys. Rev. **30**, 387 (1927); Hill and Van Vleck, Phys. Rev. **32**, 250 (1928); Mulliken, Phys. Rev. **32**, 388 (1928); Almy, Phys. Rev. **35**, 1495 (1930); and Almy and Rahrer, Phys. Rev. **38**, 1816 (1931).

[4] Steubing, Ann. d. Physik **33**, 553 (1910) and, ibid. **39**, 1408 (1912); Reiss, Zeits. f. physik. Chemie **88**, 513 (1914). See also Fortrat, reference 3.

[5] Cf. Watson, and Mulliken, reference 3.

[6] For a more complete résumé of the band structure and its interpretation, cf. Mulliken, reference 3, who has admirably summarized our present knowledge of the spectrum.

Several months ago, in the effort to detect isotopes of hydrogen[7] we made some intense exposures of λ3064 and the adjacent regions toward the red. Although unsuccessful in our immediate objective we succeeded in greatly reducing the continuous background and obtained plates which showed, throughout the spectrum, many score lines not hitherto recorded in the literature. We have recently measured the plates in the neighborhood of the (0′, 1″) band at λ3428. In addition to extending the principal branches of λ3428 to the extent of some 44 lines we have found 54 new lines (including 11 in common with λ3428) which form a new band with a band head at λ3484. The present paper presents the details of these measurements and of the assignments, which identify the band at λ3484 as a new band in the OH system.

Experimental Procedure

The arrangements for exciting the spectrum were similar, in the main, to whose employed by Watson and by Jack. The water vapor flowed through a heavy walled Pyrex capillary through which the discharge passed. The capillary was viewed end-on through a quartz window.

The continuous background which appeared in long exposures gave us some concern. By introducing a slow stream of oxygen through a capillary which extended beneath the surface of the distilled water we were successful in greatly reducing this troublesome factor, without appreciable change in the intensity of the OH bands.

The bands were photographed with a Hilger E 185 prism spectrograph, which gives a dispersion of about 4.4A per mm in the region of λ3500, and were taken on Eastman "Speedway" plates. Although one exposure was allowed to run for 40 hours we found that, because of the intensification of the background, no new features appeared after about the eighth or tenth hour. The use of Eastman's "Opaque" as a plate backing reduced halation, which was a factor in the long exposures.

Measurements of the Bands λλ3428 and 3484

Tables II, III and IV contain *all* lines which appeared on our plates between λ3429 and λ3570. Although we obtained several plates which show the new lines recorded in these tables, the measurements are all taken from a single plate, chosen because of its superior focus in the neighborhood of λ3500. This plate was a five hour exposure with a slit width of 0.001 mm. The measurements were made with a Gaertner comparator and each value recorded in the tables is an average of at least four independent readings. The values of the measurements for individual lines were ordinarily reproducible to within 0.05A (=0.4 cm^{-1}) but, in extreme cases, our measurements showed deviations, among themselves of twice this amount. Our plates were calibrated in terms of standard iron lines which were photographed both before and after the OH exposures.[8] Except where overlapping occurs, we believe that the measurements of individual lines are probably good to within about 0.05A.

Intensities are based on an empirical scale (0–10) as they appear to the eye. The letter *d* following the intensity rating indicates that the line in question has the appearance of an unresolved doublet; *h* indicates that the line appeared hazy; *t* indicates a line that is assigned in two places while *q* marks a line used in more than two assignments. In Table II lines printed in bold faced type have previously been reported by Jack although the assignments of wave-lengths are our own. Lines marked with an asterisk (*) are substitutes for assignments made by Jack. These substitutions are justified either by interpola-

[7] Since then, discovered by Urey, Brickwedde and Murphy, Phys. Rev. **39**, 164 (1932); ibid. **40**, 1 (1932).

[8] Because of a slight shift in the relative positions of the iron standards, which was found subsequently to have been due to a movement in the plate holder during the adjustments between exposures, the measurements on the original plate were employed only to give line *differences* among the lines of the OH bands. The absolute wave-lengths were determined with the aid of a later plate, in which the shifts due to plate holder adjustments were avoided. On this plate we compared the positions of fifteen of the sharpest lines of λ3428 with adjacent iron lines. The measurements on the original plate were then related to these fifteen lines as secondary standards. Our measurements of the 75 lines in λ3428 which had previously been measured by Jack averaged 0.05A higher (about 0.4 cm^{-1} lower) than his but the difference appears to be real, and not related to any source of error in our calibration, since our measurements of 200 lines in λ3064, on the same plate, agreed to within an average 0.01A of Grebe and Holtz' values for the same lines.

TABLE II. λ3428 *band.*

K	λ air	Intensity	ν vac.	λ air	Intensity	ν vac.	K	λ air	Intensity	ν vac.	λ air	Intensity	ν vac.
		R_1			R_2				Q_1			Q_2	
1	3450.44	7 *t*	28973.5	3465.66	1	28846.3	11	3477.30	4	28749.7	3481.86	4	28712.0
2	3447.95	7	28994.5	3460.52	2 *t*	28889.6	12	3480.15	4	28726.2	3484.45	5 *q*	28690.7
3	3445.34	9 *dq*	29016.5	3456.00	3	28926.9	13	3483.21	3	28700.9	3487.28	2	28667.4
4	3442.89	9	29037.1	3451.98	6	28960.6	14	3486.59	2	28673.1	3490.49	5 *t*	28641.1
5	3440.43	5	29057.9	3448.41	7	28990.7	15	3490.12	5 *q*	28644.1	3493.94	7 *dq*	28612.8
6	3438.14	5	29077.2	3445.34	9 *dq*	29016.5	16	3493.94	7 *dq*	28612.8	3497.60	8 *dq*	28582.1
7	3436.07	10 *q*	29094.7	3442.41	9 *q*	29041.2	17	3498.15	5	28578.4	3501.62	3	28550.1
8	3433.86	9 *dq*	29113.5	3439.93	3	29062.1	18	3502.72	3	28541.1	3506.04	5	28514.1
9	3432.38	10 *dt*	29126.0	3437.83	3	29079.8	19	3507.53	5 *t*	28502.0	3510.70	8 *t*	28476.2
10	3431.08	5	29137.0	3436.05	10 *q*	29094.7	20	3512.66	3	28460.4	3515.79	7 *t*	28435.0
11	3429.76	4	29148.3	3434.49	3	29108.1	21	3518.13	3	28416.1	3521.14	4 *t*	28391.8
12	3428.88	5	29155.7	3433.37	2	29117.6	22	3524.03	4 *q*	28368.6	3526.97	1	28344.8
13	3428.38	8 *t*	29160.0	3432.38	10 *dt*	29126.0	23	3530.26	2 *t*	28318.4	3533.18	1	28295.0
14	3428.02	9 *t*	29163.0	3431.91	10 *dq*	29130.0	24	3536.95	1	28264.9	3539.76	1	28242.4
15	3428.02	9 *t*	29163.0	3431.91	10 *dq*	29130.0*	25	3544.04	2 *t*	28208.3	3546.91	0	28185.5
16	3428.38	8 *t*	29160.0	3431.91	10 *dq*	29130.0	26	3551.55	0	28148.7	3554.42	1 *t*	28126.0
17	3429.18	5	29153.2	3432.93	2	29121.3	27	3559.89	0 *hq*	28082.8	3562.34	0	28063.5
18	3430.31	5	29143.6	3433.86	9 *dq*	29113.5	28	3567.78	0 *t*	28020.7			
19	3431.91	10 *dq*	29130.0	3435.43	5	29100.2							
20	3433.86	9 *dq*	29113.5	3437.30	5	29084.3			P_1			P_2	
21	3436.07	10 *q*	29094.7	3439.60	3	29064.9	1	3462.56	7	28872.2			
22	3439.02	3	29069.8	3442.41	9 *q*	29041.2	2	3468.15	10 *t*	28825.6	3480.89	6	28720.0
23	3442.41	9 *q*	29041.2	3445.34	9 *dq*	29016.5	3	3473.77	6 *t*	28778.9	3484.45	5 *q*	28690.7
24	3446.09	2	29010.2	3449.42	2	28982.2	4	3479.27	5	28733.4	3488.44	8 *dq*	28657.9
25	3450.44	7 *t*	28973.5	3453.73	1	28945.9	5	3484.88	5 *t*	28687.2	3493.01	8 *t*	28620.4
26	3455.24	1	28933.3	3458.53	10 *t*	28905.8	6	3490.49	5 *t*	28641.1	3497.60	8 *dq*	28582.1
27	3460.52	2 *t*	28889.6	3464.00	0	28860.2	7	3496.37	7 *t*	28592.9	3502.97	3	28539.1*
							8	3502.32	1	28544.4	3508.40	5 *t*	28494.9
		Q_1			Q_2		9	3508.40	5 *t*	28494.9	3514.02	6 *t*	28449.3
1	3458.53	10 *t*	28905.8	3473.77	6 *t*	28778.9*	10	3514.65	1	28444.2	3519.90	4	28401.8
2	3460.06	10	28893.0	3472.61	8 *t*	28788.5	11	3521.14	4 *t*	28391.8	3526.11	0	28351.7*
3	3461.54	10	28880.6	3472.15	10 *q*	28792.3	12	3527.54	1 *t*	28340.3	3532.51	1	28300.4
4	3463.06	9	28868.0	3472.15	10 *q*	28792.3	13	3534.51	1	28284.4	3538.99	0	28248.6
5	3464.59	10	28855.2	3472.61	8 *t*	28788.5	14	3541.74	1 *t*	28226.7*	3545.86	2 *d*	28193.9*
6	3466.31	8	28840.9	3473.33	5	28782.5	15	3548.93	0 *dt*	28169.5	3552.97	0	28137.5
7	3468.15	10 *t*	28825.6	3474.42	3	28773.5	16	3556.22	0	28111.8	3560.52	0 *t*	28077.8
8	3470.14	7	28809.0	3475.89	5	28761.3	17	3564.04	0 *t*	28050.1	3567.78	0 *t*	28020.7
9	3472.15	10 *q*	28792.3	3477.62	4	28747.0*							
10	3474.73	3	28770.9	3479.55	3	28731.1*						$P_{Q_{12}}$	
							1				3477.89	1	28744.8*

tions between the lines of the respective branches or by the combination relations.

Table IV contains the only lines, in the region included within the tables, which remain unassigned. It is possible that these lines belong to an unidentified (2′, 3″) band. Indeed, they correspond quite well with the positions of lines calculated for this band. A number of lines beyond λ3570 also correspond to calculated (2′, 3″) lines or to extensions of either λ3428 or λ3484. However, the lines are extremely weak and the number observed are insufficient to let us be certain as to their identification.

APPLICATION OF THE COMBINATION PRINCIPLE TO λ3484, AND THE ASSIGNMENT OF VIBRATIONAL QUANTUM NUMBERS

It is apparent from Fig. 1, which is a Fortrat diagram of the line assignments recorded in Tables II and III, that λ3484 possesses the same general structure as does λ3428, which is typical of other members of this system. Identification of the new band[9] is made complete by application of the combination principle. The relationships between the respective lines of the bands and the corresponding term values of the molecule are

[9] Shaw (Phys. Rev. **37**, 1548 (1931)) reported the discovery of a group of lines which had the appearance of a band head at about λ3525 and suggested that these might belong to OH. No details were published. It is probable that Shaw observed the Q_2 head at λ3523. The fact that Shaw states that he observed no new features in λ3428 precludes the possibility of his observing the true band head at λ3484. Because of their greater intensity the *Q* branches would make their appearance first.

TABLE III. λ*3484 band.*

K	λ air	Intensity	ν vac.	λ air	Intensity	ν vac.
		R_1			R_2	
1	3501.12	0	28554.1	3516.71	0	28427.6
2	3498.73	2	28573.6	3512.33	3 *t*	28463.0
3	3496.37	7 *t*	28592.9	3507.53	5 *t*	28502.0
4	3493.94	7 *dq*	28612.8	3503.70	1	28533.1
5	3492.10	1	28627.9	3500.44	1	28559.7
6	3490.12	5 *q*	28644.1	3495.60	8 *dq*	28582.1
7	3488.44	8 *dq*	28657.9	3495.09	2	28603.4
8	3487.03	0	28669.5	3493.01	8 *t*	28620.4
9	3485.58	1	28681.4	3491.32	0	28634.3
10	3484.45	5 *q*	28690.7	3490.12	5 *q*	28644.1
11	3483.80	2 *q*	28696.1	3489.06	1 *t*	28652.8
12	3483.80	2 *q*	28696.1	3488.44	8 *dq*	28657.9
13	3483.80	2 *q*	28696.1	3488.44	8 *dq*	28657.9
14	3484.08	0	28693.8	3488.44	8 *dq*	28657.9
15	3484.88	5 *t*	28687.2	3489.06	1 *t*	28652.8
16	3486.03	0	28677.7	3490.12	5 *q*	28644.1
17				3491.59	0	28632.1
		Q_1			Q_2	
1	3509.09	2	28489.3	3527.77	2 *t*	28362.6
2	3510.70	8 *t*	28476.2	3524.03	4 *q*	28368.6
3	3512.33	3 *t*	28463.0	3523.42	4 *t*	28373.5
4	3514.02	6 *t*	28449.3	3523.42	4 *t*	28373.5
5	3515.79	7 *t*	28435.0	3524.03	4 *q*	28368.6
6	3517.73	3	28419.3	3525.07	2	28360.1
7	3519.90	4	28401.8	3526.56	1	28348.1

K	λ air	Intensity	ν vac.	λ air	Intensity	ν vac.
		Q_1			Q_2	
8	3522.14	3	28383.8	3528.11	1	28335.7
9	3524.77	2 *t*	28362.6	3530.26	2 *t*	38318.4
10	3527.54	1 *t*	28340.3	3532.70	1	28298.9
11	3530.55	1	28316.1	3535.37	2 *q*	28277.5
12	3533.87	1	28289.5	3538.45	1	28252.9
13	3537.53	1	28260.2	3541.74	1 *t*	28226.7
14	3541.38	2 *t*	28229.5	3545.61	2 *dt*	28195.9
15	3545.61	2 *dt*	28195.9	3549.62	0	28164.0
16	3550.30	0	28158.6	3554.06	1	28128.8
17	3555.19	0	28119.9	3558.90	0	28090.6
18	3560.52	0 *t*	28077.8	3564.04	0 *t*	28050.1
19	3566.23	0	28032.9	3569.68	0	28005.8
		P_1			P_2	
1	3513.02	0	28457.4			
2	3518.56	1	28412.6	3531.81	1	28306.0
3	3524.03	4 *q*	28368.6	3535.37	2 *q*	28277.5
4	3529.89	0	28321.4	3539.49	1	28244.6
5	3536.38	2 *q*	28277.5	3544.04	2 *t*	28208.3
6	3541.38	2 *t*	28229.5	3548.93	0 *dt*	28169.5
7	3547.44	0	28181.3	3554.42	1 *t*	28126.0
8	3553.68	0	28131.8	3559.89	0 *hq*	28082.8
9	3559.89	0 *hq*	28082.8	3566.23	0 *t*	28032.9
10	3566.62	0	28029.8			
					$P_{Q_{12}}$	
1				3528.84	1	28329.8

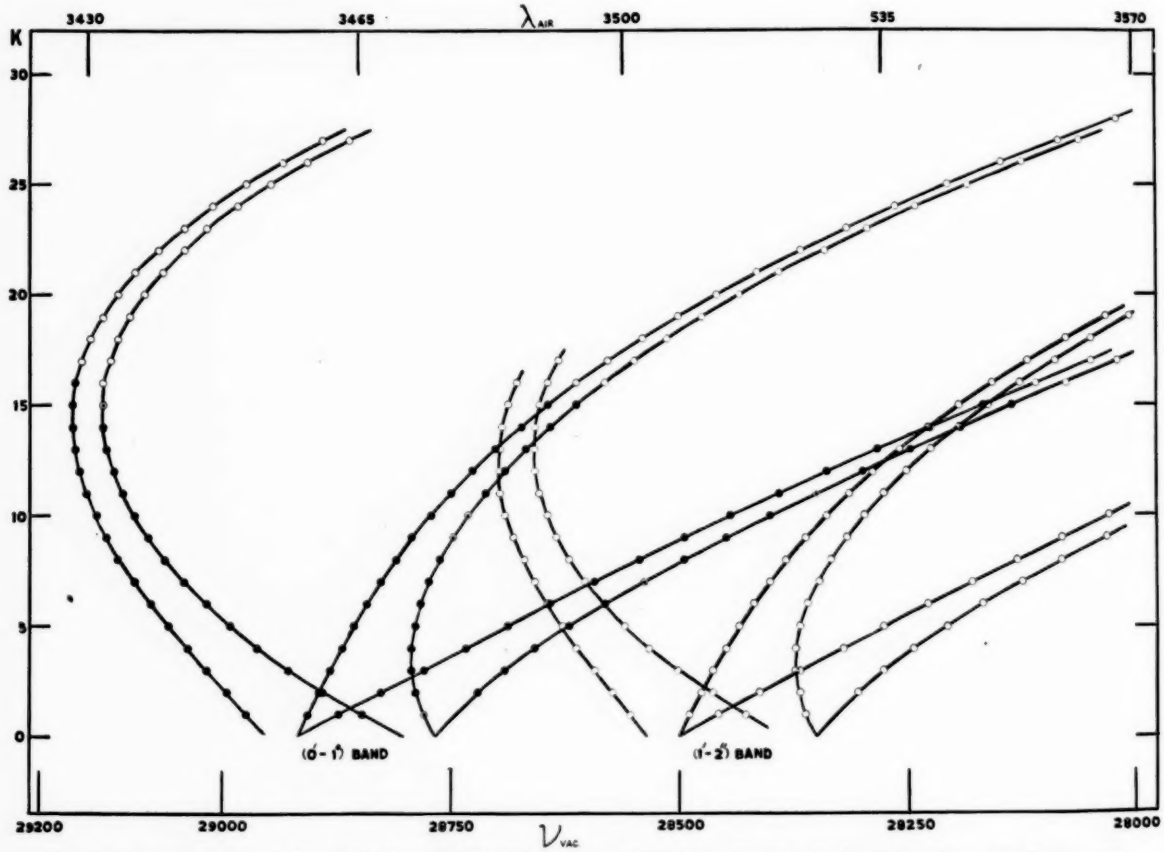

FIG. 1. Fortrat diagrams for λλ3428 and 3484. Black dots, lines identified by Jack; circle-dots, reassignments; circles, new lines.

given by the following set of equations:[10]

$$P_1(K)=F_1'(K-1)-F_{1B}''(K), \quad (1a)$$
$$P_2(K)=F_2'(K-1)-F_{2B}''(K), \quad (1b)$$
$$R_1(K)=F_1'(K+1)-F_{1B}''(K), \quad (1c)$$
$$R_2(K)=F_2'(K+1)-F_{2B}''(K), \quad (1d)$$
$$Q_1(K)=F_1'(K)-F_{1A}''(K), \quad (1e)$$
$$Q_2(K)=F_2'(K)-F_{2B}''(K). \quad (1f)$$

From the first four of these equations,

$$R_1(K)-P_1(K)=F_1'(K+1)-F_1'(K-1)=\Delta_2F_1'(K), \quad (2a)$$
$$R_2(K)-P_2(K)=F_2'(K+1)-F_2'(K-1)=\Delta_2F_2'(K), \quad (2b)$$

and from the last four,

$$R_1(K)-Q_1(K)=F_1'(K+1)-F_1'(K)+F_{1A}''(K)-F_{1B}''(K)=\Delta_1F_1'(K+\tfrac{1}{2})+\delta_1(K), \quad (3a)$$
$$R_2(K)-Q_2(K)=F_2'(K+1)-F_2'(K)+F_{2A}''(K)-F_{2B}''(K)=\Delta_1F_2'(K+\tfrac{1}{2})+\delta_2(K), \quad (3b)$$

where the δ_1 and δ_2 terms represent the intervals between the A and B components which arise from Λ type doubling and are set equal to $F_A''(K)-F_B''(K)$.

Table V gives values of Δ_2F_{12}' computed for λ3484 as well as for the six bands identified previously. Each of these figures is the *average* of the Δ_2F' values calculated by Eqs. (2a) and (2b), but differs only slightly from either Δ_2F_1' or Δ_2F_2' since the difference in these quantities is of the order of magnitude of only 0.2 cm^{-1}. From this table it is apparent that the *upper* vibrational level of λ3484 is identical with that of λ2811 and of λ3122 and so is the ($v'=1$) level. This assignment, together with the individual line assignments in the Q and R branches, is confirmed by the $(R-Q)$ combinations. These were computed for λ3484, for λ2811 and for λ3122, by the use of Eqs. (3a) and (3b) and are shown in Table VI where values of Δ_1F_1' and of Δ_1F_2' are tabulated separately.

TABLE IV. *Unassigned lines in the region between λ3429 and λ3570.*

λ air	Intensity	ν vac.
3561.17	0	28072.7
3564.78	0	28044.3
3565.24	0	28040.7
3568.73	0	28013.2

[10] For the typical energy level diagram and for the meanings of symbols cf. Mulliken, reference 3.

TABLE V.[11] $R_{12}(K)-P_{12}(K)$ *for the OH bands.*

K	λ2608	λ2811	λ2875	λ3064	λ3122	λ3428	λ3484
1	90.7	96.7		101.4		101.4	97.2
2	152.3	160.8		169.2		169.3	159.0
3	212.6	224.8	209.6	236.7		236.9	224.4
4	271.3	288.7	272.8	303.8	(288.9)	303.2	288.9
5	333.6	352.0	333.7	370.4	352.2	370.5	350.9
6	392.6	415.2	393.5	436.4	414.6	435.2	413.6
7	(451.8)	477.0	451.7	501.8	476.9	502.0	477.0
8	509.8	538.3		566.5	537.8	568.2	537.7
9	567.4	598.8		630.5	598.8	630.8	600.0
10	623.1	658.7		693.3	658.9	692.9	(660.9)

TABLE VI.

	$R_1(K)-Q_1(K)$			$R_2(K)-Q_2(K)$		
K	λ3484	λ2811	λ3122	λ3484	λ2811	λ3122
1	64.8	64.6	—	65.0	64.7	—
2	97.4	96.6	—	94.4	96.0	—
3	129.6	128.7	—	128.5	128.2	—
4	163.5	161.1	—	159.6	160.0	—
5	192.9	192.8	188.7	191.1	191.9	—
6	224.8	225.2	223.1	222.0	223.5	—
7	256.1	256.4	255.1	255.3	254.3	—
8	285.7	287.5	286.8	284.7	285.1	—
9	318.8	318.5	319.2	315.9	315.8	—
10	350.4	348.8	351.1	345.2	346.3	—
11	380.0	379.2	383.2	375.3	375.9	—
12	406.6	408.2	—	405.0	405.6	—
13	435.9	436.6	—	431.2	433.8	—
14	464.3	465.5	—	462.0	461.9	—
15	491.3	492.8	—	488.8	489.4	—
16	519.1	520.0	—	515.3	515.9	—
17	—	—	—	541.5	542.0	—

[11] In this and in the succeeding tables the frequencies for the lines in λ3428 are taken from our Table II, while the data of the following authors was employed in obtaining combination relationships in the other bands; λλ3064 and 3122, Grebe and Holtz (except in Table VI, in which the data of Fortrat was employed for λ3122); λλ2811 and 2875, Watson; and λ2608, Jack.

The following combinations give term differences in the *lower* levels of the respective bands:

$$R_1(K-1)-P_1(K+1)=F_1'(K)-F_{1B}''(K-1)-F_1'(K)+F_{1B}''(K+1)=\Delta_2F_{1B}(K)$$
$$=\Delta_2F_1''-\tfrac{1}{2}[\delta_1(K+1)-\delta_1(K-1)], \quad (4a)$$

$$R_2(K-1)-P_2(K+1)=F_2'(K)-F_{2B}''(K-1)-F_2'(K)+F_{2B}''(K+1)=\Delta_2F_{2B}''(K)$$
$$=\Delta_2F_2''-\tfrac{1}{2}[\delta_2(K+1)-\delta_2(K-1)], \quad (4b)$$

$$R_1(K-1)-Q_1(K)=F_1'(K)-F_{1B}''(K-1)-F_1'(K)+F_{1A}''(K)$$
$$=\Delta_1F_1''(K-\tfrac{1}{2})+\tfrac{1}{2}[\delta_1(K)+\delta_1(K-1)], \quad (5a)$$

$$R_2(K-1)-Q_2(K)=F_2'(K)-F_{2B}''(K-1)-F_2'(K)+F_{2A}''(K)$$
$$=\Delta_1F_2''(K-\tfrac{1}{2})+\tfrac{1}{2}[\delta_2(K)+\delta_2(K-1)]. \quad (5b)$$

By taking averages of (4a) and (4b) and of (5a) and (5b), respectively, *average* $\Delta F''$'s are obtained. These take the form:

$$\Delta_2F_{12}''=R_{12}(K-1)-P_{12}(K+1)+\tfrac{1}{4}[\delta_1(K+1)-\delta_1(K-1)+\delta_2(K+1)-\delta_2(K-1)], \quad (4c)$$

$$\Delta_1F_{12}''=R_{12}(K-1)-Q_{12}(K)-\tfrac{1}{4}[\delta_1(K)+\delta_1(K-1)+\delta_2(K)+\delta_2(K-1)]. \quad (5c)$$

Hill and Van Vleck[3] give an equation for the rotational and coupling energies which, when extended to include the rotational stretching term given by Kemble[3] may be put in the form

$$F''(K)=\pm A\Lambda/2+B''[\{(K+\tfrac{1}{2})\pm\tfrac{1}{2}\}^2-\Lambda(\Lambda\pm1)\pm(B''/A\Lambda)\{[(K+\tfrac{1}{2})\pm\tfrac{1}{2}]^2-\Lambda^2\}$$
$$+(D''/B'')(K+\tfrac{1}{2})^4+\cdots], \quad (6)$$

where $B''=h/8\pi^2I$, $\Lambda=1$ for OH, D'' is the rotational stretching constant and A is the proportionality factor in the expression for the magnetic coupling energy of the doublet II states, and is equal to the separations of the double P, Q and R branches at their origins. The upper signs go with the F_1 rotational states while the lower signs go with the F_2 levels. For average rotational term values [such as are involved in Eqs. (4c) and (5c)] Eq. (6) may be expressed in the form

$$F_{12}''(K)=B''[(K+\tfrac{1}{2})^2+\tfrac{1}{4}-\Lambda^2+(B''/A\Lambda)(K+\tfrac{1}{2})+(D''/B'')(K+\tfrac{1}{2})^4+\cdots]. \quad (7)$$

From Eq. (7) the following relationships are easily obtained:

$$\Delta_2F_{12}''(K)=4B''(K+\tfrac{1}{2})+2(B''^2/A\Lambda)+8D[(K+\tfrac{1}{2})^3+(K+\tfrac{1}{2})]+\cdots, \quad (8a)$$

$$\Delta_1F_{12}(K-\tfrac{1}{2})=2B''K+B''^2/A\Lambda+D''(4K^3+K)+\cdots. \quad (8b)$$

Table VII gives values of Δ_2F_{12}'', calculated by Eq. (4c), and of B'', calculated by Eq. (8a), for λλλ3064, 3428 and 3484. Table VIII gives values of Δ_1F_{12}'' and of B'' calculated by Eqs. (5c) and (8b), respectively. In employing Eqs. (8a) and (8b) we set A equal to 140.3 cm^{-1}, 140.9 cm^{-1} and 141.5 cm^{-1} for the respective λ3064, λ3428 and λ3484 bands. These values were obtained by graphical extrapolation of the experimentally observed doublet separations for the three bands, making use of the Q, of the P and of the R branches. We evaluated the D's for use in Eqs. (6), (7) and (8a, b) from the equation

$$D_v=D_e+\beta(v+\tfrac{1}{2}), \quad (9)$$

in which we calculated D_e and β from the theoretical formulae

TABLE VII. $R_{12}(K-1)-P_{12}(K+1)$ *combinations.*

K	λ3064		λ3428		λ3484	
	Δ_2F_{12}''	B''	Δ_2F_{12}''	B''	Δ_2F_{12}''	B''
2	182.0	18.72	175.1	17.99	167.8	17.21
3	256.5	18.72	246.5	17.98	235.4	17.16
4	330.0	18.69	318.3	18.02	305.0	17.25
5	403.2	18.67	387.8	17.95	374.0	17.30
6	476.0	18.67	458.7	17.98	440.6	17.27
7	547.8	18.64	527.7	17.95	506.3	17.22
8	619.0	18.64	596.5	17.95	573.4	17.25

$$D_e = -4B_e^3/\omega_e^2 \qquad (10)$$

$$\beta = \alpha^2/6\omega_e + (20\alpha B_e^2 + 32x_e B_e^3)/\omega_e^2. \qquad (11)$$

The latter equation is due to Kemble.[12] These equations had, of course, to be solved by a series of approximations since accurate values of B_e and of β are dependent on the solutions of Eqs. (8a, b).

Comparison of the B'''s in Tables VII and VIII show clearly that the lower vibrational level of λ3484 is the $(v''=2)$ level, heretofore unobserved.

TABLE VIII. $R_{12}(K-1)-Q_{12}(K)$ *combinations.*

K	λ3064		λ3428		λ3484	
	Δ_1F_{12}''	B''	Δ_1F_{12}''	B''	Δ_1F_{12}''	B''
2	72.1	18.65	69.1	17.85	68.4	17.63
3	109.7	18.72	105.5	17.98	100.0	17.03
4	146.9	18.73	141.4	18.01	135.9	17.30
5	183.6	18.71	176.4	17.96	170.6	17.35
6	220.0	18.68	211.5	17.95	203.0	17.22
7	256.2	18.67	245.8	17.90	236.7	17.24
8	292.2	18.67	280.8	17.93	268.4	17.14
9	327.7	18.66	315.2	17.94	301.9	17.19
10	362.9	18.66	348.7	17.93	335.0	17.23
11	397.5	18.65	381.1	17.89	366.7	17.22
12	431.9	18.66	414.9	17.93	398.6	17.23
13	465.2	18.65	447.0	17.92	428.0	17.17
14	498.3	18.65	479.5	17.95	457.9	17.15
15	530.8	18.65	510.8	17.95	488.5	17.19
16	562.3	18.65	540.6	17.94	517.8	17.19
17	593.3	18.65	571.2	17.97	546.1	17.19

ROTATIONAL AND VIBRATIONAL CONSTANTS FOR THE OH BANDS

Average values of B'' were computed, for each of the bands, from Tables VII and VIII and are given in Table IX. In obtaining averages of the B's we discarded those which were computed from ΔF_{12}'s of less than 200 cm^{-1} and weighted the remainder in proportion to the corresponding magnitudes of the ΔF_{12}'s. We did this since the errors in individual B's must lie almost entirely in the errors of measurement of the four lines used in each combination.

Our values of the B'''s and of I_e'' differ from those published by Jack[3] due, in part, to the fact that Jack neglected the last term in Eq. (4c) (which effects B to the extent of about 0.02 cm^{-1} in the region in which Jack employed the data)

[12] E. C. Kemble, J. Opt. Soc. Am. **12**, 1 (1926).

TABLE IX. *Rotational constants.*[13]

Lower state $^2\Pi$	Upper state $^2\Sigma$
$Be''=19.025$	$Be'=17.384$
$B_0''=18.663$	$B_0'=16.954$
$B_1''=17.952$	$B_1'=16.101$
$B_2''=17.216$	$B_2'=15.233$
$\alpha''=0.724$	$\alpha'=0.860$
$D_e''=-1.97\times10^{-3}$ (calc.)	$D_e'=-2.07\times10^{-3}$ (calc.)
$\beta''=5.0\times10^{-5}$ (calc.)	$\beta'=4.3\times10^{-5}$ (calc.)
$I_e''=1.454\times10^{40}$ g cm^2	$I_e'=1.591\times10^{40}$ g cm^2
$r_e''=0.964\times10^{-8}$ cm	$r_e'=1.009\times10^{-8}$ cm

but due, principally, to our use of the improved formula of Hill and Van Vleck and to our use of Eqs. (10) and (11) to evaluate De'' and β''.

For convenience, we also include in Table IX the rotational constants for the $^2\Sigma$ level. The B_v's for this level are taken from Jack. The other constants were evaluated, by us, from the same relationships employed in getting the constants for the $^2\Pi$ level.

In calculating the null lines of the various bands of the OH system we have employed the equations

$$\nu_{01} = P_1(1) + F_1''^*(1) - F_1'(0) \qquad (12a)$$

$$\nu_{02} = Q_{12}(1) + F_2''^*(1) - F_2'(0) \qquad (12b)$$

since these combinations involve the smallest corrections for null point energy. The (F')'s were calculated by the equation due to Kemble,[3]

$$F'(K) = B'(K+\tfrac{1}{2})^2 + D'(K+\tfrac{1}{2})^4 \qquad (13)$$

and the (F''^*)'s by the use of the formula

[13] Kemble[3] also gave equations for the rotational energy. For high rotational quantum numbers he gives an equation which may be put in the form

$$F''(K) = B''\left[(K+\tfrac{1}{2})^2 - \Lambda^2 + \frac{D''}{B''}(K+\tfrac{1}{2})^4 \mp \frac{P(P+2\alpha)s^3}{(K+\tfrac{1}{2})}\right]$$

where the last term, which corrects for the magnetic coupling energy of the doublet Π states and which may be evaluated from A and from other easily evaluated constants, goes out in the expression for $F_{12}''(K)$. Kemble's equation leads to respective B_0, B_1 and B_2 values of 18.50, 17.78 and 17.02 cm^{-1}, which were reported by us in a preliminary abstract [Phys. Rev. **43**, 374 (1933)]. While, with these values of B'' and Jack's values of D'', Kemble's equation empirically reproduces the data above about $(K=8)$ it lacks the theoretical soundness of Hill and Van Vleck's equation, subsequently derived. Hence, derived constants, such as (I'')'s, (r'')'s, D_e'''s, etc., are inexact by Kemble's equation but are correct by the equation of Hill and Van Vleck.

$$F''^{*}(K)=F''(K)-F''(K-\tfrac{1}{2}) \qquad (14)$$

in which the (F'')'s were evaluated by Eq. (6). The expedient represented by Eq. (14) is necessary since Eq. (6) does not solve for rotational energy alone but for a combination of rotational energy with magnetic coupling energy, the latter itself being a function of K.

Tables X and XI show the schemes of null lines, obtained by Eqs. (12a) and (12b) for the F_1 and F_2 states, respectively. Vibrational energy increments are shown in italics. An asterisk indicates that the ${}^{P}Q_{12}$ (1) line employed in (12b) has been assigned in more than one place.

From the italicized term differences in Tables X and XI we have evaluated the vibrational constants which are given in Table XII. Those term differences which involve null lines marked with one or more asterisks were given a weighting of one-third relative to the other values included in the tables. The vibrational constants for the upper electronic level agree substantially with those given by Birge[14] except for an evident printers error in Birge's tabulation.

TABLE X. *Null lines of the* ${}^{2}\Pi_{\frac{3}{2}}$ *branches of the OH bands.*

	$v''=0$		1		2
$v'=0$	32,464.96	*3569.56*	28,895.4		
	2,988.77		*2,988.8*		
1	35,453.73	*3569.50*	31,884.23	*3404.4*	28,479.8
	2,793.27		*2,793.18*		
2	38,247.00	*3569.59*	34,677.41		

TABLE XI. *Null lines of the* ${}^{2}\Pi_{\frac{1}{2}}$ *branches of the OH bands.*

	$v''=0$		1		2
$v'=0$	32,325.84	*3570.1*	28,755.7		
	2,988.70		*2,989.5*		
1	35,314.54*	*3569.35*	31,745.19**	*3404.9*	28,340.3
	2,793.80		*2,792.98*		
2	38,108.34**	*3570.17*	34,538.17		

TABLE XII. *Vibrational constants.*

$\omega_e''=3734.9$	$\omega_e'=3184.1$
$x_e''\omega_e''=82.6$	$x_e'\omega_e'=97.7$

We wish to express our thanks to Dr. H. P. Knauss, of the Department of Physics of The Ohio State University, who gave us helpful advice in connection with the production of the spectrum and, in particular, to Dr. W. R. Brode, of the Department of Chemistry, who kindly placed the facilities of his spectroscopic laboratory at our disposal and who made many helpful suggestions in the experimental phases of the work.

[14] Birge, page 232 of National Research Council Report on Molecular Spectra in Gases.

Variational Principles in Electromagnetism

H. BATEMAN, *Norman Bridge Laboratory of Physics, California Institute of Technology*

(Received December 20, 1933)

The familiar relation between the potentials in electromagnetic theory is regarded as a consequence of the principles of angular momentum and center of mass expressed by the symmetry of the stress-energy tensor. The electromagnetic equations are derived from a Lagrangian function L equal to an arbitrary function of the invariants E^2-H^2 and $E\cdot H$ of the electromagnetic field and rules different from that of Schrödinger are given for the construction of a stress-energy-tensor.

IN a recent paper Fock and Podolsky[1] have derived the equations of electromagnetism from the Lagrangian function

$$L=\tfrac{1}{2}(E^2-H^2)-\tfrac{1}{2}\left(\operatorname{div}A+\frac{1}{c}\frac{\partial\Phi}{\partial t}\right)^2 \qquad (1)$$

and have added the equation

$$E_t\equiv\operatorname{div}A+(1/c)(\partial\Phi/\partial t)=0 \qquad (2)$$

after the equations

$$\operatorname{curl}H=-\frac{1}{c}\frac{\partial E}{\partial t}+\nabla E_t,\quad \operatorname{div}E+\frac{1}{c}\frac{\partial E_t}{\partial t}=0 \qquad (3)'$$

have been derived by assuming the relations $H=\operatorname{curl}A$, $E=-(1/c)(\partial A/\partial t)-\nabla\Phi$, which imply that

$$\operatorname{curl}E=-(1/c)(\partial H/\partial t),\quad \operatorname{div}H=0. \qquad (3)''$$

A physical reason is needed for Eq. (2) and it has occurred to the author that this may be furnished by the requirement of symmetry of the stress-energy-tensor associated with Eqs. (3).

In forming this tensor we shall adopt the principle that the components of the tensor should involve only the quantities E_x, E_y, E_z, H_x, H_y, H_z, E_t occurring in the electromagnetic equations. A tensor satisfying this requirement and the laws of conservation of energy and linear momentum has already been constructed,[2] its components are

$$\begin{aligned}
X_x&=E_x^2+H_x^2+\tfrac{1}{2}(E_t^2-E^2-H^2),\\
X_y&=E_xE_y+H_xH_y-E_tH_z,\\
Y_x&=E_xE_y+H_xH_y+E_tH_z,\\
X_z&=E_xE_z+H_xH_z+E_tH_y,\\
Z_x&=E_xE_z+H_xH_z-E_tH_y,\\
G_x&=E_yH_z-E_zH_y-E_xE_t,\\
S_x&=c(E_yH_z-E_zH_y+E_xE_t),\\
W&=\tfrac{1}{2}(E^2+H^2+E_t^2),\quad\cdots.
\end{aligned} \qquad (4)$$

The conservation laws

$$\begin{aligned}
\partial X_x/\partial x+\partial X_y/\partial y+\partial X_z/\partial z&=(1/c)(\partial G_x/\partial t)\\
\cdot\quad\cdot\quad\cdot\quad\cdot\quad\cdot\quad\cdot\quad\cdot\quad\cdot&\\
\partial S_x/\partial x+\partial S_y/\partial y+\partial S_z/\partial z+\partial W/\partial t&=0
\end{aligned} \qquad (5)$$

are readily seen to be a consequence of Eqs. (3) but the law of symmetry

$$Y_z=Z_y,\ Z_x=X_z,\ X_y=Y_x,\ S_x=cG_x,\ S_y=cG_y,\ S_z=cG_z \qquad (6)$$

associated with the principle of the conservation of angular momentum and the property of the center of mass, is satisfied only when $E_t=0$ unless there is no electromagnetic field. It should be mentioned that a symmetrical tensor

$$\begin{aligned}
X_x&=E_x^2+H_x^2-\tfrac{1}{2}(E^2+H^2-E_t^2)-2E_t\frac{\partial A_x}{\partial x},\\
X_y&=E_xE_y+H_xH_y-E_t\left(\frac{\partial A_x}{\partial y}+\frac{\partial A_y}{\partial x}\right)=Y_x,\\
G_x&=E_yH_z-E_zH_y-E_t\left(\frac{1}{c}\frac{\partial A_x}{\partial t}-\frac{\partial\Phi}{\partial x}\right)=\frac{1}{c}S_x,\\
W&=\tfrac{1}{2}(E^2+H^2+E_t^2)-2E_t\frac{1}{c}\frac{\partial\Phi}{\partial t}
\end{aligned} \qquad (7)$$

[1] V. Fock and B. Podolsky, Phys. Zeits. d. Sow. **1**, 801 (1932).

[2] H. Bateman, Phys. Rev. **12**, 459 (1918).

may be derived from the Lagrangian function (1) by using Schrödinger's rule[3] but if $E_t \neq 0$ the conservation laws are not generally a consequence of (3) and, moreover, this tensor involves quantities which do not enter into the electromagnetic Eqs. (3) and so is ruled out by our requirement. It should be mentioned that Schrödinger's rule does not always associate a symmetrical stress-energy tensor with a Lagrangian function[4] so even if this rule were regarded as of universal application the principle of the conservation of angular momentum could not be regarded as a direct consequence of the variational principle alone. There are cases, however, in which Schrödinger's rule does not seem to be applicable. To construct such a case let us write[5]

$$\begin{aligned}
&h_x=\gamma_y-\beta_z-a_t-w_x, \quad e_x=b_z-c_y-\alpha_t-\phi_x,\\
&h_y=\alpha_z-\gamma_x-b_t-w_y, \quad e_y=c_x-a_z-\beta_t-\phi_y,\\
&h_z=\beta_x-\alpha_y-c_t-w_z, \quad e_z=a_y-b_x-\gamma_t-\phi_z,\\
&e_t=\alpha_x+\beta_y+\gamma_z+\phi_t, \quad h_t=a_x+b_y+c_z+w_t,\\
&\sigma=\tfrac{1}{2}(h_x^2+h_y^2+h_z^2-h_t^2)-\tfrac{1}{2}(e_x^2+e_y^2+e_z^2-e_t^2),\\
&\tau=h_xe_x+h_ye_y+h_ze_z-h_te_t
\end{aligned} \tag{8}$$

and consider the Lagrangian function

$$L=f(\sigma, \tau).$$

It is readily seen that

$$\begin{aligned}
&\frac{\partial L}{\partial \alpha_t}=\frac{\partial L}{\partial \phi_x}=\frac{\partial L}{\partial c_y}=-\frac{\partial L}{\partial b_z}=e_x\frac{\partial L}{\partial \sigma}-h_x\frac{\partial L}{\partial \tau}=E_x, \quad \text{say},\\
&\cdots\cdots\cdots\cdots\cdots\cdots\cdots\cdots\cdots\cdots\cdots\cdots\\
&\frac{\partial L}{\partial \alpha_x}=\frac{\partial L}{\partial \beta_y}=\frac{\partial L}{\partial \gamma_z}=\frac{\partial L}{\partial \phi_t}=e_t\frac{\partial L}{\partial \sigma}-h_t\frac{\partial L}{\partial \tau}=E_t, \quad \text{say},\\
&-\frac{\partial L}{\partial \alpha_t}=-\frac{\partial L}{\partial w_x}=\frac{\partial L}{\partial \gamma_y}=-\frac{\partial L}{\partial \beta_z}=h_x\frac{\partial L}{\partial \sigma}+e_x\frac{\partial L}{\partial \tau}=H_x, \quad \text{say},\\
&\cdots\cdots\cdots\cdots\cdots\cdots\cdots\cdots\cdots\cdots\cdots\cdots\\
&-\frac{\partial L}{\partial w_t}=-\frac{\partial L}{\partial a_x}=-\frac{\partial L}{\partial b_y}=-\frac{\partial L}{\partial c_z}=h_t\frac{\partial L}{\partial \sigma}+e_t\frac{\partial L}{\partial \tau}=H_t, \quad \text{say},
\end{aligned} \tag{9}$$

consequently the equations of Euler and Lagrange for the variation problem

$$\delta\int L\,dxdydzdt=0$$

take the form[6]

$$\begin{aligned}
&\nabla E_t+\partial E/\partial t=\operatorname{curl} H, \quad \operatorname{div} E+\partial E_t/\partial t=0,\\
&\nabla H_t+\partial H/\partial t=-\operatorname{curl} E, \quad \operatorname{div} H+\partial H_t/\partial t=0,
\end{aligned} \tag{10}$$

and so reduce to the equations of Maxwell when $E_t=H_t=0$. When Schrödinger's rule

$$\begin{aligned}
T_{xy}=&a_x\frac{\partial L}{\partial a_y}+b_x\frac{\partial L}{\partial b_y}+c_x\frac{\partial L}{\partial c_y}+w_x\frac{\partial L}{\partial w_y}\\
&+a_x\frac{\partial L}{\partial b_x}+a_y\frac{\partial L}{\partial b_y}+a_z\frac{\partial L}{\partial b_z}+a_t\frac{\partial L}{\partial b_t}\\
&+\alpha_x\frac{\partial L}{\partial \alpha_y}+\beta_x\frac{\partial L}{\partial \beta_y}+\gamma_x\frac{\partial L}{\partial \gamma_y}+\phi_x\frac{\partial L}{\partial \phi_y}\\
&+\alpha_x\frac{\partial L}{\partial \beta_x}+\alpha_y\frac{\partial L}{\partial \beta_y}+\alpha_2\frac{\partial L}{\partial \beta_z}+\alpha_t\frac{\partial L}{\partial \beta_t}-\delta_{xy}L,\\
&\delta_{xy}=0 \quad x\neq y\\
&\quad\;=1 \quad x=y
\end{aligned} \tag{11}$$

is applied to this function L it gives a tensor T whose components cannot be expressed simply in

[3] E. Schrödinger, Ann. d. Physik **82**, 265 (1927).

[4] H. Bateman, Proc. Nat. Acad. Sci. **13**, 326 (1927).

[5] The suffixes added to α, β, γ, ϕ, a, b, c, w are used to denote partial derivatives of the quantities. This rule does not extend to the suffixes added to e and h. For convenience the unit of time has been chosen so that the velocity of light is represented by unity.

[6] These are the equations considered by the author in Phys. Rev. **12**, 459 (1918).

terms of the quantities E_x, E_y, E_z, E_t, H_x, H_y, H_z, H_t, consequently we shall endeavor to replace it by some other rule. It is readily seen that if

$$
\begin{aligned}
2X_y &= \frac{\partial L}{\partial \alpha_t}\frac{\partial L}{\partial \phi_y} + \frac{\partial L}{\partial \alpha_x}\frac{\partial L}{\partial \alpha_y} + \frac{\partial L}{\partial \alpha_y}\frac{\partial L}{\partial \beta_y} + \frac{\partial L}{\partial \alpha_z}\frac{\partial L}{\partial \gamma_y} + \frac{\partial L}{\partial a_t}\frac{\partial L}{\partial w_y} + \frac{\partial L}{\partial a_x}\frac{\partial L}{\partial a_y} + \frac{\partial L}{\partial a_y}\frac{\partial L}{\partial b_y} + \frac{\partial L}{\partial a_z}\frac{\partial L}{\partial c_y}, \\
2Y_x &= \frac{\partial L}{\partial \beta_t}\frac{\partial L}{\partial \phi_x} + \frac{\partial L}{\partial \beta_x}\frac{\partial L}{\partial \alpha_x} + \frac{\partial L}{\partial \beta_y}\frac{\partial L}{\partial \beta_x} + \frac{\partial L}{\partial \beta_z}\frac{\partial L}{\partial \gamma_x} + \frac{\partial L}{\partial b_t}\frac{\partial L}{\partial w_x} + \frac{\partial L}{\partial b_x}\frac{\partial L}{\partial a_x} + \frac{\partial L}{\partial b_y}\frac{\partial L}{\partial b_x} + \frac{\partial L}{\partial b_z}\frac{\partial L}{\partial c_x}, \\
2X_x &= \frac{\partial L}{\partial \alpha_t}\frac{\partial L}{\partial \phi_x} + \left(\frac{\partial L}{\partial \alpha_x}\right)^2 + \frac{\partial L}{\partial \alpha_y}\frac{\partial L}{\partial \beta_x} + \frac{\partial L}{\partial \alpha_z}\frac{\partial L}{\partial \gamma_x} + \frac{\partial L}{\partial a_t}\frac{\partial L}{\partial w_x} + \left(\frac{\partial L}{\partial a_x}\right)^2 + \frac{\partial L}{\partial a_y}\frac{\partial L}{\partial b_x} + \frac{\partial L}{\partial a_z}\frac{\partial L}{\partial c_x},
\end{aligned}
\tag{12}
$$

and the other components are defined by corresponding equations, we obtain a tensor for which Eqs. (5) are satisfied. This tensor includes the tensor (4) as a particular case, indeed

$$
\begin{aligned}
X_x &= E_x^2 + H_x^2 - \tfrac{1}{2}(E^2 + H^2 - E_t^2 - H_t^2), \\
X_y &= E_xE_y + H_xH_y - E_tH_z + H_tE_z, \\
Y_z &= E_xE_y + H_xH_y + E_tH_z - H_tE_z,
\end{aligned}
\tag{13}
$$

and so the components of (4) are obtained by putting $H_t = 0$. On the other hand, a symmetrical tensor is obtained by writing

$$
\begin{aligned}
2X_y &= \frac{\partial L}{\partial \phi_x}\frac{\partial L}{\partial \phi_y} - \frac{\partial L}{\partial \alpha_x}\frac{\partial L}{\partial \alpha_y} - \frac{\partial L}{\partial \beta_x}\frac{\partial L}{\partial \beta_y} - \frac{\partial L}{\partial \gamma_x}\frac{\partial L}{\partial \gamma_y} + \frac{\partial L}{\partial w_x}\frac{\partial L}{\partial w_y} - \frac{\partial L}{\partial a_x}\frac{\partial L}{\partial a_y} - \frac{\partial L}{\partial b_x}\frac{\partial L}{\partial b_y} - \frac{\partial L}{\partial c_x}\frac{\partial L}{\partial c_y} = 2Y_x, \\
2X_x &= \left(\frac{\partial L}{\partial \phi_x}\right)^2 - \left(\frac{\partial L}{\partial \alpha_x}\right)^2 - \left(\frac{\partial L}{\partial \beta_x}\right)^2 - \left(\frac{\partial L}{\partial \gamma_x}\right)^2 + \left(\frac{\partial L}{\partial w_x}\right)^2 - \left(\frac{\partial L}{\partial a_x}\right)^2 - \left(\frac{\partial L}{\partial b_x}\right)^2 - \left(\frac{\partial L}{\partial c_x}\right)^2,
\end{aligned}
\tag{14}
$$

with similar equations for the other components. These equations give

$$
\begin{aligned}
X_x &= E_x^2 + H_x^2 - \tfrac{1}{2}(E^2 + H^2 + E_t^2 + H_t^2), \\
X_y &= E_xE_y + H_xH_y, \\
X_z &= E_xE_z + H_xH_z, \\
G_x &= S_x = E_yH_z - E_zH_y, \\
W &= \tfrac{1}{2}(E^2 + H^2 - E_t^2 - H_t^2)
\end{aligned}
\tag{15}
$$

but now the Eqs. (5) are satisfied only under certain conditions which are fulfilled when E_t and H_t are constants and there will be a density of negative energy at a great distance from all the electric and magnetic charges if these constants are different from zero. When $E_t = H_t = 0$ the tensor reduces to the familiar electromagnetic tensor, also

$$
\begin{aligned}
&\tfrac{1}{2}(H^2 - E^2) \\
&\quad = \sigma\left\{\left(\frac{\partial L}{\partial \sigma}\right)^2 - \left(\frac{\partial L}{\partial \tau}\right)^2\right\} + 2\tau\frac{\partial L}{\partial \sigma}\frac{\partial L}{\partial \tau} = S, \text{ say}, \\
E\cdot H &= \tau\left\{\left(\frac{\partial L}{\partial \sigma}\right)^2 - \left(\frac{\partial L}{\partial \tau}\right)^2\right\} - 2\sigma\frac{\partial L}{\partial \sigma}\frac{\partial L}{\partial \tau} = T, \text{ say},
\end{aligned}
$$

so that L becomes a function of S and T. It should be mentioned that S. R. Milner[7] has already suggested that $(S^2+T^2)^{\frac{1}{2}}$ can be used as a Lagrangian function and on a previous occasion the author[4] has shown that T can be used in this way. The foregoing analysis shows that a very general function of S and T can also be used for the portion of space-time not occupied by electric

[7] S. R. Milner, Proc. Roy. Soc. **A120**, 483 (1928). In Milner's case $S = \sigma$, $T = -\tau$.

charges. The conditions at the outer boundary of this region may be fulfilled for all variations if the boundary is a moving wave-front beyond which there is no field. In the region occupied by electric charges additional terms must be added to the Lagrangian function. It should be mentioned that the tensor (15) can also be found by writing

$$2X_y=\frac{\partial L}{\partial \alpha_t}\frac{\partial L}{\partial \beta_t}-\frac{\partial L}{\partial \alpha_x}\frac{\partial L}{\partial \beta_x}-\frac{\partial L}{\partial \alpha_y}\frac{\partial L}{\partial \beta_y}-\frac{\partial L}{\partial \alpha_z}\frac{\partial L}{\partial \beta_z}+\frac{\partial L}{\partial a_t}\frac{\partial L}{\partial b_t}-\frac{\partial L}{\partial a_x}\frac{\partial L}{\partial b_x}-\frac{\partial L}{\partial a_y}\frac{\partial L}{\partial b_y}-\frac{\partial L}{\partial a_z}\frac{\partial L}{\partial b_z},$$

$$2X_x=\left(\frac{\partial L}{\partial \alpha_t}\right)^2-\left(\frac{\partial L}{\partial \alpha_x}\right)^2-\left(\frac{\partial L}{\partial \alpha_y}\right)^2-\left(\frac{\partial L}{\partial \alpha_z}\right)+\left(\frac{\partial L}{\partial a_t}\right)^2-\left(\frac{\partial L}{\partial a_x}\right)^2-\left(\frac{\partial L}{\partial a_y}\right)^2-\left(\frac{\partial L}{\partial a_z}\right)^2.$$

and similarly for the other components.

Crystalline Fields of Pr, Nd and Yb from Paramagnetic Susceptibilities

W. G. PENNEY,* *Department of Physics, University of Wisconsin*

(Received January 27, 1933)

Calculations are made on the temperature variation of the paramagnetic susceptibilities of various salts of the rare earth group, employing the ideas of the crystal field developed in previous papers. It is shown that good agreement can be obtained with the experimental results on the salts $Pr_2(SO_4)_3$, Nd_2O_3 and Yb_2O_3, if the crystalline field is assumed to have the form $\Sigma_i\{Ax_i^2+By_i^2-(A+B)z_i^2\}$. This type of field, however, allows no agreement to be had for the experimental data on $Pr_2(SO_4)_3\cdot 8H_2O$; instead for the octahydrated sulphates, the assumption of a field of cubic symmetry $D\Sigma_i(x_i^4+y_i^4+z_i^4)$ is necessary. The various crystalline fields we find necessary to account for the magnetic data are in good accord with the few facts known on the crystal structure of the different compounds.

THE purpose of this note is to extend somewhat the results contained in a previous article by Penney and Schlapp.[1] It was shown in this paper that good agreement could be obtained for the variation of the paramagnetic susceptibilities of crystal powders of the salts $Pr_2(SO_4)_3\cdot 8H_2O$ and $Nd_2(SO_4)_3\cdot 8H_2O$, as measured by Gorter and de Haas,[2] on the assumption that the metallic ion is subject to a crystalline electric potential field of cubic symmetry. Measurements have now been made by Sucksmith[3] over a range of temperature 70–700°K on the oxides of several of the rare-earth elements, and among them Nd ($J=9/2$) and Yb ($J=7/2$) are amenable to calculations. Moreover, Gorter, de Haas and van den Handel[4] have made measurements on $Pr_2(SO_4)_3$ over the range of temperature 14–360°K, and Pr ($J=4$) is also very suitable for computational work. Using these data, we have made provisional calculations on the crystal fields of Pr, Nd and Yb. Although their general character is probably correct, too much importance must not be attached to the numerical results, since the experimental material is not complete enough to enable the fields to be determined with anything approaching certainty.

One difficulty which confronts us directly as we attempt to write down an expression for the Hamiltonian of the problem, is the type of symmetry to allow to the crystalline field. If the detailed crystal structure were known, this trouble would not arise, but unfortunately this state of affairs is not realized at present. The only method of procedure is to assume a likely form for the crystal field and to see whether it allows agreement to be obtained with the magnetic data. For the oxides of the rare-earths the problem is particularly disturbing because there are at least three crystallographic forms,[5] each of which is stable within a certain range of temperature depending on the particular rare-earth element. Experimentalists have not stated on which form their measurements were made, and it is quite possible that the oxides were mixtures of two or more modifications, or were even entirely of a form which was not really stable at the experimental temperatures. One would expect a discontinuity in the susceptibility on passing from one type of crystal structure to another. Perhaps the very small irregularities in the results of Sucksmith are of this origin. We shall see that the types of crystalline field which we find necessary to account for the experimental material are in satisfactory accord with the few facts known about the crystal structures of the various salts.

* Commonwealth Fund Fellow.

[1] W. G. Penney and R. Schlapp, Phys. Rev. **41**, 194 (1932). See also R. Schlapp and W. G. Penney, ibid. **42**, 666 (1932).

[2] C. J. Gorter and W. J. de Haas, Leiden Comm. 218b.

[3] W. Sucksmith, Phil. Mag. **14**, 1115 (1932).

[4] C. J. Gorter, W. J. de Haas and J. van den Handel, Leiden Comm. 218c.

[5] P. Ewald and C. Hermann, *Strukturbericht*, p. 261.

Praseodymium

As has been already stated, a field of cubic symmetry allows good agreement to be obtained with experiment for the susceptibility of the octahydrated sulphates of Pr and Nd. From analogy with the salts of Ni, Cr and Co, one would expect the paramagnetic ion to be surrounded with water molecules, and therefore, that it is these which give rise to the major part of the electric field. With the Tutton salts and also with $NiSO_4 \cdot 6H_2O$, it is known[6] that the six water molecules are arranged at the corners of a regular octahedron, around the paramagnetic ion. Hence their contribution to the electric field has cubic symmetry. Probably this is also true for the rare-earth salts mentioned above, but unfortunately their crystal structure is not known and it is impossible to check this hypothesis. There are only four water molecules to each metallic ion and this would seem to indicate that sharing of water molecules must occur. However, there is the possibility that the water molecules are arranged at the corners of a regular tetrahedron around the paramagnetic ion, since this would also give a field effectively of cubic symmetry. This follows because the third order terms contribute no diagonal elements in the secular equation, while the fourth order terms have cubic symmetry. This arrangement of water molecules would seem unlikely, since, as pointed out by Gorter,[7] it has the opposite sign of D from that which gives agreement with experiment.

The salt $Pr_2(SO_4)_3 \cdot 8H_2O$. The question arises whether any field of symmetry other than the cubic one previously treated, will also give agreement with the experimental results on the octahydrate salts described. It is possible to show that a field of the type $Ax^2+By^2-(A+B)z^2$ will not allow agreement to be obtained with the experimental results on $Pr_2(SO_4)_3 \cdot 8H_2O$. The case $A=B$ has already been considered[1] but we now extend the calculations to include $A \neq B$. Measurements have been made only on the crystal powder but these alone are sufficient to eliminate this type of rhombic field. The calculations are similar to those already described and are therefore outlined very briefly. For the Pr ion it is necessary to consider the effect of the electric field only on the lowest multiplet component, since the fields are not strong enough to break down the coupling between L and S to form J. One sets up the secular equation corresponding to the Hamiltonian

$$\Sigma_i\{Ax_i^2+By_i^2-(A+B)z_i^2\}+\beta\mathbf{H}\cdot(\mathbf{L}+2\mathbf{S}),$$

retaining only those terms diagonal in L, S and J. In our case $J=4$, and the secular equation of order $(2J+1)=9$, factors sufficiently to enable the roots to be calculated without much difficulty, up to and including terms in H^2. The susceptibility then follows in the usual way. Two fields are particularly simple, *viz.*, $A=B$, and $B=0$. All other fields of the type under consideration are intermediate to these two, since the first is symmetric around the z-axis, while the second is the most anisotropic possible around the z-axis. Fig. 1 shows the way the energy levels behave on passing from the field $A=1$, $B=1$ to the field $A=2$, $B=0$, keeping $A+B=2$. The numbers to the right of the energy levels denote to which of the four one-dimensional representations of the rhombic group

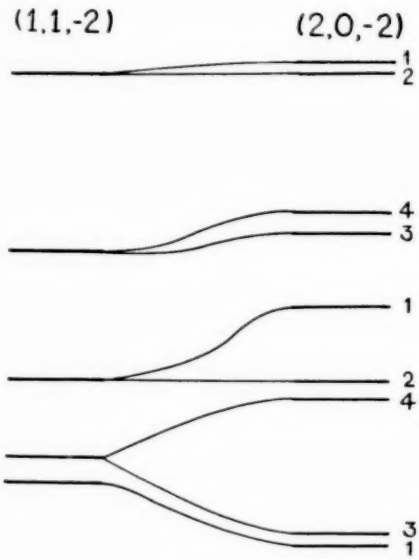

Fig. 1. Behavior of the energy levels of the Pr ion on passing from the field $A=1$, $B=1$ to the field $A=2$, $B=0$.

[6] W. Hoffmann, Zeits. f. Krist. **78**, 279 (1931); C. A. Beevers and H. Lipson, ibid. **83**, 123 (1932).

[7] C. J. Gorter, Phys. Rev. **42**, 437 (1932).

(G_1, G_2, G_3, G_4 in the notation of Bethe[8]) they belong. Of course, the energy levels are invariant of an arbitrary interchange of A, B and $-(A+B)$, and so is the mean susceptibility, but the individual principal susceptibilities undergo the corresponding interchange. Fig. 2 shows the calculated values of $n_B^2=3\chi kT/N\beta^2$, as a function of T for the particular fields (1) $40(x^2+y^2-2z^2)$, (2) $1700(x^2-z^2)$, the size of the

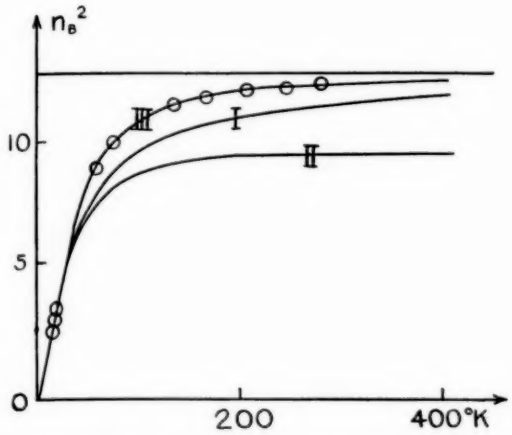

FIG. 2. Calculated and observed values of n_B^2 for $Pr_2(SO_4)_3\cdot 8H_2O$. (Circle, Gorter and de Haas; I, 40 $(x^2+y^2-2z^2)$; II, 1700 (x^2-z^2); III, -0.59 $(x^4+y^4+z^4)$.)

splitting produced by them being chosen so that n_B^2 at low temperatures agrees with the experimental results. All other rhombic fields of this type for which $(A+B)>0$, when made to fit the experimental results at low temperatures, lie between these two curves. The horizontal straight line represents Hund's law $n_B^2=g^2J(J+1)$, which is asymptotic to all our curves, where g is the Landé g-factor, and is equal to 4/5 for Pr. For comparison, we have also drawn in the theoretical curve for a field of cubic symmetry $-0.59(x^4+y^4+z^4)$. It is necessary to consider also the possibility of the energy spectrum being inverted, i.e., $(A+B)<0$, corresponding to changing the sign of the constants of the field. The disagreement with this choice is even more pronounced than with the choice assumed in Fig. 2.

The salt $Pr_2(SO_4)_3$. If the water molecules were removed from the salt $Pr_2(SO_4)_3\cdot 8H_2O$, we would expect the cubic symmetry of the field acting on the Pr ion to be lost, and for it substituted a field of lower symmetry $Ax^2+By^2-(A+B)z^2$. It seems unlikely that $Pr_2(SO_4)_3$ has a crystal structure which makes the field acting on the Pr ion possess cubic symmetry. If, for example, the salt has the same structure as the molybdate $Pr_2(MoO_4)_3$, or the hexagonal, tetragonal or monoclinic modifications of the oxide Pr_2O_3, the field would possess rhombic symmetry. If it were the same as the cubic modification of the oxide Pr_2O_3 the field would probably be a mixture of second and fourth order terms of about equal importance. Now the paramagnetic susceptibility of $Pr_2(SO_4)_3$ has been measured by Gorter, de Haas and van den Handel,[4] and it is possible to show that their experimental results and the results calculated for a field of cubic symmetry do not agree, but that the calculated values for a field of the type $Ax^2+By^2-(A+B)z^2$ do. Of course, we are at liberty to add to the terms of the second degree, terms of higher degree, but it proves that the field is already sufficiently general to give agreement as far as the mean susceptibility is concerned. The results are shown in Fig. 3,

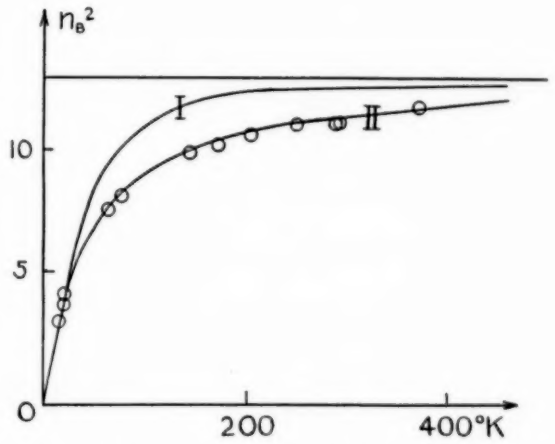

FIG. 3. Calculated and observed values of n_B^2 for $Pr_2(SO_4)_3$. (Circle, experiment 1; I, -0.59 $(x^4+y^4+z^4)$; II, $11(5x^2+3y^2-8z^2)$.)

where it can be seen that the field $11(5x^2+3y^2-8z^2)$ gives a very good representation of the experimental points. The energy levels for this field are 0, 56, 280, 572, 615, 1250 (narrow doublet), 2200 (narrow doublet) cm^{-1}. The overall splitting produced by the electric field on

[8] H. Bethe, Ann. d. Physik **3**, 133 (1929).

the lowest J level is comparable with the interval between the two lowest J levels for the free ion, and hence we should really have considered a much more extended secular determinant including the other J levels. The level $J=5$, however, is not affected quite so much by the electric field as is the lowest J level.[9] The effect would have been to add to n_B^2 a term proportional to T, not of much importance at room temperatures, and not sufficiently large to prevent agreement being obtained with experiment with slightly different values of A and B.[10]

There still remains one type of field which must be investigated to see if it will give agreement with experiment for the salt $Pr_2(SO_4)_3$, that where there is a dominant term of cubic symmetry, together with a smaller term of rhombic symmetry. We have satisfied ourselves that no agreement can be obtained. This remains true even when the energy spectrum is inverted, corresponding to a change in the sign of D. It may not be out of place here to remark that if a small rhombic field be superposed on a dominant cubic field, the average susceptibility is altered only in second approximation, but the appearance of the energy level diagram changes a good deal, degeneracies usually being removed in first approximation. This makes the comparison with absorption spectra very difficult.

Neodymium

It is possible to make calculations for neodymium very similar to those made for praseodymium. However, there is one distinct difference between the two elements. Unlike the corresponding Pr salts, $Nd_2(SO_4)_3\cdot 8H_2O$ and Nd_2O_3 show very similar behavior as regards magnetic properties, and the mean susceptibility of either may be fitted equally well with a field of cubic symmetry or a field of rhombic symmetry. This feature is probably peculiar to neodymium and is certainly not displayed by either praseodymium or ytterbium. For the octahydrate salt we prefer the field of cubic symmetry and for the oxide, the field of rhombic symmetry. The oxide on which the measurements were made was probably monoclinic or tetragonal, or even a mixture of these two, and the crystal field in either of these cases would possess rhombic symmetry. Fig. 4 shows the experimental results on the oxide Nd_2O_3 and the values calculated for the field $82(x^2+y^2-2z^2)$ cm^{-1}. The levels for the latter are 0, 492, 1476, 2952, 4920 cm^{-1}, each of them possessing the Kramers double-degeneracy. The over-all splitting for this field is rather large but there is no need to consider the matrix elements of the magnetic moment off-diagonal in J, since their effect could not affect the agreement to any extent at low temperatures. The level $J=11/2$ is not split by the crystal field as much as is the level $J=9/2$, as can be seen by working out the coefficients of the matrix elements of the squares of the coordinates.[9] We do not plot the values for the octahydrate salt because they are very close to those for the oxide, and would therefore confuse the figure. It may be mentioned, however, that the most sensitive way of plotting the results, n_B^2 against T, reveals that the experimental results of Gorter and de Haas[2] at 14–20°K are rather less than the values calculated for a field of cubic symmetry.

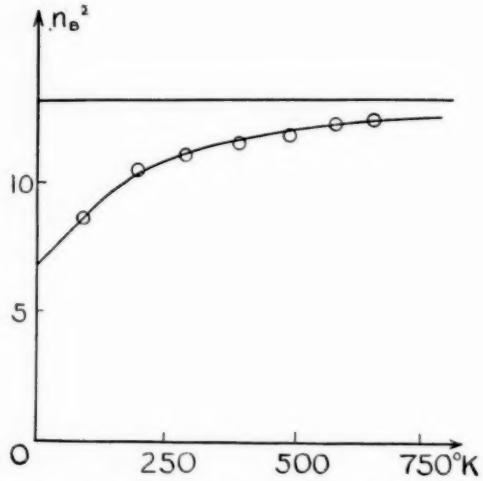

FIG. 4. Calculated and observed values of n_B^2 for Nd_2O_3. (Circle, Sucksmith; curve, 82 $(x^2+y^2-2z^2)$.)

[9] We have $\Sigma_i\{Ax_i^2+By_i^2-(A+B)z_i^2\}(M;\ M)=\text{const.}+\frac{1}{2}a(A+B)\{3M^2-J(J+1)\}$. By the spur theorem developed in paper (1), the ratio of the coefficient a for the three ions Pr, Nd and Yb can be calculated, and the product $a(A+B)$ is determined from the magnetic data.

[10] However, at room temperatures the correction due to the matrix elements of the moment off-diagonal in J is about two percent. The correction is particularly important in the case of Sm, and will be considered shortly in a paper by Miss Frank.

Ytterbium

Ytterbium is interesting for two reasons. First, because it is possible to make a fairly accurate prediction of the variation with temperature of the susceptibility of the salt $Yb_2(SO_4)_3 \cdot 8H_2O$. Second, because the oxide Yb_2O_3 shows a very pronounced deviation from Hund's law, even at 700°K (the square of the magneton number at 700°K is 17.5 while Hund's law gives 20.6).

The salt $Yb_2(SO_4)_3 \cdot 8H_2O$. From analogy with the similar salts of Pr and Nd, we assume that the Yb ion in $Yb_2(SO_4)_3 \cdot 8H_2O$ is subject to a field of cubic symmetry. The energy levels in the presence of the field of cubic symmetry $D\Sigma_i(x_i^4+y_i^4+z_i^4)$, and a magnetic field H can be calculated up to terms in H^2 by the method already described.[1] Yb is one electron short of a closed shell, and the problem is therefore that of a one electron system, with an inverted energy spectrum. The sign of D has been taken to be positive, as in all cases previously considered. The energy levels are

$$W_1 = -14a + 1.167G - 0.3240G^2/a,$$
$$W_2 = -\ 2a + 1.833G + 0.3240G^2/a,$$
$$W_3 = -\ 2a + 0.500G - 0.1500G^2/a,$$
$$W_4 = \ 18a - 1.500G + 0.1500G^2/a,$$

and four more obtained from these by changing the sign of G. Here $a = 12pD$ and $G = g\beta H$, g being the Landé g-factor (8/7 for Yb). The susceptibility of $Yb_2(SO_4)_3 \cdot 8H_2O$ has been measured at 290°K by Cabrera[11] ($n_B^2 = 19.10$), St. Meyer[12] ($n_B^2 = 21.0$) and Zernike and James[13] ($n_B^2 = 19.75$). We now choose the constant a to pass through the mean of these values ($n_B^2 = 19.95$; $a = -9.4$ cm^{-1}), and then we obtain the curve for n_B^2 against T which is plotted as curve II in Fig. 5. More accurate measurements may require adjustment of this curve, but it should be necessary only to expand or contract it along the T axis. The experimental results on $Yb_2(SO_4)_3$, as measured by Cabrera and Duperier,[14] are also shown for comparison. However, we have not attempted to fit these points, since nothing much can be done until measurements are made at low temperatures. The greater the deviations from Hund's law, the more precise is the determination of the crystal field, and with $Yb_2(SO_4)_3$ these occur only at low temperatures.

The oxide Yb_2O_3. Let us now consider the oxide Yb_2O_3. Two sets of experimental data are

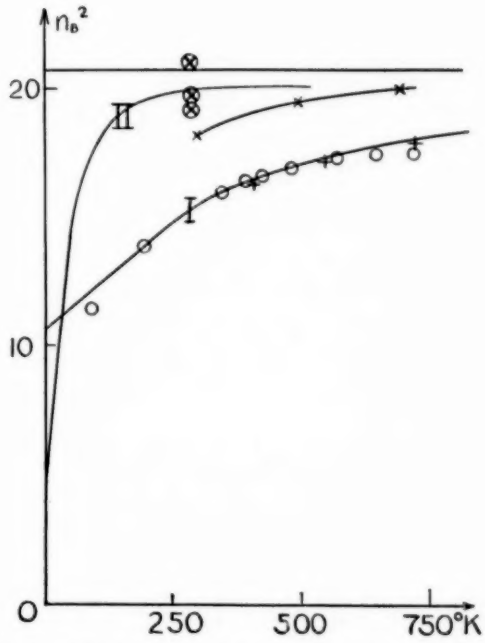

FIG. 5. Calculated and observed values of n_B^2. (For Yb_2O_3: circle, Sucksmith; plus, Cabrera and Duperier; I, 143 $(x^2+y^2-2z^2)$.) (For $Yb_2(SO_4)_3 \cdot 8H_2O$: circled cross, various experimenters; II, -0.78 $(x^4+y^4+z^4)$.) (For $Yb_2(SO_4)_3$: cross, Cabrera and Duperier.)

available, by Sucksmith[3] and Cabrera and Duperier,[14] respectively, and the two agree within two percent over the whole range measured by the latter observers. The nearest approach to the experimental results that we have been able to obtain are those for the axial field $143(x^2+y^2-2z^2)$, although we have tried many others. The difficulty is to get a field which will give as low a value of the magneton number at low temperatures as is observed. The second order rhombic field without axial symmetry does not agree as well as that with this symmetry, and the addition of a field of cubic symmetry does not improve matters. As can be seen on referring to Fig. 5, the disagree-

[11] B. Cabrera, C. R. **180**, 669 (1925).

[12] St. Meyer, Phys. Zeits. **26**, 51, 478 (1925).

[13] J. Zernike and C. James, J. Am. Chem. Soc. **48**, 2827 (1926).

[14] B. Cabrera and A. Duperier, C. R. **188**, 1640 (1929).

ment is not very serious. There seems little doubt that good agreement could be obtained by assuming a field which allowed the levels $M=7/2,\ 3/2,\ -1/2,\ -5/2$, to be mixed arbitrarily, still preserving the Kramers degeneracy. However, the problem is very complicated in its full generality, and the best simple solution seems to be the one given. The energy levels for this field are 0, 860, 2580, 5160 cm^{-1}. It will be noticed that the sign of the coefficients of the crystal field is the same for all three ions Pr, Nd and Yb. In order to compare the electric fields acting on the ions, it is necessary to investigate the coefficients of the matrix elements of the squares of the coordinates for the different ions. It is found that this coefficient is negative for all three, and hence the electric field has in each case the form $\Sigma_i\{Ax_i^2+By_i^2-(A+B)z_i^2\}$ where $(A+B)$ is negative. The relative magnitudes of $(A+B)$ for the Pr ion in $Pr_2(SO_4)_3$, the Nd ion in Nd_2O_3, and the Yb ion in Yb_2O_3 are Pr : Nd : Yb = 1.88 : 1.00 : 0.54. These ratios are very satisfactory, considering that the agreement between the theoretical and experimental results was not perfect.

In conclusion, I would like to express my thanks to Professor J. H. Van Vleck for helpful suggestions during the course of this work.

The Positive Electron

CARL D. ANDERSON, *California Institute of Technology, Pasadena, California*

(Received February 28, 1933)

Out of a group of 1300 photographs of cosmic-ray tracks in a vertical Wilson chamber 15 tracks were of positive particles which could not have a mass as great as that of the proton. From an examination of the energy-loss and ionization produced it is concluded that the charge is less than twice, and is probably exactly equal to, that of the proton. If these particles carry unit positive charge the curvatures and ionizations produced require the mass to be less than twenty times the electron mass. These particles will be called positrons. Because they occur in groups associated with other tracks it is concluded that they must be secondary particles ejected from atomic nuclei.

Editor

ON August 2, 1932, during the course of photographing cosmic-ray tracks produced in a vertical Wilson chamber (magnetic field of 15,000 gauss) designed in the summer of 1930 by Professor R. A. Millikan and the writer, the tracks shown in Fig. 1 were obtained, which seemed to be interpretable only on the basis of the existence in this case of a particle carrying a positive charge but having a mass of the same order of magnitude as that normally possessed by a free negative electron. Later study of the photograph by a whole group of men of the Norman Bridge Laboratory only tended to strengthen this view. The reason that this interpretation seemed so inevitable is that the track appearing on the upper half of the figure cannot possibly have a mass as large as that of a proton for as soon as the mass is fixed the energy is at once fixed by the curvature. The energy of a proton of that curvature comes out 300,000 volts, but a proton of that energy according to well established and universally accepted determinations[1] has a total range of about 5 mm in air while that portion of the range actually visible in this case exceeds 5 cm without a noticeable change in curvature. The only escape from this conclusion would be to assume that at exactly the same instant (and the sharpness of the tracks determines that instant to within about a fiftieth of a second) two independent electrons happened to produce two tracks so placed as to give the impression of a single particle shooting through the lead plate. This assumption was dismissed on a probability basis, since a sharp track of this order of curvature under the experimental conditions prevailing occurred in the chamber only once in some 500 exposures, and since there was practically no chance at all that two such tracks should line up in this way. We also discarded as completely untenable the assumption of an electron of 20 million volts entering the lead on one side and coming out with an energy of 60 million volts on the other side. A fourth possibility is that a photon, entering the lead from above, knocked out of the nucleus of a lead atom two particles, one of which shot upward and the other downward. But in this case the upward moving one would be a positive of small mass so that either of the two possibilities leads to the existence of the positive electron.

In the course of the next few weeks other photographs were obtained which could be interpreted logically only on the positive-electron basis, and a brief report was then published[2] with due reserve in interpretation in view of the importance and striking nature of the announcement.

MAGNITUDE OF CHARGE AND MASS

It is possible with the present experimental data only to assign rather wide limits to the

[1] Rutherford, Chadwick and Ellis, *Radiations from Radioactive Substances*, p. 294. Assuming $R \propto v^3$ and using data there given the range of a 300,000 volt proton in air S.T.P. is about 5 mm.

[2] C. D. Anderson, Science **76**, 238 (1932).

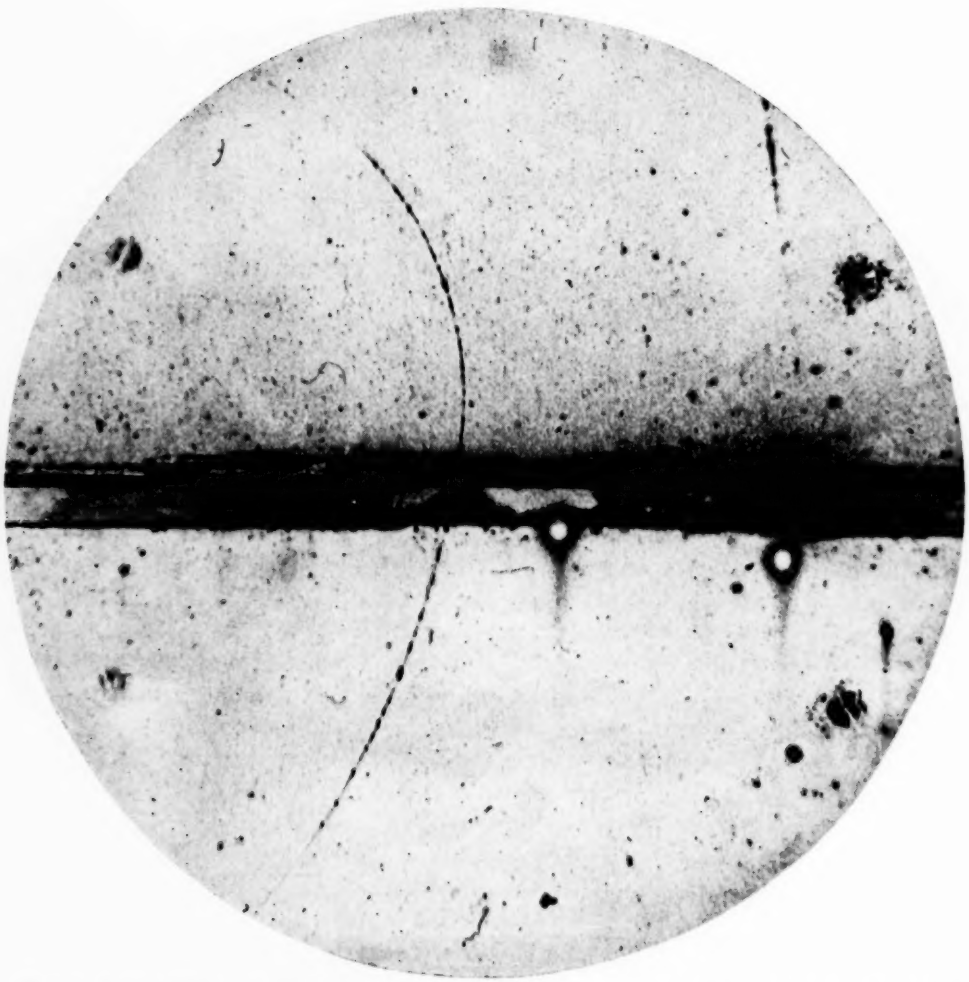

FIG. 1. A 63 million volt positron ($H\rho = 2.1 \times 10^5$ gauss-cm) passing through a 6 mm lead plate and emerging as a 23 million volt positron ($H\rho = 7.5 \times 10^4$ gauss-cm). The length of this latter path is at least ten times greater than the possible length of a proton path of this curvature.

magnitude of the charge and mass of the particle. The specific ionization was not in these cases measured, but it appears very probable, from a knowledge of the experimental conditions and by comparison with many other photographs of high- and low-speed electrons taken under the same conditions, that the charge cannot differ in magnitude from that of an electron by an amount as great as a factor of two. Furthermore, if the photograph is taken to represent a positive particle penetrating the 6 mm lead plate, then the energy lost, calculated for unit charge, is approximately 38 million electron-volts, this value being practically independent of the proper mass of the particle as long as it is not too many times larger than that of a free negative electron. This value of 63 million volts per cm energy-loss for the positive particle it was considered legitimate to compare with the measured mean of approximately 35 million volts[3] for negative electrons of 200–300 million volts energy since the rate of energy-loss for particles of small mass is expected to change only very slowly over an energy range extending from several million to several hundred million volts. Allowance being made for experimental uncertainties, an upper limit to the rate of loss of energy for the positive particle can then be set at less than four times that for an electron, thus fixing, by the usual relation between rate of ionization and

[3] C. D. Anderson, Phys. Rev. **43**, 381A (1933).

charge, an upper limit to the charge less than twice that of the negative electron. It is concluded, therefore, that the magnitude of the charge of the positive electron which we shall henceforth contract to positron is very probably equal to that of a free negative electron which from symmetry considerations would naturally then be called a negatron.

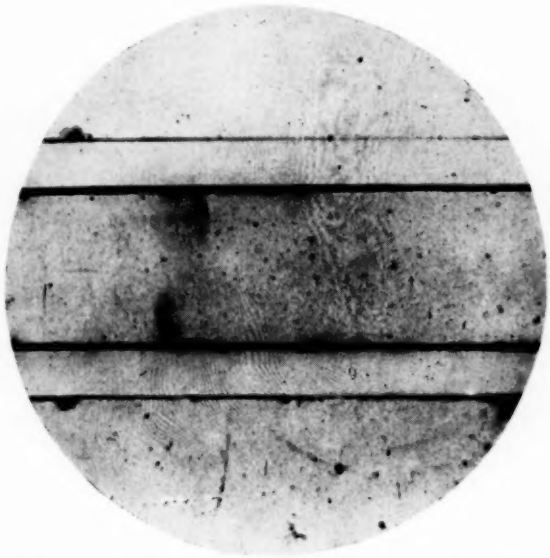

FIG. 2. A positron of 20 million volts energy ($H\rho = 7.1 \times 10^4$ gauss-cm) and a negatron of 30 million volts energy ($H\rho = 10.2 \times 10^4$ gauss-cm) projected from a plate of lead. The range of the positive particle precludes the possibility of ascribing it to a proton of the observed curvature.

It is pointed out that the effective depth of the chamber in the line of sight which is the same as the direction of the magnetic lines of force was 1 cm and its effective diameter at right angles to that line 14 cm, thus insuring that the particle crossed the chamber practically normal to the lines of force. The change in direction due to scattering in the lead,[3] in this case about 8° measured in the plane of the chamber, is a probable value for a particle of this energy though less than the most probable value.

The magnitude of the proper mass cannot as yet be given further than to fix an upper limit to it about twenty times that of the electron mass. If Fig. 1 represents a particle of unit charge passing through the lead plate then the curvatures, on the basis of the information at hand on ionization, give too low a value for the energy-loss unless the mass is taken less than twenty times that of the negative electron mass. Further determinations of $H\rho$ for relatively low energy particles before and after they cross a known amount of matter, together with a study of ballistic effects such as close encounters with electrons, involving large energy transfers, will enable closer limits to be assigned to the mass.

To date, out of a group of 1300 photographs of cosmic-ray tracks 15 of these show positive particles penetrating the lead, none of which can be ascribed to particles with a mass as large as that of a proton, thus establishing the existence of positive particles of unit charge and of mass small compared to that of a proton. In many other cases due either to the short section of track available for measurement or to the high energy of the particle it is not possible to differentiate with certainty between protons and positrons. A comparison of the six or seven hundred positive-ray tracks which we have taken is, however, still consistent with the view that the positive particle which is knocked out of the nucleus by the incoming primary cosmic ray is in many cases a proton.

FIG. 3. A group of six particles projected from a region in the wall of the chamber. The track at the left of the central group of four tracks is a negatron of about 18 million volts energy ($H\rho = 6.2 \times 10^4$ gauss-cm) and that at the right a positron of about 20 million volts energy ($H\rho = 7.0 \times 10^4$ gauss-cm). Identification of the two tracks in the center is not possible. A negatron of about 15 million volts is shown at the left. This group represents early tracks which were broadened by the diffusion of the ions. The uniformity of this broadening for all the tracks shows that the particles entered the chamber at the same time.

From the fact that positrons occur in groups associated with other tracks it is concluded that they must be secondary particles ejected from an atomic nucleus. If we retain the view that a nucleus consists of protons and neutrons (and α-particles) and that a neutron represents a close combination of a proton and electron, then from the electromagnetic theory as to the origin of mass the simplest assumption would seem to be that an encounter between the incoming primary ray and a proton may take place in such a way as to expand the diameter of the proton to the same value as that possessed by the negatron. This process would release an energy of a billion electron-volts appearing as a secondary photon. As a second possibility the primary ray may disintegrate a neutron (or more than one) in the nucleus by the ejection either of a negatron or a positron with the result that a positive or a negative proton, as the case may be, remains in the nucleus in place of the neutron, the event occurring in this instance without the emission of a photon. This alternative, however, postulates the existence in the nucleus of a proton of negative charge, no evidence for which exists. The greater symmetry, however, between the positive and negative charges revealed by the discovery of the positron should prove a stimulus to search for evidence of the existence of negative protons. If the neutron should prove to be a fundamental particle of a new kind rather than a proton and negatron in close combination, the above hypotheses will have to be abandoned for the proton will then in all probability be represented as a complex particle consisting of a neutron and positron.

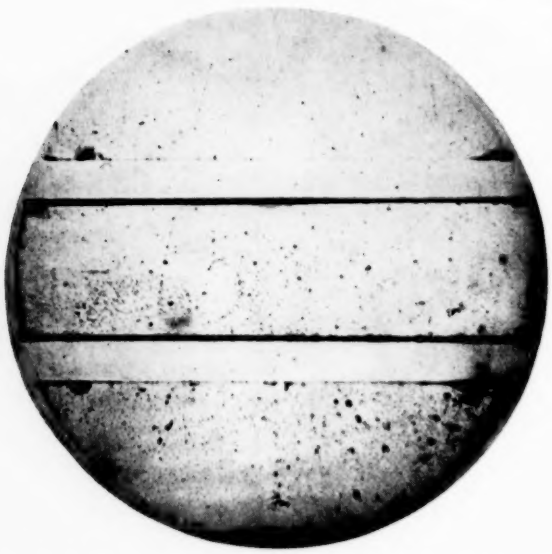

FIG. 4. A positron of about 200 million volts energy ($H\rho = 6.6 \times 10^5$ gauss-cm) penetrates the 11 mm lead plate and emerges with about 125 million volts energy ($H\rho = 4.2 \times 10^5$ gauss-cm). The assumption that the tracks represent a proton traversing the lead plate is inconsistent with the observed curvatures. The energies would then be, respectively, about 20 million and 8 million volts above and below the lead, energies too low to permit the proton to have a range sufficient to penetrate a plate of lead of 11 mm thickness.

While this paper was in preparation press reports have announced that P. M. S. Blackett and G. Occhialini in an extensive study of cosmic-ray tracks have also obtained evidence for the existence of light positive particles confirming our earlier report.

I wish to express my great indebtedness to Professor R. A. Millikan for suggesting this research and for many helpful discussions during its progress. The able assistance of Mr. Seth H. Neddermeyer is also appreciated.

LETTERS TO THE EDITOR

Prompt publication of brief reports of important discoveries in physics may be secured by addressing them to this department. Closing dates for this department are, for the first issue of the month, the twentieth of the preceding month; for the second issue, the fifth of the month. The Board of Editors does not hold itself responsible for the opinions expressed by the correspondents.

Resonance Spectrum of Bromine

It has been found possible to excite a resonance spectrum of nine terms in bromine vapor at very low pressure. The λ5461 line of the mercury arc was used in the excitation of the fluorescence. Two types of light furnace were used. In the first type a large mercury arc was constructed concentrically about a tube 70 cm in length containing the bromine vapor. In the second type two powerful mercury arcs, vertical and operated in series at 5 to 10 amperes, were mounted inside an elliptical reflector with the bromine tube. Each arc was connected to the vacuum line and was equipped with a third 10,000 volt electrode to facilitate starting.

The bromine resonance tube was connected to the high vacuum line as well as to a reservoir in which solid bromine was maintained at −63°C, by immersion in melting chloroform. The bromine vapor pressure was accordingly about 0.2 mm. Plates were obtainable in 3 hours on a Steinheil three prism spectrograph. Wave-length measurements were made from microphotometer traces.

Insofar as could be determined on the low dispersion plates, each line was actually a doublet of wave number separation equal to 22. All of the terms were included fairly accurately by the series formula:

$$1/\lambda_n = 18{,}307.6 - 326n + 2n^2.$$

In this expression, n represents the positive order of the line, with the use of Wood's resonance spectrum notation, and λ_n is the wave-length of the short wave-length component of the doublet of n^{th} order. The wave-lengths of the shorter components of all but one of the nine orders are given in Table I.

TABLE I.

Order	Wave-length	Order	Wave-length
1	5559.8A	5	5975.5A
2	5659.9	6	6089.0
3	(masked by	7	6199.5
	the yellow lines	8	6316.0
	of mercury)	9	6437.0
4	5863.5		

It is of interest to compare the iodine resonance spectra found by Wood with the bromine series. In the case of iodine with excitation by λ5461 the series is expressed by:

$$1/\lambda_n = 18{,}307.6 - 213n + 0.6n^2.$$

The separation of the doublets for iodine is 5 wave numbers. The bromine resonance spectrum is exceedingly less intense than the iodine spectrum.

It is not certain that the true bromine rotation doublets have been resolved. The presumable long wave components are much weaker than the short wave components and in some cases seem to be absent entirely.

HAROLD PLUMLEY

Physics Department,
University of Chicago,
February 22, 1933.

On the Statistical Foundation of Debye's Theory of Electrolytes

Professor V. K. La Mer has recently drawn my attention to some paradoxical inconsistencies in the thermodynamic evaluation of the free energy of electrolytes if expressions for the ionic potentials are used which have been derived by a consistent application of the well-known Debye-method. These difficulties though pointed out six years ago in a paper by Gronwall, La Mer and Sandved have not hitherto found a satisfactory explanation. They can be summarized in the statement that the free energy of an electrolytic solution seems to depend on the way in which the ions are assumed to be charged (either simultaneously or successively) while the initial and final state are kept constant. This would mean that the free energy at constant temperature is no longer a function of the instantaneous state alone but also of its previous history—in contradiction to the principles of thermodynamics.

As a result of a closer investigation it has been found that the Debye-method *in general* leads to expressions which do not obey the integrability relations of thermodynamics. More specifically, it can be stated that the limiting law (without ionic diameters) satisfies the thermodynamic requirements. Expressions which contain individual ionic diameters as well as all higher approximations for ions of nonsymmetrical valence-type do not conform to the integrability conditions. This explains also the paradox mentioned above.

A more detailed publication will follow soon.

OTTO HALPERN

New York University,
University Heights,
February 27, 1933.

Low States of the Heaviest Elements

With the aid of Fermi's potential for positive ions,[1] the energies of the $5f$, $6d$, $7s$ and $7p$ states of the atoms and ions built upon the radon core have been calculated from Schrödinger's equation by the approximation method of Wentzel-Kramers-Brillouin. It leads to the "phase integral" of the classical quantum theory with half-integer quantum numbers, except for the f states of uranium and singly ionized uranium (and Ac, Ac^+, Th, Th^+, Pa, Pa^+), in which cases the eigenvalues are given by an expression obtained from the quantum mechanical problem of two unequal potential minima.[2] The energy ϵ has to satisfy the relation

$$\int_{x_1}^{x_2} d\rho(\epsilon - v)^{\frac{1}{2}} = (n - l - \tfrac{1}{2})\pi - \tan^{-1}\left[\tfrac{1}{4}\exp\left\{-2\int_{x_2}^{x_3} d\rho(v-\epsilon)^{\frac{1}{2}}\right\}\tan\int_{x_3}^{x_4} d\rho(\epsilon - v)^{\frac{1}{2}}\right]$$

where $x_1 < x < x_2$, $x_3 < x < x_4$ are the two regions of possible classical motion and $x_2 < x < x_3$ is the region under the potential hill.

The table below gives the results of the calculation of the energies in terms of the Rydberg constant as unity.

	U^{+++++}	U^{++++}	U^{+++}	U^{++}	U^{+}	U
$5f$	−3.22	−2.35	−1.45	−0.74	−0.256	−0.0625
$6d$	−3.15	−2.40	−1.70	−1.10	−0.55	−0.14
$7s$			−1.38	−0.90	−0.54	−0.20
$7p$			−1.30	−0.85	−0.47	−0.165

Calculations show that the energies of the different states depend chiefly on the degree of ionization and change very little with change of nuclear charge from $Z=92$ to 89. Hence the relative position of the levels in the uranium ions will be very similar to that for the corresponding ions of Pa, Th and Ac. The calculations involved are only approximations but nevertheless they give information as to which configurations can be expected to form the lowest states of the four heaviest elements; they are

89	Ac	Radon core +	$6d^2$	$7s$
			$6d$	$7s^2$
90	Th	Radon core +	$6d^3$	$7s$
			$6d^2$	$7s^2$
91	Pa	Radon core +	$6d^4$	$7s$
			$6d^3$	$7s^2$
92	U	Radon core +	$5f$	$6d^4$ $7s$
			$5f$	$6d^3$ $7s^2$
				$6d^5$ $7s$
				$6d^4$ $7s^2$

The interesting point is that with U the $5f$ state begins to be prominent, in contradiction with the older calculations of Sugiura and Urey.[3] Because of the approximate nature of the calculations it is not certain whether the lowest state of uranium already contains a $5f$ electron. However, beginning with element 93 we have to consider the six-fold ionized atom to obtain the ion with the radon core and in this ion the $5f$ is certainly the lowest level. This makes it very probable that the neutral atom 93 in its normal state contains at least one $5f$ electron. This points to the possible beginning of a series of elements similar to the rare earths in their relation to the periodic table, though the outer electron configurations and thus the chemical properties of these hypothetical elements will be different from those of the rare earths.

It is obvious that the results concerning the low states of the heaviest elements have to be confirmed by the analysis of the spectra of their ions, which has been started in this laboratory.

TA-YOU WU
S. GOUDSMIT

Department of Physics,
University of Michigan,
March 1, 1933.

[1] E. Fermi, Mem. della reale Acad. d'Italia I, 1930. A. Sommerfeld, Zeits. f. Physik **78**, 283 (1932).

[2] This has also been applied to the calculation of the quantum defects of states of heavy elements and shows why the quantum defects of penetrating orbits are in several cases near to integers. Details will be published shortly.

[3] Y. Sugiura and H. C. Urey, Kgl. Danske Vid. Selsk. **7**, 13 (1926).

The Separation of Hydrogen Isotopes by Fractional Desorption

Eyring[1] has recently emphasized the significance of zero point energy in the separation of hydrogen isotopes and has linked this with the observation of Washburn and Urey[2] on the separation by electrolysis and with the concept of activated adsorption and desorption of gases on surfaces developed by Taylor.[3] This theoretical approach lent especial importance to an experimental study of the possible separation of hydrogen isotopes by desorption from surfaces on which they are adsorbed with an activation energy. The experiments of Taylor and Sherman[4] on the para-hydrogen conversion at surfaces as a criterion of activated adsorption of hydrogen suggested at once that active charcoal surfaces would be the best for such experiments. Accordingly we have examined the desorption of electrolytic hydrogen, purified by passage over platinized asbestos and suitable drying agents, from an active adsorbent charcoal maintained at liquid air temperatures. We have examined, by the method developed by Bleakney,[5] the final samples of hydrogen desorbed from charcoal under these circumstances. A one stage desorption process yielded

a final sample of 35 cc from an initial adsorption of 5025 cc. This revealed a three-fold enrichment of H^1H^2. A two stage desorption was then made in which, from 5715 cc adsorbed, an end desorption was secured amounting to 440 cc, which was then readsorbed and fractionally desorbed to give a final sample of 90 cc. This sample showed a five-fold enrichment of H^1H^2 over that present in the hydrogen after passing the purification train. While this enrichment may not be as large as that to be expected theoretically on the basis of zero-point energy and activated adsorption, it appears to be much larger than would be expected from a simple distillation process of separation. Since, theoretically, this method of separation by desorption involving zero-point energy will be enormously more efficient at the temperature of liquid hydrogen we are taking steps to extend our experiments to these lower temperature ranges.

HUGH S. TAYLOR
AUSTIN J. GOULD
WALKER BLEAKNEY

Frick Chemical Laboratory,
Palmer Physical Laboratory,
Princeton University,
March 2, 1933.

[1] H. Eyring, Proc. Nat. Acad. Sci. **19**, 78 (1933).
[2] E. W. Washburn and H. C. Urey, Proc. Nat. Acad. Sci. **18**, 496 (1932).
[3] H. S. Taylor, J. Am. Chem. Soc. **53**, 578 (1931).
[4] H. S. Taylor and A. Sherman, Trans. Faraday Soc. **28**, 247 (1932).
[5] W. Bleakney, Phys. Rev. **41**, 32 (1932).

Scattering and Absorption of Neutrons

In these experiments the neutron source consisted of beryllium powder in one or more glass bulbs 4 mm diameter filled with radon, in amounts up to 1200 millicuries. Alpha-radiation equivalent to 3600 millicuries of polonium was thus utilized, making a much more powerful neutron source than hitherto reported, although de Broglie, le Prince-Ringuet, Thibaud and La Tour used a radon-beryllium source without stating the amount of radon.[1] Neutrons were ejected from the beryllium by the alpha-particles from radon, radium *A* and radium *C'*, to a number around 10^5 per second. To measure the intensity of the neutron stream a small ionization chamber was used, connected to an amplifier-oscillograph system described previously, which registered ionizations by single high-speed particles above the unavoidable background of gamma-radiation.[2] The ionizing particles were atoms projected from the paraffin front and the other materials of the chamber by neutron impact.

For the scattering measurements, annular ring scatterers were used, the direct beam being largely blocked out of the chamber by a cylinder of lead 19 cm long, and the scattering, measured by the increase in the number of neutrons registered with the scattering ring in place, was determined for positions giving several scattering angles.

TABLE I.

Material	*Angle of Scattering*				
	46±15	51±20	82±27	125±25	151±15
Paraffin	3.68	3.65	2.18	1.48	0.21
Water	3.59	3.45	2.50	1.48	0.56
Carbon	2.96	2.17	2.01	1.62	0.79
Lead	2.75	2.52	2.49	1.71	0.58

Table I shows the relative scattering by rings 15.5 cm mean radius and square cross section of 25 cm^2 in numbers of neutrons registering in ionization chamber per minute, the distance from source to chamber being 31.5 cm.

As might be expected, paraffin and water, containing much hydrogen, show small backward scattering, no more than would be indicated for the carbon or oxygen contained, while carbon and lead show more nearly uniform scattering.

The computation of the scattering coefficients requires approximations as to geometrical quantities and absorption. The following figures are probably relatively correct to within ±15 percent: fraction scattered (per unit volume of scatterer) from an incident beam of unit intensity into unit solid angle in the specified direction: lead 2.28×10^{-2} at 45°, 1.2×10^{-2} at 125°; carbon 2.12×10^{-2} at 45°, 0.96×10^{-2} at 125°.

Since the absorption of neutrons is largely scattering, the greatest absorption will be shown by an absorber just filling the geometrical path, because any material outside the direct beam scatters neutrons back into the chamber. For example, paraffin in the form of a cylinder 3 cm diameter and 4 cm long shows twice as much absorption as a large plate of paraffin 4 cm thick. Absorbers 3 cm in diameter were uniformly used in this work. Absorption curves were taken for carbon, lead, water and paraffin, the neutron beam having been filtered through 4 cm of lead to reduce the gamma-radiation. These curves are approximately exponential, and appear to approach a minimum which is probably the residual scattering from the room. A study was also made of the absorption by cylinders, 4 cm long, of various materials, as shown in Fig. 1. Copper has the highest absorption per cm of any material yet tested.

As to correlation of the atomic absorption with atomic weight, the simple hypothesis of elastic sphere collision between the neutron and the nucleus, with a definite radius for the neutron and a radius for the nucleus proportional to the cube root of its atomic weight, can be made to fit the absorption results very well, a radius of 4.6×10^{-13} cm being required for the neutron and one of 7.8×10^{-13} cm

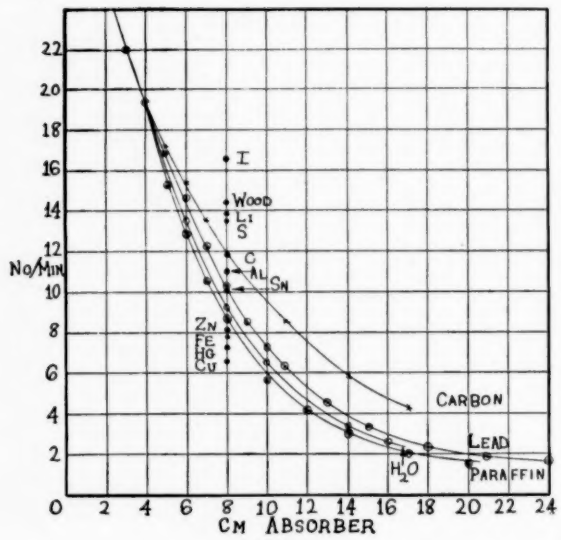

FIG. 1

for the lead nucleus. The size of the lead nucleus accords with radioactive disintegration theory, but the radius assigned to the neutron seems too large to permit it to fit into nuclei. If we introduce the hypothesis of an angle function for the scattering, such that small angle scattering is relatively greater for heavier atoms, the neutron radius will need to be smaller. Professor Rabi has kindly investigated the wave mechanics picture far enough to conclude that the scattering function for small angles is really of this type, and that our data lead to a more reasonable value, of the order of 1.2×10^{-13} cm, for the neutron collision radius.

J. R. DUNNING
G. B. PEGRAM

Columbia University,
March 6, 1933.

[1] de Broglie, le Prince-Ringuet, Thibaud and La Tour, Comptes Rendus **194** (1932).
[2] J. R. Dunning, Phys. Rev. **43**, 380A (1933).

Evaporation Technique for Aluminum

Mirrors made from aluminum by the evaporation technique are superior to silver in several respects as listed below. The reflectivity of aluminum is very nearly as high as silver for green light but is much higher for the ultraviolet[1] making possible the use of mirrors for ultraviolet optics where the lack of achromatism in a lens system is often objectionable.

The aluminum mirrors, now exposed for over six months, show no tarnish. The permanence of the high reflectivity definitely exceeds that of silver protected by an evaporated quartz layer.[2] The aluminum is inert toward corrosive agents because of a layer of oxide which forms on the aluminum upon contact to the air.

The aluminum adheres to glass more tenaciously than silver so that dust, etc., may be washed off with soap and water. One small glass grating coated with aluminum has been washed several times a week for a period of about three months without any harmful effect to the mirror and, furthermore, without introducing the small scratches which silver exhibits after being cleaned.

Other features, such as its apparent uniformity of reflectivity and transmission in the visible, may make of aluminum an important material for coating interferometer plates.

The evaporation of aluminum from a tungsten helix may be successfully effected when the proper size of tungsten wire and helix are chosen.

The technique of evaporation depends upon the fact that tungsten has a limited solubility in liquid aluminum. When the wire of the tungsten helix is large enough it is possible for the aluminum to become saturated with tungsten before the wire is dangerously reduced in diameter. For the successful evaporation of aluminum the helix may be 8 turns of 30 mil tungsten wire wound (in a Bunsen flame at red heat) on an 8 d. finishing nail to form a coil about one inch long. When the pitch of the helix is much less than 8 turns per inch the aluminum shorts the coil and is inefficiently heated by the electric current. When, however, the diameter of the helix is greater, the ratio of aluminum to tungsten is too great and the coil burns out. Furthermore, when a helix is made of wire of diameter larger than 30 mil the coil is excessively brittle.

The tungsten which is dissolved by the aluminum is deposited back on the helix as the evaporation proceeds. This may be sintered to the helix by a final heating of the empty coil and so approximately compensates for the dissolution of metal by the aluminum. Ordinarily one coil of tungsten lasts for some dozen charges of aluminum. The aluminum is cut in the form of a cylinder which fits easily into the helix. As the purest aluminum gives best results as regards tarnishing and adhesion, it is advisable to melt the aluminum to the helix to free it from gas and oxide before the mirror is uncovered. This may also be accomplished by a preliminary run to fuse the aluminum after which the apparatus is dismounted and the mirror introduced into the vacuum chamber. Other than this the technique is the same as has been described before[1] for the vacuum evaporation of metals.

JOHN STRONG*

California Institute of Technology,
March 8, 1933.

* National Research Fellow.

[1] W. W. Coblentz and R. Stair, Bur. Standards J. Research **4**, 189 (1930).
[2] C. Hawley Cartwright and John Strong, Rev. Sci. Inst. **2**, 189 (1931).

Effect of Spin Interaction in the Diffraction and Polarization of Electrons

The main features of electron diffraction may be explained without considering the orientation of the spins of the electrons in a diffracting crystal. This theory however appears to be inadequate for explaining some of the phenomena of diffraction such as have been reported by Farnsworth.[1] If, in addition to the usual considerations, we assume that the reaction of a crystal upon an incident electron will depend upon the orientation of that electron's spin with respect to some distinguishable direction in the portion of the crystal which is involved, we would then expect certain phenomena very similar to some of those reported by Farnsworth.

According to prevalent ideas, a single crystal of a ferromagnetic metal is subdivided into domains in which all the electrons of a certain type are coupled together with their spins parallel. The direction of the common axis of spin for a given domain may lie in any one of a number of possible directions with respect to the crystal axes. It has further been suggested[2] that a single crystal of any metal is likewise subdivided into domains in which all the electrons of a certain type are coupled together with their spins antiparallel. Such a domain will be characterized by a unique direction for the spin axes of the coupled electrons but it will not exhibit a magnet moment. We may therefore expect anisotropic effects in any crystal, but the direction of this "spintropism" may be different in different domains of the same crystal.

Consider an electron beam diffracted by a crystal such as has been described in the preceding paragraph. If we assume that the reaction between the crystal and any electron of the beam depends upon the orientation of the spin of the incident electron with respect to the anisotropy of the various domains involved, we may expect phenomena somewhat analogous to the double refraction of light beams. Since more than one domain may be involved, we may expect multiple beams such as have been observed by Farnsworth, and the index of refraction would be different for the different beams. However satisfactory this suggested explanation might prove to be in all other respects, it would be a bit hard to accept unless marked polarization could be detected in the diffracted beams.

The theoretical and experimental evidence in regard to the existence of any considerable degree of polarization in electron beams is mostly negative to date. On the other hand, if the above ideas concerning the structure of metal crystals are correct—they appear to be so for ferromagnetics at least—there must exist in the interior of a crystal periodic magnetic fields of considerable magnitude along with the electric fields. If both electric and magnetic fields exist in a crystal there will be a polarizing effect on an electron beam according to Darwin[3] who did not believe that such a crystal could be used for diffraction experiments. The various experiments on electron polarization showing a negative or small effect may have failed to detect this polarization because the analyzers and polarizers which were used were not effective. Even the very careful experiments of Davisson and Germer[4] are not necessarily conclusive because it is apparently not certain that the anisotropy of the crystal was uniform in direction throughout the effective volume of the crystal. Experiments are planned to see if it is possible to find a more effective diffractor to use as a polarizer and analyzer.

J. H. Howey

Sloane Physics Laboratory,
Yale University,
March 3, 1933.

---

[1] H. E. Farnsworth, Phys. Rev. **40**, 684 (1932).

[2] F. Bitter, Phys. Rev. **42**, 731 (1933); F. Zwicky, Phys. Rev. **38**, 1772 (1931).

[3] Darwin, Proc. Roy. Soc. **A120**, 631 (1929).

[4] Davisson and Germer, Phys. Rev. **33**, 760 (1929).

Proceedings of The New England Section of the American Physical Society

MINUTES OF THE CAMBRIDGE MEETING, FEBRUARY 4, 1933

THE second regular meeting of the New England Section was held in Cambridge, Massachusetts on Saturday, February 4, jointly with a meeting of the Eastern Association of Physics Teachers. The morning sessions of the two Societies were separate, while the afternoon session was a joint one. The Presiding Officers for the morning sessions of the Physical Society were Professor E. C. Kemble, Chairman of the Section, and Professor G. F. Hull. The Presiding Officers of the joint afternoon session were Professor E. C. Kemble and Mr. L. A. Wendelstein, President of the Eastern Association of Physics Teachers.

About 80 were present at the Physical Society's morning sessions, and about 250 at the afternoon session.

The morning sessions were devoted to the reading of contributed papers, the abstracts of which appear below.

A meeting of the Program Committee was held at noon. The date of the fall meeting at Middletown, Connecticut was tentatively set as October 14, 1933. A number of suggestions were made for subjects for the invited papers at that meeting. It was decided that since the program of the Section's meetings was still in an experimental stage, further efforts would be made to get suggestions from members as to possible improvements in these programs.

A vote of thanks was extended to the members of the Department of Physics at M.I.T. for their hospitality.

Luncheon was held at the Walker Memorial Dining Halls.

The afternoon session was devoted to invited papers. The first three constituted a Colloquium on *Nuclear Physics*. Dr. M. A. Tuve of the Carnegie Institute of Washington, Bureau of Terrestrial Magnetism, talked on *Recent Advances in Nuclear Physics*, Dr. R. J. Van de Graaff of M.I.T. talked on *High Voltage Methods in Nuclear Physics*, and Mr. E. H. Bramhall of M.I.T. demonstrated an Electrostatic High-Voltage Generator.

The fourth invited paper was by Professor D. H. Menzel of Harvard Observatory on *Physics of the Sun*.

The Program of the Section consisted of 16 papers, the abstracts for which are given below.

PHILIP M. MORSE, *Secretary-Treasurer*

ABSTRACTS

1. The Weiss law for Rochelle salt. HANS MÜLLER, *Massachusetts Institute of Technology.*—The dielectric constant of Rochelle salt has been measured between 23° and 50° with help of a capacitance bridge by using 1000 cycle a.c. Between 34° and 50° Weiss's law is satisfied. The Curie constant is 128.5 and the "dielectric" Curie point 24.9°C. From these data the Lorenz-Lorentz factor is calculated to 2.315. Assuming the dielectric effect is due to the freely rotating molecules of the water of crystallization the same factor must be 2.314. Below 34° the dielectric constant is a function of the applied field. The maximum value 1540 of the dielectric constant is reached at the "ferromagnetic" Curie point 23.75°.

2. X-ray study of crystal structure of Rochelle salt and effect of temperature. B. E. WARREN AND H. M. KRUTTER, *Massachusetts Institute of Technology.*—From oscillation and rotation patterns of small crystals of Rochelle salt an orthorhombic unit cell has been found with dimensions $a=11.85$A, $b=14.25$A, $c=6.21$A and space group V^3. The unit cell contains four molecules of $NaKC_4H_4O_6\cdot 4H_2O$. With the low symmetry of V^3 a structure determination by direct methods is impossible. Unusually large values of dielectric constant have been found between $+20$°C and -20°C and it was of interest to see whether there was an appreciable change in structure above and below this region. Integrated intensities were measured with a Bragg ionization spectrometer for h00, 0k0 and 001 at -50°C and $+25$°C. The measurements at -50°C showed only a normal increase such as would be expected from the usual Debye temperature factor.

3. Variational atomic wave functions. PHILIP M. MORSE AND L. A. YOUNG, *Massachusetts Institute of Technology.*—Wave functions are chosen for $1s$, $2s$ and $2p$ states of the form suggested by Slater (Phys. Rev. **42**, 33 (1932)). They are made mutually orthogonal, to simplify calculations. Four parameters are used, giving more possibilities of variation than the forms used by Zener (Phys. Rev. **36**, 51 (1930)). The values of all the integrals occurring in the energy expression are computed for a wide range of these parameters. The energies and wave functions of any atom with less than eleven electrons can be computed by taking the proper linear combination of these integrals and minimizing the resulting function of the four parameters. The procedure is not complicated. The discrepancy between these calculated energies and the observed ones for lithium-like atoms is no greater than the difference between the observed energies of helium-like atoms and the $2(Z-5/16)^2$ value.

4. Application of the mechanical interval recorder to analysis of the spectrum of Os I. WALTER ALBERTSON, *Massachusetts Institute of Technology.*—A number of energy levels of Os I have been found with the aid of the mechanical interval recorder (G. R. Harrison, R.S.I. **3**, 753 (1932)). The wave numbers of the 184 strongest lines were punched on a tape by using a scale of 1 mm per wave number. Intervals up to 9400 cm^{-1} were recorded on the machine. A rapid survey of the chart showed several intervals for which a comparatively large number of coincidences appeared. Most of these intervals when linked together were found to give a term array. Comparison with the term array of Os I by C. P. Snyder (unpublished data through courtesy of Dr. W. F. Meggers) shows that all of Snyder's terms except one are included in the new array and that the new array is more extensive. Further application of the machine to analysis of this spectrum is being carried out by the inclusion of weaker lines in the record.

5. Predissociation and the crossing of molecular potential energy curves. O. K. RICE, *Harvard University.*—The calculation of the width and shape of a line which is broadened because of predissociation has been extended so as to include perturbations of intermediate size. By "perturbations of intermediate size" we mean perturbations which are not so great that lines (of given rotational quantum number) belonging to two adjacent vibrational levels are broadened so as to overlap appreciably; they may be any size up to that limit. These calculations have been applied to the case where a potential curve giving molecule formation is intersected by a repulsive curve at a point corresponding to a rather great distance between the two atoms forming a diatomic molecule, the curves which cross being the unperturbed curves. It is found that the discrete lines are not only broadened, but they are distorted in shape and shifted in position. The exact amount of broadening of a line depends very greatly upon its energy relative to the energy at which the potential curves cross, and in general a line which is much broadened will also be much shifted in position. Further, there is present a series of subsidiary maxima of the absorption coefficient. It is found that this theory gives a satisfactory explanation of many of the features of the complex predissociation phenomena (isolated groups of sharp and diffuse lines superimposed on a faint background of blurred bands) observed by Brown and Gibson (Phys. Rev. **40**, 529 (1932)) in the case of iodine chloride.

6. On a molecular spectrum emitted from atomic iodine vapor. O. OLDENBERG, *Harvard University.*—Iodine vapor at high temperature shows a paradox in its spectrum (W. Gerlach and F. Gromann, Zeits. f. Physik **18**, 239 (1923)). Although *monatomic* to 99.9 percent, it emits an intense continuous band which in a previous discussion (O. Oldenberg, Zeits. f. Physik **25**, 142 (1924)) was shown to belong to *molecules*. It was concluded that in the discharge through *atomic* iodine *excited molecules* are formed by the collision of two atoms, which must possess a store of energy sufficient for emitting this spectrum. It was suggested that a positive and a negative atomic ion, pulled together by the Coulomb force, meet this requirement. In recent experiments, however, it was found that the intensity of the continuous spectrum decreases strongly with decreasing pressure. The obvious interpretation is that it is emitted from a molecule just formed by a pair of atoms, one of which is excited; the small intensity at low pressure is explained by a lifetime of the excited state shorter than the interval between collisions at low pressure.

7. A new modulator for use in Kennelly-Heaviside layer recording. HARRY R. MIMNO, P. H. WANG AND P. B. KING, *Harvard University.*—Satisfactory automatic devices for recording the effective heights of the Kennelly-Heaviside layers have recently been constructed. These devices impose new requirements on the design of the associated transmitting circuits. The simple synchronous grid-blocking circuit, developed for our eclipse expedition, is well adapted for such field measurements, but it should not be used in a permanent laboratory installation. A more elaborate system is now being employed in order to reduce all possible sources of interference with other radio channels. The carrier frequency is determined by a temperature-controlled crystal. A multi-stage radiofrequency amplifier is modulated by a Thyratron pulse generator. The duration of the pulse may be altered at will. When taking 24 hour records, the number of pulses per minute may be greatly reduced, without loss of accurate synchronization. The transmitting station is identified by call letters transmitted at 15 minute intervals.

8. The elastic constants of rocks and their relation to seismic wave speeds. W. A. ZISMAN, *Harvard University.*—Previous comparisons between the elastic constants of rocks determined statically and those computed by applying the theory of elastic waves to the seismically observed wave speeds had led to serious discrepancies. In attempting to clarify this situation, measurements were made on Young's modulus, E, Poisson's ratio σ, and the compressibility, χ, of rocks taken from quarries in which Leet

had measured the speeds of explosion waves. Discrepancies existing in already published values of E and σ were found to be due to neglect of previous experimenters to study the large changes in E and σ with the mean applied stress. Inconsistencies in the compressibility determinations of Adams and Williamson were shown to exist and suggest the presence of a 10 percent error in their methods. Their prediction of a rapid increase in compressibility with decreasing pressure was verified and shown to be caused by the porosity of rocks. It was also discovered that water contained in the rocks had an important influence upon the elastic constants, Leet's values of χ for Quincy Granite and for Norite from Sudbury, Canada agreed with our static measurements to within a few percent. These results are of fundamental importance to geophysicists, for they establish their right to apply the theory of elastic waves to the results of seismologists in order to determine from the wave speeds the values of E, σ, and χ for that locality, and hence make it possible to identify the kind of rock existing there.

9. Ferromagnetism of the iron nickel alloys under hydrostatic pressure. R. L. STEINBERGER, *Harvard University.*—The application of pressure to a well annealed specimen causes a relatively large change in flux density; usually a decrease, and an incomplete recovery on release of pressure. In pure iron, 20 percent and 80 percent nickel the change is negative and linear. Forty, fifty, ninety percent nickel alloys and pure nickel exhibit pressure hysteresis of varying amounts. In the 30 and 60 percent specimens the rate of change of flux decreases with increasing pressure. The change is nearly 100 percent in the case of the 30 percent specimen. That is, the metal is made nonmagnetic by the application of pressure.

10. The effect of tension on the electrical resistance of the single trigonal crystals, bismuth and antimony. MILDRED ALLEN, *Harvard University.*—The compensated potentiometer method of measuring small changes in resistance developed by P. W. Bridgman has been used in the study of the effect of tension, applied parallel to the direction of current flow, on the resistance of the two trigonal single crystals, bismuth and antimony. The adiabatic tension coefficient of resistance at 30°C of both has been found to depend on the orientations of the principal and secondary cleavage planes. For the limiting cases of the principal cleavage plane perpendicular and parallel to the tension, the coefficient is found to be independent of the secondary orientation. The coefficient shows trigonal symmetry, as is to be expected. Professor Bridgman has shown on the basis of symmetry considerations that six constants are sufficient entirely to define the change of resistance of trigonal crystals under deforming forces. These have been found for both bismuth and antimony; the constants for antimony are about ten times smaller than for bismuth. The changes in resistance resulting from the *deformation* due to the tension, have been computed and applied as corrections to the observed changes.

11. The viscosity of mixtures of liquids at high pressures. R. B. DOW, *Harvard University.*—The effect of pressure on the viscosity of organic, binary mixtures has been investigated by methods developed and used by P. W. Bridgman. Six mixtures have been examined over the entire composition range at two temperatures, 30° and 75°C, and at pressures extending to 12,000 kg/cm². The isobaric curves on the viscosity-composition graphs for *n*-hexane-*n*-decane and *n*-hexane-carbon disulphide are linear at both temperatures. The corresponding curves for *n*-hexane-chlorobenzene, *n*-hexane-diethyl ether, and uegenol-carbon disulphide are complex. Irregularities in certain regions of composition and sags in the curves appear. The qualitative and quantitative natures of these vary both with change in pressure and temperature. The *n*-pentane-*n*-benzene isobaric curves show unusual sags, with few irregularities, which are functions of temperature. The thermodynamic properties of the mixtures give no explanation of these effects. It is probable that the interlocking between molecules of unlike sizes and shapes is the cause of the great increase in viscosity with increase in pressure.

12. Energy distribution of photoelectrons from zinc surfaces. NORRIS E. BRADBURY, *Massachusetts Institute of Technology.*—The energy distribution of photoelectrons emitted from zinc surfaces by the 2537 line of mercury has been studied for various surface conditions. The classical method of retarding potentials was employed by using a small spherical source with a large collecting sphere. Machined and polished zinc gives a distribution curve of which the most probable energy lies at approximately 0.4 of the maximum energy. The work function determined from this maximum energy is about 3.1 volts in agreement with results of other investigators. If the zinc is heated to 375° with consequent evaporation of the surface, the work function increases to 3.24 volts and the character of the energy distribution curve changes. This change consists of a displacement of the most probable energy to about 0.55 of the maximum and a decrease in the number of electrons emitted with lower velocities. Allowing the surface to stand in contact with nitrogen restored the original broad distribution but did not bring the work function down to the value for the polished surface.

13. Recent advances in nuclear physics. M. A. TUVE, *Bureau of Terrestrial Magnetism, Carnegie Institution of Washington.*

14. High-voltage methods in the investigation of nuclear structure. R. J. VAN DE GRAAFF, *Massachusetts Institute of Technology.*

15. Demonstration of an electrostatic high-voltage generator. E. H. BRAMHALL, *Massachusetts Institute of Technology.*

16. Physics of the sun. D. H. MENZEL, *Harvard Observatory.*

AUTHOR INDEX TO ABSTRACTS OF THE CAMBRIDGE MEETING OF THE NEW ENGLAND SECTION

Albertson, Walter—No. 4
Allen, Mildred—No. 10

Bradbury, Norris E.—No. 12
Bramhall, E. H.—No. 15

Dow, R. B.—No. 11

King, P. B.—see Mimno
Krutter, H. M.—see Warren

Menzel, D. H.—No. 16
Mimno, Harry R., P. H. Wang and P. B. King—No. 7
Morse, Philip M. and L. A. Young—No. 3
Müller, Hans—No. 1

Oldenberg, O.—No. 6

Rice, O. K.—No. 5

Steinberger, R. L.—No. 9

Tuve, M. A.—No. 13

Van de Graaff, R. J.—No. 14

Wang, P. H.—see Mimno
Warren, B. E. and H. M. Krutter—No. 2

Young, L. A.—see Morse

Zisman, W. A.—No. 8

THE AMERICAN INSTITUTE OF PHYSICS

INCORPORATED

GOVERNING BOARD

For The American Physical Society:

KARL T. COMPTON, *Chairman*
Massachusetts Institute of Technology

GEORGE B. PEGRAM, *Secretary*
Columbia University

JOHN T. TATE
University of Minnesota

For The Optical Society of America:

PAUL D. FOOTE
The Gulf Companies

LOYD A. JONES
Eastman Kodak Company

F. K. RICHTMYER
Cornell University

For The Acoustical Society of America:

H. D. ARNOLD
Bell Telephone Laboratories

HARVEY FLETCHER
Bell Telephone Laboratories

DAYTON C. MILLER
Case School of Applied Science

For The Society of Rheology:

E. C. BINGHAM
Lafayette College

WHEELER P. DAVEY
Pennsylvania State College

A. STUART HUNTER
du Pont Rayon Company

For The American Association of Physics Teachers:

HOMER L. DODGE
University of Oklahoma

PAUL E. KLOPSTEG
Central Scientific Company

FREDERIC PALMER
Haverford College

ADMINISTRATIVE STAFF

HENRY A. BARTON, *Director*
JOHN T. TATE, *Adviser on Publications*
MADELINE M. MITCHELL, *Editorial Secretary*
Office: 11 East 38th Street, New York, New York

JOURNALS

THE PHYSICAL REVIEW
REVIEWS OF MODERN PHYSICS
PHYSICS
JOHN T. TATE, *Editor*
J. W. BUCHTA, *Assistant Editor*
E. C. BINGHAM, *Rheology Editor*

THE JOURNAL OF THE OPTICAL SOCIETY OF AMERICA
THE REVIEW OF SCIENTIFIC INSTRUMENTS WITH PHYSICS NEWS AND VIEWS
F. K. RICHTMYER, *Editor*

THE JOURNAL OF THE ACOUSTICAL SOCIETY OF AMERICA
F. R. WATSON, *Chairman, Editorial Board*
WALLACE WATERFALL, *Managing Editor*

THE JOURNAL OF CHEMICAL PHYSICS
HAROLD C. UREY, *Editor*

THE AMERICAN PHYSICS TEACHER
DUANE ROLLER, *Editor*

The American Institute of Physics is a membership corporation of which five societies are the founding members. These five societies are the principal national societies devoted to pure and applied physics in America. Their names, and those of their representatives who form the Governing Board of the Institute, are given above. The principal work of the Institute is the publication of journals sponsored by the societies or by itself. The names and the editors of the journals are also listed above.

The broad purpose of the Institute is to represent, in all matters of wide or common interest, the five thousand or more members and subscribers associated with the Founder Societies and the journals. It aims to advance the science and profession of physics, and to promote cooperation between pure research, the applied sciences and the industries. To achieve these aims, it is greatly in need of an endowment and is empowered by law to administer grants and funds of any kind.

Notice: This issue does not contain a volume index because the volume has been extended to include twelve issues. An index will appear in the June 15th number.

CONTENTS

MARCH 15, 1933

Geographic Study of Cosmic Rays . . . . . ARTHUR H. COMPTON 387

Determination of e/m for an Electron by a New Deflection Method . . . . . FRANK G. DUNNINGTON 404

Determination of e/m by Means of Photoelectrons Excited by X-Rays . . . . . G. G. KRETSCHMAR 417

Masses of Ne^{20} and B^{11}. The Mass of Ne^{22} and the Disintegration of F^{19} . . . . . K. T. BAINBRIDGE 424

Thermionic and Adsorption Characteristics of Thorium on Tungsten . . . . . WALTER H. BRATTAIN AND JOSEPH A. BECKER 428

Transformations in the Theory of Complex Spectra . GEORGE H. SHORTLEY 451

Zeeman Effect of Lead II, III and IV . . J. B. GREEN AND R. A. LORING 459

Infrared Absorption Bands of Methane . . . . . WILL V. NORRIS AND HILBERT J. UNGER 467

New Band in the Spectrum of the OH Molecule . . . . . HERRICK L. JOHNSTON, DAVID H. DAWSON AND MARGERY K. WALKER 473

Variational Principles in Electromagnetism . . . . . H. BATEMAN 481

Crystalline Fields of Pr, Nd and Yb from Paramagnetic Susceptibilities . . . . . W. G. PENNEY 485

Positive Electron . . . . . CARL D. ANDERSON 491

Letters to the Editor:

Resonance Spectrum of Bromine . . . . . HAROLD PLUMLEY 495

On the Statistical Foundation of Debye's Theory of Electrolytes . OTTO HALPERN 495

Low States of the Heaviest Elements . . . TA-YOU WU AND S. GOUDSMIT 496

Separation of Hydrogen Isotopes by Fractional Desorption . . . . . HUGH S. TAYLOR, AUSTIN J. GOULD AND WALKER BLEAKNEY 496

Scattering and Absorption of Neutrons . J. R. DUNNING AND G. B. PEGRAM 497

Evaporation Technique for Aluminum . . . . . JOHN STRONG 498

Effect of Spin Interaction in the Diffraction and Polarization of Electrons . . . . . J. H. HOWEY 499

Proceedings of the American Physical Society 500

CAMBRIDGE MEETING OF THE NEW ENGLAND SECTION, February 4, 1933; Minutes and Abstracts 1–16, Author Index

LANCASTER PRESS, INC., LANCASTER, PA.